Characterization of cell biological and physiological functions of the phosphoglycolate phosphatase AUM

Charakterisierung zellbiologischer und physiologischer Funktionen der Phosphoglykolat-Phosphatase AUM

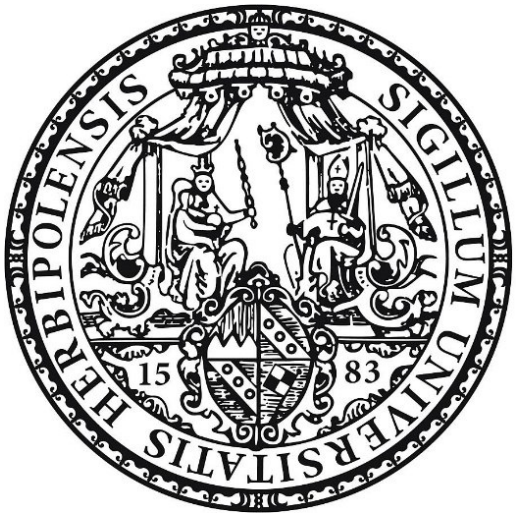

Dissertation for a doctoral degree
at the Graduate School of Life Sciences,
Julius-Maximilians-Universität Würzburg
(Section Biomedicine)

submitted by

Gabriela Segerer

from Kitzingen am Main

Würzburg, November 2015

Submitted on: ……

Members of the *Promotionskomitee*:

Chairperson:	Prof. Dr. Manfred Gessler
Primary Supervisor:	Prof. Dr. Antje Gohla
Supervisor (Second):	Prof. Dr. Dr. Manfred Schartl
Supervisor (Third):	PD Dr. Heike Hermanns

Date of Public Defence: ……

Date of Receipt of Certificates: ……

Table of contents

Figure and table index

Abbreviations

2D	two-dimensional
µg	microgramm
µL	microliter
µM	micromolar
ADP	adenosine diphosphate
ATP	adenosine triphosphate
CDR	Circular dorsal ruffle
CIN	Chronophin
DDR	DNA damage response
DG	diglyceride
DHAP	dihydroxyacetone phosphate
DNA	deoxyribonucleic acid
DSB	double-strand break
E	embryonic day
ECM	extracellular matrix
EGF	epidermal growth factor
EGFR	epidermal growth factor receptor
FA	fatty acid
F-actin	filamentous actin
FN	fibronectin
FAK	focal adhesion kinase
FN	fibronectin
G3P	glycerol 3-phosphate
G-actin	globular actin
GADP	glyceraldehyde 3-phosphate
GC1	mouse spermatogonial cell line
GPCR	G-protein coupled receptor
HAD	haloacid dehalogenase
ICAM-1	intercellular adhesion molecule-1
LC	lymphocyte
kDa	kilo Dalton
MEF	mouse embryonic fibroblast
MG	monoglyceride
mL	milliliter

MLEC	mouse lung endothelial cell
mM	millimolar
ng	nanogramm
nm	nanometer
OCR	oxygen consumption rate
OXPHOS	oxidative phosphorylation
PC	phosphatidylcholine
PCR	polymerase chain reaction
PG	phosphoglycolate
PDE	phosphodiesterase
PDXP	pyridoxal phosphate phosphatase
PEP	phosphoenolpyruvate
PEPCK	phosphoenolpyruvate carboxykinase
PGP	phosphoglycolate phosphatase
PI3K	phosphatidylinositol-4,5-bisphosphate 3-kinase
PK	pyruvate kinase
PKC	protein kinase C
PL	phospholipid
PLC	phospholipase C
PLL	poly-L-lysine
PLP	pyridoxal 5'-phosphate
p-NPP	*para*-nitrophenylphosphate
PPM	protein phosphatase, metal-dependent
PPP	phosphoprotein phosphatase
PTP	protein tyrosine phosphatase
PS	phosphatidylserine
PUFA	polyunsaturated fatty acid
pY	phosphotyrosine
RNA	ribonucleic acid
ROS	reactive oxygen species
RTK	receptor tyrosine kinase
SDF-1	stromal-derived factor-1
SDS-PAGE	sodium dodecylsulphate polyacrylamide gel electrophoresis
S.E.M.	standard error of the mean
SFK	Src family kinase
shRNA	short hairpin RNA
SSB	single-strand break

TCA	tricarboxylic acid
TG	triglyceride
TPI	triose phosphate isomerase
v/v	volume/volume
w/v	weight/volume
WT	wildtype
x *g*	multiples of Earth's standard gravity (9.81 m/s^2)
Y	tyrosine
YFP	yellow fluorescent protein

1 Introduction

1.1 Phospho-regulation by kinases and phosphatases

Regulation of enzyme activity is critical for cellular signal transduction and for governing cell behavior. One major way to alter protein function consists of reversible, posttranslational modifications. The predominant eukaryotic modification is phosphorylation of proteins (Khoury et al., 2011). Phospho-regulation is the dynamic and highly organized process of phosphorylation and its counterpart, dephosphorylation, and is governed by the opposing functions of kinases and phosphatases. Phosphorylation is the addition of the gamma phosphate group $(PO_4)^{3-}$, derived from adenosine triphosphate (ATP) to particular amino acids in proteins, or to small substrates with a free hydroxyl group such as lipids, sugars or other metabolites. There are nine amino acids, which can function as a phosphate acceptor, namely arginine, lysine, aspartate, cysteine, glutamate, histidine, serine, threonine and tyrosine. The majority of phosphorylation events occurs on serine, threonine and tyrosine residues with a distribution of 86.5%, 11.8% or 1.8%, respectively (Olsen et al., 2006). Protein phosphorylation typically leads to changes of protein conformation because a highly polar, two times negatively charged phosphate group is introduced. By affecting the chemical and sterical properties, phosphorylation can directly alter the enzymatic activity of a protein, or otherwise change its interactions with other binding partners, and thereby modulates its function (Cohen, 2000).

Dephosphorylation is the removal of covalently bound phosphate by hydrolysis, and is accomplished by the action of phosphatases. The regulation of protein activity and/or their subcellular localization by phosphorylation and dephosphorylation is involved in almost every known signaling pathways (Graves and Krebs, 1999) and plays a fundamental role in a wide range of cellular processes such as cell proliferation, migration and adhesion. Abnormal phospho-regulation is associated with a variety of pathophysiological processes and diseases such as cancer, diabetes or cardiovascular disorders (Blume-Jensen and Hunter, 2001, Cohen, 2001).

In eukaryotes, it has been estimated that approximately 30% of all cellular proteins are phosphorylated on at least one residue (Cohen, 2000) and around 700,000 phosphorylation sites have been characterized *in vivo* using mass spectrometry (Newman et al., 2013, Ubersax and Ferrell, 2007). Because of the enormous number of potential phosphorylation sites, kinase- as well as phosphatase signaling has to be tightly regulated to coordinate cellular processes.

Meanwhile, more than 500 protein kinases and about 20 lipid kinases have been identified, making kinases one of the largest protein families (Duong-Ly and Peterson, 2013). Protein

kinases have emerged as promising therapeutic targets because mutations in their activities are often linked to cancer and have been extensively studied.

Right now, about 200 catalytic subunits of human phosphatases have been identified (Liberti et al., 2013). This comparatively small number, together with the promiscuous activity of some isolated phosphatase catalytic domains *in vitro*, has led to the assumption that phosphatases are broadly specific and dephosphorylate many substrates. However, whereas kinases are derived from a common ancestor and exhibit a highly conserved sequence similarity in their catalytic domains, protein phosphatases have many ancestors and display therefore, a higher diversity (Virshup and Shenolikar, 2009).

In the last decades, it has become clear that phosphatases can indeed be highly specific and control signal transduction in a dominant and non-redundant manner (Ren et al., 2011, Seifried et al., 2014, Shi, 2009).

1.2 Classification of phosphatases

According to their structural and mechanistic properties, protein phosphatases are classified into six subfamilies (**Figure 1**). Four families, representing ~80% of the identified phosphatases, control the phosphorylation state of serine, threonine and tyrosine residues (Pils and Schultz, 2004, Hunter, 1995).

The largest class is constituted by protein tyrosine phosphatases (PTPs), which are further subdivided into classical PTPs (receptor-like and non-transmembrane PTPs), the dual specificity PTPs (DUSPs) and low molecular weight PTPs (Cdc25 isoforms) (Alonso et al., 2004). Protein serine/threonine phosphatases comprise phosphoprotein phosphatases (PPPs) and the metal-dependent protein phosphatases (PPMs) (Shi, 2009). The fourth class consists of the largely unexplored family of haloacid dehalogenase- (HAD-) type phosphatases (Seifried et al., 2013). The phosphoglycolate phosphatase AUM, which is characterized in this thesis, belongs to this family.

The remaining two phosphatase families are lipid phosphatases, which dephosphorylate phosphorylated lipids, such as sphingosines (Sigal et al., 2005) and NUDT (nucleoside diphosphate linked to moiety X, also termed Nudix) phosphatases, acting on pyrophosphates and nucleotide sugars (Mildvan et al., 2005).

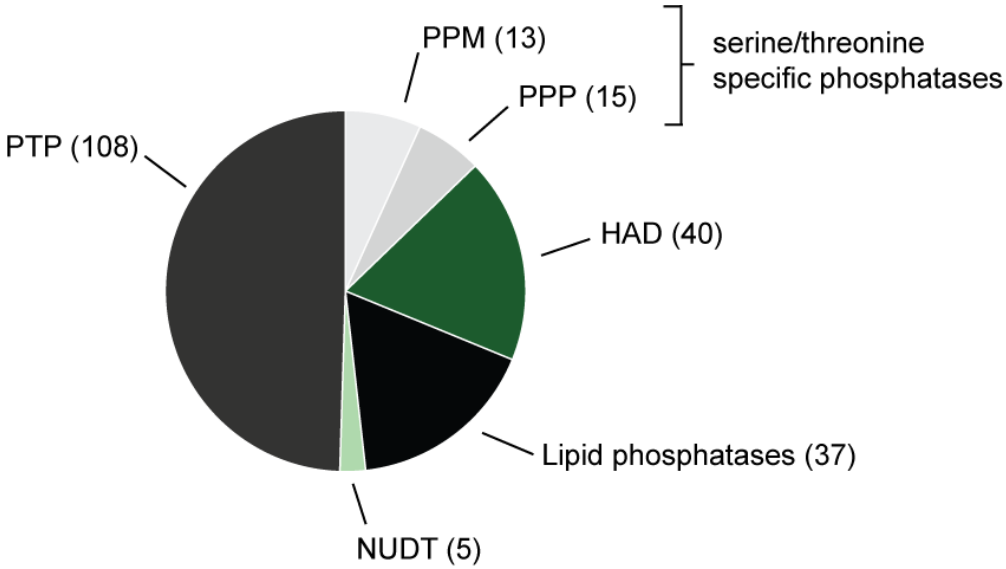

Figure 1: Human phosphatome.
The pie chart shows the classification of 218 human phosphatase catalytic subunits into six subfamilies: Protein tyrosine phosphatase (PTP), phosphoprotein phosphatases (PPPs), metal-dependent protein phosphatases (PPMs), haloacid dehalogenase phosphatases (HAD), lipid phosphatases and nucleoside –diphosphate-linked moiety X phosphatases (NUDT). The numbers of the constituent family members are displayed in parentheses. The figure was adapted from (Liberti et al., 2013) and (Seifried et al., 2013).

1.3 Haloacid dehalogenase (HAD) phosphatases

The superfamily of HAD hydrolases is a very large, ubiquitous and conserved archaic family of proteins, present in organisms from all three super kingdoms of life (Pandya et al., 2014, Seifried et al., 2013). Most members of this superfamily are phosphotransferases (~79% phosphatases and ~20% ATPases) (Allen and Dunaway-Mariano, 2009).

1.3.1 Structural features of HAD phosphatases

Although the overall sequence similarity between HAD phosphatases is very low on the amino acid level, members of this family can nevertheless be identified based on the presence of four HAD signature motifs containing the conserved catalytic residues. HAD signature motif 1 hhhDXDXT/V (h, hydrophobic residue; D, aspartate; X, any amino acid; T, threonine; V, valine) contains the essential nucleophilic aspartate, which catalyzes the phosphoryl transfer. Together with the second aspartate, it additionally coordinates the obligatory cofactor Mg^{2+} in the active site. Dephosphorylation of a substrate occurs by forming a phosphoaspartate intermediate. After removal of the substrate-leaving group, a water molecule exerts a nucleophilic attack on the phosphoaspartate intermediate, resulting in the release of free

phosphate and the regeneration of the aspartate (Allen and Dunaway-Mariano, 2009, Seifried et al., 2013).

HAD phosphatases can dephosphorylate, often highly specifically, a broad field of low and high molecular weight substrates, ranging from metabolite, carbohydrates or lipids to serine/threonine - or tyrosine-phosphorylated proteins (Allen and Dunaway-Mariano, 2009, Aravind and Koonin, 1998). A structural element inserted in the catalytic domain of HAD phosphatases, termed cap domain, plays a decisive role in the selectivity for low or high molecular weight substrates (Burroughs et al., 2006). According to their structure and their insertion sites, caps can be divided into three classes, C0, C1 and C2. **Figure 2** shows the structural diversity of HAD phosphatase cap domains.

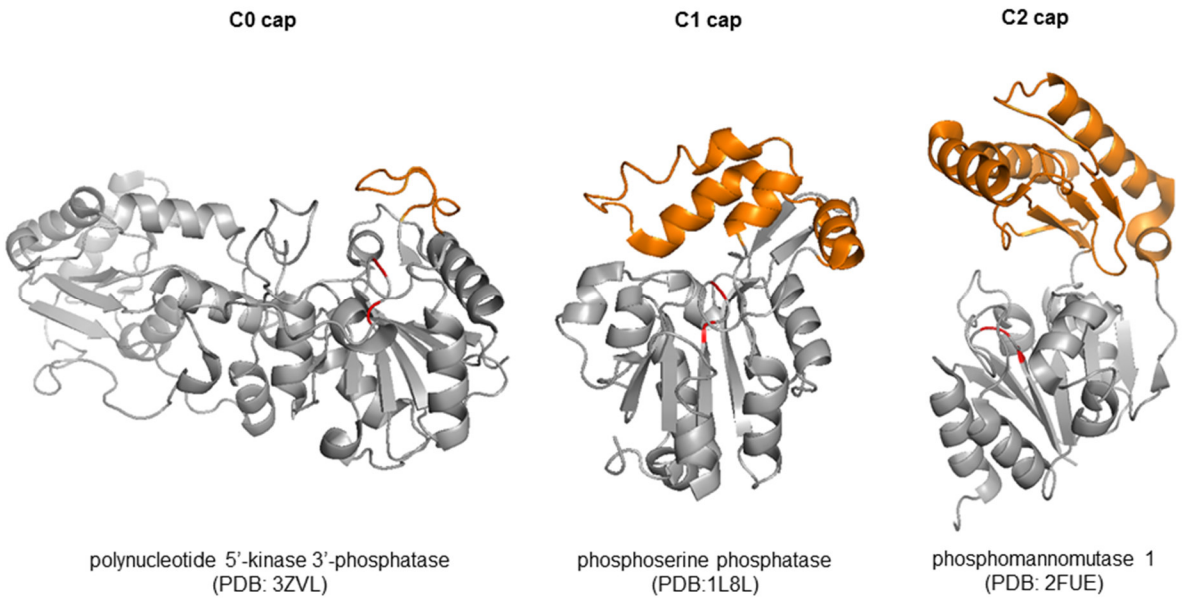

Figure 2: Structural diversity of HAD phosphatase cap domains.
Displayed are X-ray crystal structures of polynucleotide 5'- kinase 3'-phosphatase (PNKP, with an unstructured loop as cap), phosphoserine phosphatase (PSPH, with a C1 cap consisting of a four-helical bundle), and phosphomannomutase1 (PMM1, with a C2 cap consisting of an α/β fold). The catalytic domain is depicted in gray, cap domains are colored in orange and the catalytic aspartates of the HAD signature motif 1 are colored in red. The figure is adapted from (Seifried et al., 2013).
John Wiley and Sons license: 3736980762499.

C0 domains are very small and structurally simple. Phosphatases containing this domain are termed cap-less and generally prefer high molecular weight substrates. Some members may also dephosphorylate small substrates by 'pseudocapping' after oligomerization via cap domains (Lu et al., 2009).

C1 and C2 cap domains are much larger and sterically restrict access to the active site (see **Figure 2**). Thus, C1 and C2 phosphatases generally process low molecular weight substrates.

However, two members of C1 and C2 phosphatases are known which exceptionally dephosphorylate also high molecular weight protein substrates (Seifried et al., 2013). The C2-capped phosphatase Chronophin (gene name pyridoxal phosphatase; PDXP) for example dephosphorylates as a small molecule pyridoxal 5'-phosphate (PLP; Vitamin B6) (Fonda, 1992) and targets as protein substrates serine 3- phosphorylated cofilin (Gohla et al., 2005) and the serine/threonine -phosphorylated steroid receptor 3 (Li et al., 2008), and the C1-capped Eyes absent family member Eya 3 dephosphorylates tyrosine-phosphorylated histone H2AX (Krishnan et al., 2009).

1.3.2 HAD phosphatases in health and diseases

HAD-type phosphatases are a very large and diverse family of at least 40 human members. A growing number of them has been linked to human diseases such as cardiovascular or metabolic disorders and cancer (Seifried et al., 2013).

One prominent example is the Eyes absent (Eya) phosphatase family consisting of four paralogs in humans. They were originally characterized in eye development of *Drosophila melanogaster* and are involved in tissue- and organ formation of muscle, eye, ear and kidney (Jemc and Rebay, 2007, Rebay et al., 2005). Eya proteins are defined by a conserved so-called Eya domain that mediates protein-protein interactions with DNA binding proteins. Eyes absent phosphatases were initially identified as transcription factors, acting through interaction with homeodomain-containing Sine oculis proteins (also known as Six) and their phosphatase activity was discovered later (Li et al., 2003, Tootle et al., 2003, Rayapureddi et al., 2003). Thus, the characterization of Eya revealed for the first time the existence of transcription factors that also exhibit phosphatase activity. As already mentioned, Eya 3 proteins dephosphorylate tyrosine-phosphorylated histone H2AX, resulting in the recruitment of DNA repair complexes and an increase in the resistance of cells to apoptotic signals (Krishnan et al., 2009). Mutations in Eya proteins are linked to various congenital disorders including the multi-organ diseases bronchio-oto-renal syndrome (BOR1) and bronchio-otic syndrome (BOS1) (Abdelhak et al., 1997, Clarke et al., 2006). Overexpression of Eya proteins results in tissue overgrow and malignant tumors and downregulation suppresses tumor growth (Zhang et al., 2005, Reichenberger et al., 2005). Recently, it was shown that the tyrosine phosphatase activity of Eya is essential to promote cell migration and invasion of tumor cells (Pandey et al., 2010).

Another phosphatase family whose causal link to human diseases is supported by genetic data, are the lipins 1-3. All lipins, but mainly lipin-1, catalyze the magnesium-dependent dephosphorylation of phosphatidic acid to form diglyceride. They may also regulate the expression of genes involved in lipid metabolism in the nucleus (Donkor et al., 2007, Csaki and Reue, 2010). Lipin-1 polymorphisms in humans are linked to rhabdomyolysis (Zeharia et al.,

2008) and metabolic disorders such as insulin resistance and diabetes, whereas lipin-2 deficiency causes multifocal bone and skin inflammation, known as *Majeed* syndrome (Reue, 2009).

Our research group is interested in the characterization of two novel members of the HAD-phosphatase family, namely chronophin and phosphoglycolate phosphatase AUM (gene annotation PGP). Chronophin was initially identified as pyridoxal 5'-phosphate (PLP) phosphatase (gene annotation PDXP) (Fonda, 1992). Fundamental processes for example synthesis of neurotransmitters (Awapara et al., 1962, Baxter and Roberts, 1958), amino acid metabolism (Schirch and Szebenyi, 2005, Raboni et al., 2003, Bettati et al., 2000), and lipid metabolism (Combs, 2008), are PLP-dependent. Many diseases are associated with PLP deficiencies, such as epilepsy, depression, cardiovascular diseases and cancer (Zhang et al., 2013, Hvas et al., 2004, Mills et al., 2014, Lin et al., 2006). Additionally, chronophin dephosphorylates the actin severing protein cofilin on its inhibitory serine residue (Gohla et al., 2005). Recently, our group was able to demonstrate that chronophin regulates glioblastoma growth and invasiveness in a cofilin-dependent manner (Schulze et al. 2015). Thus, chronophin acts on the one hand, as a metabolic phosphatase by dephosphorylation of PLP and on the other hand, as a protein phosphatase.

1.4 Characterization of phosphoglycolate phosphatase PGP

The closest paralog of chronophin is the mammalian phosphoglycolate phosphatase AUM (from now on referred to as PGP). PGP was identified by database mining and phylogenetic analysis (Seifried et al., 2014). A sequence alignment demonstrated that PGP and chronophin share 45% identity on amino acid level and 87% similarity of predicted secondary structure motifs (Seifried et al., 2014). The murine protein has a predicted molecular weight of 34.5 kDa and consists of 321 amino acids. PGP was termed AUM (aspartate-based, ubiquitous, Mg^{2+}-dependent phosphatase) because of its biochemical characteristics. As a HAD phosphatase, PGP needs an aspartate as a nucleophile in its active site. The point mutation of aspartate on position 34 in the HAD motif 1 to an asparagine leads to a phosphatase inactive mutant (PGP^{D34N}) (Seifried et al., 2014). Phosphatase activity of this mutant was tested against the artificial substrate *para*-nitrophenylphosphate (*p*NPP). PGP^{WT} was able to dephosphorylate *p*NPP, whereas PGP^{D34N} was not. For catalytic activity of PGP, Mg^{2+} is required as cofactor. Western blot analysis using a PGP specific polyclonal antibody, showed that PGP is ubiquitously expressed in all major tissues. The highest expression was detected in testis (Seifried et al., 2014).

1.4.1 PGP dephosphorylates phosphoglycolate *in vitro*

In vitro phosphatase assays with phosphoglycolate (PG) as a substrate showed that highly purified, recombinant murine PGP acts as a PG phosphatase *in vitro*, with K_m = 0.3 mM, k_{cat} = 2.13 ± 0.05 s^{-1}, and a k_{cat}/K_m = 7.1 × 10^3 s^{-1} mM^{-1} (**Figure 3**). To confirm the specificity of this reaction, the phosphatase-inactive catalytic point mutant PGP^{D34N} (PGP^{DN}) and the closest PGP homolog chronophin (PDXP) were tested in parallel. However, neither PGP^{DN}, nor PDXP exhibited *in vitro* phosphatase activity against PG. Additionally, PGP did not detectably dephosphorylate other substrates containing PG-like structural features (unpublished data).

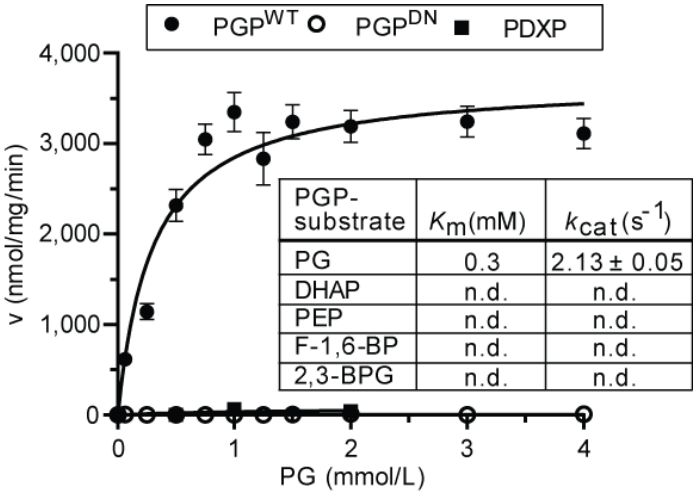

Figure 3: PGP is a PG phosphatase *in vitro*.
In vitro phosphatase activity of purified recombinant murine PGP towards phosphoglycolate (PG; n=8), dihydroxyacetone phosphate (DHAP), phosphoenolpyruvate (PEP), fructose 1,6-bisphosphate (F-1,6-BP) or 2,3-bisphosphoglycerate (2,3 BPG) (n=2 for each of these compounds). Free inorganic phosphate that was released after PGP-catalyzed dephosphorylation was quantified using a malachite green assay. PGP^{D34N} (PGP^{DN}; n=6) and PDXP (n=2) were tested as well. Results represent mean values ± S.E.M. Experiments were performed with two independently purified protein batches. Note that some error bars are masked by the symbols. n.d., not detectable. The experiments were performed by Annegrit Seifried.

1.4.1.1 Source of mammalian phosphoglycolate (PG)

The origin of mammalian phosphoglycolate (PG) is not known with certainty. In plants, PGP is one of the core enzymes of photosynthetic carbon dioxide (CO_2) assimilation. Here, PG is formed during photorespiration, and PGP is essential to provide glycolate that can be salvaged by re-entry into the Calvin cycle (Bauwe et al., 2010).

In humans, there is one source of PG known in the context of DNA-repair. Life in aerobic conditions favors the formation of oxygen free radicals that constantly cause DNA damage. Reactive oxygen species (ROS) generated by endogenous oxidative stress or by ionizing radiation can trigger single- or double-strand DNA breaks (SSBs, DSBs), which typically bear a 3'-phosphate or a 3'-phosphoglycolate (3'-PG) terminus (Iyama and Wilson, 2013) as a

consequence of free radical attack on the DNA sugar moiety. Mass spectrometric quantification showed that 3'-PG termini constitute ~10% of all DNA sugar oxidation products produced by γ-irradiation or by treatment with the radiomimetic drug bleomycin (Chen et al., 2007); earlier studies estimated that ~25% of oxidative stress-induced (Bertoncini and Meneghini, 1995), or up to 50% of radiation-induced DNA strand breaks bear 3'-PG termini (Henner et al., 1983). Because these 3'-ends preclude direct DNA re-ligation, they need to be enzymatically processed to enable DNA repair and thus to maintain genomic integrity. Phosphodiesterases (PDEs) cleave 3'-PG DNA ends and release free PG (Zhou et al., 2009, Zhou et al., 2005). This step enables DNA repair. Free PG is further hydrolyzed to glycolate by dedicated phosphoglycolate phosphatases (PGPs) in the cytosol **(Figure 4)**.

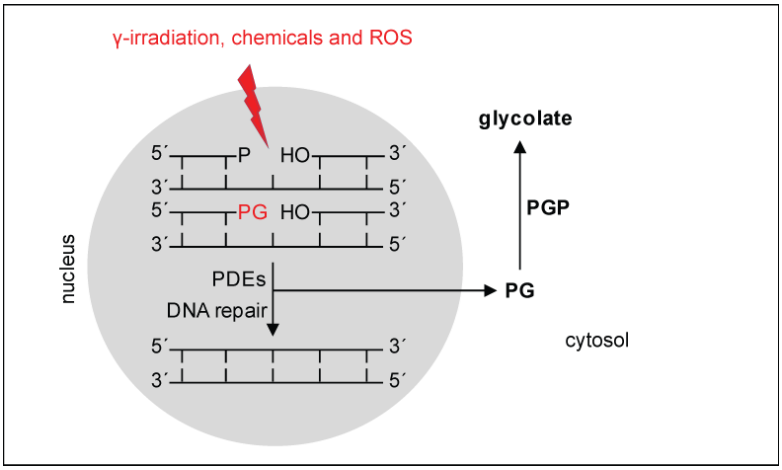

Figure 4: Origin of mammalian phosphoglycolate (PG).
Oxidative damage triggers single- and double-strand DNA breaks with a 3'-phosphoglycolate (3'-PG) terminus. After cleavage of these ends by phosphodiesterases (PDE), PG is released to the cytosol and can be dephosphorylated by dedicated PGPs.

1.4.1.2 Function of mammalian phosphoglycolate (PG)

The function of PG or glycolate is not yet known in mammals. Despite the widespread expression of mammalian PGPs in all tissues and cells examined so far (Seifried et al., 2014, Knight et al., 2012), their biological roles remain elusive. Human PGP was first purified and biochemically characterized from red blood cells, based on the biochemical enrichment of a PG-hydrolyzing activity (Badwey, 1977, Zecher and Wolf, 1980, Rose, 1981). PG was initially thought to activate the bisphosphoglycerate mutase-dependent hydrolysis of 2,3-bisphosphoglycerate (2,3-BPG), a major modifier of the oxygen affinity of hemoglobin. However, a physiological role of PGP and PG for controlling 2,3-BPG levels in human erythrocytes could not be substantiated (Somoza and Beutler, 1983). Early genetic linkage studies suggested an involvement of the *Pgp* gene locus in polycystic kidney disease and manic depressive illness, but these associations were later weakened (Breuning et al., 1990, Ewald et al., 1995).

There are some reports identifying PG as an inhibitor of enzymes involved in glucose homeostasis. PG inhibits phosphoenolpyruvate carboxykinase (Stiffin et al., 2008), an enzyme used in gluconeogenesis and inhibits two enzymes involved in glycolysis, the pyruvate kinase (Dougherty and Cleland, 1985) and triose phosphate isomerase (Hartman et al., 1975) *in vitro* because of its structural similarity to the endogenous substrates of these enzymes.

Pyruvate kinase catalyzes the final step of the glycolytic pathway, the transfer of a phosphate group from phosphoenolpyruvate to ADP. Triosephosphate isomerase (TPI) isomerizes dihydroxyacetone phosphate (DHAP) and glyceraldehyde 3'-phosphate (GADP), which are produced in glycolysis from glucose-derived fructose 1,6-bisphosphate.

It was demonstrated that PG inhibits purified TPI activity *in vitro* by functioning as a reversibly binding transition state analog of TPI substrates (Wolfenden, 1969) (**Figure 5**).

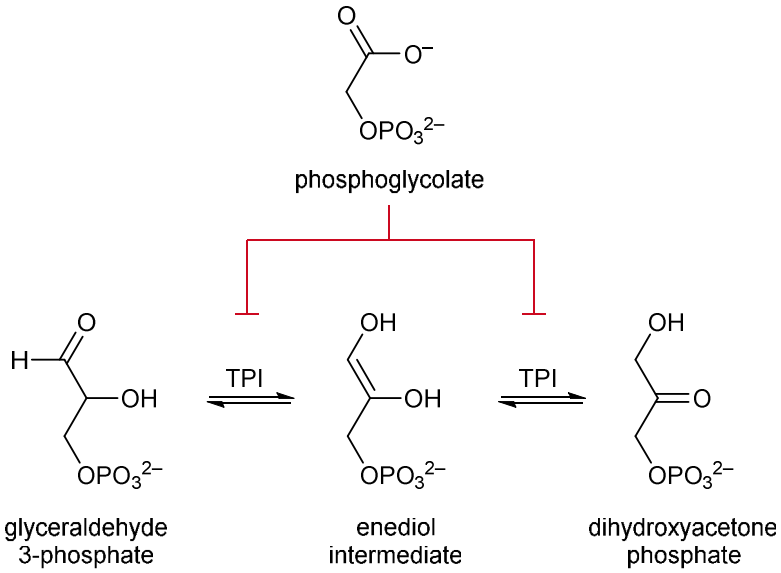

Figure 5: TPI inhibition by phosphoglycolate.
For details, see text below.

The isomerization of GADP and DHAP occurs via a proposed enediol intermediate. Because of its structural similarity to this intermediate, PG can bind at the active site of TPI and inhibits catalytic activity towards the endogenous substrate (Dwyer et al., 2004).

The inhibition of TPI activity as a potential physiological PG function is especially interesting because TPI constitutes a branch point between carbohydrate and lipid metabolism.

1.4.1.3 TPI controls a branch point between glucose- and lipid metabolism

The reversible interconversion of DHAP and GADP by TPI constitutes the transition from glycolysis to lipogenesis. Glycerol 3-phosphate dehydrogenase converts DHAP to glycerol 3-phosphate that provides the carbohydrate backbone that activated fatty acids (FA-CoA) are esterified with to build triglycerides (TGs) during lipogenesis. Fatty acids derived from cellular uptake or from fatty acid synthesis are activated by acyl-CoA synthase (ACSL) and utilized together with glycerol 3-phosphate (G3P) for lipogenesis (**Figure 6**).

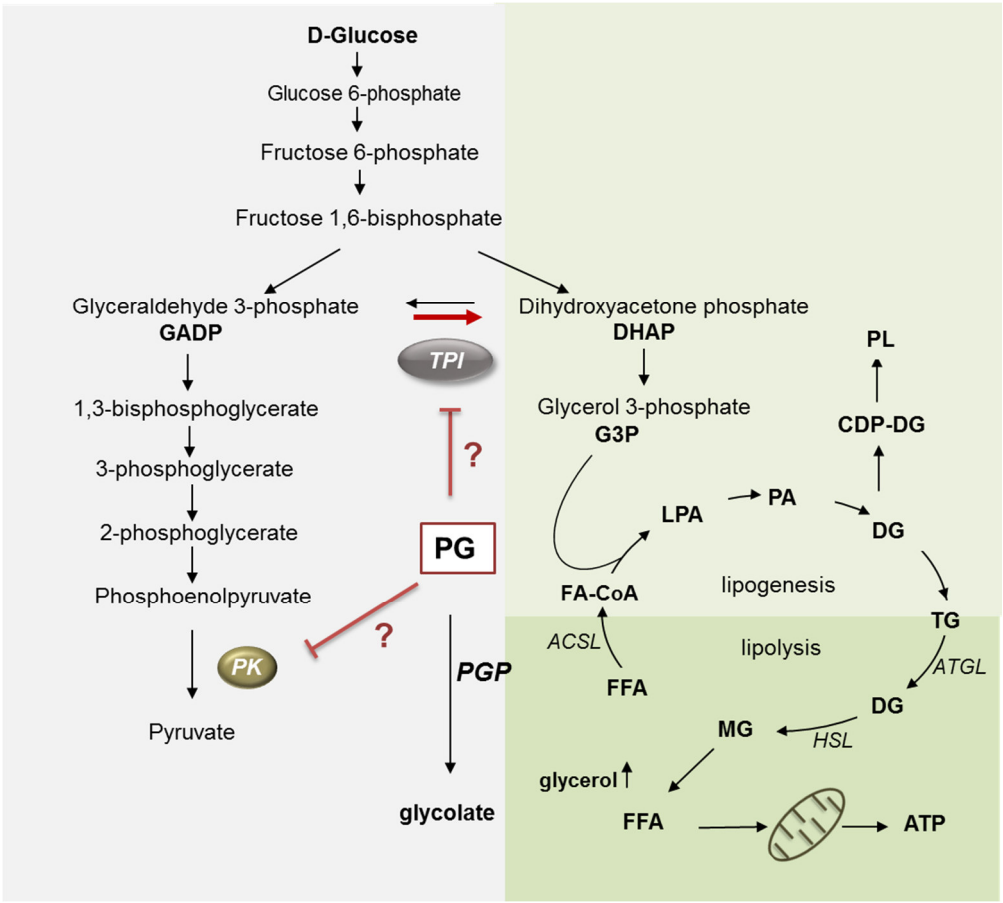

Figure 6: Carbohydrate- and lipid metabolism.
Together with free fatty acids, activated by acyl-CoA synthase (ACSL), DHAP-derived G3P forms lysophosphatidic acid (LPA) and drives triglyceride (TG) synthesis. By acylation of LPA phosphatidic acid (PA) is formed, which is acylated to diglyceride (DG). DGs are utilized as precursor for phospholipids (PL) or acylated to form TGs. During lipolysis, TG is hydrolyzed by the adipose TG lipase (ATGL) to DG, which is hydrolyzed to monoglyceride (MG) by the hormone sensitive lipase (HSL). The released fatty acids (FFA) can be utilized for ATP production by β-oxidation in the mitochondria. (Berg JM, Tymoczko JL, Stryer L. Biochemistry. 5th edition; 2002).

During lipogenesis, several intermediate lipids are generated. Initially, lysophosphatidic acid (LPA) is formed after condensation of G3P with FA-CoA. LPA further reacts to phosphatidic acid (PA). PA is acylated to form diglycerides (DG). DG acylation to triglyceride (TG) is the final step of lipogenesis. DG can also be utilized after conversion to cytidine diphosphate activated diglycerides (CTP)-DG for the production of phospholipids (PL) such as phosphatidylcholine, phosphatidylethanolamine and phosphatidylserine, which are abundant

in the plasma membrane. Lipolysis is the breakdown of TGs and starts with hydrolysis of TG to DG, which is further hydrolyzed to monoglycerides (MG). Two different lipases are responsible for this process, the adipose TG lipase (ATGL) which hydrolyzes TG and releases DG, and the hormone sensitive lipase (HSL) which hydrolyzes DG to MG. The released fatty acids can be utilized for ATP production by β-oxidation in the mitochondria (Berg JM, Tymoczko JL, Stryer L. Biochemistry. 5th edition; 2002).

So far, PG was only used experimentally as an *in vitro* inhibitor of pyruvate kinase (PK) and TPI. It has not been proven, if PG physiologically inhibits PK- or TPI activity and if there are any consequences for carbohydrate and lipid metabolism.

1.4.2 PGP acts as a tyrosine-directed phosphatase *in vitro*

Similar to its closest relative chronophin which dephosphorylates the small molecule PLP (Fonda, 1992) as a metabolic phosphatase (Kestler et al., 2014), our data show that PGP dephosphorylates the low molecular weight substrate PG (see **Figure 3**;unpublished data), and suggest that it might thereby play a role in carbohydrate and lipid metabolism. In contrast to the serine/threonine -directed phosphatase chronophin (Li et al., 2008, Gohla et al., 2005), it was demonstrated that PGP acts as a tyrosine-directed phosphatase *in vitro.* In a phospho-peptide screen with over 720 phosphorylated peptides, purified PGP exclusively dephosphorylates a small number of tyrosine-phosphorylated peptides and directly hydrolyzes tyrosine-phosphorylated proteins from HeLa cell extracts in a phosphatase overlay assay (Seifried et al., 2014). Additionally, it was shown in spermatogonial GC1 cells that stimulation with the epidermal growth factor (EGF) leads to an increase of tyrosine phosphorylation especially of high molecular weight proteins upon RNA interference-mediated depletion of endogenous PGP (**Figure 7**).

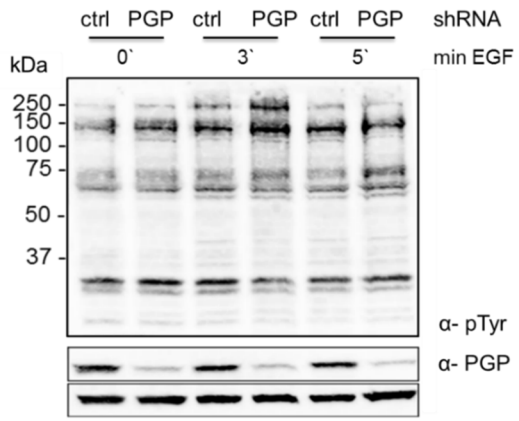

Figure 7: PGP is implicated in growth factor signaling.
Control shRNA and PGP shRNA expressing spermatogonial GC1 cells were seeded on poly-L-lysine coated surface, serum-starved overnight and stimulated with 100 ng/mL EGF for the indicated time points. Cells were lysed, and proteins were separated by SDS-PAGE and transferred onto nitrocellulose membranes for immunoblotting. Cellular tyrosine phosphorylation levels were analyzed with 4G10 α-phosphotyrosine antibody. After 3 min of stimulation, specific changes in tyrosine phosphorylation levels were detectable (Seifried et al., 2014).

Though it was shown that high concentrations of purified PGP can directly dephosphorylate tyrosine-phosphorylated peptides and proteins from HeLa cell extracts (Seifried et al., 2014), a physiological tyrosine-phosphorylated substrate has not been identified yet.

In the peptide screen, the EGF receptor (EGFR) itself and some of its downstream signaling molecules have appeared as possible substrates of PGP (Seifried et al., 2014).

The EGFR is a transmembrane receptor and constitutes a member of the ErbB receptors, a subfamily of four closely related receptor-tyrosine kinases (RTK) (Herbst, 2004). Upon ligand binding, the receptor dimerizes and its intrinsic intracellular protein-tyrosine kinase activity is induced. This leads to the auto-phosphorylation on multiple tyrosine residues (pY) including pY992, pY1045, pY1068, pY1148 and pY1173 and to the recruitment and binding of scaffolding and downstream effector proteins such as GRB2, SHC, GAB1 or PLCγ (Downward et al., 1984, Carpenter, 2000).

A simplified model of EGF-dependent signaling is displayed in **Figure 8**.

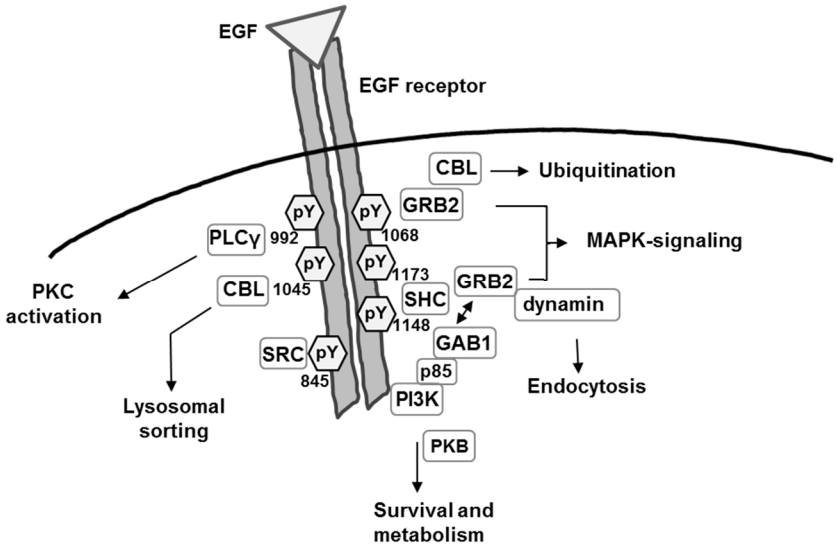

Figure 8: Simplified model of EGF receptor signaling.
After ligand binding, the receptor dimerizes and the enhancement of the intrinsic tyrosine kinase activity leads to auto-phosphorylation of tyrosine residues 992, 1045, 1068, 1148 and 1173 and subsequently to the recruitment and binding of effector proteins. For details, see text below. The figure is adapted from (Kolch and Pitt, 2010).

GRB2 can either bind directly to the EGFR (pY1068) or indirectly via SHC (binds at pY1173) binding which results in the activation of the RAS GTPases (Lowenstein et al., 1992) and mitogen-activated protein kinases (MAPKs) (Avruch et al., 2001). GRB2 interacts with several proteins including dynamin, which is implicated in EGFR endocytosis (Wang and Moran, 1996) and recruits them to the EGFR.

The E3 ubiquitin-protein ligase CBL is also a substrate of the EGFR. CBL associates with the receptor either by binding to GRB2 or by direct binding to the EGFR (pY1045) leading to lysosomal sorting and ubiquitination of the receptor (Grovdal et al., 2004).

GAB1, another GRB2 interacting protein, recruits PI3K to the EGFR by the binding of its p85 subunit (Rodrigues et al., 2000) resulting via protein kinase B activation in survival signaling (Brunet et al., 1999).

The tyrosine kinase Src is activated by the EGFR upon receptor activation and phosphorylates the receptor on tyrosine 845 resulting in the modulation of the mitogenic function of the receptor (Biscardi et al., 1999).

Another prominent enzyme activated by EGFR is PLCγ1 (Rotin et al., 1992, Kim et al., 1991) which catalyzes the hydrolysis of PIP_2, leading to the generation of the second messengers diglyceride (DG) and inositol trisphosphate (IP_3). IP_3 production results in the release of stored Ca^{2+} from the endoplasmic reticulum (Kadamur and Ross, 2013). Together with DG, Ca^{2+} activates protein kinase C (PKC) (Huang, 1989). By PKC-mediated phosphorylation of several proteins, PLCγ1 is involved in the regulation of growth (Xia et al., 1996) or actin remodeling (Nishizuka, 1995, Laux et al., 2000).

These examples represent only a fraction of signaling proteins and signaling pathways involved in RTK signal transduction.

PGP-dependent changes in tyrosine phosphorylation of proteins upon EGFR activation suggest a role of PGP in RTK signaling. However if PGP directly dephosphorylates a tyrosine-phosphorylated substrate downstream of EGF receptor signaling has not been proven yet.

1.4.3 PGP is a regulator of integrin-dependent cell adhesion

PGP was also identified as a regulator of integrin-mediated cell adhesion. By performing cell adhesion assays with control shRNA or PGP shRNA expressing GC1 cells, it was shown that cells lacking PGP adhere faster on different integrin ligands such as fibronectin, vitronectin and collagen I/IV (PhD thesis, A. Saxena and Diploma thesis, M. Radenz).
Figure 9 shows fibronectin-mediated cell adhesion of control shRNA or PGP shRNA expressing GC1 cells.
Fibronectin is a high molecular weight glycoprotein and one of the main components of the extracellular matrix (Halper and Kjaer, 2014, Wierzbicka-Patynowski and Schwarzbauer, 2003). It contains an Arg-Gly-Asp (RGD) motif, which is recognized by integrins and results in ligand binding (D'Souza et al., 1991). Peptides containing a RGD motif and thereby inhibiting integrin-ligand interaction normalized PGP-dependent cell adhesion on fibronectin,

demonstrating that integrin engagement is critical for PGP-dependent effects on cell adhesion (PhD thesis, A. Saxena).

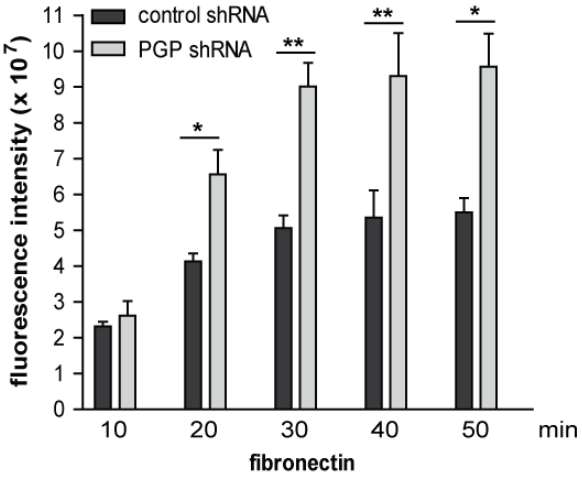

Figure 9: Role of PGP for cell adhesion.
Control shRNA and PGP shRNA expressing cells were labeled with calcein, seeded on fibronectin (15 µg/mL) pre-coated surface and allowed to attach for the indicated time points. Unbound cells were washed away and the fluorescence was measured. Calcein was excited at 485 nm and the light emitted at 520 nm was recorded. The resulting fluorescence intensity was plotted and is proportional to the number of cells that adhered to the surface.

Based on the biochemical and cellular characteristics of PGP discussed so far, an emphasis of this thesis was to study the role of PGP for cell adhesion and migration downstream of integrin- and RTK-signaling and to elucidate PGP-dependent signaling. Therefore, integrin-signaling leading to cell adhesion and migration will be explained in more detail in the following sections.

1.5 Integrins

Integrins are heterodimeric transmembrane receptors consisting of an α- and β-subunit. They are required for cell-extracellular matrix (ECM) adhesion by mediating interactions between the actin cytoskeleton of the cell and ECM, and are needed for cell-cell adhesion by binding to adhesion proteins such as intercellular adhesion molecule-1 (ICAM-1) (Diamond et al., 1991) or vascular cell adhesion protein-1 (VCAM-1) (Klemke et al., 2007), expressed on the plasma membrane of neighboring cells.

Integrins have a large *N*-terminal extracellular part (~800 amino acids), which binds to the ECM, a transmembrane helix (~20 amino acids) and a shorter intracellular *C*-terminal domain (~13-70 amino acids) lacking enzymatic activity (Hynes, 1992). Integrins are ubiquitously expressed and show a great diversity in higher organisms. The non-covalent hetero-dimerization of 19 α and 8 β subunits is thought to yield 25 integrins. Additionally, splice variants increase the diversity. Each integrin heterodimer has a preferred ECM molecule that

it can bind to. RGD containing proteins such as fibronectin are the main ligands of α5β1 integrins. Vitronectin is a ligand of αVβ3 integrins, and α1β1 and α2β1 are the major collagen-binding integrins (Campbell and Humphries, 2011, Plow et al., 2000).

1.5.1 Integrin signaling

Structural studies showed that integrins exist in an inactive (low affinity) and an active (high affinity) conformation (Campbell and Humphries, 2011). Integrins exclusively bind to the ECM in their active extended conformation and are capable for signaling (Zhu et al., 2008, Arnaout et al., 2002). Different signaling pathways lead to integrin activation. Integrin activators such as kindlin and talin are FERM domain containing proteins. FERM (four-point-one, ezrin, radixin, moesin) is a widespread domain, which localizes and links cytosolic proteins to the plasma membrane (Chishti et al., 1998). After translocation to the membrane, talin and kindlin can bind to the β-subunit of integrins (Tadokoro et al., 2003a, Moser et al., 2008, Harburger et al., 2009). The interaction between talin and kindlin and their binding to the β-subunit lead to a conformational change of the integrin. The extracellular domain is extended resulting in the transition to a high affinity state. (Tadokoro et al., 2003b, Ye and Petrich, 2011). Concomitantly, talin can bind directly to actin, whereas kindlin bind actin through adaptor proteins such as α-actinin, thereby providing a link between the receptor and the cytoskeleton (Moser et al., 2009). This signaling pathway leading to integrin activation is termed inside out signaling and allows the cell to react for example to adhesion- or migration stimuli (Ginsberg et al., 1992).

As signaling receptors located at the plasma membrane, integrins are also able to transduce external signals inside cells. Integrins are converted to their active conformation by binding to their ligands. After ECM binding, integrins start to cluster at the plasma membrane and protein-interaction sites of the cytoplasmic domain get modified for the recruitment and binding of signaling- and adaptor proteins. The so-called outside-in signaling mediates processes such as cell polarity, cell adhesion and cell migration (Legate et al., 2009).

Thus, signal transduction of integrins occurs bi-directionally across the plasma membrane (**Figure 10**).

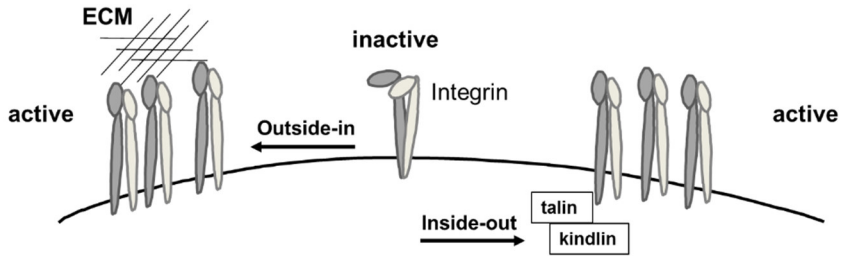

Figure 10: Integrin activation signaling.
Integrin activation upon talin- and kindlin binding is termed inside-out signaling. Integrin ligand binding to external domains leads to a conformational change into the high affinity state and to integrin activation via outside in signaling.

Upon integrin clustering, adhesive structures, the so-called focal adhesions are formed (Zaidel-Bar, 2009). Concomitantly, cytoplasmic α- and β- tails of integrins are more separated from each other in their active, extended conformation and allow the recruitment of integrin signaling proteins. The interaction of the cytoplasmic domain with downstream signaling molecules leads to the formation of a large multi-protein complex, the so-called adhesion complex or adhesome (Wozniak et al., 2004, Zaidel-Bar and Geiger, 2010) and to the activation of a number of signal transduction cascades (Winograd-Katz et al., 2014).

Integrins do not have any enzymatic activity. Thus, the formation of the adhesome is critical for integrin signal transduction. Many enzymes of this complex are actin-binding proteins such as vinculin and talin. They link integrins to the actin cytoskeleton to provide mechanical stability to the cell (Mitra et al., 2005). Additionally, adaptor proteins such as p130cas, kindlin and paxillin, transmembrane proteins and effector proteins such as kinases and phosphatases are involved. The interplay between kinases and phosphatases has to be a well-orchestrated to ensure proper signal transduction.

Especially tyrosine phosphorylation of signaling- and cytoskeletal proteins is critical for integrin signaling (Bass et al., 2008, Maher et al., 1985). The tyrosine kinases focal adhesion kinase (FAK) and Src kinase are key players in integrin signaling leading to cell adhesion and migration (Sieg et al., 1999, Cary et al., 2002). Upon integrin activation, FAK initially gets auto-phosphorylated on tyrosine residue 397, which leads to an activation of FAK. After FAK binding, Src is also activated and carries out subsequent phosphorylation events, such as phosphorylation of the adaptor proteins p130cas or paxillin (Mitra and Schlaepfer, 2006, Webb et al., 2004, Pellicena and Miller, 2001).

The protein tyrosine phosphatases PTP-PEST, PTP1B and PTPα are key phosphatases in integrin signal transduction. They regulate integrin-mediated cell adhesion and migration for example by regulation of p130cas phosphorylation (Liang et al., 2005, Angers-Loustau et al., 1999, Garton et al., 1996) or by dephosphorylation and thereby activation of Src (Pallen, 2003).

Besides tyrosine kinases, serine/threonine kinases such as members of protein kinase C family and lipid kinases such as PI3 kinase are also involved in integrin signaling (Miranti et al., 1999, Guidetti et al., 2015)

1.5.2 Integrin-dependent cell adhesion, spreading and migration

A balance between cell adhesion and migration is essential for many physiological processes including tissue homeostasis, wound healing and immune responses. A mismatch in the balance often results in pathophysiological processes such as metastasis and inflammation.

Cell-cell adhesion as well as cell-matrix adhesion enable cells to communicate with their environment, and both processes are essential for maintaining multicellular structures. Adhesive interactions are also critical for cell migration. Movement of a cell starts by building membrane protrusions and the formation of adhesion sites at the cell front, the so-called leading edge. After ECM binding of integrins at the leading edge, initially dot-shaped and short-lived nascent adhesion are formed (Webb et al., 2002). After integrin clustering, they start to grow to focal complexes and afterwards to even more organized focal adhesions (Kanchanawong et al., 2010). Through the formation of the adhesion complex, the actin cytoskeleton is linked via adaptor proteins such as talin to the ECM, and traction force can be generated. In parallel, old adhesion sites at the rear end have to be removed by dispersal of adhesion components to enable movement of the cells (Huttenlocher and Horwitz, 2011). The dynamic process of assembly and disassembly of focal adhesion structures is termed focal adhesion turnover and is controlled by a complex interplay of kinases and phosphatases. Prominent examples in the regulation of this process are FAK, Src or PTP1B (Westhoff et al., 2004, Burdisso et al., 2013)

1.6 Cytoskeletal rearrangements during cell adhesion and migration

Next to FA turnover, a highly dynamic and well-orchestrated cytoskeleton remodeling enables cells to carry out cellular processes such as cell adhesion, spreading and migration.

The cytoskeleton of eukaryotic cells consists of three main components (Alberts B, Johnson A, Lewis J, et al. Molecular Biology of the Cell. 4th edition; 2002).

Microfilaments are composed of polymerized actin monomers and provide protrusive and contractile forces for cell movement. They undergo rapid cycles of polymerization and depolymerization to allow the cell to react properly to internal and external cues.

The second component consists of microtubules. The diameters of microtubules are larger than actin filaments, consist of tubulin and play a role in cell communication, directed cell migration and cell division.

The third type of cytoskeleton filaments are flexible intermediate filaments. They are composed of different monomer proteins and provide mechanical stability to the cell.

The cytoskeleton needs to be highly dynamic to react to requirements of the cell. For cell events such as cell adhesion, spreading and migration actin microfilaments play a critical role because of their contractile capacity (Fletcher and Mullins, 2010, Wehrle-Haller and Imhof, 2003).

Therefore, actin remodeling and its regulation will be described in greater detail. **Figure 11** shows actin reorganization, which accompanies and enables cell adhesion, cell spreading and cell migration.

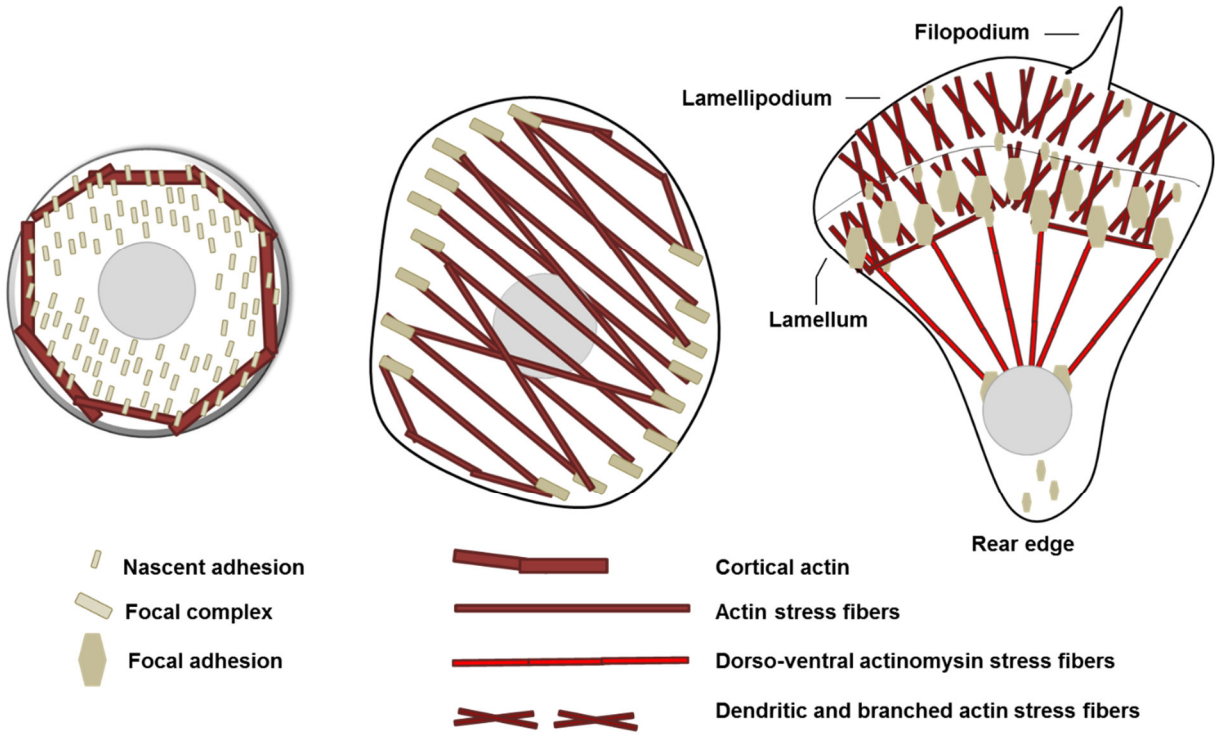

Figure 11: Actin dynamics and focal adhesion turnover during cell spreading and migration.
After attachment to the substratum, nascent adhesion are formed and actin is assembled as cortical actin bundles near the plasma membrane. During cell spreading, stress fibers are formed concomitantly with adhesion maturation. After receiving migratory stimuli, the cell forms protrusions (lamellipodia and filopodia) at the leading edge and the more adhesive lamellum. The lamellipodium as well as the lamellum consist of a dendritic, branched actin network. After integrin clustering and the formation of focal adhesion complexes, the actin cytoskeleton is linked to the substratum and traction force can be generated. In parallel, old adhesion sites at the rear end have to be disassembled by dispersal of adhesion components to enable movement of the cell. (Huttenlocher and Horwitz, 2011, Chhabra and Higgs, 2007)

Upon cell attachment to the ECM, actin cytoskeleton is extended and linked via integrins to the extracellular, ventral cell surface. During cell spreading, actin is reorganized near the plasma membrane and initially builds cortical actin fibers. At later time points, thin stress fibers are formed, which are anchored to the plasma membrane at focal complexes and focal adhesions. Stress fibers are composed of cross-linked actin filaments and myosin, together forming contractile actomyosin bundles. Anchoring of these fibers to focal adhesions results in mechano-transduction. Concomitantly, traction force exerted by actomyosin contractions promote adhesion maturation.

After receiving migratory stimuli, adhering cells form protrusions, the so-called lamellipodia and filopodia at the leading edge of the cells. These structures consist of a branched network of actin filaments and are driven by the polymerization of actin. Small GTPases such as Rho and Rac mediate stress fiber assembly (Arthur and Burridge, 2001, Fukata et al., 2003, Guillou et al., 2008).

1.6.1 Regulation of actin remodeling

Actin binding proteins are important modulators of actin reorganization by promoting assembly and disassembly of actin filaments. Profilin elongates and actin-depolymerizing factor (ADF, also known as cofilin) shortens the size of actin filaments. The ARP2/3 complex nucleates and branches new filaments by binding actin monomers and the side of pre-existing actin filaments. Repetition of actin branching results in a dendritic actin meshwork (Chhabra and Higgs, 2007).

Mature actin filaments are often crosslinked. Actin cross-linking proteins such as α-actinin and fascin regulate actin filaments organization into secondary structures. Disassembly of actin filaments is coordinated by capping and severing proteins such as cofilin (Dos Remedios et al., 2003, Bamburg and Bernstein, 2010).

Kinases as well phosphatases contribute to the upstream regulation of actin cytoskeleton reorganization by phosphorylation and dephosphorylation of actin binding proteins. LIM-kinases, which phosphorylate and inactivate the actin severing protein cofilin, and chronophin, which dephosphorylates and reactivates cofilin (Arber et al., 1998, Gohla et al., 2005) are only two examples for kinases and phosphatases involved in actin turnover.

The serine-threonine kinase PKC is another important regulator of actin reorganization. It was demonstrated that PKC isoforms influence actin dynamics and thereby regulate cellular processes that are affected by remodeling of actin microfilaments, such as cell adhesion and migration (Harrington et al., 1997, Iwabu et al., 2004, Volkov et al., 2001). PKCs control these processes either by modulating integrin localization and their signal transduction or by direct phosphorylation of cytoskeletal regulators (Larsson, 2006). Several PKC substrates are involved in cytoskeleton reorganization. The myristoylated alanine-rich C kinase substrate (MARCKS) is one of the first characterized PKC substrates and identified as an actin cross-linking protein, involved in the regulation of anchoring actin cytoskeleton to the plasma membrane (Hartwig et al., 1992).

Activation of PKC isoforms leads on the one hand to the suppression of stress fibers and the formation of pro-migratory ruffles, but on the other hand also induces stress fiber formation (Larsson, 2006). For example, it was demonstrated that PKC induces the formation of focal adhesions and stress fibers in fibroblasts after spreading on fibronectin (Woods and Couchman, 1992).

1.6.2 Actin-based membrane structures

To regulate cellular processes such as cell adhesion and migration actin filaments can be assembled into various cellular structures at the plasma membrane including lamellipodia, filopodia and membrane ruffles (**Figure 12**).

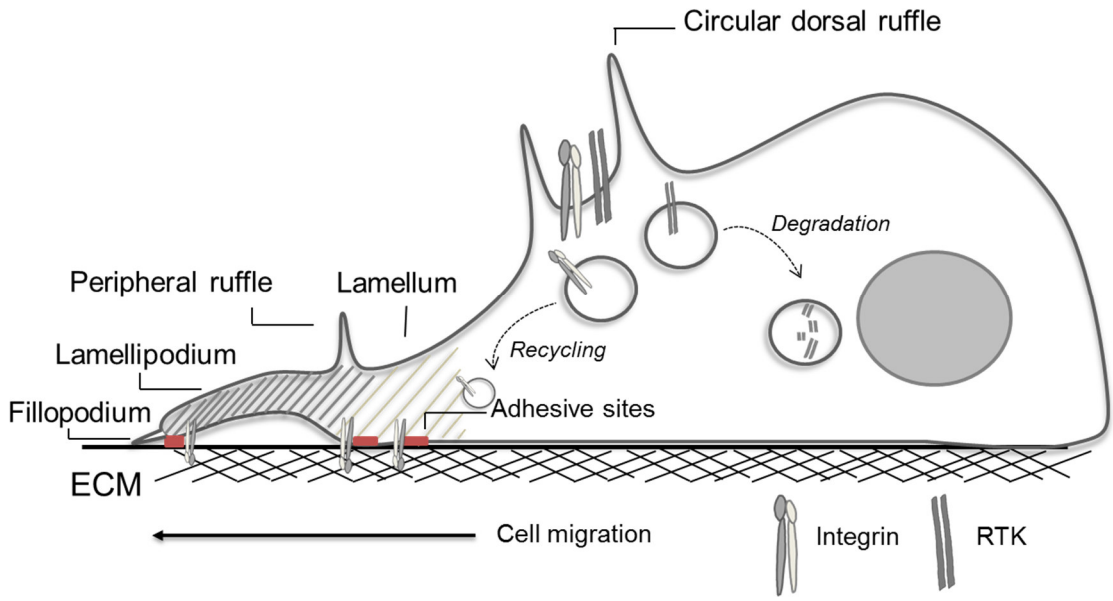

Figure 12: Protrusive actin structures.
For details, see text below. The figure is adapted from (Chhabra and Higgs, 2007).

Lamellipodia are sheet-like protrusive structures. Together with the lamellum, they build the protrusive edge of the cell as a thin sheet of membrane-enclosed cytoplasm (Pollard et al., 2000). The lamellum is thicker, more adhesive and closer to the cell body than the lamellipodium (Abercrombie et al., 1971). Actin filaments are dendritically branched at the protrusive edge (Svitkina and Borisy, 1999) and it was shown that two filament populations, which are independently nucleated, exist in in the lamellipodium and the lamellum (Ponti et al., 2004).

Filopodia are finger-like actin structures protruding from the leading edge of motile cells. They contain long parallel actin filament bundles, which are anchored deep into to the lamellipodium and the lamellum (Svitkina et al., 2003).

Ruffles are transient, sheet-like actin structures and can be classified into peripheral ruffles, occurring at the leading edge of motile cells, and circular dorsal ruffles (also known as dorsal ruffles or actin waves), assembling on the apical cell surface. When the attachment between the leading edge and the substratum is lost, actin filaments and plasma membrane move rearward leading to the formation of peripheral ruffles. There is evidence that lamellipodia and peripheral ruffles are generated by the same actin filament assembly mechanisms (Abercrombie et al., 1970). Dorsal ruffles are assembled at the apical surface and form ring-like structure before they disappear. The function of this membrane structure as well as the signaling leading to circular dorsal ruffle formation are just poorly understood.

1.6.3 Circular dorsal ruffles (CDRs)

CDRs were first observed in migrating fibroblasts (Abercrombie et al., 1970). In contrast to peripheral ruffles which are formed upon stimulation and persisitently cycle between assembly and disassembly, CDRs are transient and assemble only once upon cell stimulation (Hoon et al., 2012).

CDRs appear after 3 to 5 minutes of growth factor stimulation and disappear within 10 to 20 minutes. It is assumed, that they are formed by the generated force of newly polymerized F-actin against the dorsal plasma membrane (Orth et al., 2006). Some proteins, which are involved in actin remodeling and are associated with the actin cytoskeleton, such as cortactin, dynamin 2 and actin-related protein 2/3 (Arp 2/3), localize to CDRs (Krueger et al., 2003).

CDR formation has also been observed in primary cells. Mouse embryonic fibroblast display CDRs upon platelet-derived growth factor (PDGF) stimulation (Mellström et al., 1988), and endothelial cells upon vascular endothelial growth factor (VEGF) stimulation (Wu et al., 2003). Though CDRs were mentioned in the literature almost five decades ago (Abercrombie et al., 1970), the function of circular dorsal ruffles still remains unclear.

1.6.3.1 Functions of CDRs

CDRs are implicated in macropinocytosis. It has been demonstrated that macropinosomes are generated concomitantly with the closure of CDRs (Dowrick et al., 1993). Cells use macropinocytosis for example for nutrient uptake or membrane transfer (Commisso et al., 2013, Dharmawardhane et al., 2000).

CDR are mostly linked to receptor internalization. Receptor tyrosine kinases (RTK), in particular the EGF receptor is sequestered and internalized via CDRs (Orth et al., 2006). Upon internalization, RTKs can be either recycled or degraded (Sigismund et al., 2008). It was also reported that several other RTKs such as PDGF receptor (Huang et al., 2011a) and the hepatocyte growth factor receptor (HGFR) (Abella et al., 2010) are internalized by CDR formation.

In the last few years, it has become clear that integrins can be endocytosed via CDRs. After internalization, integrins are then delivered to endosomes and are recycled back on the ventral surface to create new adhesive sites (Gu et al., 2011, Margadant et al., 2011).

It is also assumed that CDRs are involved in the transition of a cell from a static to a motile state. As mentioned in **1.6**, upon a migratory stimulus, cells have to rearrange their actin cytoskeleton. Lamellipodia are formed at the leading edge and the rear edge has to retract to promote cell motility. During this process, actin has to re-localize to the leading edge and has to be reorganized there. In parallel, plasma membrane and potentially also integrins are

internalized by macropinocytosis via CDRs and translocate to the leading edge to form lamellipodia and to mediate cell-substrate adhesion (Hoon et al., 2012). CDRs contain a dendritically branched meshwork of actin, which is potentially derived from the disassembly of stress fibers close to CDRs. Consistently, proteins that are involved in actin branching such as cortactin and the Arp 2/3 complex localize to CDRs (Krueger et al., 2003). When CDRs are disassembled, actin might be recycled for lamellipodia formation to promote cell migration (Hoon et al., 2012).

1.6.3.2 CDR formation signaling

Next to actin bundling and branching proteins, more than 20 proteins are already identified which localize to CDRs and regulate their formation (Hoon et al., 2012). Many of these proteins regulate CDR formation at multiple stages in the same pathway. Because of the complexity and the still existing open questions, signaling pathways leading to CDR formation will be discussed only briefly below.

As already mentioned, CDRs are induced by RTK signaling. However, previously it was demonstrated that β1 integrin crosstalk with RTKs is also critical for CDR formation (Azimifar et al., 2012). Cells lacking β1 integrin are not able to form CDRs (King et al., 2011). Integrin activation triggers FAK- and Src-mediated activation of p130CAS, resulting in CDR formation (Rivera et al., 2006).

In addition, Src activation by RTK- or integrin signaling leads to the activation of PI3 kinase (PI3K). PI3K phosphorylates phosphatidylinositol (4,5)-bisphosphate (PIP_2) to phosphatidylinositol (3,4,5)-trisphosphate (PIP_3). Upon PIP_3 accumulation, the large GTPase dynamin and other actin remodeling proteins such as WASP/WAVE family proteins, Arp 2/3 complex and cortactin are recruited to the plasma membrane (Krueger et al., 2003, Legg et al., 2007). Furthermore, increased PI3K activity also activates the small GTPase Rac1. Rac1 activation and the recruitment of actin remodeling proteins to the plasma membrane results in CDR formation (Welch et al., 2003, Dharmawardhane et al., 2000) (**Figure 13**).

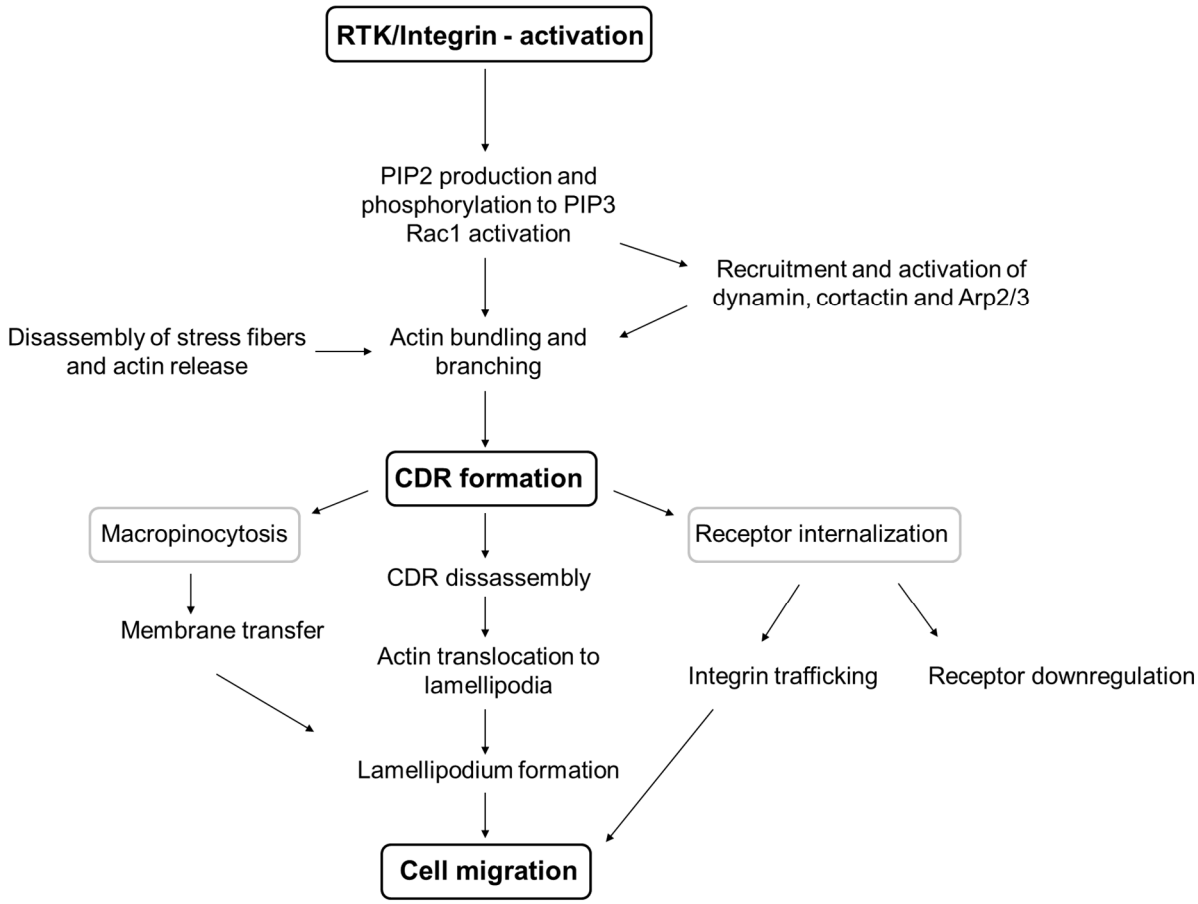

Figure 13: CDR formation signaling.
Stimulation of RTKs and or integrins leads to activation of Src and PI3K, resulting in the activation of the small GTPases Rac1 and the accumulation of PIP3 at the cell membrane. Dynamin, Arp 2/3 complex and cortactin are recruited to the membrane leading to actin remodeling at the plasma membrane and subsequently to CDR formation. The actin, which is required for CDR formation is likely derived from disassembly of stress fibers. CDRs are implicated in macropinocytosis and receptor internalization, for example of integrins. Integrin trafficking results in the formation of new adhesive sites, required for cell migration. After CDR disassembly, actin is recycled to form lamellipodia, promoting cell migration. The figure is adapted from (Hoon et al., 2012).

1.7 Role of PGP *in vivo*

The second main emphasis of the thesis was to investigate the physiological role of PGP. For this purpose, *Pgp*-deficient mice were characterized.

Conditionally PGP-inactivated mice were generated by using a Cre/*loxP*-based conditional *Pgp*-knockout approach linked to the simultaneous knockin of a minigene encoding for the phosphatase-inactive *Pgp* point mutant Pgp^{D34N} (Pgp^{DN}) (Seifried et al., 2014) into the endogenous Pgp locus of C57BL/6J mice (**Figure 14**).

Upon FLPe-mediated removal of the neomycin resistance cassette and Cre-mediated excision of the floxed *Pgp, Pgp*^{DN} is expressed under the control of the endogenous *Pgp* promoter. By using different tissue specific Cre-lines, various conditional phosphatase inactive mouse models can be generated.

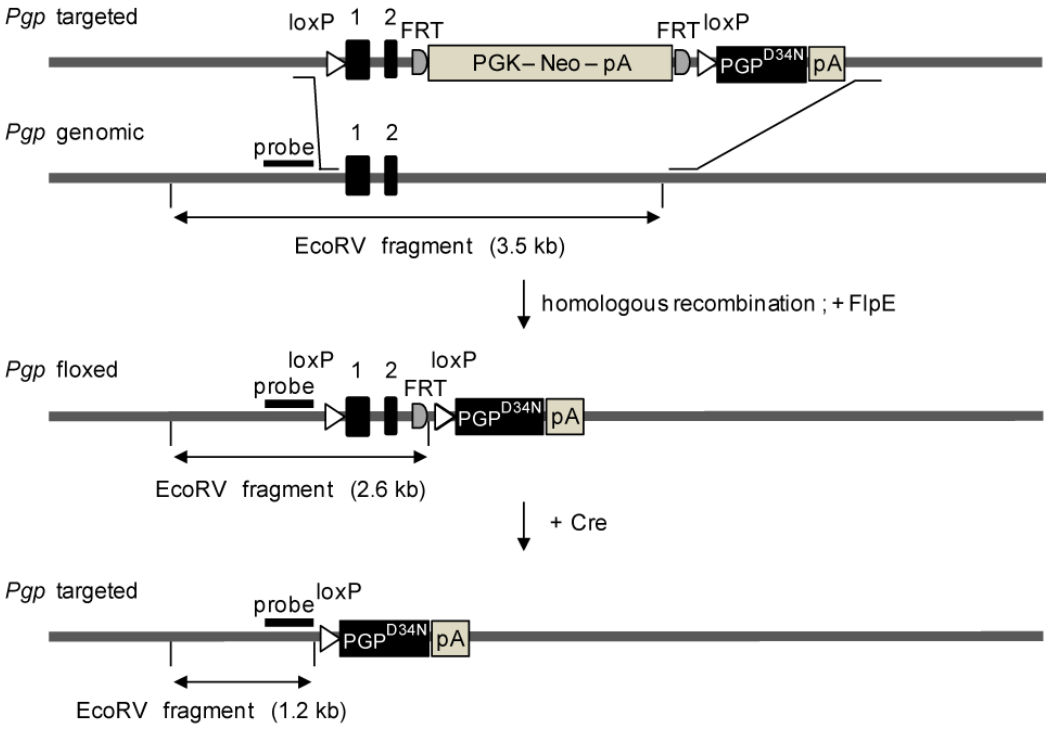

Figure 14: Pgp targeting strategy.
For details, see text above.

Two Cre-lines were used. Breeding *Pgp*$^{flx/flx}$ mice with the whole-body Cre deleter strain EIIa-Cre led to a global *PGP* inactivation in every mouse tissue (*Pgp*$^{flx/flx}$*; EIIa-Cre)* and breeding with the Tie2-Cre driver line led to a *PGP* inactivation in endothelial cells and in cells of the hematopoietic system such as red blood cells or lymphocytes (*Pgp*$^{flx/flx}$*; Tie2-Cre).*

2 Aim of the study

Mammalian haloacid dehalogenase (HAD)-type phosphatases are a large and ubiquitous, yet poorly understood class of enzymes. Although a growing number of these phosphatases is linked to important diseases such as cardiovascular or metabolic disorders and cancer, the cellular and physiological functions of many HAD phosphatases remain elusive.
Our laboratory has previously identified the mammalian phosphoglycolate phosphatase PGP (also referred to as AUM) as a member of the HAD-type superfamily of hydrolases. *In vitro* experiments had identified PGP as a tyrosine-directed phosphatase, implicated in RTK signaling and initial cellular studies suggested that PGP was involved in cell adhesion downstream of integrin signaling.

The aim of the present study is to provide a mechanistic understanding of the cellular functions of PGP and to gain first insights into *in vivo* roles.

Four main questions were addressed:

(1) What is the physiological substrate of PGP?
(2) Does PGP depletion affect cell migration?
(3) What are the mechanisms underlying the effects of PGP depletion on actin reorganization?
(4) What are the consequences of whole-body ablation of PGP activity in mice?

Answering these questions is expected to provide important insights into the physiological roles of PGP.

3 Materials and Methods

3.1 Materials

3.1.1 Chemicals and reagents

2-Propanol	Carl Roth
3-(N-morpholino)propanesulfonic acid (MOPS)	Sigma Aldrich
12-*O*-tetradecanoylphorbol-13-acetate	Sigma Aldrich
acetic acid (glacial)	Carl Roth
acetone	Carl Roth
acrylamide/bisacrylamide (30% /0.8%)	Carl Roth
adenosine triphosphate (ATP)	Sigma Aldrich
agarose (gene technology quality, GTQ)	Carl Roth
ammonium chloride	Carl Roth
ammonium persulfate (APS)	Sigma Aldrich
amphotericin B	Sigma Aldrich
aprotinin	Sigma Aldrich
ascorbic acid	Lifeline
benzamidine	AppliChem
bis-benzimide trihydrochloride (Hoechst 33342)	Sigma Aldrich
bovine serum albumin, fraction V (BSA)	AppliChem
bromophenol blue	Merck Millipore
calcium chloride ($CaCl_2$)	Merck Millipore
citric acid	Carl Roth
collagenase type II	Worthington
4′,6-diamidino-2-phenylindole (DAPI)	Sigma Aldrich
deoxyribonucleotide triphosphates (dNTPs)	Invitrogen
dextran sulfate (M_r >500,000)	AppliChem
dextrose	Carl Roth
dimethyl sulfoxide (DMSO)	AppliChem
dithiothreitol (DTT)	Sigma Aldrich
di-sodium hydrogen phosphate dehydrate (Na_2HPO_4)	AppliChem
Dulbecco`s phosphate buffered saline [PBS (w/o $MgCl_2$/$CaCl_2$)]	PAN Biotech
Dulbecco's modified Eagle's medium (DMEM)	PAN Biotech

Dulbecco's modified Eagle's medium [DMEM (w/o phenolred)]	PAN Biotech
Dynabeads	Invitrogen
endothelial cell growth supplement (EnGS)	Lifeline
epidermal growth factor (EGF, human)	Sigma Aldrich
ethanol	Carl Roth
ethidium bromide solution (1%)	Carl Roth
ethylene-glycol tetraacetic acid (EGTA)	AppliChem
ethylenediamine tetraacetic acid (EDTA)	Merck
fetal bovine serum (FBS, Lifefactor)	Lifeline
fetal calf serum (FCS)	PAN Biotech GmbH
fibronectin (FN, human)	Calbiochem
Ficoll PM 400	AppliChem
formamide	AppliChem
gelatin from porcine skin	Sigma Aldrich
glacial acetic acid (CH_3CO_2H)	Sigma Aldrich
glucose	Merck Millipore
glycerol	AppliChem
glycine	Carl Roth
goat serum	Sigma Aldrich
heparin sulfate	Lifeline
hydrochloric acid (HCl)	Carl Roth
hydrocortisone hemisuccinate	Lifeline
hydrogen peroxide (30%)	AppliChem
leupeptin	Carl Roth
L-glutamine	PAN Biotech GmbH
L-glutamine (LifeFactor)	Lifeline
Lipofectamine 2000	Invitrogen
malachite green solution	Enzo Life sciences
methanol	Carl Roth
N, N, N', N'-tetramethylethylenediamine (TEMED)	Carl Roth
nonfat dry milk powder	AppliChem
nonyl phenoxypolyethoxylethanol (NP-40)	Fluka
Opti-MEM	Invitrogen
para-formaldehyde (PFA)	Carl Roth
Pefabloc SC	Roche
penicillin G sodium salt	PAN Biotech GmbH

pepstatin A	Sigma Aldrich
phosphatase inhibitor cocktail I and II	Sigma Aldrich
poly-L-lysine (PLL)	Sigma Aldrich
polyvinylpyrrolidone (M_r ~360,000)	AppliChem
Ponceau S	Invitrogen
potassium hydrogen carbonate ($KHCO_3$)	AppliChem
Protein G sepharose	GE Healthcare
Precision Plus Protein Standard Dual Color	Bio-Rad
ProLong mounting medium	Invitrogen
puromycin	Calbiochem
recombinant human epidermal growth factor (rh EGF)	Lifeline
RPMI 1640	PAN Biotech GmbH
salmon sperm DNA (sheared)	Ambion
sodium azide (NaN_3)	Merck
sodium chloride (NaCl)	Carl Roth
sodium citrate ($Na_3C_6H_5O_7$)	Carl Roth
sodium dihydrogen phosphate (NaH_2PO_4)	Merck
sodium dodecyl sulfate (SDS), ultra pure	Carl Roth
sodium fluoride (NaF)	Sigma Aldrich
sodium hydroxide (NaOH)	Carl Roth
sodium orthovanadate (Na_3VO_4)	Sigma Aldrich
sodium pyrophosphate ($Na_4P_2O_7$)	Sigma Aldrich
sodium sulfite (Na_2SO_3)	Carl Roth
soybean trypsin inhibitor (STI)	Sigma Aldrich
streptomycin sulfate	PAN Biotech GmbH
stromal derived factor-1 (SDF-1)	Immunotools
triethanolamine (TEA)	AppliChem
tris(hydroxymethyl)aminomethan (Tris) base/Tris-HCl	Carl Roth
trisodium 2-hydroxypropane-1,2,3-tricarboxylate	Sigma Aldrich
trisodium citrate	Sigma Aldrich
Triton X-100	Sigma Aldrich
Trypan Blue	Sigma Aldrich
Tween-20	AppliChem
VascuLife Basal medium	Lifeline
β-glycerophosphate	Sigma Aldrich
β-mercaptoethanol	Sigma Aldrich
XF Calibrant	Seahorse Bioscience

3.1.2 Technical equipment

5424 R centrifuge	Eppendorf
5804 centrifuge	Eppendorf
BBD 6229 incubator	Heraeus
BDK laminarflow	Thermo Scientific
C1000TM thermal cycler	Bio-Rad
DMI6000 Total internal reflection (TIRF) microscope	Leica
DMIL LED fluorescence microscope	Leica
E.A.S.Y Win32 gel documentation system	Herolab
Eclipse TE 2000 epifluorescence microscope	Nikon
EnVision 2104 multilabel reader	Perkin Elmer
FACS Calibur flow cytometer	BD Biosciences
H35 hypoxystation	Don Whitley Scientific
hypoxia incubator chamber	Stemcell-Technologies
ImageQuant LAS 4010 Digital Imaging System	GE Healthcare
Lab 850 pH meter	Schott Instruments
Laborvert FS microscope	Leitz
Mini-PROTEAN Tetra cell polyacrylamide gel system	Bio-Rad
Mini-Sub Cell GT agarose gel system	Bio-Rad
MM 301 Mixer Mill;	Retsch GmbH
MR Hei-MixL magnetic stirrer	Heidolph
Neubauer counting chamber	Marienfeld
Seahorse XF96e extracellular flux analyzer	Seahorse Bioscience
Systec V-150 autoclave	Systec
TCS SP5 confocal microscope	Leica
Thermomixer comfort 1.5 mL	Eppendorf
Trans-Blot SD semi-dry transfer cell	Bio-Rad
Unimax 1010 plate mixer	Heidolph
Universal 16R centrifuge	Hettich
VORTEX-GENIE 2 mixer	Scientific Industries

3.1.3 Consumable supplies

8-well chamber (uncoated, ibidi treated)	Ibidi
12-well chamber (removable: microscopy glass slide)	Ibidi
96-well plate Nunclon Delta Surface	Thermo Scientific
96-well plate, white	Thermo Scientific
Amicon Ultra-0.5 mL centrifugal filters	Merck Millipore

culture dishes Nunclon Delta Surface	Nunc
culture multi-well dishes Nunclon Delta Surface (6-,12-, 48 well)	Nunc
cell scraper	Biologix
cell strainer (70 µM)	Corning
cryo vials	Nalgene
Falcon tubes (15 and 50 ml)	BD Biosciences
Hybond C nitrocellulose membrane	Amersham
Omnifix - F syringe and needles	B. Braun
PCR tubes	Hartenstein
polystyrene tubes	BD Biosciences
ProbeQuant G-50 micro columns	GE Healthcare
reaction tubes (1.5 and 2 mL)	Eppendorf
Sartolon polyamide 0.2 µm filter	Sartorius Biotech
SuperFrost Plus cover slips	Thermo Scientific
surgical disposable scalpel	B. Braun
Transwell inserts 6.5 mm, 3.0 µm	Costar
Whatman paper	Ahlstrohm

3.1.4 DNA- and protein ladders

100 bp DNA ladder	NEB
1 kb DNA ladder	NEB
GeneRuler 100bp DNA ladder	Fermentas
Precision Plus Protein Standards Dual color	Bio-Rad

3.1.5 Commercial kits

ATP determination kit (A22066)	Molecular Probes
Click-iT EdU Alexa Fluor 488 imaging kit	Invitrogen
Deca Prime II DNA labeling kit	Invitrogen
DNeasy kit	Qiagen
Glycerol-3-phosphat (G3P) colorimetric assay kit	Biovision
Micro BCA kit	Thermo Scientific
PKC activity assay	Enzo Life sciences
Super Signal West Pico chemiluminescent substrate	Thermo Scientific
Triose Phosphate Isomerase (TPI) activity assay kit	Biovision
XF Cell Mito stress kit	Seahorse Bioscience

3.1.6 Commercial buffers

10x Dream tag buffer	Invitrogen
10x Pfx buffer	Invitrogen

3.1.7 Cell lines and mouse models

GC1 spg	ATCC
B6.Cg-Tg(Tek-cre)1Ywa/J (Tie2-Cre)	The Jackson Laboratory
B6.FVB-Tg(EIIa-cre)C5379Lmgd/J	The Jackson Laboratory
C57Bl/6J mice	Charles River Laboratories
C57Bl/6 *Pgp*^{tm1Goh} mice	Ozgene Ltd.

3.1.8 Cell culture medium

Complete DMEM:

DMEM supplemented with:	4.5 g/L glucose
	10% FCS
	2 mM L-glutamine
	100 U/mL penicillin
	100 µg/mL streptomycin

DMEM starving medium:

DMEM supplemented with:	4.5 g/L glucose
	2 mM L-glutamine
	100 U/mL penicillin
	100 µg/mL streptomycin

Phenol red-free DMEM:

DMEM w/o phenol red supplemented with:	4.5 g/L glucose
	10% FCS
	2 mM L-glutamine
	100 U/mL penicillin
	100 µg/mL streptomycin

RPMI:

RPMI supplemented with:	2.0 g/L glucose
	2 mM L-glutamine
	100 U/mL penicillin
	100 µg/mL streptomycin

Complete VascuLife:

VascuLife Basal Medium supplemented with:	5% FBS
	0.2% EnGS
	5ng/mL rh EGF
	50 µg/mL ascorbic acid
	10 mM L-glutamine
	1.0 µg/mL hydrocortisone hemisuccinate
	0.75U/ml heparine sulfate
	100 U/mL penicillin
	100 µg/mL streptomycin
	25 µg/mL amphotericin B

VascuLife starving medium:

VascuLife Basal medium supplemented with:	10 mM L-glutamine
	100 U/mL penicillin
	100 µg/mL streptomycin.
	25 µg/mL amphotericin B

3.1.9 Antibodies

α-Actin mouse monoclonal (clone C4)	Merck Millipore
α-AUM rabbit polyclonal, anti-full-length protein antibodies glycine /magnesium eluate	Charles River, A. Seifried, PhD thesis
α-AUM rabbit polyclonal anti-peptide antibodies	Charles River, P. Duraphe, PhD thesis
α-alpha-tubulin mouse monoclonal (DM1A)	Sigma Aldrich

α-CD 3 anti-mouse monoclonal (DaA3)	Immunotools
α-CD 28 anti-mouse monoclonal (37.51)	Immunotools
α-CD 31/ Pecam rat anti-mouse monoclonal (MEC 13.3)	BD Biosciences
α-CD 102/ ICAM-2 rat anti-mouse monoclonal [3C4(mIC2/4)]	BD Biosciences
α-rat/ α-rabbit biotinylated goat antibodies	BD Biosciences
α- EGF receptor rabbit polyclonal	Cell Signaling technologies
α-rabbit and α-mouse secondary antibodies, HRP-conjugated	Thermo Scientific
α- PLCγ1 total rabbit monoclonal (D9H10)	Cell Signaling technologies
α-pY416 Src family rabbit polyclonal	Cell Signaling technologies
α-pY527 Src family rabbit polyclonal	Cell Signaling technologies
α-pY783 PLCγ1 rabbit monoclonal (D6M9S)	Cell Signaling technologies
α-pY1068 EGF receptor mouse polyclonal	Cell Signaling technologies
α-pY1173 EGF receptor rabbit monoclonal (53A5)	Cell Signaling technologies

3.1.10 Immunocytochemistry reagents

Alexa Fluor 488 phalloidin	Invitrogen
Alexa Fluor 546 phalloidin	Invitrogen
Alexa Fluor 488 conjugated goat anti-rabbit	Invitrogen
Alexa Fluor 488 conjugated goat anti-rat	Invitrogen
Alexa Fluor 546 conjugated goat anti-rabbit	Invitrogen
Alexa Fluor 633 conjugated goat anti-rabbit	Invitrogen

3.1.11 Pharmacological inhibitors and negative controls

Dynasore	Sigma Aldrich
GÖ6983	Sigma Aldrich
PP2	Merck Millipore
PP3	Merck Millipore
sotrastaurin	Selleckchem
U73122	Tocris
U73334	Tocris
wortmannin	Sigma Aldrich

3.1.12 Inhibitors for metabolic studies

2-Deoxyglucose	Sigma Aldrich
antimycin A	Seahorse Bioscience
atglistatin	Sigma Aldrich
etomoxir	Sigma Aldrich
oligomycin A	Seahorse Bioscience
rotenone	Seahorse Bioscience

3.1.13 Enzymes and purified proteins

Catalase (#219261)	Calbiochem
Dreamtaq polymerase (#EP0701)	Invitrogen
EcoRV (#RO195)	New England Biolabs
ICAM-1, recombinant mouse (#796-IC)	RD systems
Pfx polymerase (#12344-024)	Invitrogen
PGP^{wt}, recombinant, purified	Annegrit Seifried
PGP^{D34N}, recombinant, purified	Annegrit Seifried
PLCγ1 human (#TP316448-OR)	Origene
superoxide dismutase (#574591)	Calbiochem
Syk, active (#14-314)	Merck Millipore
trypsin/EDTA	PAN Biotech GmbH

3.1.14 Radioactive nucleotides

[α-^{32}P] dCTP	Hartmann Analytik

3.1.15 Plasmids

pcDNA3	Invitrogen
pdEYFP	Invitrogen
pdEYFP-C1-hAUM (human)	A. Saxena, PhD thesis
pdEYFP-C1-$hAUM^{D34N}$ (human)	A. Saxena, PhD thesis

3.1.16 Solutions and buffers

Unless otherwise noted, chemicals given in percent (%) designate volume per volume (v/v).

SDS-PAGE

SDS-PAGE sample buffer (Laemmli's buffer, 4 x):	62.5 mM	Tris-HCl
	10%	glycerol
	5%	β-mercaptoethanol
	2% (w/v)	SDS
	0.02% (w/v)	Bromophenol Blue
	pH 6.8	
running buffer (SDS-PAGE):	25 mM	Tris base
	200 mM	glycine
	1% (w/v)	SDS
	pH 8.7	
SDS-PAGE stacking gel:	4% (w/v)	acrylamide
	0.02%	APS
	0.002%	TEMED
	0.1%	SDS
	125 mM	Tris-HCl
	pH 6.8	
SDS-PAGE running gel (8%):	8% (w/v)	acrylamide
	0.05%	APS
	0.003%	TEMED
	0.1%	SDS
	375 mM	Tris-HCl
	pH 8.8	
SDS-PAGE running gel (12%):	12% (w/v)	acrylamide
	0.05%	APS
	0.003%	TEMED
	0.1%	SDS
	375 mM	Tris-HCl
	pH 8.8	

Immunoblotting

anode buffer I:	0.3 M	Tris base
	40%	methanol
anode buffer II:	25 mM	Tris base
	40%	methanol
cathode buffer:	25 mM	Tris base
	40 mM	glycine
	10%	methanol

For the transfer of high molecular weight proteins, 20% methanol was used in anode buffers I and II, and 0.005% SDS was added to the cathode buffer.

blocking buffer:	50 mM	Tris-HCl
	2 mM	$CaCl_2$
	80 mM	NaCl
	5% (w/v)	nonfat dry milk
	0.2%	NP-40
	pH 8.0	
stripping buffer:	62.5 mM	Tris-HCl
	2% (w/v)	SDS
	100 mM	β-mercaptoethanol
	pH 6.7	
TBS (10x):	0.5 M	Tris-HCl
	1.5 M	NaCl
	pH 7.5	
TBS-T:	50 mM	Tris-HCl
	150 mM	NaCl
	0.05 %	Tween-20
	pH 7.5	

antibody diluent:	10 mM	HEPES
	0.5 M	NaCl
	1% (w/v)	BSA
	0.2%	Tween-20
	0.02% (w/v)	NaN_3
	pH 7.4	
Ponceau S solution:	0.1% (w/v)	Ponceau S
	5%	CH_3CO_2H

Tissue and cell lysis buffer

digestion buffer:	25 mM	NaOH
	0.2 mM	EDTA
neutralization buffer:	40 mM	Tris-HCl
	pH 5.5	
lysis buffer (for cell lysates and IPs):	50 mM	Tris-HCl
	150 mM	NaCl
	1%	Triton X-100
	1 mM	EDTA
	1 mM	β-glycerophosphate
	7.5 mM	sodium pyrophosphate
	3 mM	orthovanadate
	10 µg/mL	aprotinin
	10 µg/mL	leupeptin
	1 mM	Pefabloc
	10 µg/mL	pepstatin
	1:300	phosphatase inhibitor cocktail I
	1:300	phosphatase Inhibitor cocktail II
	pH 7.5	
PKC lysis buffer:	20 mM	MOPS
	50 mM	β-glycerophosphate

	50 mm	sodium fluoride
	1 mM	sodium orthovanadate
	5 mM	EGTA
	2 mM	EDTA
	1 mM	benzamidine
	1 mM	Pefabloc
	10 µg/mL	leupeptin
	10 µg/mL	aprotinin
	10 µg/mL	pepstatin
	1%	Triton X-100
red blood cell lysis buffer (RBC):	155 mM	NH_4Cl
	12 mM	$KHCO_3$
	0.1 mM	EDTA
	pH 7.3	

others

ACD (acid-citrate-dextrose) buffer:	39 mM	citric acid
	75 mM	sodium citrate
	135 mM	dextrose
	pH 7.4	
prehybridization solution	50%	formamide
	10%	dextran sulfate
	1 M	NaCl
	1%	SDS
	50 mM	Tris base
	pH 7.4	
	0.2%	BSA
	0.2%	polyvinylpyrrolidone
	0.2%	Ficoll PM 400
	3.76 mM	sodium pyrophosphate
	0.01%	salmon sperm DNA

reaction buffer:	150 mM	NaCl
	25 mM	HEPES
	10%	glycerol
	1%	NP-40
	125 U/mL	superoxide dismutase
	250 U/mL	catalase
	0.5 µg/mL	leupeptin
	0.5 µg/mL	aprotinin
SCC (saline sodium citrate) buffer I:	0.1%	SDS
	15 mM	NaCl
	1.5 mM	$Na_3C_6H_5O_7$
	pH 7.0	
SCC (saline sodium citrate) buffer II:	0.5%	SDS
	15 mM	NaCl
	1.5 mM	$Na_3C_6H_5O_7$
	pH 7.0	
Syk kinase buffer:	40 mM	Tris base
	20 mM	$MgCl_2$
	0.1 mg/mL	BSA
	50 µM	DTT
TAE:	40 mM	Tris base
	20 mM	CH_3CO_2H
	1 mM	EDTA
	pH 8.5	
TMN:	50 mM	TEA
	5 mM	$MgCl_2$
	250 mM	NaCl
	pH 7.5	

Trypan Blue solution:	0.4% (w/v) Trypan blue in PBS

3.1.17 Software

GraphPad Prism version 6.0	GraphPad software
ImageJ version 1.45i	NIH
ImageJ colocalization finder	NIH
ImagePro Software version 7.0	Media Cybernetics
MassLynx software version 4.1	Waters
QuantLynx software	Waters
RLA-Tools	developed by Dr. Agnes Fekete and Prof. Dr. Martin J. Müller, Julius von Sachs Institute, Pharmaceutical Biology, University of Würzburg
TransOmics software	Waters
Wave software version 2.2.0	Seahorse Bioscience

3.2 Methods

3.2.1 Generation and breeding of Pgp knockout PGP^{D34N} knockin mice

Floxed *Pgp* mice (*Pgp*^{tm1Goh}*; Pgp*$^{flx/flx}$) were generated on a C57Bl/6J background by Ozgene Pty Ltd. Australia. The neomycin resistance cassette was removed by breeding with the global FLPe deleter strain B6.129S4-Gt(ROSA)26Sor<tm1(FLP1)Dym>/RainJ. Whole-body or hematopoietic/endothelial cell-specific PGP inactivation was achieved by breeding with B6.FVB-Tg(EIIa-cre)C5379Lmgd/J (EIIa-Cre) or B6.Cg-Tg(Tek-cre)1Ywa/J (Tie2-Cre) transgenic mice. Transgenic mice were obtained from The Jackson Laboratory. Timed matings were determined by vaginal plugs. Mouse experiments were approved by the Regierung von Unterfranken, and all analyses were carried out in strict accordance with all German and European Union applicable laws and regulations concerning care and use of laboratory animals.

3.2.2 Genotyping of mice

For **Southern blotting**, genomic DNA was isolated from mouse tail tips with DNeasy and digested with EcoRV. DNA was subjected to agarose gel electrophoresis, denatured, blotted onto nitrocellulose and crosslinked with UV light. The probe was generated by PCR using Pfx polymerase and labeled with [α-^{32}P] dCTP employing the DecaPrime II DNA labeling kit. Unincorporated labeled nucleotides were removed with illustra ProbeQuant G-50 micro columns. The labeled probe was added to the prehybridization solution, incubated overnight at 42°C, and washed extensively in SCC buffer I at 42°C and in SCC buffer II at 68°C. Products are 3.5 kb (*Pgp*^{WT}), 2.6 kb (*Pgp* floxed) and 1.2 kb (*Pgp*^{D34N}).

For genotyping by **PCR**, yolk sacs or ear-punch biopsies of *Pgp*$^{flx/flx}$ or *Pgp*$^{flx/flx}$*; EIIa-Cre* mice were lysed for 60 min at 95°C in 35 µL digestion buffer, lysates were neutralized with 35 µL of neutralization buffer, and insoluble material was removed by centrifugation for 3 min at 1,500 × *g*. PCR was performed using DreamTaq polymerase. The primers are complementary to the 50 bp intron that is lacking in the knocked-in *Pgp* minigene, and detect the wildtype (212 bp) or targeted (163 bp) allele.

Genotyping of Tie2-Cre-transgenic mice was performed as recommended by The Jackson Laboratory. Primers detect the *Pgp* wildtype allele at 367 bp and the floxed allele at 401 bp.

Primer: *Pgp* intron forward: 5'-AAT GAG CGT CCC GGA GGC-3'

Pgp intron reverse: 5'-AAA CCC AAG CGCCTT AGC-3'

The PCR reaction mix contained:

2 µL 10x DreamTaq-Buffer

0.6 µL 10mM dNTP

1 µL 10µM forward primer

1 µL 10µM reverse primer

2 µL DNA

0.2 µL DreamTaq polymerase

sterile $H_2O_{dest.}$ was added to reach a final volume of 20 µL.

PCR protocol:

(1) initialization step: 95°C → 3 min
(2) denaturation step: 98°C → 20 sec
(3) annealing step: 51°C → 15 sec
(4) final elongation step: 72°C → 25 sec
(5) final hold: 12°C → ∞

(2) to (4) 35 reaction cycles

3.2.3 Agarose gel electrophoresis

For the separation of DNA fragments after PCR, agarose gel electrophoresis was performed. The required gel was generated by melting 2.5% agarose (w/v) in TAE buffer, which was also used as running buffer. Before pouring the gel, 0.005% ethidium bromide was added. As a standard, a 100 bp ladder was used. DNA was separated electrophoretically according to molecular size at a constant voltage of 80 V. For UV-light detection, a gel documentation system was used.

3.2.4 Embryo explants and isolation of primary cells

E8.5 embryos from *Pgp*$^{flx/flx}$ or *Pgp*$^{flx/flx}$*; EIIa-Cre* mice were explanted on 24-well microtiter plates precoated with 0.1% porcine gelatin (see **3.2.5.5** coating protocols) and cultured in complete DMEM in a 37°C, humidified cell culture incubator (5% CO_2).

To generate **mouse embryonic fibroblasts** (MEFs), explants were trypsinized after seven days, and isolated MEFs were cultured in complete DMEM in a 37°C, humidified cell culture incubator (5% CO_2).

For the isolation of **red blood cells**, ~600 µL blood from *Pgp*$^{flx/flx}$ or *Pgp*$^{flx/flx}$*; Tie2-Cre*$^{+/-}$ mice was collected into 250 µL acid citrate dextrose (ACD) buffer. Blood was centrifuged at 410 x *g* for 5 min at room temperature, the supernatant and buffy coat was discarded, and the pellet was washed three times in 500 µL 0.9% NaCl.

Lymphocytes were isolated from lymph nodes of *Pgp*$^{flx/flx}$ or *Pgp*$^{flx/flx}$*; Tie2-Cre*$^{+/-}$ mice. Here, superficial (cervical, axillary, brachial and inguinal) lymph nodes and deep mesenteric lymph nodes (**Figure 15**) were dissected and washed in RPMI medium. Afterwards, lymph nodes were homogenized with a plunger of a sterile syringe and passed through a cell strainer mounted on a 50 mL Falcon tube. The strainer was rinsed five times with 1 mL RPMI. The cell suspension was centrifuged at 800 x *g* for 8 min at room temperature and the supernatant was discarded. The cell pellet was resuspended in 1 mL of RBC lysis buffer and incubated for 8 min at room temperature. Afterwards, 9 mL RPMI was added, and the suspension was centrifuged again at 800 x *g* for 8 min. The supernatant was removed, and the lymphocytes were resuspended in RPMI medium containing 10% fetal calf serum.

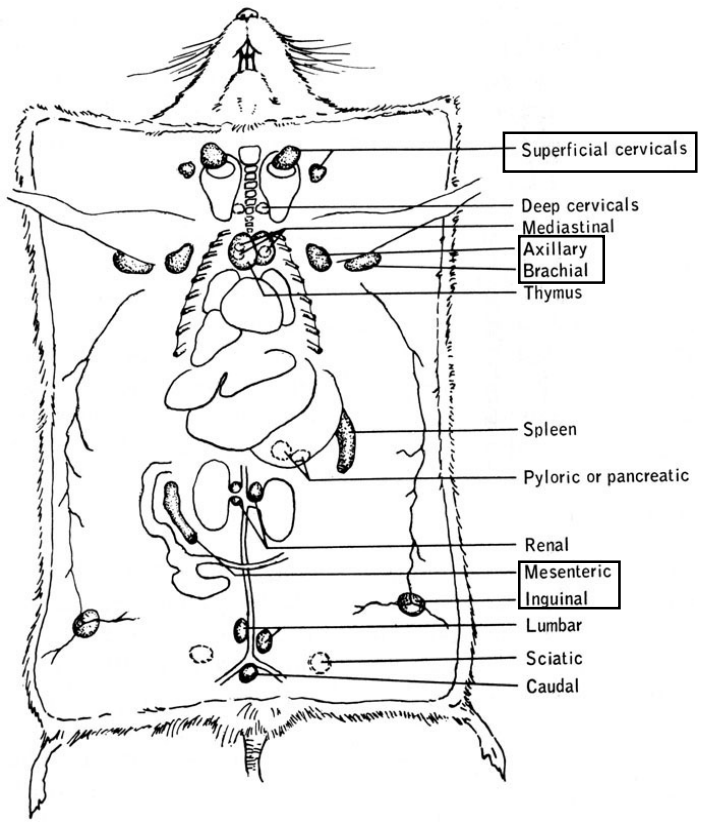

Figure 15: Lymph node atlas.
adapted from (Dunn, 1954).

For the isolation of **endothelial cells,** lungs of 6 day old *Pgp$^{flx/flx}$* or *Pgp$^{flx/flx}$; Tie2-Cre$^{+/-}$* mice were dissected and washed in DMEM on ice. The medium was carefully removed, and the lobes mashed with a scalpel. The mashed lung was taken up into a 15 mL Falcon tube using 5 mL of 0.2% collagenase type II solution in DMEM and digested under rotation for 60 min at 37°C. After 30 min, the lung suspension was passed through a 20G-needle ten times. The procedure was repeated ten times at the end of the 60 min incubation period before passing the cell/tissue suspension through a cell strainer mounted on a 15 mL falcon tube. The cell strainer was washed with 5 ml DMEM supplemented with 20% FCS, and the cell suspension was centrifuged for 5 min at 250 x *g* at room temperature. The supernatant was removed, and the cell pellet was resuspended by pipetting in 1 mL of ice-cold PBS + 0.1% BSA. The cell suspension was transferred into a 5 mL polystyrene tube, and 6 µL of α-CD31 (PECAM1)-coated dynabeads (see coating protocols, **3.2.5.5**) were added. The mixture was rotated for 30 min at 4°C and transferred to a reaction tube fixed on a magnetic rack. After 2 min the medium was removed, and 1 mL cold PBS + 0.1% BSA was added. The tube was removed from the magnet and the cells/beads were resuspended. The tube was placed again on the magnetic rack, and the washing steps were repeated four times. The cells/beads were resuspended in 1 mL of complete VascuLife medium and plated in a gelatin-precoated 6 cm dish (see coating protocols, **3.2.5.5**) containing 4 mL of medium. As soon as the cells were confluent, the second sorting was performed. For this purpose, cells were washed with PBS, trypsinized and resuspended in DMEM containing 20% FCS. The cell suspension was then centrifuged for 5 min at 250 x *g* at room temperature, the pellet was resuspended in 1 mL of ice-cold PBS containing 0.1% BSA, and the cell suspension was transferred to a 5 mL polystyrene tube. Six µL of α-CD102 (ICAM-2)-coated beads (see coating protocols, **3.2.5.5**) were added. After 30 min rotation at 4°C, five washing steps, as described above for the first sorting step, were performed. The cells were resuspended in 1 mL of complete VascuLife medium and plated on a 10 cm gelatin-precoated dish containing 9 mL of VascuLife medium.

3.2.5 Cell culture techniques

3.2.5.1 Cell lines, primary cells and cell culture

Besides primary cells, a murine spermatogonial cell-line, termed **GC1-spg** (from now on referred to as GC1 cells), was used. For RNA interference-mediated knockdown of PGP, lentiviral particles containing PGP-directed or nontargeting control shRNAs (MISSION shRNA panel SHCLND-NM_025954 or SHC002) were generated as previously described (Seifried et al., 2014). Cells stably expressing the shRNA constructs were selected for 2-3 days in complete DMEM containing 1 µg/mL puromycin. The cells were maintained at 37°C and 7% CO_2 in a humidified cell culture incubator.

E8.5 embryos from *Pgp$^{flx/flx}$* or *Pgp$^{flx/flx}$; EIIa-Cre* mice were explanted on 24-well microtiter plates precoated with 0.1% porcine gelatin and cultured in complete DMEM. Heart beats were assessed daily and the medium was changed every third day.

MEFs derived from the explants were cultured in complete DMEM. **Isolated red blood** cells were used immediately. **Lymphocytes** were maintained for 24 h in RPMI supplemented with 10% FCS before performing experiments. Three million lymphocytes were seeded per well. **Endothelial cells** were cultured for up to two weeks in complete VascuLife medium on plates precoated with 2% porcine gelatin.

Primary cells as well as embryo explants were cultured at 37°C and 5% CO_2 in a humidified cell culture incubator.

3.2.5.2 Freezing cells

A 10 cm dish with confluent cells was washed with PBS. Cells were trypsinized and resupended in complete DMEM. After centrifugation at 250 x *g* for 5 min at room temperature, cell pellet was resuspended in 1.5 mL of complete DMEM. Afterwards, 1.5 mL of complete DMEM containing 10% sterile DMSO was added, and the cell suspension was immediately aliquoted into three 2 mL cryo vials. The vials were stored in a cryo box overnight at -80°C. The next day, the vials were transferred to a liquid nitrogen tank.

3.2.5.3 Thawing cells

The frozen cells were thawed in a waterbath at 37°C. When only a small ice crystal was left in the cryo vial, the cell suspension was resuspended and transferred into 9 mL of prewarmed complete DMEM. After centrifugation at 250 x *g* for 5 min, the cell pellet was resuspended in 1 mL of complete DMEM and transferred to a 10 cm dish containing 9 mL of prewarmed complete DMEM. After 24 h the medium was changed.

3.2.5.4 Transfection

Cells were transiently transfected with Lipofectamin 2000. For PGP add-back experiments, 150,000 of control shRNA or PGP shRNA expressing cells were seeded on 3 cm diameter dishes. After 24 h, PGP shRNA cells were transfected either with 140 ng of RNA interference-insensitive human PGP^{WT}-YFP construct or with 130 ng RNA interference-insensitive human PGP^{DN}–YFP construct. As controls, PGP shRNA or control shRNA expressing cells were either transfected with 140 ng pcDNA3-YFP, or with 140 ng empty pcDNA3 vector. For the transfection, the plasmid DNA was added to 250 µl Opti-MEM, and 3 µL Lipofectamine 2000 were mixed separately with 250 µL Opti-MEM in polystyrene tubes. After a 5 min incubation period, DNA- and Lipofectamine 2000 solutions were mixed together and incubated for another 20 min to allow formation of transfection complexes. Meanwhile, cells were washed with 1 mL

of warm Opti-MEM and 1 mL of Opti-MEM as well as 0.5 mL of DNA/Lipofectamine/Opti-MEM mix was added to the cells. After a 4 h incubation at 37°C, medium was replaced with 2 mL of complete DMEM. To check transfection efficiency, YFP expression was examined by fluorescence microscopy 24 h after transfection.

3.2.5.5 Coating of cell culture dishes, endothelial cell sorting and lymphocyte activation

The culture dishes of endothelial cells were precoated with an autoclaved solution of 2% porcine **gelatin** in desalted water. The solution was added to the cell culture dishes to cover the surface completely and removed after 2 min. Afterwards, dishes were air-dried in a laminar flow hood before medium or cells were added.

For the cultivation of E8.5 embryo explants, surface of culture dishes was coated with a solution of 0.1% porcine **gelatin** in desalted water and processed as described above.

For **fibronectin** coating, plates were incubated for 90 min at 37°C with 10 µg/mL fibronectin in PBS (unless otherwise specified). Afterwards, plates were rinsed with PBS, and cells were added.

Poly-L-lysine coated plates were prepared with a 0.1 mg/mL poly-L-lysine solution in PBS. After one hour incubation at 37°C, liquid was removed, plates were dried in a laminar flow hood and were washed two times with PBS prior to addition of cells.

For **endothelial cell sorting,** magnetic dynabeads were coated either with α-CD31 or α-CD102 antibodies. Here, 200 µL of anti-rat IgG Dynabeads were transferred to a reaction tube and resuspended in 1 mL of sterile 0.1% BSA in PBS. Afterwards, the tube was fixed on a magnetic rack, medium was removed, and the beads were resuspended in 1 mL of sterile 0.1% BSA in PBS. After three washing steps, the beads were taken up in 500 mL 0.1% BSA in PBS and 10 µL of the antibody (either α-CD 31 or α-CD 102) was added. The tubes were tumbled for 2 h at room temperature. After two washing steps with 0.1% BSA in PBS, beads were resuspended in 200 µL of PBS containing 0.1% BSA and stored at 4°C.

For **lymphocyte activation,** 12-well culture dishes were precoated for 2 h with α-CD3 antibodies in PBS (5 µg/mL). Afterwards, dishes were washed three times with PBS. Three million lymphocytes were seeded per well and were co-activated by the addition of α-CD 28 (5 µg/mL) and IL-2 (100 U/mL) for 18 h.

Lymphocyte two-dimensional (2D) migration assays were performed on **ICAM-1** coated 8-well slides. Slides were coated for 2 h with ICAM-1 in PBS (3 µg/mL) prior to blocking 3 times for 5 min with 2% BSA in PBS.

3.2.5.6 Immunocytochemistry

For immunostaining, cells were fixed in 4% *para*-formaldehyde (PFA) for 20 min at room temperature. After permeabilization with 0.5% Triton-X-100 for 15 min and blocking with 3% BSA in PBS for 1 h, primary antibodies were added at a 1:200 dilution in 1% BSA in PBS, and cells were incubated for 1 h at room temperature. The cells were washed 3 times for 5 min with PBS before Alexa-conjugated secondary antibodies or phalloidin was added at a 1:400 dilution in 1% BSA in PBS. Afterwards, cells were incubated for 1 h at room temperature in the dark and washed 3 times for 5 min with PBS. In the last washing step, DAPI was added at a concentration of 1 µg/mL to counterstain the nuclei. After 3 min, cells were washed again with PBS, and coverslips were mounted in Pro Long mounting medium.

3.2.6 Cellular assays

3.2.6.1 Pharmacological inhibitors

Pharmacological inhibitors with their appropriate negative control or with a solvent control were used as follows (unless otherwise specified): PP2/PP3 (10 µM, 30min), dynasore (100 µM, 30min), wortmannin (50 nM, 30min), Gö6983 (3.3 µM; 3h), sotrastaurin (500 nM; 4h) and U73122/U73343 (0.5 µM, 30min).

3.2.6.2 Proliferation assays

Per condition, 1,000 MEFs were seeded in complete DMEM in duplicate wells of 96-well microtiter plates precoated with 0.1% gelatin. The effect of hypoxia on cell proliferation was assessed using a hypoxia chamber, and cells were kept either at ~20% O_2, 5% CO_2 or at ~1% O_2, 5% CO_2 for 16 h in the presence of 10 µM 5-ethynyl-2′-deoxyuridine (EdU) to assay for DNA synthesis. Cells were counterstained with DAPI and imaged on a Nikon TE Eclipse epifluorescence microscope equipped with a 4 × objective, and EdU- and/or DAPI-labeled cells were analyzed using Image Pro software version 7.0. Approximately 500-800 cells were scored per condition. Growth curves of GC1 cells stably expressing PGP-directed shRNA or control shRNA were obtained by seeding 250 cells per time point in duplicate wells of a 96-well microtiter plate precoated with fibronectin (10 µg/mL). Cells were cultured in phenol red-free complete DMEM. Each day, cells in predetermined wells were stained with Hoechst 33342 and imaged on a Nikon TE Eclipse epifluorescence microscope as described above.

3.2.6.3 Quantification of circular dorsal ruffles (CDR)

For analysis of CDR formation, GC1 cells expressing PGP shRNA or control shRNA were seeded on 12-well slides (8,000 cell per well) precoated with fibronectin or poly-L-lysine. After 4 h, cells were serum-starved overnight. The next day, cells were treated with or without inhibitors (see **3.2.6.1**), and CDR formation was stimulated with EGF (100 ng/mL) for 3 min at

37°C. The reaction was stopped by fixing cells in 4% PFA and cells were stained as described in 3.2.5.6 with Alexa-Fluor-488-conjugated phalloidin to stain filamentous (F)-actin and with DAPI to counterstain the nuclei. Cells were analyzed on a Leica confocal microscope equipped with Leica Application Suite software. Per condition, 200-300 cells were counted and the percentage of cells showing CDRs was calculated. For the determination of the number of CDRs per ruffling cell, 150 cells showing CDRs were scored per condition.

3.2.6.4 Cell spreading assays

For spreading experiments, 1 x 10^6 control shRNA and PGP shRNA expressing cells were seeded on 6 cm dishes and serum-starved for 4 h after seeding. Next day, cells were treated with or without inhibitors (see **3.2.6.1**), washed with PBS, trypsinized and resuspended in starving medium containing 0.1% BSA and 0.5 mg/mL soybean trypsin inhibitor (STI). The cells were centrifuged at 250 x *g* for 5 min at room temperature and resuspended in starving medium containing 0.1% BSA to a concentration of 120,000 cells/mL. Inhibitors with a reversible mode of action were added again, and cells were stimulated or not with EGF (100 ng/mL) in suspension. Afterwards, 70 µL of the cell suspension were added to 8-well slides, which had been precoated with fibronectin (10 µg/mL) and blocked with 0.1% BSA in starving medium for 1 h. The cells were allowed to attach and spread for 10 min before they were fixed with 4% PFA for 20 min at room temperature. The cells were permeabilized and stained with phalloidin and DAPI, as described in **3.2.5.6**. Afterwards, they were imaged on a Nikon TE Eclipse epifluorescence microscope. The spread cell areas of 30-50 cells per condition were determined by using ImagePro software.

3.2.6.5 PGP-rescue experiments

To determine the impact of PGP activity on CDR formation, 8,000 GC1 cells, either transfected with human PGP^{WT}-YFP constructs or with human PGP^{DN}–YFP constructs (see **3.2.5.4**), were seeded per well of 12-well slides precoated with fibronectin. After 4 h, cells were serum-starved overnight and CDR formation was stimulated by addition of EGF (100 ng/mL). To allow the identification of transfected cells, cells were additionally stained with an α-GFP/YFP antibody (see **3.2.5.6**). Only YFP-positive cells were considered for the evaluation.

For spreading experiments, 2 x 10^5 transfected cells were seeded on 3 cm diameter dishes, and medium was changed to starving medium 4 h later. The next day, spreading experiments and identification of transfected cells were performed as described above. Cell areas of 30-50 cells per condition were determined by using ImagePro software. Also here, only YFP-positive cells were considered for the calculation.

3.2.6.6 Endothelial cell spreading assays

Endothelial cells derived from lungs of *Pgp*$^{flx/flx}$ or *Pgp*$^{flx/flx}$*; Tie2-Cre*$^{+/-}$ mice were seeded on gelatin-precoated 3 cm dishes (70,000 cells/dish). Four h later, cells were serum-starved overnight. The next day, cells were washed with PBS, trypsinized and resuspended in Vasculife starving medium containing 0.1% BSA and 0.5 mg/mL STI. Cells were centrifuged at 250 x *g* for 5 min at room temperature, resuspended in starving medium containing 0.1% BSA to a concentration of 400,000 cells/mL and stimulated or not with EGF (100 ng/mL). One hundred µL of the cell suspension were added to 8-well slides (precoated with fibronectin and blocked with 0.1% BSA in starving medium for 1 h). Cells were allowed to attach and spread for 15 min before they were fixed with 4% PFA for 20 min at room temperature. Afterwards, cells were stained with phalloidin, with DAPI and with an α-CD31 antibody (see **3.2.5.6**) to identify endothelial cells. Imaging was performed on a Nikon TE Eclipse epifluorescence microscope. Cell areas of 30-50 endothelial cells per condition were determined by using ImagePro software.

3.2.6.7 Time lapse cell migration assays

For 2D migration assays, 6,000 GC1 cells expressing PGP shRNA or control shRNA were seeded on 8-well slides precoated with fibronectin at concentrations ranging from 0 to 15 µg/mL and serum-starved overnight 4 h later. The next day, cells were stimulated or not with EGF (100 ng/mL), the accumulated distance was monitored on Nikon TE Eclipse epifluorescence microscope for 17 h and determined by tracking 40 cells per condition using ImagePro software.

To assay 2D cell migration of lymphocytes isolated from *Pgp*$^{flx/flx}$ or *Pgp*$^{flx/flx}$*; Tie2-Cre*$^{+/-}$ mice, cells were activated overnight by seeding on 12-well dishes precoated with α-CD3 and addition of α-CD28 and IL-2 (see **3.2.5.5**). Next day, cells were resuspended and counted in a Neubauer chamber. Dead cells determined by Trypan blue uptake were excluded from the analysis. To follow lymphocyte migration, 10,000 cells were seeded per well of a 8-well slide precoated with ICAM-1 (see **3.2.5.5**). Cells were stimulated or not with SDF-1 (200 ng/mL), and cell tracks were followed for 30 min on a Nikon TE Eclipse epifluorescence microscope. The accumulated distances (= length of cell migration track from starting point A to end point B) were determined by tracking 40 cells per condition using ImagePro software.

3.2.6.8 Transwell cell migration assays

Lymphocytes were isolated from *Pgp*$^{flx/flx}$ or *Pgp*$^{flx/flx}$*; Tie2-Cre*$^{+/-}$ mice and seeded overnight in a 12-well culture dish as described in **3.2.5.1**. Next day, cells were treated with or without inhibitors (see **3.2.6.1**), counted and a cell suspension at a concentration of 10^6 cells/100 µL in RPMI/0.25% BSA was prepared. One hundred µL of the suspension was added to the upper

compartment of 3.0 µm pore diameter transwell inserts precoated with fibronectin or poly-L-lysine. The lower compartment of the transwell chamber contained 600 µL of RPMI/0.25% BSA. To start the migration assay, 100 ng/mL SDF-1 was added as a chemoattractant to the medium reservoir in the lower chamber (**Figure 16**).

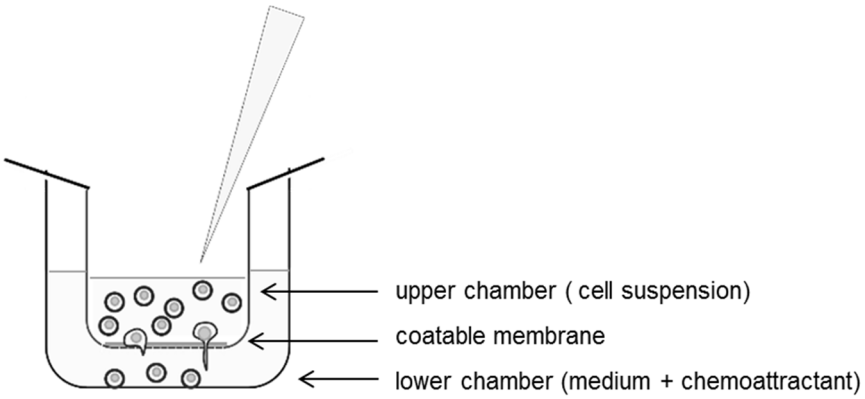

Figure 16: Transwell assay based on the Boyden chamber method.

After 3 h, the assay was stopped by removing the insert. Transmigrated cells were stained using Hoechst 33342 for 30 min and imaged on a Nikon TE Eclipse epifluorescence microscope. Cell numbers were counted semi-automatically using ImagePro software.

3.2.6.9 PKC activity assay

To analyze PKC activity lymphocytes were isolated from *Pgp*$^{flx/flx}$ or *Pgp*$^{flx/flx}$*; Tie2-Cre*$^{+/-}$ mice and seeded overnight in a 12-well culture dish as described above (**3.2.5.1**). Next day, cells were counted in a Neubauer chamber. Dead cells were assessed by using Trypan blue solution and were excluded from cell number determination. A concentrated cell suspension of 16 x 10^6 cells per 100 µL of RPMI was prepared and stimulated with 200 ng/mL SDF-1. One hundred µL of the stimulated cell suspension was added to a 3 cm dish precoated with fibronectin and blocked with 0.1% BSA in starving medium for 1 h. The cells were allowed to attach for 10 min, and were subsequently lysed with 200 µL of ice-cold PKC lysis buffer. After 10 min incubation on ice, cells were scraped from the plate using a rubber policeman and collected in pre-chilled tubes. Cell lysates were incubated for 20 min at 4°C under constant agitation. Insoluble cell components were removed by centrifugation at 10,000 × *g* for 12 min at 4°C. The supernatant was collected and protein concentrations were determined using the Micro BCA Protein Assay Kit. Lysates were diluted with PKC lysis buffer to comparable protein concentrations, and PKC activity was determined in 30 µL of the cell lysates according to the manufacturer's instructions.

3.2.6.10 Flow cytometry

Flow cytometry is a method for quantification of fluorescently labeled molecules either on the cell surface or -after permeabilization- inside the cell. This method can also be used to analyze cell size. Flow cytometric analysis was performed with non-starved or overnight serum-starved endothelial cells isolated from *Pgp*$^{flx/flx}$ or *Pgp*$^{flx/flx}$*; Tie2-Cre*$^{+/-}$ mice. To this end, cells were washed with PBS, trypsinized and resupended either in Vasculife complete medium or in Vasculife starving medium. After counting the cells in a Neubauer counting chamber, a cell suspension of 100,000 cells per condition was centrifuged at 250 x *g* for 5 min at room temperature and cell pellets were resuspended in 1 mL of PBS. Cell size was analyzed by detection of forward scatter signals in a FACS Calibur flow cytometer.

3.2.7 Metabolic studies

3.2.7.1 Determination of glycerol 3-phosphate (G3P) levels

Glycerol 3-phosphate levels in E8.5 embryo explant cultures were determined using a Glycerol 3-phosphate Colorimetric Assay Kit. Three embryo explants per genotype were pooled and lysed in 120 µL of ice-cold G3P assay buffer. Lysates were centrifuged at 10,000 × *g* at 4°C for 5 min to remove insoluble cell components, and cell supernatants were kept on ice. Fifty µL of the cleared embryo explant lysates were used, and glycerol 3-phosphat levels were determined according to the manufacturer's instructions. To calculate G3P levels per µg of protein, protein concentrations of the embryo lysates were determined using the Micro BCA Protein Assay Kit.

3.2.7.2 Lipidomics

The analysis of results from lipidomic studies was performed by Matthias Zundler according to published procedures (Schiebel et al., 2013) with modifications, and will be explained in more detail in his MD thesis (unpublished). Briefly, all solvents were LC-MS grade and purchased from Biosolve. Lipids were extracted using *tert*-butylmethylether (TBME) as described with minor modifications (Chen et al., 2013). Per experiment, ten pooled E8.5 embryos (*Pgp*$^{WT/WT}$, *Pgp*$^{WT/DN}$ or *Pgp*$^{DN/DN}$; ~50 µg total protein) were extracted with 600 µL ice-cold 100% methanol for at least 24 h at -80°C. After the addition of 200 µL distilled water, samples were treated for 5 min at 21 Hz in a ball mill equipped with 5 mm zirconium oxide grinding balls. One mL TBME was added. Samples were rocked on a thermocycler for 1 h at room temperature, vortexed for 1 min, 250 µL of distilled water was added, samples were vortexed again for 1 min, and centrifuged at 9,400 × *g* for 3 min to achieve phase separation. The upper phase was evaporated, dissolved in 50 µL isopropanol and analyzed by LC/MS as described previously (Schiebel et al., 2013). Processing of chromatograms, peak detection and integration were

performed using MassLynx software. TransOmics software was used for data preprocessing for untargeted metabolomics and for marker identification. Glycerolipid profiling was conducted using the in-house developed software RLA-Tool (developed by Dr. Agnes Fekete and Prof. Dr. M. Müller, Julius von Sachs Institute/Pharmaceutical Biology, University of Würzburg). Defined lipid species were searched for in the samples based on their exact m/z in the low energy function and two integral fragments (fatty acyl side chains) in the high energy function with an error tolerance of 3 mDa. The identification was confirmed by the linear coherence between retention time and m/z (Hummel et al., 2011). The identified species were then assembled into an automated method within QuantLynx embedded in MassLynx for the systematic integration of the identified lipid species in the extracts. For the analysis of GC1 control shRNA or PGP shRNA cells, 5.5×10^6 cells per cell type and experiment were extracted in 450µL ice-cold 100% methanol for at least 24 h at -80°C. After the addition of 150 µL distilled water, samples were processed and analyzed as described above.

3.2.7.3 Determination of ATP levels

ATP levels of GC1 cells and E8.5 embryos from *Pgp*$^{flx/flx}$ or *Pgp*$^{flx/flx}$*; EIIa-Cre* mice were quantified with recombinant firefly luciferase using an ATP determination kit. GC1 cells seeded in 3 cm dishes were grown to a confluent monolayer by overnight culture in complete DMEM. Cells were then serum-starved for six h, and incubated for 1 h in the absence or presence of glucose, sodium palmitate [coupled to fatty acid- and globulin-free bovine serum albumin (for details see www.seahorsebio.com); final concentration, 200 µM] or inhibitors [final concentrations of atglistatin and etomoxir, 50 µM; 2-deoxyglucose (2-DG), 100 mM]. ATP concentrations were determined according to the manufacturer's instructions, using 10 µL of the cell lysates. To calculate ATP levels per µg of protein, protein concentrations were determined using the Micro BCA Protein Assay Kit.

3.2.7.4 Analysis of triose phosphate isomerase (TPI) activity

TPI activity in E8.5 embryo explant cultures from *Pgp*$^{flx/flx}$ or *Pgp*$^{flx/flx}$*; EIIa-Cre* mice and red blood cells isolated from *Pgp*$^{flx/flx}$ or *Pgp*$^{flx/flx}$*; Tie2-Cre*$^{+/-}$ mice was determined using the Triose Phosphate Isomerase activity kit. Embryo explants were lysed in 175 µL, and snap-frozen red blood cell pellets were lysed in 1 mL of the provided TPI assay buffer. Lysates were kept on ice for 10 min, and cell debris was removed by centrifugation for 10 min at 10,000 × *g*. Fifty µL of the cleared embryo explant lysates, or 5 µL of the cleared red blood cell lysates were used in a final assay volume of 50 µL. Enzyme kinetics were followed spectrophotometrically at 450 nm in 96-well microplates on a multilabel plate reader, and the values were extrapolated to a NADH standard curve. To calculate TPI activity per µg of protein, protein concentrations were determined using the Micro BCA Protein Assay Kit.

3.2.7.5 Analysis of cellular respiration

Oxygen consumption rates (OCRs) were measured using a Seahorse XF96e extracellular flux analyser and XF Cell Mito Stress kits according to the manufacturer's recommendations. Each assay cycle consisted of a 1 min mix, 2 min wait, and 3 min measurement period. The mitochondrial ATP synthase inhibitor oligomycin (2 µM) was added after three basal assay cycles to determine the fraction of respiration used to drive ATP synthesis. Carbonyl cyanide-4-(trifluoromethoxy)phenylhydrazone (FCCP, 0.5 µM) was injected after three further assay cycles to uncouple ATP synthesis from electron transport and thus to induce maximal respiration. After another three assay cycles, a mix of the complex I inhibitor rotenone (0.5 µM) and the complex III inhibitor antimycin A (0.5 µM) was added to determine the non-mitochondrial respiratory rate. For inhibitor experiments, cells were pretreated for 30 min with 40 µM etomoxir, 50 µM atglistatin or 100 mM 2-DG. The principle of a mitochondrial stress assay is depicted in **Figure 17**.

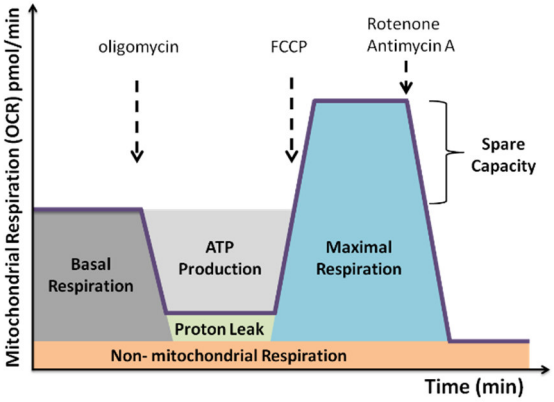

Figure 17: Mitochondrial stress assay.

For OCR measurements under oxygen-deprived conditions, cells were grown overnight in a hypoxia incubator at 3% O_2 and 5% CO_2. The oxygen scavenger sodium sulfite (final concentration, 100 mM) was added to wells containing only XF Calibrant to provide a 'zero' oxygen reference parameter. Cells were washed twice under hypoxic conditions with bicarbonate-free XF assay medium, followed by a 1 h preincubation at 37°C and 3% O_2. OCR measurements were conducted as described above. Analyses were performed using Wave software. To correct the OCR values for variations in cell numbers, cells were fixed in 75% ethanol for 15 min, dried and stained with 0.1% (w/v) crystal violet in 20% ethanol for 20 min. Cells were dried overnight, the dye was extracted with 10% acetic acid, and A_{562} was read on a microplate reader. Standard curves were constructed by extrapolating the crystal violet values to a protein concentration standard curve determined using the Micro BCA Protein Assay Kit, obtained from cells seeded in parallel.

3.2.8 Protein analytics

3.2.8.1 Sodium dodecyl sulfate polyacrylamide gel electrophoresis (SDS-PAGE)

Proteins were separated according to their molecular mass using SDS-PAGE. In the first step, proteins were denatured by boiling in sample buffer for 3 min. Proteins with lower molecular mass such as PGP (~34 kDa), were run on 12% SDS-PAGE gels, and larger proteins such as Src (~60 kDa) or PLCγ1 (~155 kDa) were resolved in 8% SDS-PAGE gels (Laemmli, 1970). Proteins were concentrated in the stacking gel at a constant voltage of 75 V and the separation took place at a constant voltage of 130 V in the running gel.

3.2.8.2 Western Blot analysis

Proteins separated by SDS-PAGE were transferred onto nitrocellulose membranes via semi-dry transfer. For this purpose, a "Western blot sandwich" was built (**Figure 18**). Two sheets of Whatman paper soaked with anode buffer I and one sheet soaked in anode buffer II formed the bottom of the sandwich. The nitrocellulose membrane was first soaked in H_2O_{dest} and then in anode buffer II and added to the Whatman paper sheets. The gel rinsed in cathode buffer was added on the membrane followed by three sheets of Whatman paper equilibrated in cathode buffer. Proteins with lower molecular mass were electrophoresed in "low" buffers, and proteins with higher molecular mass in "high" buffers. "Low" transfer buffers contain more methanol than "high" buffers to promote binding of lower MW proteins to the membrane. SDS is added to "high" buffers to promote elution of the higher MW proteins from gels. Proteins were blotted at a constant electric current of 70 mA per gel.

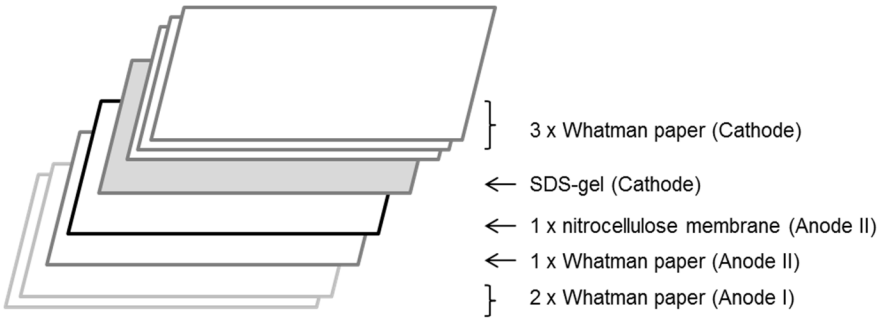

Figure 18: Western blot sandwich.
For details, see text above.

Blotting times ranged from 30 min for PGP to 90 min for PLCγ1. Afterwards, membranes were stained with Ponceau S to visualize the transferred proteins, and scanned for documentation. After incubation with blocking buffer for 20 min to avoid unspecific binding of the antibodies, membranes were rinsed with H_2O_{dest} and incubated with primary antibodies overnight at 4°C under agitation. The primary antibodies were diluted 1:1,000 in antibody diluent. The next day, membranes were rinsed three times with H_2O_{dest} and incubated with horseradish peroxidase

(HRP)-labelled secondary antibodies for 1 h at room temperature. Secondary antibodies were diluted 1:10,000 in blocking buffer. For analysis of tubulin expression levels, the first antibody was diluted 1:10,000, and the membrane was incubated for 1 h at room temperature, followed by washing and the incubation with the secondary antibody. The blot was developed using Super Signal West Pico Stable Peroxide Solution and Luminol/Enhancer Solution mixed in a ratio of 1:1 for 3 min. ImageQuant LAS 4010 Digital Imaging System was used to detect protein signals. Bands were densitometrically analyzed with ImageJ software (see **3.2.10**).

3.2.8.3 Immunoblot stripping

The membrane was placed in 50 mL Falcon tubes containing freshly prepared stripping buffer and was incubated for 45 min at 50°C. The tube was vigorously vortexed every 5 min. Afterwards, membrane was extensively rinsed with desalted water for 15 min before washing three times with 200 mL of TBS containing 0.05% Tween for 10 min under constant agitation. Prior to reprobing, the membrane was incubated with blocking buffer for 30 min.

3.2.8.4 Preparation of cell lysates

Lysates generated to assess PGP expression levels in cultured or primary cells or tissues were prepared in Laemmli`s sample (2 x) buffer. For analysis of phosphorylation levels of PLCγ1, Src family kinases or of the EGF receptor, cells expressing control or PGP-directed shRNAs were seeded on fibronectin or poly-L-lysine, serum-starved overnight after 4 h, and stimulated or not with EGF (100 ng/mL) for 0, 3 or 5 min before lysis with ice-cold lysis buffer on ice. For inhibitor experiments, cells were pretreated with the Src family kinase inhibitor PP2 or its negative control PP3 before stimulation with EGF and cell lysis. The lysates were rotated for 15 min at 4°C, and insoluble material was removed by centrifugation at 21,000 x *g* for 15 min. Protein concentrations of the cleared supernatants were determined using the Micro BCA kit, according to the manufacturer`s instructions. To adjust protein concentrations Laemmli`s sample buffer (4 x) was added.

3.2.8.5 Immunoprecipitation

To immunoprecipitate tyrosine-phosphorylated (pY783) PLCγ1, 1.5 x 10^6 control shRNA or PGP shRNA expressing GC1 cells were seeded on fibronectin-coated 10 cm dishes. To analyze maximal PLCγ1 phosphorylation levels, a second dish with GC1 cells expressing control shRNA was prepared in parallel. Four h after seeding, these cells were serum-starved overnight and subsequently treated with 100 µM freshly prepared pervanadate solution (obtained by a 1:1 mixture of 100 mM H_2O_2 and 100 mM $NaVO_4$) for 30 min (Daum et al., 1998). Cells were stimulated with 100 ng/mL EGF for 3 min before cell lysis in 500 µL ice-cold lysis buffer. The lysates were rotated for 15 min at 4°C, and insoluble material was removed by centrifugation at 21,000 x *g* for 15 min. Protein concentrations of the cleared supernatants

were determined using the Micro BCA kit, and samples were diluted to comparable protein concentrations in a final volume of 500 µL lysis buffer. Five µL of pY783 PLCγ1 antibody was added per sample, and lysates were rotated overnight at 4°C. The next day, protein G sepharose beads (20 µL packed beads per sample) were pre-equilibrated and blocked in lysis buffer containing 3% BSA for 1.5 h at room temperature. The beads were washed three times with 1 mL lysis buffer by centrifugation at 400 x *g* for 2 min at room temperature. After the last washing step, beads were resuspended in 1.2 mL lysis buffer. Four hundred µL of the resuspended beads were aliquoted in three 1 mL reaction tubes. After centrifugation (400 x *g*; 2 min) the supernatant was removed, and 500 µL of the cell lysates were added to the beads. The mixture was rotated for 2 h at 4°C. After washing the beads three times in lysis buffer, proteins were eluted from the beads by boiling in 30 µL of Laemmli's buffer (2 x) for 5 min. After a high speed centrifugation step (10,000 x *g*; 10 min) the entire supernatant was used for Western blot analysis.

3.2.9 Experiments with purified proteins

3.2.9.1 Cellular PLCγ1 dephosphorylation assays

To analyze whether PLCγ1 is a direct substrate of PGP, 1.5 x 10^6 GC1 cells expressing control shRNA were seeded on fibronectin-coated 10 cm dishes and serum-starved overnight. Three dishes were prepared in parallel. The next day, cells were treated for 30 min with 100 µM freshly prepared pervanadate solution (prepared as decribed above, **3.2.8.5**). The cells were stimulated with 100 ng/mL EGF for 3 min before cell lysis in 500 µL ice-cold lysis buffer. The lysates were rotated for 15 min at 4°C, and insoluble material was removed by centrifugation at 21,000 x *g* for 15 min. After pooling the lysates, an immunoprecipitation of tyrosine-phosphorylated (pY783) PLCγ1 was performed as described above (**3.2.8.5**). After a 2 h incubation period under agitation at 4°C, the beads–lysate mixture was aliquoted into three reaction tubes. The beads were washed three times by centrifugation (400 x *g*, 2 min, 4°C) with 1 mL lysis buffer and resuspended in 300 µL of TMN buffer containing 1 mM DTT. Highly purified, recombinant murine PGP^{WT} or PGP^{DN} (10 µg each) or 1% BSA control protein were added to the samples. After a 2 h rotation step at 37°C, the beads were washed with TMN buffer, and proteins were eluted from the beads by boiling in Laemmli's buffer (2 x) for 5 min. The samples were centrifuged at 10,000 x *g* for 10 min, and the supernatant was subjected to Western blotting to determine phosphorylation levels of tyrosine 783 of PLCγ1. For this purpose, lysates were blotted onto nitrocellulose, and Western blots were performed with total PLCγ1 or pY783-PLCγ1 antibodies. The assay was also performed with lower concentration of purified PGP (0.05 µg, 0.5 µg and 1 µg), with shorter incubation times (45/60 min) and in presence or absence of 10 µM of the Src family kinase inhibitor PP2.

3.2.9.2 Recombinant PLCγ1 dephosphorylation assays

One µg of purified PLCγ1 was incubated with 1 µg of active Syk and 500 µM ATP in 300 µL of Syk kinase buffer. The solution was rotated for 1 h at 37°C. Afterwards, proteins were concentrated and washed three times with TMN using Amicon Ultra-0.5 mL Centrifugal Filters (14,000 x *g,* 10 min, room temperature*)* according to the manufacturer's instructions. In the last centrifugation step, the concentrated proteins were collected in a reaction tube, 500 µl of TMN containing 1 mM DTT was added, and two 250 µL aliquots were prepared and incubated either with 1 µg PGP^{WT} or with 1 µg PGP^{DN}. After 1 h of incubation at 37°C under agitation, the proteins were again concentrated using Amicon Ultra-0.5 mL Centrifugal Filters as described above. Laemmli's buffer (2 x) was added, and samples subjected to Western blotting using a pY783-PLCg1 antibody to analyze phosphorylation levels of this residue.

3.2.10 Image quantification

Western blots were analyzed densitometrically using ImageJ, version 1.45i. To normalize for protein loading, values were adjusted to tubulin expression levels. For the evaluation of phosphorylation levels of the EGF receptor the values were adjusted to total EGF receptor expression levels.

3.2.11 Statistical analysis

Unpaired Student`s *t*-test were performed using Graph pad prism version 6.0. Data are expressed as mean ± S.E.M. * $P< 0.05$; ** $P< 0.01$; *** $P< 0.001$; **** $P< 0.0001$

4 Results

4.1 Role of phosphoglycolate phosphatase (PGP) for cell spreading and cell migration

The first part of the thesis deals with the question how PGP regulates integrin- and RTK-mediated cell adhesion. Additionally, the question arises if PGP also regulates other cellular functions that are mediated by actin cytoskeleton reorganization, such as cell migration.

As already mentioned. PGP-depleted cells adhered faster on integrin ligands such as fibronectin (see **1.4.3**). For cell adhesion, cells have to profoundly reorganize their actin cytoskeleton. This suggests that PGP might play a role in integrin-dependent actin reorganization. Previously, PGP was identified as a regulator of receptor tyrosine kinase- (RTK-) induced signaling (Seifried et al., 2014). Important pathways through which RTK activation influences actin dynamics include the regulation of phosphatidylinositide 3- (PI3-) kinase- (Jimenez et al., 2000) and protein kinase C- (PKC-) signaling (Laux et al., 2000, Brandt et al., 2002).

Cellular processes such as cell spreading and cell migration also require a dynamic and organized rearrangement of the actin cytoskeleton. To study the role of PGP for cell spreading and migration downstream of integrin- and RTK-signaling, the following cell lines were used.

The spermatogonial cell line GC1 is a suitable model to study actin dynamics because GC1 cells exhibit a well-elaborated actin cytoskeleton. They are derived from mouse testis and express high levels of PGP. Targeting of PGP by RNA interference using short hairpin RNA (shRNA) resulted in a reduction of PGP protein levels by ~80%, as determined by densitometric analysis of PGP expression in control shRNA and PGP shRNA expressing cells (**Figure19**).

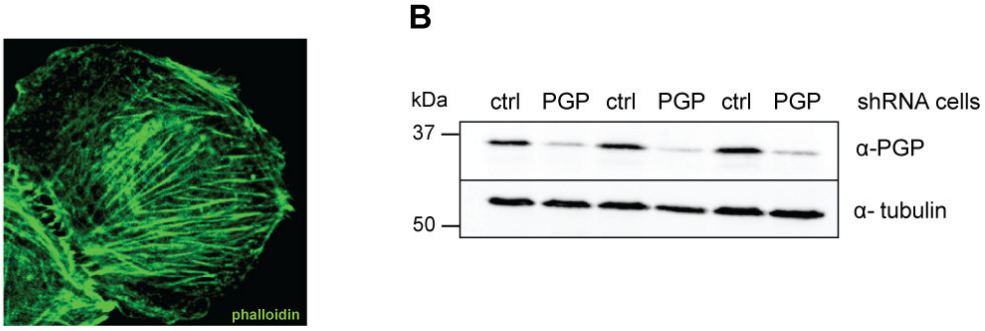

Figure 19: Spermatogonial GC1 cell line.
A: Control shRNA cells stained with phalloidin to visualize actin filaments.
B: Western blot showing the expression levels of endogenous PGP in murine GC1 cells stably expressing control (ctrl) shRNA or shRNA directed against murine PGP.

The regulation of cell adhesion and migration in lymphocytes as well as in endothelial cells is essential for physiological processes such as wound healing and immune responses. To begin to analyze a potential role of PGP in these processes, primary endothelial cells and lymphocytes were isolated from *Pgp*$^{flx/flx}$ and *Pgp*$^{flx/flx}$; *Tie2-Cre*$^{+/-}$ mice. Breeding of *Pgp*$^{flx/flx}$ mice with the Tie2-Cre driver line leads to a *Pgp* inactivation in endothelial cells and in cells of the hematopoietic system such as red blood cells or lymphocytes (see **1.7**). Mouse lung endothelial cells were isolated from the lung lobes of five to seven day old pubs, and primary lymphocytes were isolated from superficial (cervical, axillary, brachial and inguinal) and deep mesenteric lymph nodes.

4.1.1 Cellular effects of PGP

4.1.1.1 PGP activity regulates integrin- and RTK- induced circular dorsal ruffle formation

As a first step, EGF- and integrin-mediated actin reorganization was analyzed in spermatogonial GC1 cells. Control shRNA as well as PGP-directed shRNA expressing cells were seeded on the integrin ligand fibronectin and were serum-starved overnight. Upon EGF stimulation, cells were monitored for 45 minutes by differential interference contrast (DIC) microscopy using an epifluorescence microscope. After about three minutes, a ring-like membrane structure appeared on the dorsal plasma membrane of the cells and disappeared after some minutes. To characterize this transient membrane projections further, immunostaining experiments were performed. Control shRNA and PGP shRNA expressing cells were treated, as described above, and fixed after three minutes of EGF stimulation. To visualize actin filaments, the cells were stained with phalloidin and stained with DAPI to identify the nucleus. The ring-like membrane ruffle was enriched with F-actin.

There were some reports published describing a ring-like, transient and actin-rich dorsal membrane structure which is inducible by growth factor stimulation, the so-called circular dorsal ruffle (see **1.6.3**) (Suetsugu et al., 2003, Orth and McNiven, 2006). Thus, the dorsal membrane projections observed in GC1 cells upon EGF stimulation may also represent circular dorsal ruffles (CDRs, see **Figure 20**).

The percentage of cells showing CDRs was quantified. CDR formation was significantly increased in PGP-depleted cells, and the numbers of CDRs per ruffling cell was also markedly higher after PGP depletion (**Figure 20A** and **20B**). As already mentioned, growth factor stimulation is necessary for the induction of CDRs (Mellstrom et al., 1988, Tamura and Iwamoto, 1989, Wu et al., 2003). Recently, it was reported that integrin activation is essential for this process as well (Azimifar et al., 2012). To examine whether this was the case for PGP-dependent CDR formation, GC1 cells expressing PGP shRNA or control shRNA were

seeded on poly-L-lysine (PLL), a positively charged polymer. PLL interacts with the negatively charged plasma membrane of seeded cells and improves cell adherence. In contrast to cell seeding on fibronectin, attachment of cells on PLL does not lead to integrin activation. **Figure 20C** shows that a dramatic decrease in CDR formation was observed in both control- and PGP-depleted cells upon seeding on PLL compared to seeding on fibronectin and that this decrease was particularly pronounced in PGP-deficient cells.

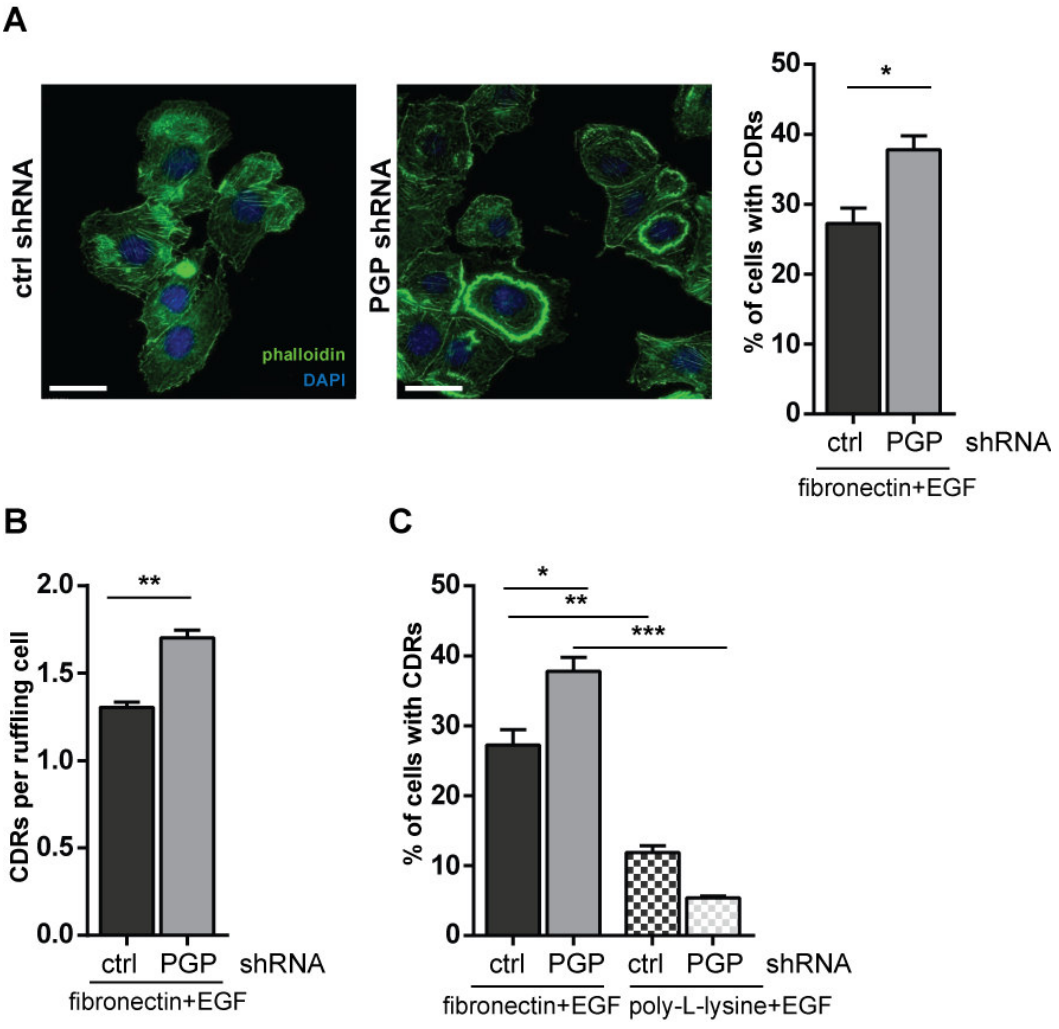

Figure 20: Characterization of PGP-dependent CDR-formation.
A: For immunofluorescence analysis of CDR formation control shRNA and PGP shRNA expressing cells were seeded on fibronectin, serum-starved overnight, fixed 3 min after EGF stimulation (100 ng/mL) and stained with Alexa 488-conjugated phalloidin to identify CDRs and with DAPI to counterstain the nuclei. For the quantification of CDR formation, 200-300 cells per condition and experiment were analyzed and the percentage of cells showing CDRs was calculated. Results are mean values ± S.E.M. of n=4 independent experiments. *, p< 0.05.
B: For the quantification of the numbers of CDRs per ruffling cells, 150 cells showing CDRs for each cell type were analyzed and the numbers of CDRs per cell were counted. n=3 independent experiments were performed. Data are expressed as means ± S.E.M. **p< 0.01.
C: Quantification of CDR formation in GC1 cells seeded on poly-L-lysine (0.1 mg/mL) in comparison to cells seeded on fibronectin (10 µg/mL) demonstrated that integrin activation is essential for PGP-dependent CDR formation. Results are mean values ± S.E.M. of n=4 independent experiments.
*, p< 0.05; **, p< 0.01; ***, p< 0.001.

Integrin- and RTK- signaling is mediated by a complex network of effector- and scaffolding proteins. To investigate whether the catalytic phosphatase activity of PGP, or the potential functions of PGP as scaffolding protein were essential for PGP-dependent CDR formation, PGP add-back experiments were performed (**Figure 21**). If the loss of PGP phosphatase activity was responsible for the observed effect, the re-expression of PGP^{DN} should recapitulate the PGP shRNA phenotype, whereas the re-expression of wildtype PGP should phenocopy the degree of CDR formation in control shRNA cells. In contrast, if PGP would function primarily as a scaffolding protein to regulate CDR formation, re-expression of either wildtype or the inactive mutant should abolish the enhanced CDR formation observed upon PGP depletion.

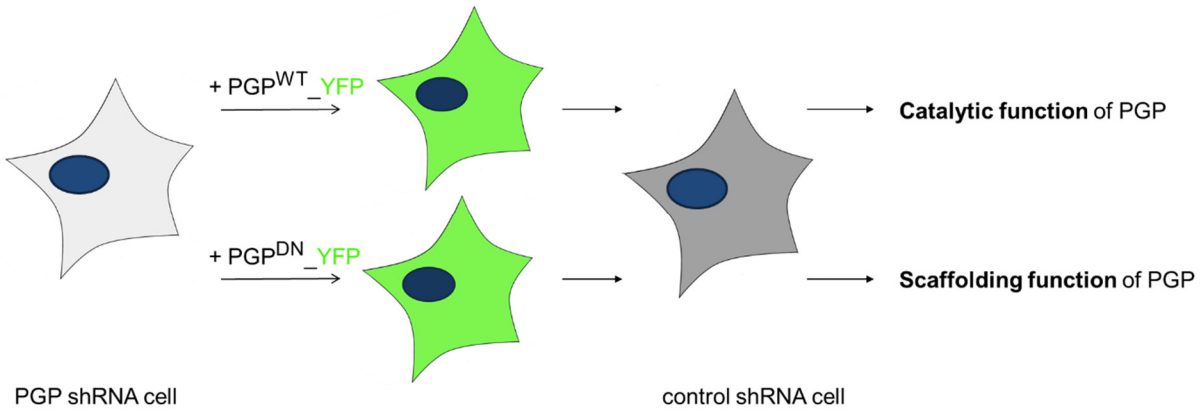

Figure 21: The principle of PGP add-back experiments.
For details, see text above.

To exclude that CDR formation was affected by cell transfection *per se*, control shRNA and PGP shRNA expressing cells were transfected with an empty YFP-tagged vector. The transfected cells displayed same levels of CDR-formation as non-transfected cells (**Figure 22B**).

For the add-back experiments, cells expressing PGP shRNA were transfected either with RNA interference-resistant human PGP^{WT} or with the phosphatase-inactive catalytic point mutant PGP^{DN} to endogenous PGP expression levels (**Figure 22A**). The remaining endogenous PGP expression in PGP shRNA cells (which was about 20% of PGP expression in control cells) was also considered. Cells, transfected with the inactive point mutant showed CDR formation levels similar to PGP-depleted cells. Only cells, transfected with wild type PGP showed the same effects on CDR formation as control shRNA cells. Thus, PGP phosphatase activity regulates integrin- and RTK- mediated CDR formation (**Figure 22B**).

Taken together, it was demonstrated that PGP activity controlled EGF-induced CDR formation in an integrin-dependent manner.

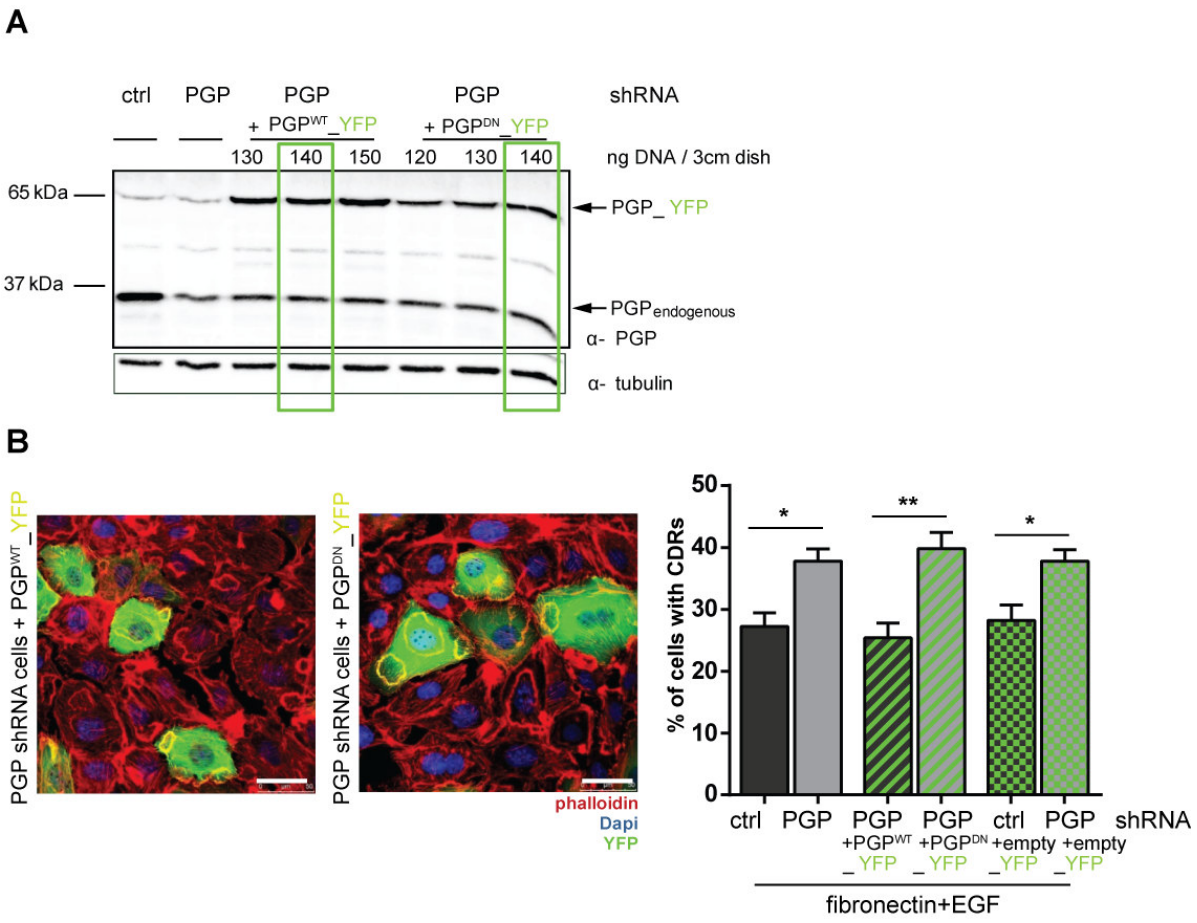

Figure 22: Effects of add-back experiments with phosphatase active- or inactive PGP versions on CDR formation.
A: Lysates of cells expressing PGP shRNA and transfected either RNA interference-resistant human PGP^{WT} or with human PGP^{DN} were immunoblotted with an α-PGP antibody to make sure that PGP^{WT} or PGP^{DN} were re-expressed at endogenous levels. The remaining PGP expression in PGP silenced cells, which was about 20% of control shRNA cells was also considered. PGP expression in control shRNA cells was used as standard, and tubulin expression was examined as loading control.
B: PGP shRNA expressing cells transfected with either PGP^{WT} or PGP^{DN} to endogenous expression levels of PGP were seeded on fibronectin, serum-starved overnight, fixed 3 min after EGF stimulation (100 ng/mL) and stained with Alexa 546-conjugated phalloidin to identify CDRs, with DAPI to counterstain the nuclei and with an α-YFP/GFP antibody to detect transfected cells. For the quantification of CDR- formation 100-200 of YFP-positive cells per condition and experiment were scored, and the percentage of cells showing CDRs was calculated. Results are mean values ± S.E.M. of n=4 (non-transfected cells) n=5 (PGP^{WT} - or PGP^{DN} -transfected cells). As a control PGP shRNA and control shRNA expressing cells were transfected with an empty-YFP vector and CDR formation of YFP-positive cells was determined as described above. n=3 independent experiments were performed. *, $p < 0.05$; **, $p < 0.01$.

4.1.1.2 PGP localizes to circular dorsal ruffles

It is already known that important proteins involved in actin remodeling such as the Neural Wiskott-Aldrich syndrome protein (N-WASP), the actin related protein 2/3 (ARP2/3) complex, WASP-family verprolin-homologous protein (WAVE) or Src are required for the formation of CDRs, and localize to CDRs (Legg et al., 2007, Suetsugu et al., 2003, Azimifar et al., 2012, Yang et al., 2006). To further characterize the transient actin-rich membrane structure, whose formation was enhanced upon PGP depletion, subcellular localization of endogenous PGP during EGF- and fibronectin- induced CDR formation was analyzed by immunocytochemistry. To this end, control shRNA expressing cells were seeded on fibronectin and were serum-starved overnight. The next day, cells were stimulated with EGF for three minutes before fixation and staining. By using an antibody against endogenous PGP, it was demonstrated that PGP localized to circular dorsal ruffles. The co-localization of PGP with F-actin, stained with phalloidin, was confirmed with a co-localization finder software provided from Image J. The Pearson`s correlation coefficient (PCC) is a statistic measure of linear correlation and is often used to quantify co-localization. Here, peak maxima of signal intensities of different channels are compared. A PCC value of 1 indicates a perfect linear correlation/co-localization, and a PCC value close to zero indicates that the fluorescence intensities of two images are uncorrelated (Dunn et al., 2011). PCC was set to a value higher than 0.75. Co-localized data points are displayed in white (**Figure 23**).

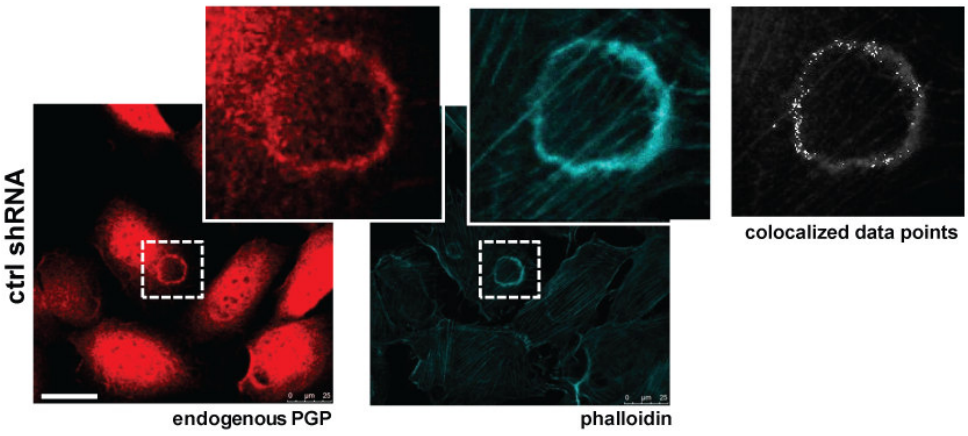

Figure 23: Analysis of the subcellular localization of endogenous PGP localization.
Control shRNA cells were seeded on fibronectin (10 µg/mL), were serum-starved overnight and stimulated with EGF (100 ng/mL). After fixation with 4% PFA, cells were stained for endogenous PGP expression (shown in red) and with Alexa 633-conjugated phalloidin (shown in cyan) to visualize actin structure. Co-localization studies were performed using ImageJ co-localization finder software. Co-localized data points with a Pearson's correlation coefficient above 0.75 are displayed in white.

4.1.1.3 PGP regulates integrin- and RTK-induced cell spreading in a CDR-dependent manner

CDRs have been implicated in integrin trafficking (see **1.6.3**). Integrins are internalized via CDRs at the apical surface, traffic through the cell and are recycled to the ventral surface to create new adhesive sites (Gu et al., 2011, Margadant et al., 2011). In this way, CDRs can regulate integrin-mediated cellular processes such as cell adhesion, spreading and migration. To investigate if increased CDR formation in PGP-depleted cells affects these processes, cell spreading experiments were performed. To this end, cells were kept in suspension, and the spreading of PGP shRNA or control shRNA expressing GC1 cells on integrin ligand fibronectin was analyzed. The cells were serum-starved overnight and brought in suspension before seeding on a fibronectin-precoated dish for 10 minutes. The reaction was stopped by fixation of the cells. In preliminary experiments, we observed that GC1 cells exhibit prominent cortical actin bundles during initial cell spreading. These actin filaments can be stained with phalloidin, thus enabling the visualization and quantification of the cell spread area. **Figure 24A** demonstrates that PGP-depleted cells showed significantly increased cell spread areas upon seeding on fibronectin.

To investigate how RTK- and integrin co-stimulation affects PGP-dependent cell spreading, control shRNA and PGP shRNA cells were stimulated with EGF in suspension before seeding on fibronectin for 10 min. Co-activation of both receptors further increased the PGP-dependent effect on cell spreading (**Figure 24A**).

As a next step, it was investigated whether the catalytic phosphatase activity of PGP or PGP as scaffolding protein was essential for PGP-dependent cell spreading. For this purpose, PGP-add-back experiments were performed (see **Figure 21**). Comparable cell spreading of PGP-depleted cells transfected with the catalytically inactive point mutant PGP^{DN} and non-transfected control shRNA cells would indicate that PGP functions as a scaffolding protein. If cell spreading of PGP-depleted cells transfected with wildtype PGP and non-transfected control shRNA were comparable, it would mean that PGP phosphatase activity is essential for the observed effects on cell spreading.

To make sure that cell spreading was not affected by cell transfection *per se*, control shRNA and PGP shRNA expressing cells were transfected with an empty YFP-tagged vector. After quantification of cell spread areas of YFP positive cells, PGP-dependent effect on cell spreading was still observable (**Figure 24B**).

The re-expression of wildtype PGP in PGP shRNA expressing cells led to equal cell spreading as observed in control shRNA cells (**Figure 24B**).

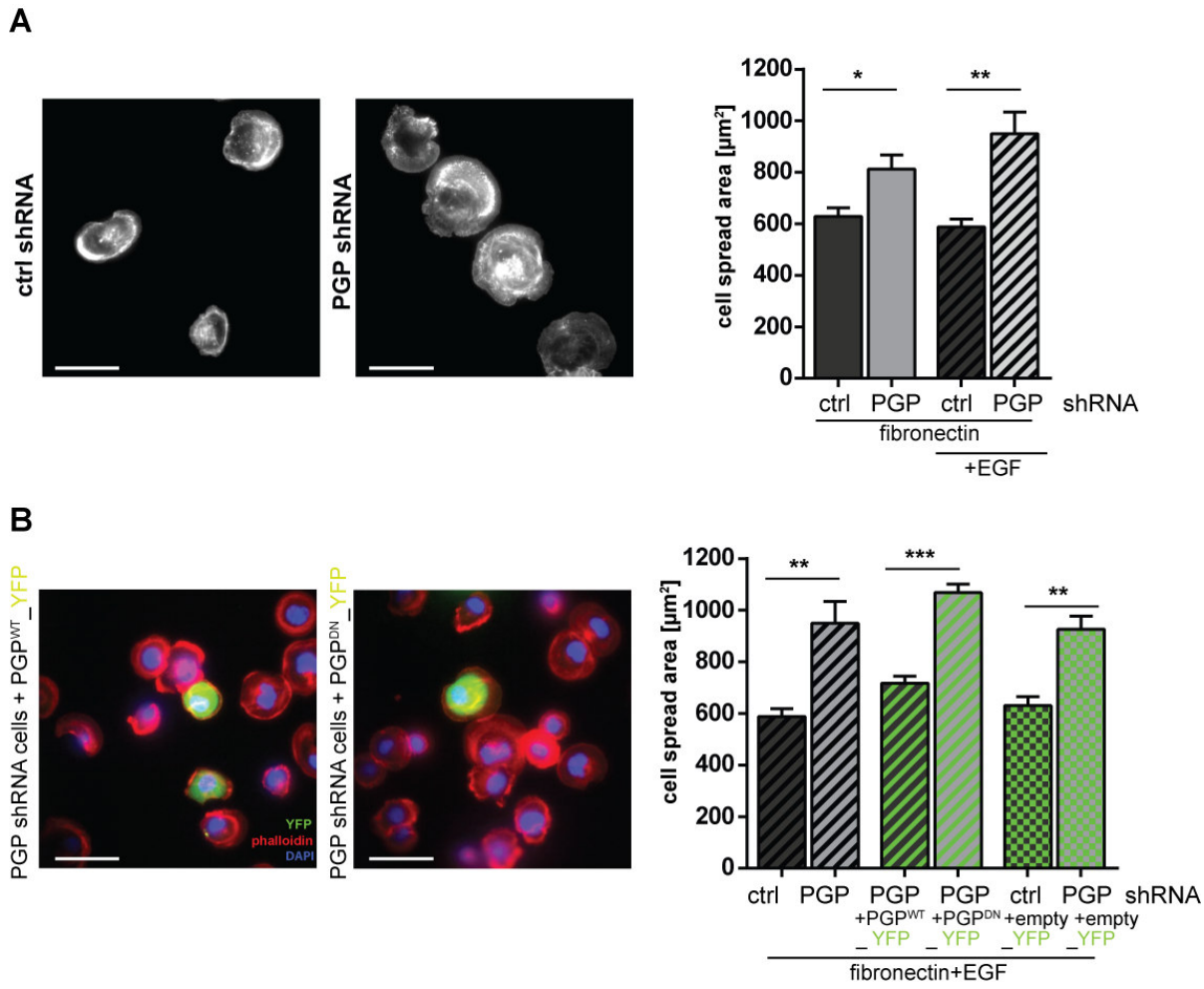

Figure 24: Cell spreading assays.
A: For immunofluorescence analysis and quantification of cell spreading, control shRNA and PGP shRNA expressing cells were seeded on 6-cm dishes and serum-starved after 4 hours. The next day, cells were washed with PBS, trypsinized, resuspended in starving medium containing 0.1% BSA and stimulated or not with EGF (100 ng/mL). Cells were plated on a 8-well slides, precoated with fibronectin (10 µg/mL) and allowed to spread for 10 minutes before fixation and staining with Alexa 488-conjugated phalloidin to visualize cell area and with DAPI to counterstain the nuclei. Cells were imaged with a Nikon epifluorescence microscope. Cell areas [µm^2] of 30-50 cells per condition were determined by using ImagePro software. Results are mean values ± S.E.M. of n=5 independent experiments. *, p< 0.05; **, p< 0.01.
B: To analyze whether effects on cell spreading were dependent on PGP activity, PGP add-back experiments were performed. PGP-silenced cells were transfected with PGP^{WT} or the inactive point mutant PGP^{DN} to endogenous PGP expression levels. Cell spreading assays were performed as explained in **A,** and cells were additionally stained with an α-YFP/GFP antibody to identify transfected cells. Cell areas [µm^2] of 30-50 YFP-positive cells were determined. n=5 (non-transfected cells) and n=6 (PGP^{WT} or PGP^{DN} transfected cells) independent experiments were performed. As a control experiment control shRNA or PGP shRNA expressing cells were transfected with an empty-YFP vector and cell spreading of the YFP-positive cells were determined as described above. Results are mean values ± S.E.M. of n=3 independent experiments. Data are expressed as mean + S.E.M. **, p< 0.01; ***, p< 0.001.

Taken together, these data demonstrated that PGP phosphatase activity regulates RTK- and integrin- induced cell spreading and that cells lacking PGP activity formed more CDRs and displayed accelerated cell spreading.

Whereas some key players of CDR formation signaling have recently been identified (Hoon et al., 2012), signal pathways leading to the formation of dorsal ruffles after growth factor stimulation remain poorly understood. Integrin- and growth factor signaling lead to the activation of Src family kinases, resulting in the activation of PI3 kinase (PI3K). PI3K phosphorylates phosphatidylinositol (4,5)-bisphosphate (PIP_2) to phosphatidylinositol (3,4,5)-trisphosphate (PIP_3). PIP_3 accumulation leads to the recruitment of the large GTPase dynamin to the plasma membrane. Increased PI3K activity also activates the small GTPase Rac1. Dynamin recruitment (Krueger et al., 2003) and Rac1 activation (Welch et al., 2003, Dharmawardhane et al., 2000) subsequently result in the formation of CDRs.

To investigate the effect of CDR on RTK- and integrin- induced cell spreading, CDR formation was blocked by pharmacological inhibition of important signaling molecules that have been implicated in CDR formation. Src family kinase (SFK) activities were blocked with PP2, PI3K activity with wortmannin and the activity of dynamin with dynasore (**Figure 25**).

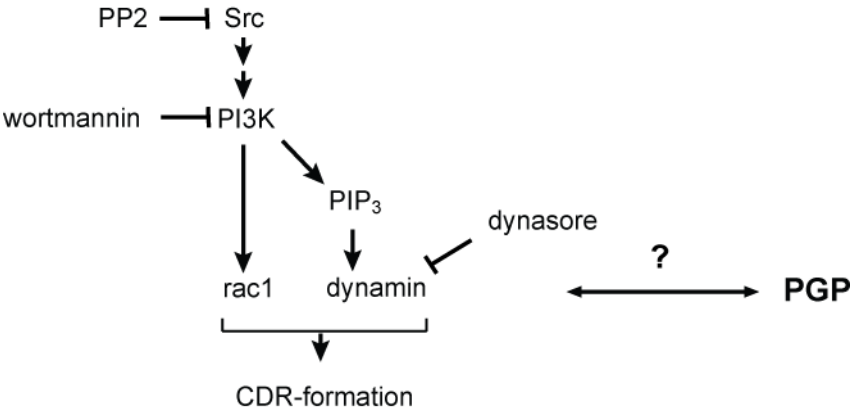

Figure 25: Simplified model of key signaling pathways involved in CDR-formation.
Pharmacological inhibitors that were used to probe PGP-dependent CDR formation are indicated.
The figure is adapted from (Hoon et al., 2012).

The inhibition of PI3K and dynamin activities led to a complete blockade of CDR formation. Treatment with PP2 normalized the PGP-dependent effect on CDR formation (see **4.1.2.2**).

To examine the impact of CDR formation on cell spreading, control shRNA and PGP shRNA expressing cells were serum-starved overnight before treatment with either wortmannin, dynasore, or PP2 for 30 minutes. The cells were brought in suspension, and inhibitors with a reversible mode of action (PP2 and dynasore) were added again. After stimulation with EGF, cells were plated on a fibronectin-precoated well. The inhibition of SFK activities, PI3K activity as well as the inhibition of dynamin activity led to a complete normalization of PGP-dependent effects on integrin- and RTK- induced cell spreading (**Table 1**).

Table 1: Inhibition of CDR formation signaling proteins.
In control (ctrl) shRNA and PGP shRNA expressing GC1 cells, activities of Src family kinases were blocked with PP2 (10 µM), PI3K activity with wortmannin (50 nM) and dynamin activity with dynasore (100 µM). The cells were stimulated with EGF and allowed to spread for 10 min on fibronectin-coated wells. The area of 30-50 cells per condition was determined by using ImagePro software. n=4 independent experiments were performed. Data are expressed as means ± S.E.M. ns = not significant.

	control		PP2		wortmannin		dynasore	
shRNA	ctrl	PGP	ctrl	PGP	ctrl	PGP	ctrl	PGP
cell area [µm²] (mean± S.E.M.)	588.0 ± 30.3	949.6 ± 84.4	785.3 ± 117.7	729.3 ±136.2	530.0 ± 14.1	475.3 ±15.9	716.0 ±98.1	644.5 ±83.6
p-value:	0.0038		ns		ns		ns	

These data argued that PGP activity regulated RTK- and integrin-induced cell spreading in a CDR-dependent manner.

4.1.1.4 Loss of PGP activity increases cell spreading of mouse lung endothelial cells

Cell spreading as well as cell adhesion are cellular processes, which have to be well coordinated, for example in endothelial cells to ensure vascular integrity (Dejana et al., 2009).

To investigate if cell spreading of endothelial cells is also regulated in a PGP-dependent manner, mouse lung endothelial cells (MLECs) were isolated from lungs of 6 day-old *Pgp*$^{flx/flx}$; and *Pgp*$^{flx/flx}$*; Tie2-cre*$^{+/-}$mice, and spreading assays of wildtype and PGP-inactivated MLECs were performed. Consistent with the results obtained in GC1 cells, PGP-inactivated endothelial cells displayed larger cell spread areas after seeding on fibronectin (**Figure 26A**) and the co-activation of integrins and RTKs increased PGP-dependent effects on cell spreading (**Figure 26A**). Thus, elevated cell spreading of PGP-depleted GC-1 cells was confirmed in genetically PGP-inactivated endothelial cells.

To examine whether the genetic approach lead to the expression of the same levels of wildtype-PGP and catalytic inactive PGP, lysates of endothelial cells isolated from *Pgp*$^{flx/flx}$; and *Pgp*$^{flx/flx}$*; Tie2-cre*$^{+/-}$mice were run in a SDS-gel and immunoblotted using an antibody against endogenous PGP. It was shown that PGP^{WT} and PGP^{DN} were expressed in comparable levels. (**Figure 26B**).

Flow cytometry was used to examine relative cell sizes of wildtype and PGP-inactivated MLECs. The cells were either unstarved or starved overnight.

In both cases, cell sizes of endothelial cells lacking PGP activity were comparable to wildtype endothelial cells (**Figure 26C**).

Thus, it was demonstrated that loss of PGP activity led to elevated RTK- and integrin-mediated cell spreading, and that this was not due to differences in cell size or PGP^{WT}/PGP^{DN} expression levels.

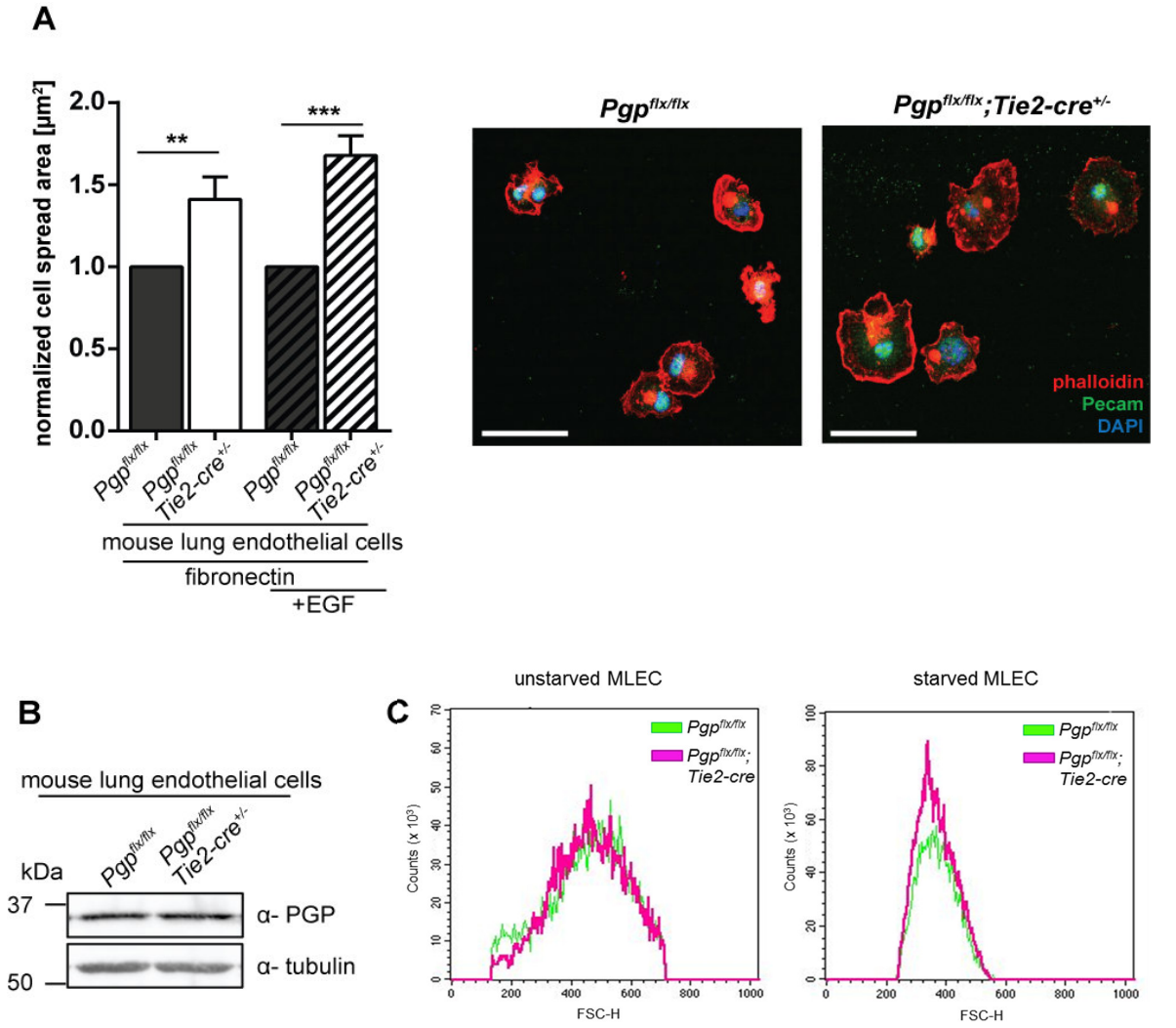

Figure 26: Effects of PGP on cell spreading of mouse lung endothelial cells (MLECs).
A: Endothelial cells were isolated from lungs of *Pgp*$^{flx/flx}$; and *Pgp*$^{flx/flx}$*; Tie2-cre*$^{+/-}$mice. The cells were serum-starved overnight, brought in suspension, stimulated or not with EGF (100 ng/mL) and allowed to spread on fibronectin-precoated surfaces for 15 min. Afterwards, cells were stained with phalloidin to identify the cell area, with DAPI to counterstain the nuclei and with a α-Pecam antibody to identify endothelial cells. Cells were imaged with a Nikon epifluorescence microscope and cell areas [µm²] of 30 MLECs per genotype and condition were determined. Results are normalized mean values of cell spread areas ± S.E.M. of n=3 independent experiments.
**, p< 0.01; ***p, < 0.001.
B: PGP expression levels were analyzed by immunoblotting of cell lysates of mouse lung endothelial cells isolated from *Pgp*$^{flx/flx}$; and *Pgp*$^{flx/flx}$*; Tie2-cre*$^{+/-}$mice using and α-PGP antibody.
C: Cell sizes of unstarved and starved endothelial cells were analyzed with flow cytometry. Forward light scatter (FSC-H) was measured.

4.1.1.5 PGP regulates cell migration

The results obtained so far demonstrate that PGP activity regulates CDR-formation, cell adhesion and spreading in an integrin and RTK-dependent manner. In order to investigate whether PGP is also involved in the regulation of cell migration, time-lapse experiments were performed. Cell migration of GC1 cells upon integrin activation was analyzed first. Control shRNA and PGP shRNA expressing cells were seeded on fibronectin and serum-starved overnight before the experiment was started. Cell migration was monitored for 17 hours. Single cell tracks were analyzed and the accumulated distance was determined. PGP-depleted cells showed a significant increase in migration (**Figure 27A**). To investigate if co-stimulation of integrins and RTKs affects PGP-dependent cell migration, cells were plated on fibronectin and serum-starved overnight. The experiment was started by the addition of EGF into the medium and the accumulated distance after 17 hours was analyzed. Consistent with the effects of RTK- and integrin- co-stimulation on PGP-dependent cell spreading, stimulation of both receptors classes further increased the difference in migration between control shRNA and PGP shRNA expressing cells.

In the next step, the impact of different fibronectin concentrations on PGP-dependent cell migration was assessed. Cell motility is a balance between cell adhesion and cell migration. Low fibronectin concentrations lead to decline of adhesive force between the cell and its substratum, resulting in a decrease of cell migration. Likewise, high fibronectin concentrations can also lead to an attenuation of cell motility because fibronectin-mediated cell adhesion predominates over cell migration (DiMilla et al., 1993). Thus, cell migration as function of fibronectin concentration results in a Gaussian distribution curve, depicted in a simplified manner in **Figure 27B**.

Cells were seeded on different fibronectin concentrations and serum-starved overnight. The next day, cells were stimulated or not with EGF. The experiment was started and the accumulated distance after 17 hours was analyzed. In every condition PGP-depleted cells show elevated cell migration and the effect was further augmented upon EGF stimulation. The highest accumulated distance and thus, cell speed was observed at low fibronectin levels (2.5 µg/mL). High fibronectin concentrations (>10 µg/mL) led to a shift from cell migration to the side of cell adhesion, resulting in decreased cell motility. Interestingly, the PGP-dependent effect on cell migration was also observable without integrin- and RTK activation (**Figure 27C**).

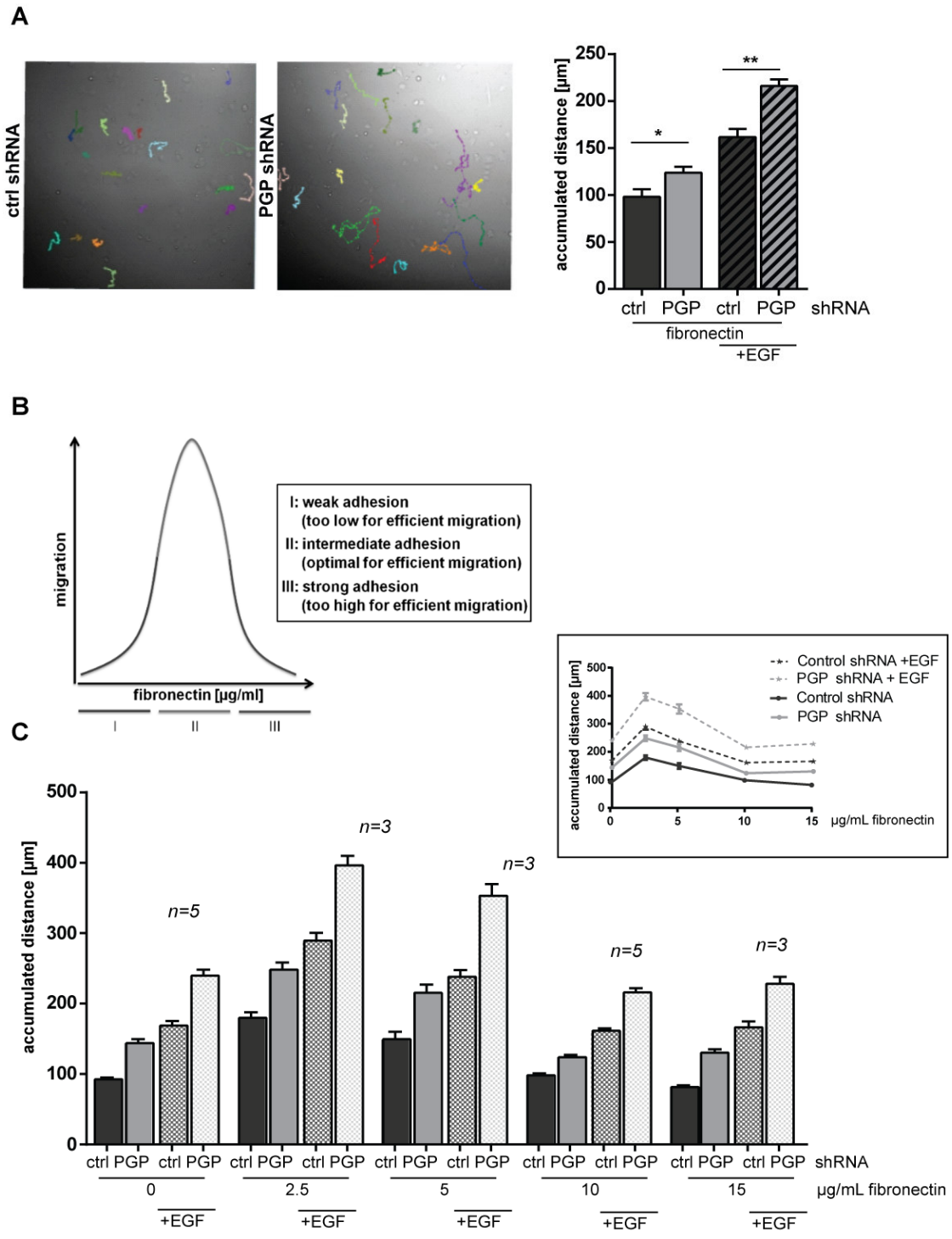

Figure 27: Analysis of PGP-dependent cell migration.
A: For 2D-migration assays, PGP shRNA and control shRNA expressing cells were seeded on 8-well slides, pre-coated with fibronectin (10 µg/mL). After 4 hours, cells were serum-starved overnight and stimulated or not with EGF (100 ng/mL). The accumulated distance was monitored in a Nikon epifluorescence microscope for 17 hours and determined by tracking 40 cells per condition using ImagePro software. n=5 independent experiments were performed Data are expressed as means ± S.E.M. *, p< 0.05; **, p< 0.01.
B: Scheme representing the effect of different fibronectin concentrations on the balance of cell adhesion and cell migration.
C: 2D-migration assays with various concentrations of fibronectin (0-15 µg/mL). PGP shRNA and control shRNA expressing cells were seeded on 8-well slides, pre-coated with different concentrations of fibronectin. After 4 hours, cells were serum-starved overnight and were stimulated or not with EGF (100 ng/mL). The accumulated distance was monitored in a Nikon epifluorescence microscope for 17 hours and determined by tracking 40 cells per condition using ImagePro software. The number of n independent experiments performed for each condition is indicated above the bars.

4.1.1.6 PGP inactivation in lymphocytes lead to an increase in cell migration

To investigate PGP-dependent cell motility in primary cells, lymphocytes were isolated from lymph nodes of *Pgp*$^{flx/flx}$; and *Pgp*$^{flx/flx}$*; Tie2-cre*$^{+/-}$ mice. Lymphocytes are fast moving cells and a well-established cell model to analyze cell migration.

By performing a genomic PCR screening of isolated lymphocytes, the purity of the cells was confirmed and it was demonstrated that our genetic approach led to the removal of the *Pgp*$^{flx/flx}$ intron in lymphocytes (**Figure 28A**).

As a first step, lymphocyte motility was analyzed in a 2D-migration assay. To this end, lymphocytes were activated overnight by stimulation with α-CD3 and α-CD28 antibodies. The co-stimulation partially mimics stimulation by antigen-presenting cells and activates the T-cell receptor (Zappasodi et al., 2008). Additionally, the autocrine cytokine IL-2 was added to boost activation (Weiss and Littman, 1994, Cho et al., 2013). The next day, cells were seeded on dishes precoated with the intercellular adhesion molecule-1 (ICAM-1). ICAM-1 is expressed on the surfaces of endothelial cells and lymphocytes and is a ligand of the lymphocyte function-associated antigen-1 (LFA-1, αLβ2), an integrin found on lymphocytes. As a chemoattractant stromal derived factor-1 (SDF-1) also known as C-X-C motif chemokine 12 (CXCL12) was added or not to the medium. SDF-1 is a cytokine usually produced in inflamed areas to induce the recruitment of lymphocytes. Cell migration was monitored for only 30 minutes. Single cell tracks were analyzed and the accumulated distance was determined. Interestingly, PGP-inactivated primary lymphocytes showed no difference in cell migration in the absence of the chemokine SDF-1. However, in the presence of the chemoattractant, PGP-inactivated lymphocytes displayed significant higher accumulated distances (**Figure 28B**). To investigate the effect of PGP activity on lymphocyte migration further, transwell assays in Boyden chambers were performed. By adding a chemoattractant to the lower chamber, a concentration gradient is generated and cells start to migrate towards higher concentrations of the chemoattractant. In contrast to 2D-migration assays, in which un-directed cell migration (chemokinesis) can be analyzed, transwell assays allow analysis of directed cell migration. The semi-permeable membrane of the insert was coated with fibronectin and 10% FCS was initially added to the medium as chemoattractant (**Figure 28C**). Cells were inoculated into the upper chamber and those, which transmigrated through the pores of the membrane and reached the lower chamber after a defined time, were quantified semi-automatically with an epifluorescence microscope. A higher number of PGP-inactivated lymphocytes migrated through the membrane and was counted in the lower chamber. Next, SDF-1 was used as chemoattractant. PGP-inactivated lymphocytes again displayed elevated migration levels (**Figure 28C**). However, without fibronectin coating (that is, without integrin activation), no difference was observable (**Figure 28C**). Without supplying a chemoattractant cell migration

was also comparable in transgenic and wildtype lymphocytes (**Figure 28C**). This was consistent with the results made in the 2D-migration assays.

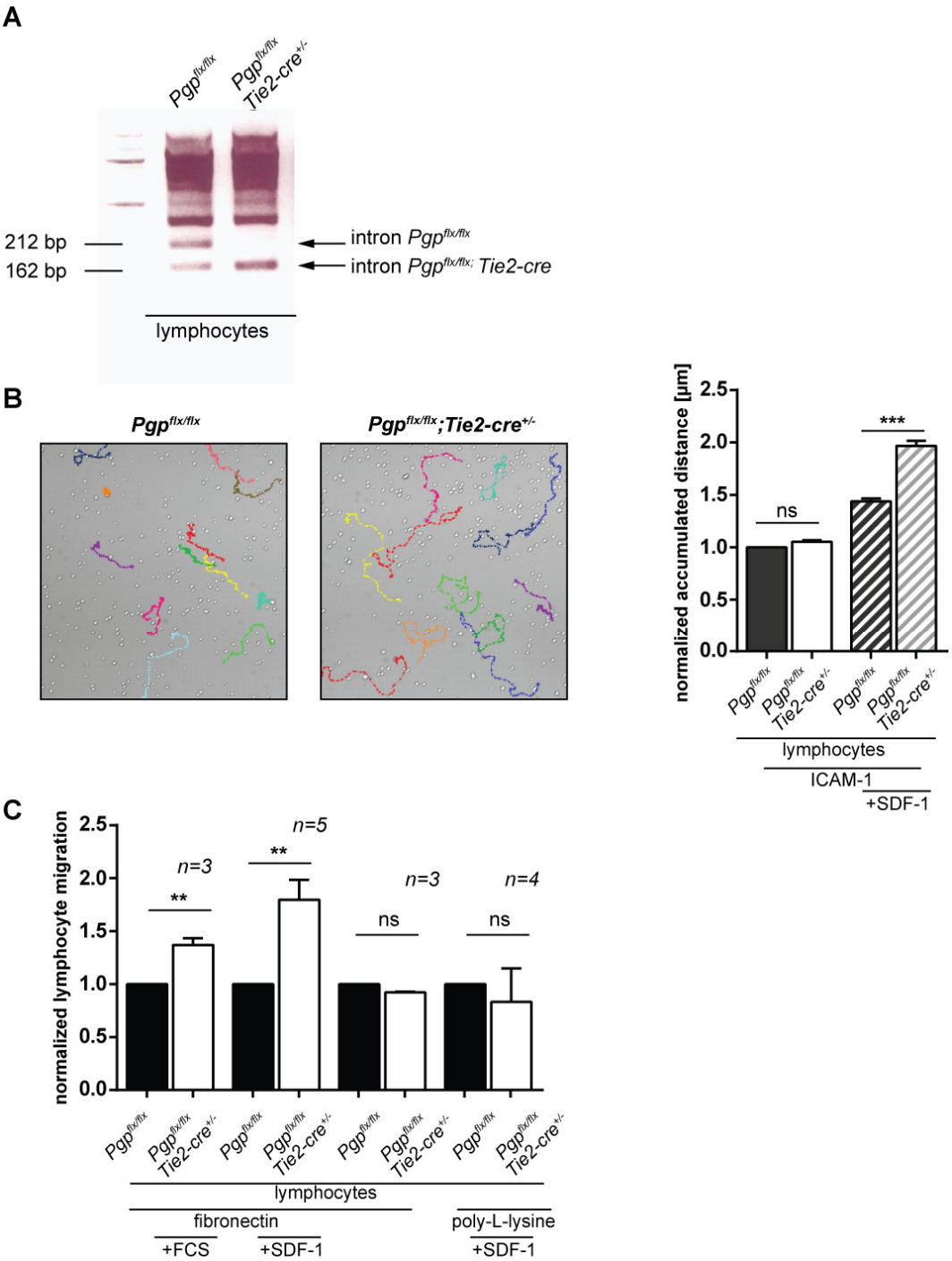

Figure 28: Analysis of PGP-dependent lymphocyte migration.
A: Genotyping by PCR. The wildtype or targeted *Pgp* allele is detected at 212 or 163 bp, respectively.
B: For 2D-migration assays, lymphocytes were activated overnight by co-stimulation with α-CD3/α-CD28 antibodies and with IL-2, and seeded on 8-well slides pre-coated with ICAM-1 (3 µg/mL). The next day, cells were stimulated or not with SDF-1 (200 ng/mL). The accumulated distance was monitored with a Nikon epifluorescence microscope for 30 minutes and determined by tracking 40 cells per condition using ImagePro software. n=3 independent experiments were performed. Data are expressed as normalized means of the accumulated distance ± S.E.M.
***, $p < 0.001$. ns = not significant.
C: Lymphocytes were kept in culture for 24 hours before performing transwell assays. The membrane of the insert was coated either with fibronectin or poly-L-lysine. A chemoattractant (either 10% FCS or 200 ng/mL SDF-1) or no chemoattractant was added. Results are normalized mean values ± S.E.M. The number of n independent experiments performed for each condition is indicated above the bars. **, $p < 0.01$. ns = not significant.

EGFR is thought to be absent in hematopoietic cells. However, there are some reports that suggest that EGFR signaling plays also a role within the immune system (Zaiss et al., 2013, Chan et al., 2009). Hence, EGF as chemoattractant was tested. However, there was no directed cell migration observable (data not shown). Thus, EGF turned out to be an unsuitable chemoattractant for lymphocytes.

Taken together, PGP-dependent lymphocyte migration occurred in an integrin- and SDF-1-dependent manner. SDF-1 is a ligand of the C-X-C chemokine receptor type 4 and 7 (CXCR4 and CXCR7), which belong to receptor classes of G-protein coupled receptors (GPCRs). Downstream effects are G_i protein-mediated. Thus, the co-activation of both receptor classes was essential for the PGP-dependent effects on lymphocyte migration. The impact of PGP depletion on cell motility was confirmed in PGP-inactivated lymphocytes. Thus, it was demonstrated that cell motility is regulated by PGP phosphatase activity.

4.1.2 Molecular mechanisms of PGP-dependent effects on CDR formation, cell spreading and cell migration

To understand how PGP regulates CDR-formation, cell spreading and cell migration, PGP-dependent signaling has to be clarified in more detail. The data obtained so far indicated that cellular effects can take place downstream of three surface receptor classes, namely integrin-, RTK- and G-protein coupled-receptors (**Figure 29**).

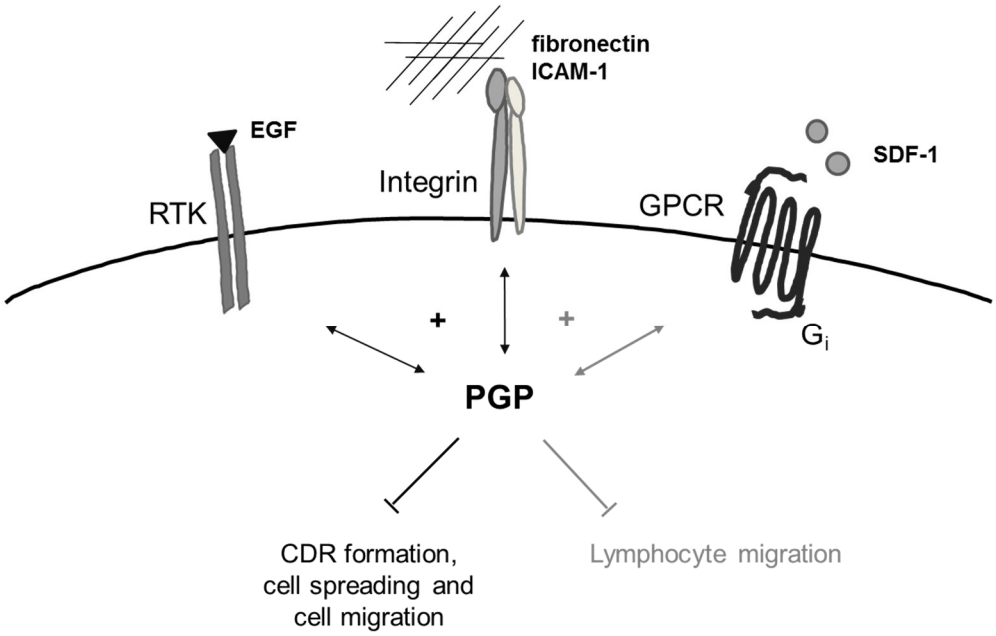

Figure 29: Model of PGP-dependent signaling.
PGP is a negative regulator of CDR-formation, cell spreading and cell migration downstream of integrin-, RTK- and GPCR signaling.

4.1.2.1 Role of PGP in EGF-receptor signaling

Because PGP was identified as a tyrosine-directed phosphatase involved in RTK signaling, it initially was investigated if PGP affects EGF receptor signaling on receptor level. As described in **1.4.2**, PGP-depleted cells show an increase in tyrosine-phosphorylated proteins 3 min after EGF stimulation. The EGFR is a ~180 kDa tyrosine kinase receptor, and EGF binding leads to auto-phosphorylation on multiple tyrosine residues (Bazley and Gullick, 2005). As a consequence, various adaptor- and scaffolding- proteins are recruited to propagate growth factor signaling affecting for example cytoskeletal changes, cell adhesion and motility (Biscardi et al., 2000). In a peptide screen with over 720 tested phospho-peptides, the EGFR itself and some of its downstream signaling molecules have appeared as possible substrates of PGP (Seifried et al., 2014). Additionally, it was shown that total EGFR expression levels were increased after PGP depletion, and that tyrosine residue 1045 of the EGFR, which plays a potential role in EGFR ubiquitination and trafficking (Grovdal et al., 2004) was hyper-phosphorylated in PGP-depleted cells upon EGF stimulation (PhD thesis; Prashant Duraphe). These results argued that an increase in total EGFR levels might be due to changes in receptor ubiquitination and degradation.

After co-stimulation with fibronectin and EGF, elevated EGFR expression levels were observed in PGP-deficient compared to control shRNA cells (**Figure 30A**). Interestingly, the difference was most pronounced after 3 minutes of EGF treatment. To examine the phosphorylation status of the receptor upon integrin and EGFR co-activation, cells expressing either control shRNA or PGP shRNA were seeded on fibronectin and serum-starved overnight. The next day, cells were stimulated with EGF (100 ng/mL) for different time points before cell lysis. The lysates were used for Western blot analysis of phosphorylation levels using phospho-specific antibodies against different phosphorylation sites of the EGF receptor. Due to technical limitations, the same blot could subsequently not be re-probed with other phospho-specific EGFR antibodies. Cell lysates from the same experiment were therefore loaded on separate gels and probed for total EGFR expression and changes in phosphorylation levels. Protein expression was adjusted to tubulin expression as a loading control, and possible differences in the phosphorylation status were adjusted to total EGFR levels. The EGF receptor was hyper-phosphorylated in PGP-depleted cells on two auto-phosphorylation sites, tyrosine residues 1068 and 1173 upon three minutes of EGF stimulation and co-activation with fibronectin (**Figure 30B**). Phosphorylation on tyrosine 1068 leads to GRB2 or GAB1 binding and subsequently activates downstream signaling pathways via RAS GTPase and MAP kinase activation to regulate actin-based cell motility (Giubellino et al., 2008). Phosphorylated tyrosine residue 1173 provides a docking site of SHC scaffold protein, and signaling proteins such as PLCγ1 can bind to this residue and subsequently get activated (Soler et al., 1994, Kim et al.,

1991, Rotin et al., 1992). Without EGF treatment, no phosphorylation of these two tyrosine residues was detectable. Interestingly, already 5 minutes after EGF stimulation, no significant differences in phosphorylation levels of tyrosine 1068 and 1173 were observable any more when comparing control shRNA and PGP shRNA expressing cells, indicating that PGP-dependent effects on RTK signaling occurred very early upon stimulation and were rapidly reversible.

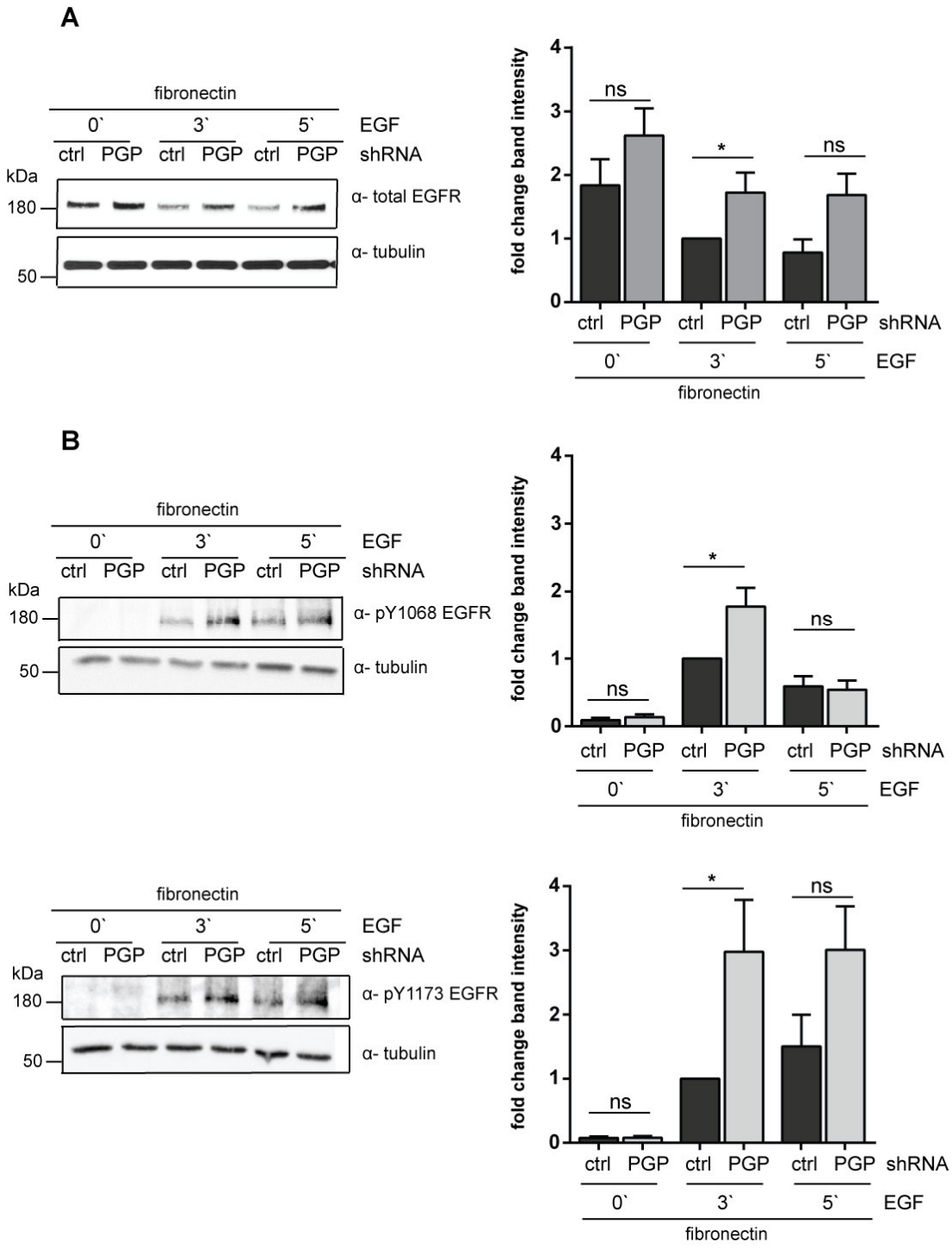

Figure 30: Effects of PGP on EGF receptor expression and phosphorylation levels upon co-stimulation with EGF and fibronectin.
A: Densitometric analysis of total EGF receptor expression levels. Control shRNA and PGP shRNA expressing GC1 cells were seeded on fibronectin and serum-starved overnight. The next day, cells were stimulated with EGF (100 ng/mL) for different time points. The cells were lysed on ice. To determine EGF receptor levels lysates were immunoblotted and probed for total EGFR and for α-tubulin to control for comparable protein loading. The densitometric analysis of EGFR band intensities normalized to α-tubulin is displayed beside. n=5 independent experiments were performed. Results are normalized mean values ± S.E.M. *, $p < 0.05$. ns = not significant.
B: Densitometric analysis of tyrosine 1068- (top) and tyrosine 1173- (bottom) phosphorylated EGF receptor. Control shRNA and PGP shRNA expressing GC1 cells were treated as explained in **A**. To determine EGF receptor phosphorylation status lysates were immunoblotted and probed for tyrosine 1068 phosphorylated EGFR and for α-tubulin to control for comparable protein loading. The densitometric analysis of band intensities normalized to α-tubulin and total EGFR amounts is displayed beside. n=4 independent experiments were performed. Results are normalized mean values ± S.E.M. *, $p < 0.05$. ns = not significant.

4.1.2.2 PGP regulates CDR–formation and cell migration by modulating PLCγ1 activity downstream of Src kinase family signaling

To elucidate the signaling pathways affected by PGP in more detail, key enzymes downstream of the EGF receptor, which may play a role in the cross-signaling between integrins and GPCRs, were inhibited pharmacologically.

The role of phospholipase C (PLC), a key protein family that acts downstream of the EGF receptor was analyzed first. The mammalian PLC family consists of thirteen members classified according to their structural properties into six isoform classes, namely PLCβ, PLCγ, PLCδ, PLCε, PLCζ and PLCη. PLC can hydrolyze the membrane-bound phospholipid phosphatidylinositol 4,5-bisphosphate (PIP_2) into diglycerides (DG) and inositol 1,4,5-trisphosphate (IP_3) (Kadamur and Ross, 2013). Thus, PLC can transduce signals that activate extracellular plasma membrane receptors such as integrins or the EGF receptor to mediate cellular effects. The isoform PLCγ1 for example was identified as an integrator of integrin and EGF receptor signaling to regulate cell motility (Jones et al., 2005, Piccolo et al., 2002).

To analyze the role of PLC in integrin-, RTK- and GPCR- induced PGP-dependent effects the pan-PLC activity inhibitor U73122 and its negative control U73343 were used.

Control shRNA and PGP shRNA expressing GC1cells were treated with U73122 or its negative control prior to analysis of CDR formation. The inhibition of PLC activity led to a normalization of CDR-formation levels, whereas treatment with the negative control did not (**Figure 31A**).

Furthermore, U73122, but not U73343 (negative control) treatment of lymphocytes abolished the increased chemotaxis observed upon PGP inactivation (**Figure 31B**).

As described in **4.1.2.1**, it has been reported that the PLC isoform PLCγ1 is recruited to the EGF receptor upon EGF stimulation (Soler et al., 1994). PLCγ1 binds to different tyrosine residues of the EGF receptor and subsequently gets activated (Kim et al., 1991). In addition, PLCγ1 has been involved in integrin signaling to mediate cell adhesion (Tvorogov et al., 2005). The fact that PLCγ1 has been implicated in both integrin and growth factor signaling suggested that PLCγ1 may function in PGP-dependent signaling.

PLCγ1 can be phosphorylated on different tyrosine residues. By determination of the phosphorylation level on tyrosine 783 (Y783), it is possible to make a statement about PLCγ1 activity (Kim et al., 1991). Besides to activation after RTK binding, PLCγ1 is activated by Syk kinase-mediated phosphorylation on Y783 (Law et al., 1996). The receptor-type protein tyrosine phosphatase PTPmu can dephosphorylate PLCγ1 on Y783, leading to attenuation of PLCγ1-mediated cellular processes such as cell migration (Phillips-Mason et al., 2011).

The role of PLCγ1 was examined in more detail. By Western blot analysis, phosphorylation levels on Y783 of PLCγ1 were analyzed in GC1 cells. PGP-depleted cells seeded on poly-L-lysine, serum-starved overnight and stimulated for three minutes with EGF displayed higher phosphorylation levels compared to control shRNA expressing cells (**Figure 31C**). This was even clearer when cells were plated on fibronectin-precoated wells and co-stimulated with EGF. Without EGF treatment, only a slight phosphorylation of tyrosine 783 was detectable, and no difference between control- and PGP shRNA cells was observable (**Figure 31D**).

PLCγ1 can also be activated in a Src-dependent manner (Haendeler et al., 2003). To test if altered Src activity influences changes in phosphorylation levels of PLCγ1, phosphorylation levels on tyrosine residue 416, the mayor activation site of Src (Roskoski, 2005), was examined. There were no detectable differences between control shRNA and PGP shRNA expressing cells (**Figure 31D**).

Taken together, these results argued that PGP regulates CDR-formation as well as lymphocyte motility downstream of PLC signaling. PLCγ1 was hyper-activated upon EGF stimulation in PGP-depleted cells and this was even more marked after co-stimulation of integrins.

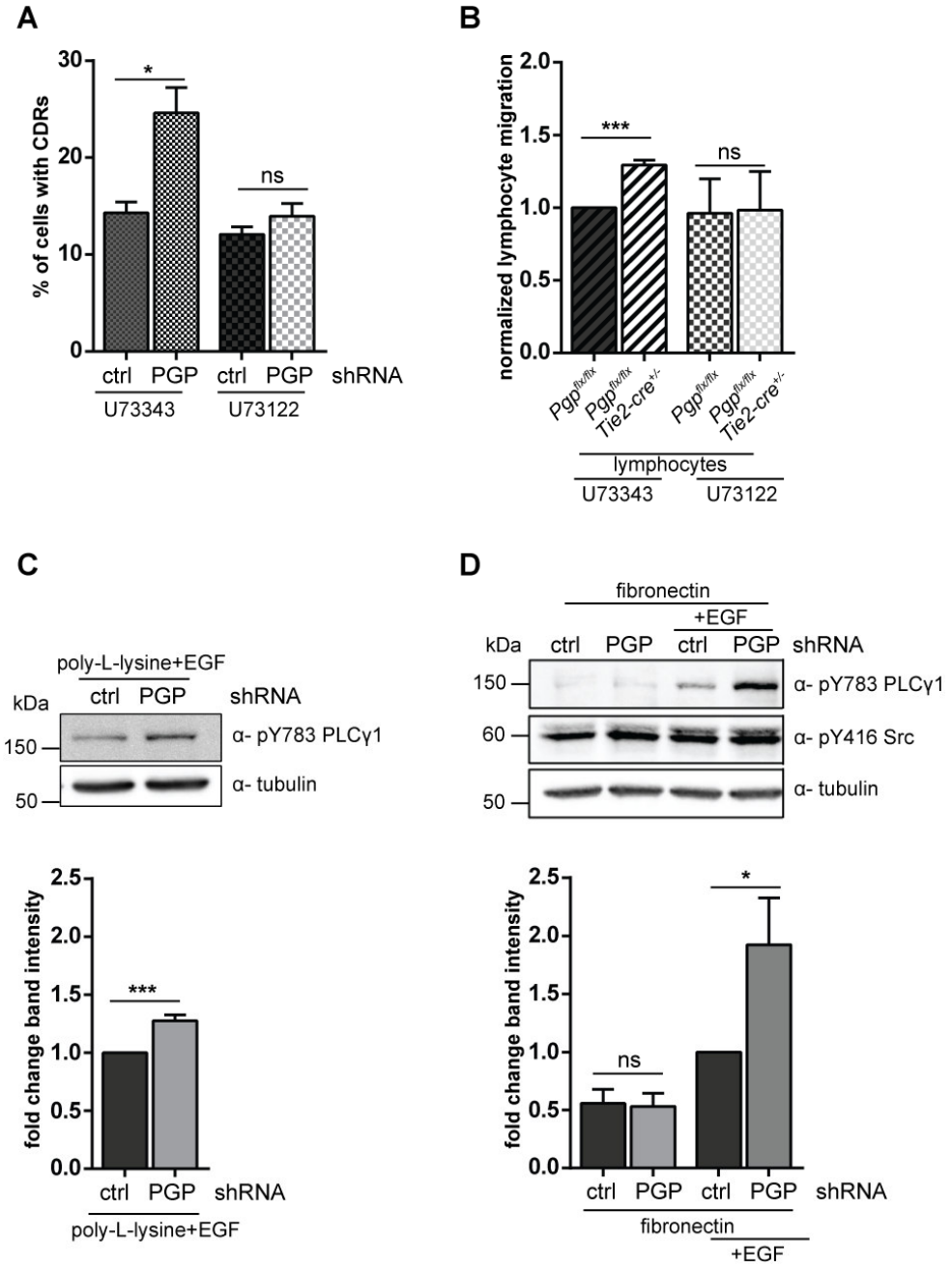

Figure 31: Analysis of PLC-mediated effects on PGP-dependent CDR formation and lymphocyte migration.
A: Quantification of CDR formation of control shRNA and PGP shRNA expressing GC1 cells pretreated with phospholipase C inhibitor U73122 (0.5 µM) or its negative control U73343 (0.5 µM).The inhibition normalizes PGP-dependent effects on CDR formation. n=5 independent experiments were performed. Data are expressed as means ± S.E.M. *, p< 0.05. ns = not significant.
B: Analysis of migration of lymphocytes isolated from *Pgp$^{flx/flx}$*; and *Pgp$^{flx/flx}$; Tie2-cre$^{+/-}$*mice with PLC inhibitor U73122 (0.5 µM) or its negative control U73343 (0.5 µM). PLCγ inhibition normalizes PGP-dependent effect on lymphocyte migration. Results are normalized mean values ± S.E.M. of n=3 experiments. ***, p< 0.001.
C: Densitometric analysis of tyrosine 783 phosphorylated PLCγ 1. Control shRNA and PGP shRNA expressing cells were seeded on poly-L-lysine and serum-starved overnight. The next day, cells were stimulated with EGF (100 ng/mL). After 3 minutes of stimulation, the cells were lysed on ice. To determine PLCγ1 activity the cell lysates were immunoblotted and probed for Y783 phosphorylated PLCγ1 and for α-tubulin to control for comparable protein loading. The densitometric analysis of band intensities normalized to α-tubulin is displayed below. n=9 independent experiments were performed. Results are normalized mean values ± S.E.M. *, p< 0.05.
D: Control shRNA and PGP shRNA expressing cells were seeded on fibronectin and serum-starved overnight. On the next day the cells were stimulated or not with EGF (100 ng/mL).Cell lysates were prepared as described above, were immunoblotted and probed for Y783 phosphorylated PLCγ1, for tyrosine 416-phosphorylated Src and for α-tubulin to control for comparable protein loading. The densitometric analysis of band intensities normalized to α-tubulin is displayed below. Results are normalized mean values ± S.E.M. of n=7 experiments. *, p< 0.05.

Src family kinase (SFK) members including the tyrosine kinases Src, Hck, Fyn, Lck, Lyn and Yes1 play a key role in intracellular signal transduction (Parsons and Parsons, 2004). Src is the prototype of this family and ubiquitously expressed. It acts downstream of integrin-, EGFR- as well as GPCR- signaling and is implicated in CDR-formation, cell spreading and migration.

To test if Src activity plays a role for PGP-dependent effects in general, its activity was inhibited with the SFK inhibitor PP2. Treatment of control shRNA and PGP shRNA expressing cells with PP2 led to a normalization of CDR-formation, whereas treatment with the negative control PP3 did not (**Figure 32A**). Lymphocyte migration was examined in transwell assays using cells isolated from *Pgp*$^{flx/flx}$; and *Pgp*$^{flx/flx}$*; Tie2-cre*$^{+/-}$ mice and treated with PP2 or its negative control PP3. Inhibition of Src kinase activities led to an equalization of lymphocyte migration levels (**Figures 32B**).

To analyze if SFK activity *per se* is essential for the PGP-dependent modulation of PLCγ1 activity, cells expressing either control shRNA or PGP-directed shRNA were seeded on fibronectin, treated with PP2 or its negative control PP3 and stimulated with EGF. PP2 treated cells exhibited no phosphorylation on tyrosine residue 783 and phosphorylation levels on tyrosine residue 527, the inhibitory site of Src kinase, was also unaltered (**Figure 32C**).

Taken together, PGP regulates PLCγ1 activation downstream of SFK signaling, whereas Src activity seems not to be affected, but required. Furthermore, these results do not exclude the possibility that other ubiquitously expressed SFK members such as Fyn and Yes are responsible for PGP-dependent effects on PLCγ1 activation, PLC-mediated CDR-formation and lymphocyte migration.

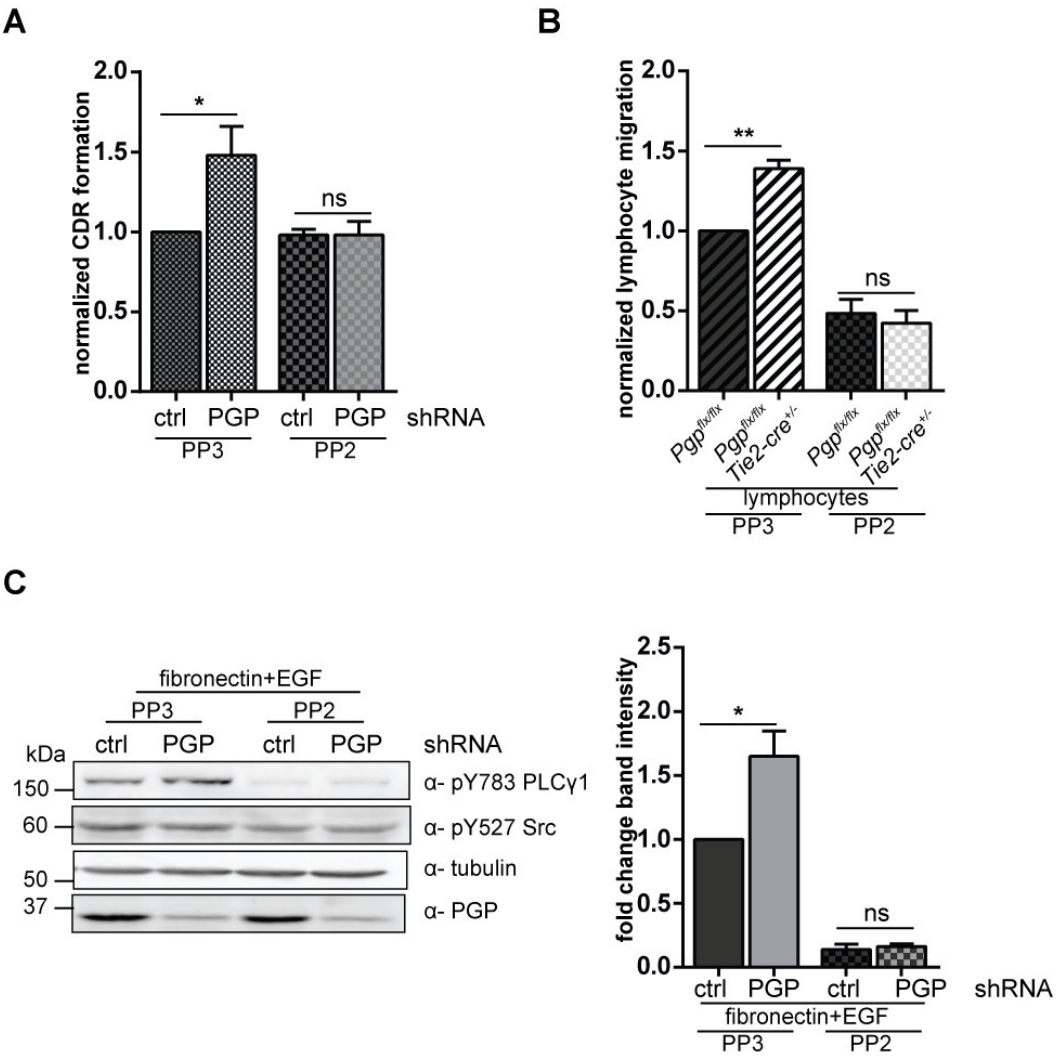

Figure 32: Analysis of the role of Src kinases for PGP-dependent cellular effects.
A: Quantification of CDR formation of control shRNA and PGP shRNA expressing GC1 cells pretreated with Src kinase inhibitor PP2 (10 µM) or its negative control PP3 (10 µM).The inhibition of Src kinase activities normalizes the PGP-dependent effects on CDR formation. n=5 independent experiments were performed.
Data are expressed as normalized means ± S.E.M. *, p< 0.05. ns = not significant.
B: Analysis of migration of lymphocytes isolated from *Pgp$^{flx/flx}$*; and *Pgp$^{flx/flx}$; Tie2-cre$^{+/-}$*mice, pretreated with Src kinase inhibitor PP2 (10 µM) or its negative control PP3 (10 µM). The inhibition of Src kinase activities normalizes PGP-dependent effects on lymphocyte migration. Results are normalized mean values ± S.E.M. of n=3 independent experiments. **, p< 0.005. ns = not significant.
C: Cells expressing control shRNA or PGP shRNA cells were seeded on fibronectin, serum-starved overnight, treated either with PP2 or with PP3 and stimulated with EGF for 3 minutes before cell lysis. The cell lysates were immunoblotted and probed for tyrosine 783-phosphorylated PLCγ1, for tyrosine 527-phosphorylated Src kinase and for α-tubulin to control for comparable protein loading. The densitometric analysis of band intensities normalized to α-tubulin is displayed in the right-hand panel. n=5 independent experiments were performed.
Data are expressed as normalized means ± S.E.M. *, p< 0.05. ns = not significant.

4.1.2.3 Decrease in PLCγ1 activity leads to a reduction of PKC-mediated effects

Activated PLCγ1 catalyzes the cleavage of the membrane phospholipid phosphatidylinositol 4,5-bisphosphat (PIP_2) to inositol 3-phosphate (IP_3) and diglycerides

(DG). DG stays membrane-bound, whereas IP_3 is released into the cytosol and can bind to its receptor at the endoplasmic reticulum resulting in calcium release (Kadamur and Ross, 2013). Calcium and DG activate protein kinases C (PKCs) at the plasma membrane.

PKCs belong to the large superfamily of serine /threonine kinases. By phosphorylation of their substrates, they mediate essential cellular signals for proliferation, actin reorganization, CDR-formation and cell motility (Even-Faitelson and Ravid, 2006, Xing et al., 2013, Laux et al., 2000). There are more than ten PKC isoforms known, which differ in tissue expression and function. They are subdivided into three classes based on their structure and activation mechanisms. Classical PKCs (cPKCs) contain α-, β_{1-}, β_{2-} and γ-isoforms. They get activated by calcium, DG and the phospholipid phosphatidylserine. The novel PKCs (nPKCs) consist of δ- , ε-, η-, and θ- isoforms. For their activation only DG is required. Thus, these two PKC classes get activated by the same second messengers that PLCs require for their activation. The last class consists of the atypical ζ-, and ι/λ-PKCs (aPKCs), which exclusively require phosphatidylserine for their activation (Mochly-Rosen et al., 2012).

To assay the impact of PKCs on PGP-mediated effects, their activity was inhibited using the pan-PKC inhibitor GÖ6983 (Gschwendt et al., 1996). Upon treatment with GÖ6983, CDR formation was completely normalized in control shRNA and PGP shRNA expressing cells (**Figure 33A**). Furthermore, directed primary lymphocyte migration, examined in transwell assays, was also normalized after treatment with the inhibitor (**Figure 33B**).

The main PKC isoform in lymphocytes is the novel PKC theta (Evenou et al., 2009). Using a specific inhibitor of this isoform, namely sotrastaurin, the elevated migration of PGP-deficient lymphocytes was also abolished (**Figure 33C**).

To investigate if hyper-activation of PLCγ1 leads to changes in PKC activity, a PKC activity assay was performed with lymphocytes isolated from *Pgp*$^{flx/flx}$; and *Pgp*$^{flx/flx}$*; Tie2-cre*$^{+/-}$mice. The assay is based on the specific phosphorylation of a pan-PKC peptide substrate precoated onto the assay wells. By using a phospho-specific antibody, phosphorylation levels of the PKC substrate can be detected as a measure of PKC activity. **Figure 33D** demonstrates that upon fibronectin and SDF-1 stimulation (that is, under the conditions that reveal PGP-dependent effects on lymphocyte migration), PKC was more active in PGP-inactivated lymphocytes. Without fibronectin and SDF-1 stimulation, PKC activity was unaltered.

Taken together, these data argue that the loss of PGP activity increases PLCγ1 activation downstream of Src kinase family signaling, leading to elevated PKC activity and finally to elevated PKC-mediated cellular effects such as CDR-formation and lymphocyte motility.

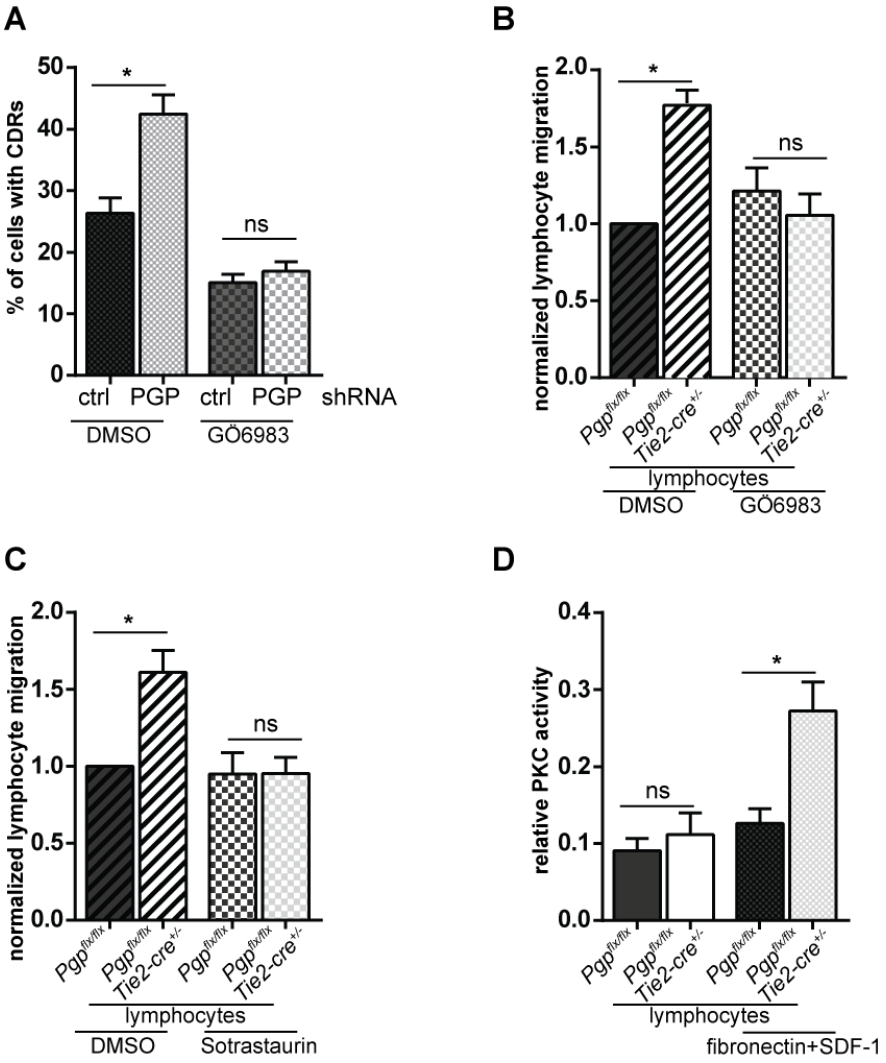

Figure 33: Role of protein kinase C for PGP-dependent cellular effects.
A: Quantification of CDR formation of control shRNA and PGP shRNA expressing GC1 cells pretreated with the pan-PKC inhibitor Gö6983 (3.3 µM) or with the same percentage of DMSO as control. PKC inhibition normalized PGP-dependent effects on CDR formation. n=5 independent experiments were performed. Data are expressed as means ± S.E.M. *, p< 0.05. ns = not significant.
B: Analysis of cell migration of lymphocytes isolated from *Pgp$^{flx/flx}$*; and *Pgp$^{flx/flx}$; Tie2-cre$^{+/-}$* mice, pretreated with the pan-PKC inhibitor Gö6983 (10 µM) or with the same percentage of DMSO as control. PKC inhibition normalizes PGP-dependent effects on lymphocyte migration. Results are normalized mean values ± S.E.M. of n=3 independent experiments. *, p< 0.05. ns = not significant.
C: Analysis of cell migration of lymphocytes isolated from *Pgp$^{flx/flx}$*; and *Pgp$^{flx/flx}$; Tie2-cre$^{+/-}$* mice pre-treated with the selective PKC theta inhibitor sotrastaurin (0.5 µM) or with the same percentage of DMSO as control. PKC theta inhibition normalizes PGP-dependent effect on lymphocyte migration. Results are normalized mean values ± S.E.M. of n=4 independent experiments; *, p< 0.05. ns = not significant.
D: PKC activity assay of lymphocytes isolated from *Pgp$^{flx/flx}$*; and *Pgp$^{flx/flx}$; Tie2-cre$^{+/-}$* mice and stimulated or not with 10 µg/mL fibronectin and 200ng/mL SDF-1. Results are from three individual mice per genotype and condition; shown are mean values ± S.E.M. of n=3 independent experiments. *, p< 0.05. ns = not significant.

4.1.2.4 Loss of PGP catalyzes PKC-mediated effects on cytoskeleton

Interestingly, PGP-depleted/inactivated cells adhere, spread and migrate faster than control cells. All these cellular processes are dependent on a rapid reorganization of the actin cytoskeleton. It was therefore hypothesized that actin remodeling proceeds faster in the

absence of PGP activity. Because PKC is a well-known regulator of actin dynamics a time course experiment was performed with control shRNA cells and PGP shRNA expressing cells plated on fibronectin and stimulated with 12-O-tetradecanoylphorbol-13-acetat (TPA) also known as phorbol 12-myristat-acetat (PMA). TPA is a phorbol ester and is able to activate classical and novel PKCs because of its structural similarity to diglycerides (Arcoleo and Weinstein, 1985).

The cells were treated with TPA for up to one hour. After three minutes of stimulation, cells showed CDR-like transient actin structure, as described in human bronchial epithelial cells (Xiao et al., 2009). At later time points, it became more and more obvious that the PKC-mediated breakdown of the actin cytoskeleton was much more pronounced and faster in PGP-depleted cells (**Figure 34**).

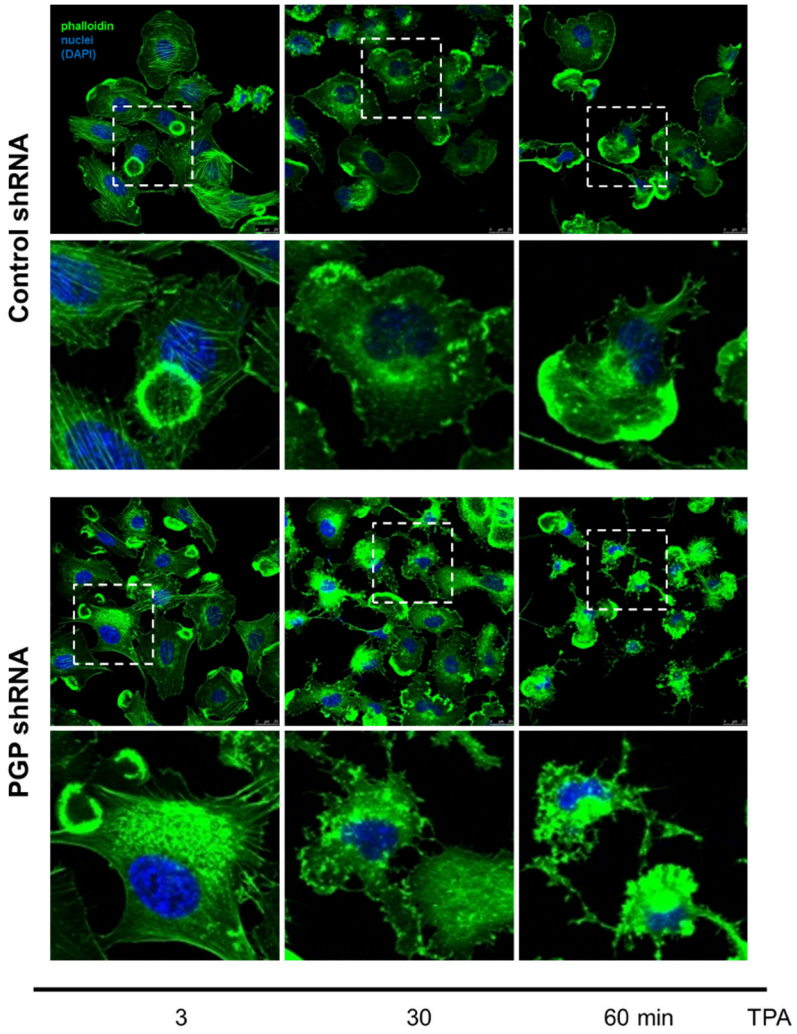

Figure 34: Effects of PKC activation by TPA on PGP-dependent actin cytoskeletal reorganization.
GC1 cells expressing control shRNA or PGP shRNA were seeded on a 12-well slide precoated with fibronectin (10 µg/mL). The next day, cells were treated with TPA (1 µM) and fixed after indicated time points. The cells were stained with phalloidin to visualize actin stress fibers and with DAPI to counterstain the nuclei. Images were taken on a confocal microscope. A magnified detail is displayed below the respective image.

The results suggest that elevated CDR-formation, cell spreading and migration in absence of PGP activity were due to accelerated PKC-mediated actin cytoskeleton remodeling.

4.1.2.5 PLCγ1 is not a direct protein substrate of PGP

PGP was previously described as a tyrosine-directed phosphatase (Seifried et al., 2014). To answer the question how exactly PGP regulates actin dynamics downstream of integrin-, RTK- and GPCR-signaling, it was investigated whether PGP can directly dephosphorylate PLCγ1 on tyrosine 783. The dephosphorylation on this residue is expected to attenuate PLCγ1 activity (Kim et al., 1991) and would therefore lead to a decrease of PKC-mediated effects on the actin cytoskeleton. To confirm the results of hyper-phosphorylation made by Western blot analysis of whole cell lysates (see **Figure 31**), an immunoprecipitation of tyrosine 783-phosphorylated PLCγ1 was performed. Here, control and PGP shRNA expressing cells were seeded on fibronectin, were serum-starved overnight and stimulated with EGF for 3 minutes. To induce maximal phosphorylation levels of PLCγ1, control cells were additionally treated with freshly prepared pervanadate, a general phosphatase inhibitor. The hyper-phosphorylation of PLCγ1 of tyrosine residue 783 was clearly observable in PGP shRNA expressing cells compared to control shRNA cells (**Figure 35A**).

To analyze if PLCγ1 is a substrate of PGP, *in vitro* dephosphorylation assays were performed. For this purpose, immunoprecipitation was repeated with control shRNA expressing cells pretreated with pervanadate. The beads conjugated with tyrosine 783-phosphorylated PLCγ1 were washed several times to remove pervanadate and unspecifically bound proteins, and were incubated with either BSA control protein, purified wildtype PGP or with the phosphatase inactive point mutant PGP^{DN}. **Figure 35B** shows that no PGP-mediated dephosphorylation of PLCγ1 could be observed. Neither variations of PGP concentrations or incubation times, nor the addition of the SFK inhibitor PP2 (to avoid re-phosphorylation at this tyrosine residue by SFKs that may be present in the immunoprecipitates) led to a detectable effect of PGP on PLCγ1 phosphorylation on tyrosine 783 (data not shown).

The next attempt was to dephosphorylate purified PLCγ1. To this end, PLCγ1 was site-specifically phosphorylated on tyrosine 783 by incubation with Syk kinase in the presence of ATP. However, the subsequent incubation with purified wildtype PGP did not show any detectable dephosphorylation of PLCγ1 (**Figure 35C**).

Thus, these data demonstrate that PGP is not able to dephosphorylate PLCγ1 on Y783 and exclude PLCγ1 as potential protein substrate of PGP.

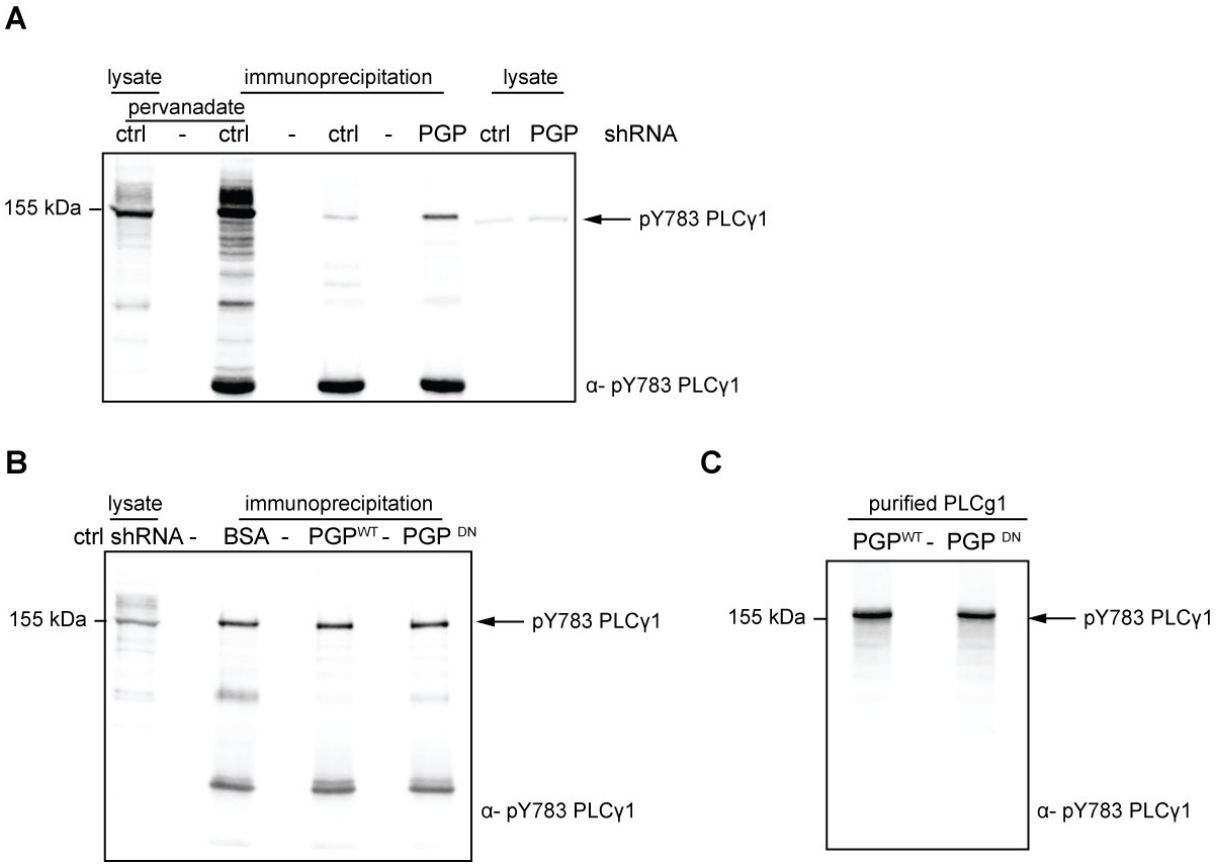

Figure 35: PLCγ1-dephosphorylation assays.
A: Immunoprecipitation of tyrosine 783-phosphorylated PLCγ1 performed with control shRNA or PGP shRNA expressing GC1 cells, seeded on fibronectin, serum-starved overnight and stimulated with EGF. The cells were pretreated or not with the general phosphatase inhibitor pervanadate (100 µM). The lysates were immunoblotted using an α-pY783 PLCγ1 antibody.
B: Immunoprecipitation of tyrosine 783-phosphorylated PLCγ1 in control shRNA expressing cells pretreated with freshly prepared general phosphatase inhibitor pervanadate (100 µM). The beads conjugated with tyrosine-phosphorylated PLCγ1 were incubated for 2 h at 37°C either with BSA control protein or with wildtype PGP or the phosphatase inactive point mutant PGP^{DN} (10 µg each). Samples were immunoblotted using an α-pY783 PLCγ1 antibody.
C: Purified recombinant PLCγ1 (1 µg) was pre-phosphorylated on tyrosine 783 by incubation with Syk and afterwards incubated either with wildtype PGP or the phosphatase inactive point mutant PGP^{DN}. The lysates were immunoblotted using an α-pY783 PLCγ1 antibody.

4.1.2.6 PGP inactivation leads to altered membrane composition

Next, a potential link between PGP-mediated phosphoglycolate dephosphorylation and actin cytoskeleton remodeling was investigated. As explained in **4.2** in more detail, studies on the role of PGP *in vivo* have revealed a new function of PGP in the regulation of lipid metabolism.

During lipogenesis not only triglycerides, but also lipid signaling molecules such as DG or membrane lipids such as phosphatidylcholine, phosphatidylethanolamine and phosphatidylserine are generated (Fagone and Jackowski, 2009).

PGP-dependent effects on cell adhesion and migration are downstream of transmembrane receptors localized at the plasma membrane, and mediated by key proteins such as PLC and PKC, which are recruited to the plasma membrane to promote signal transduction. It was therefore hypothesized that the described PGP-regulated effects could be due to altered membrane composition.

An untargeted lipidomic analysis of control shRNA and PGP shRNA expressing GC1 cells using high resolution liquid chromatography/mass spectrometry were performed together with Matthias Zundler. More than 1400 compounds with different abundance in the two cell types were found. TransOmics software was used for data preprocessing and glycerolipid profiling was conducted using software RLA-Tool (developed by Dr. A. Fekete and Prof. Dr. M. Müller, Julius von Sachs Institute/Pharmaceutical Biology, University of Würzburg).

After statistical sorting and further sorting steps (e.g. by chemical properties and similarities), four high abundance (**Figure 36A**) and 20 low abundance compounds (**Figure 36B**) were identified, which were highly up-regulated in PGP-deficient cells. After data bank analysis (Metabolite and Tandem MS Database Metlin), the exact mass to charge ratio (m/z) of the compounds and the corresponding retention times were examined (Hummel et al., 2011). With help of the received fragmentation patterns (Kirkwood et al., 2013), the high abundance compounds were identified as phosphatidylserine species.

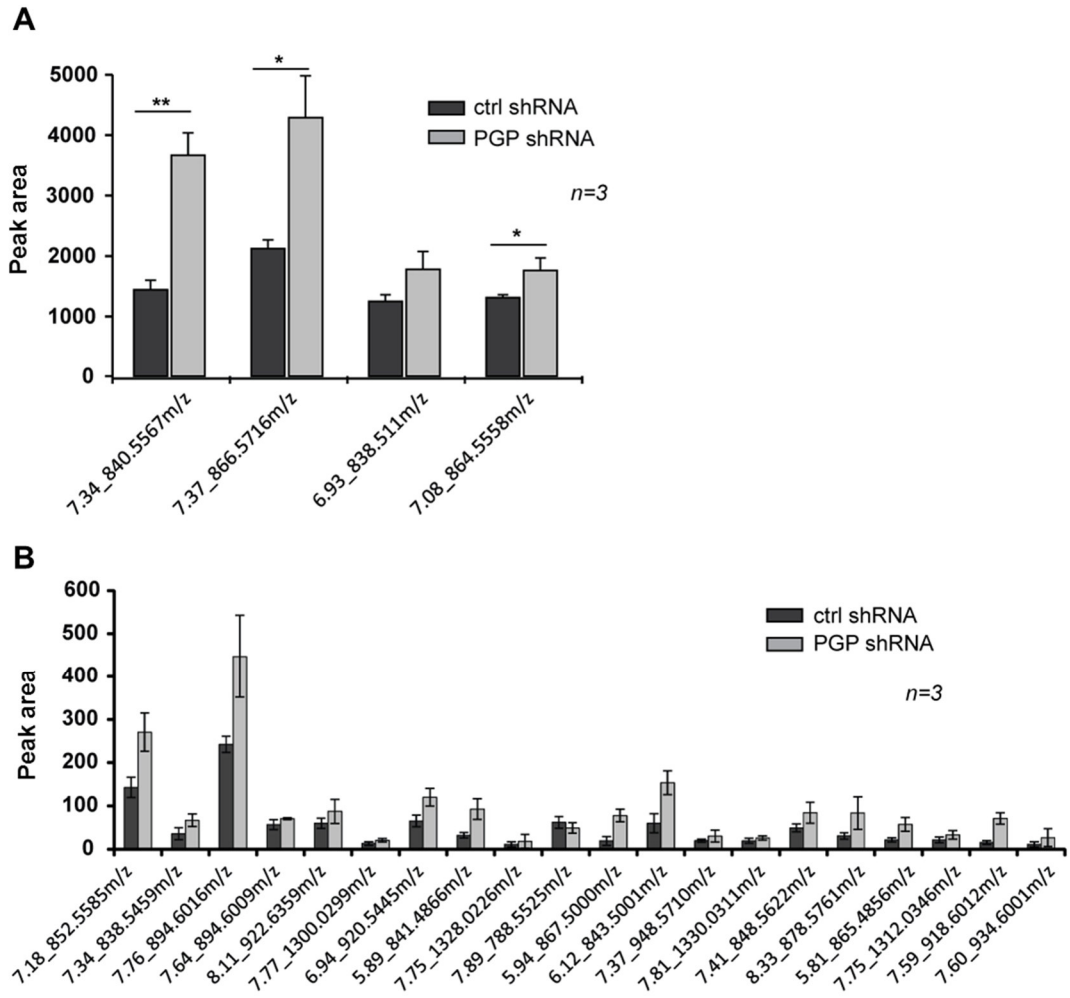

Figure 36: **Mass spectrometry-based glycerolipid profiling of control shRNA and PGP shRNA GC1 cells.** Unstimulated control shRNA and PGP shRNA expressing GC1 cells were analyzed. Four high (**A**) and 20 low (**B**) abundance compounds were found, which were highly up-regulated in PGP-deficient cells. The high abundance compounds were identified as phosphatidylserine species. Mass to charge ratio (m/z) is displayed on the x-axis and peak areas on the y-axis. Results are mean values ± S.E.M. of n=3 experiments. *, $p<0.05$.

Phosphatidylserine (PS) is a negatively charged membrane phospholipid. It consists of a glycerol backbone, which is esterified with two fatty acids. The hydroxyl group of the third glycerol carbon (C1) is esterified with a phosphoric acid-serine ester (**Figure 37**).

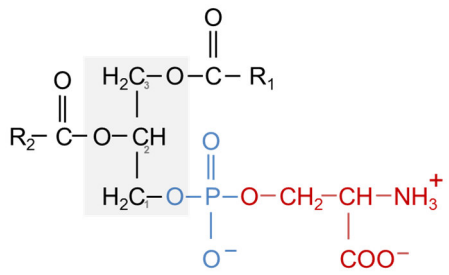

Figure 37: Structural formula of phosphatidylserine.
R_1,R_2 = (un-)saturated fatty acyl chains. The glycerol backbone is marked by the light gray box, the phosphate is shown in blue and serine is displayed in red.

PS is a well-known regulator of apoptosis. It is located on the inner side of the plasma membrane because it is bound by the enzyme flippase (Leventis and Grinstein, 2010). When a cell undergoes apoptosis, PS moves to the extracellular side of the membrane, which is a signal for phagocytosis by macrophages (Marino and Kroemer, 2013b). PS also is implicated in signal transduction by recruitment and binding of signal proteins such as vinculin, a protein of the integrin adhesome (Case and Waterman, 2015). Importantly, PLCs and PKCs also can bind to PS (Stace and Ktistakis, 2006), and as already mentioned, PS is necessary for the activation of classical and atypical PKCs (Geraldes and King, 2010).

In summary, the data obtained so far, are consistent with the hypothesis that accumulation of PS in the plasma membrane of PGP-depleted cells might lead to a pre-assembly of signaling molecules such as PLCγ1 or PKCs that couple the activation of integrins, the EGF receptor and GPCRs to accelerated cytoskeletal remodeling (**Figure 38)**.

Future experiments (see discussion) will address the validity of this model.

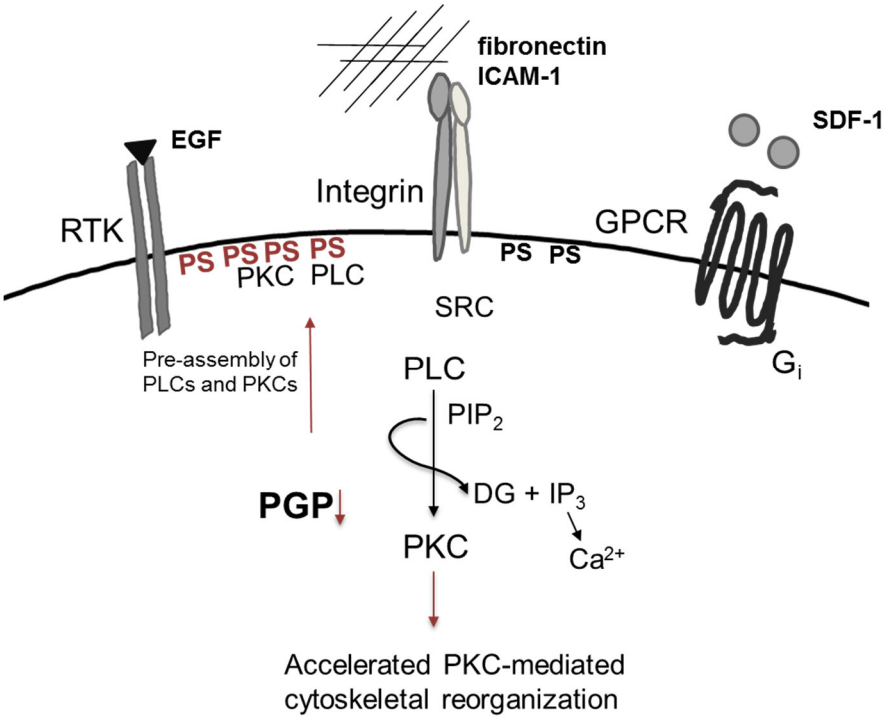

Figure 38: Model of PGP-dependent signaling.
Accumulation of phosphatidylserine (PS) in the plasma membrane after loss of PGP activity may lead to the pre-recruitment and PS-binding of signaling protein such as PLCs and PKCs. As a result, RTK-, integrin- and GPCR-induced and PLCγ1/PKC-mediated effects on the actin cytoskeleton may be accelerated and enhanced.

4.2 The role of phosphoglycolate phosphatase *in vivo*

The second part of the thesis addresses the physiological roles of PGP.

To study the function of PGP activity *in vivo*, conditionally PGP-inactivated mice were generated. For this a Cre/*loxP*-based conditional *Pgp*-knockout approach linked to the simultaneous knockin of phosphatase-inactive Pgp^{D34N} (Pgp^{DN}) into the endogenous Pgp locus of C57BL/6J mice was used. Upon FLPe-mediated removal of the neomycin resistance cassette and Cre-mediated excision of the floxed *Pgp* locus, the expression of Pgp^{DN} is placed under the control of the endogenous *Pgp* promoter (see **1.7**).

4.2.1 Whole-body PGP inactivation (EIIa-mouse) is embryonic lethal

Breeding of $Ppg^{flx/flx}$ mice with the whole-body Cre deleter strain EIIa-Cre is expected to lead to a loss of PGP phosphatase activity in all mouse tissue. The EIIa promoter drives Cre recombinase expression already in the early embryo, prior to implantation in the uterine wall (Lakso et al., 1996). Southern blot analysis of EcoRV-digested genomic DNA demonstrated homologous recombination (**Figure 39A**) and the same results were obtained by PCR screening that detects the wildtype (212 bp) or targeted (163 bp) allele (**Figure 39B**). By immunoblotting experiments using an antibody against endogenous PGP, it was shown that PGP protein expression became detectable in the embryo as well as in the allantois and yolk sac around embryonic day 8.5 (E8.5) (**Figure 39C**). Additionally, it was demonstrated that protein expression levels of wildtype or point-mutated PGP yolk sacs isolated from $Pgp^{WT/WT}$ and $Pgp^{DN/DN}$ embryos were comparable at E11.5 (**Figure 39D**).

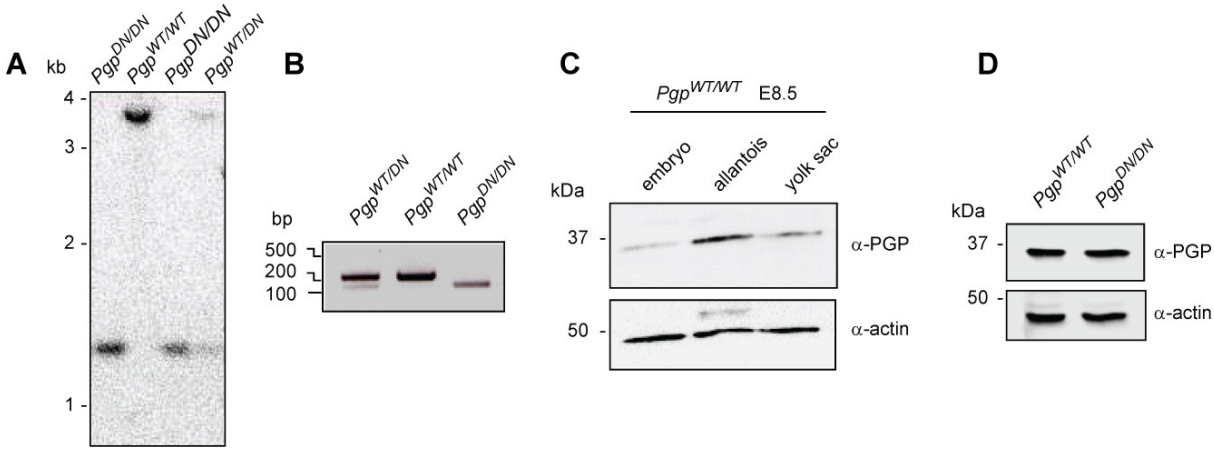

Figure 39: Generation and breeding of Pgp knockout/ Pgp^{DN} knockin mice.
A: Southern blot analysis for the detection of homologous recombination after breeding $Pgp^{flx/flx}$ mice with the global Cre-deleter strain EIIa-Cre. Upon removal of the FRT-flanked neomycin resistance cassette, Cre-mediated excision of the floxed *Pgp* gene and knockin of Pgp^{D34N} (Pgp^{DN}) results in the generation of a 1.2 kb fragment that can be detected with the probe (pr). Pgp^{WT} is detected at 3.5 kb.
B: Genotyping by PCR. The wildtype or targeted *Pgp* allele are detected at 212 or 163 bp, respectively.
C: Western blot analysis of PGP protein expression levels in allantois, yolk sac and in the embryo proper at E8.5.
D: Comparison of PGP protein expression levels in E11.5 yolk sacs isolated from $Pgp^{WT/WT}$ and $Pgp^{DN/DN}$ embryos.

Heterozygote *Pgp*$^{WT/DN}$ mice were indistinguishable from their wildtype littermates in terms of fertility and growth. Intercrossing *Pgp*$^{WT/DN}$ mice produced offspring, of which ~64% were heterozygotes, and ~36% wildtype (**Table 2**). However, no *Pgp*$^{DN/DN}$ mice were born indicating an essential function for PGP before birth.

To investigate embryonic lethality upon EIIa-Cre-driven whole body *Pgp* inactivation further, embryos from timed matings of heterozygous parents were analyzed by Kerstin Hadamek. The examination of more than 600 embryos from *Pgp*$^{WT/DN}$ intercrosses at different stages of gestation revealed that genotype ratios were consistent with the expected Mendelian distribution between E8.5 and E11.5, whereas only one homozygous *Pgp* mutant embryo was found at E12.5 (**Table 2**). Thus, *Pgp*$^{DN/DN}$ embryos seemed to die around E11.5.

Table 2: Characterization of progeny from heterozygous intercrosses.

	genotype		
stage	*Pgp*$^{WT/WT}$	*Pgp*$^{WT/DN}$	*Pgp*$^{DN/DN}$
E8.5	69	147	52
E9.5	13	34	12
E10.5	25	49	30
E11.5	16	29	18
E12.5	6	18	1
P21	30	53	0

E, embryonic day; P, postnatal day.

Somite pair numbers were comparable at E8.5 in *Pgp*$^{WT/WT}$, *Pgp*$^{WT/DN}$ and *Pgp*$^{DN/DN}$ embryos, but further somitogenesis stagnated in *Pgp*$^{DN/DN}$ embryos already one day later (**Table 3**). This indicates that PGP inactivation led to an impaired development beyond E8.5.

Table 3: Embryo staging.
The number of somite pairs in the different genotypes is indicated at E8.5 and E9.5
n are the numbers of scored embryos. n.d. = not definable.

	number of somite pairs		
stage	*Pgp*$^{WT/WT}$	*Pgp*$^{WT/DN}$	*Pgp*$^{DN/DN}$
E8.5	4-6 (*n*=4; n.d.=2)	4-6 (*n*=12; n.d.= 3)	4-6 (*n*=4; n.d.=1)
E9.5	18-24 (*n*=4; n.d.= 2)	16-23 (*n*=9; n.d.=6)	4-6 (*n*=3; n.d.=1)

Figure 40 demonstrates that at E9.5, *Pgp*$^{DN/DN}$ embryos resembled E8.5 *Pgp*$^{WT/WT}$ embryos in size.

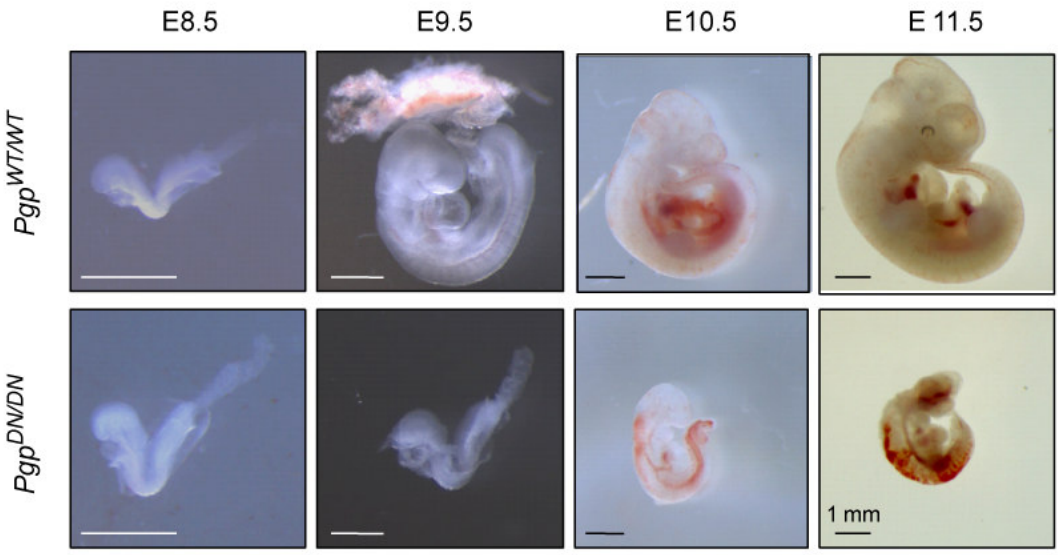

Figure 40: Comparison of Pgp$^{DN/DN}$ and Pgp$^{WT/WT}$ embryos from the E8.5 to E11.5 stage of development.
The scale bar represents 1 mm in all panels.

Additionally, *Pgp*$^{DN/DN}$ embryos showed a delay in axial rotation (turning), a hallmark of the transition from the E8.5 to E9.5 stage of development. Eight of ten *Pgp*$^{WT/WT}$ and 22 of 24 *Pgp*$^{WT/DN}$ embryos, but none of eight investigated *Pgp*$^{DN/DN}$ embryos had concluded the turning by day E9.5. **Table 4** shows that at E10.5, ~80% of *Pgp*$^{DN/DN}$ embryos were growth-retarded, as judged by a size comparable to E9.5 *Pgp*$^{WT/WT}$ embryos. In addition, beating hearts could only be detected in a fraction of *Pgp*$^{DN/DN}$ embryos. Whereas heart beats were detectable in almost 50% of the embryos at E10.5, one day later heart beats could only be observed in a third of *Pgp*$^{DN/DN}$ embryos. Interestingly, some embryos displayed cranial, dorsal and abdominal bleedings in addition to the growth defect, and these characteristics were aggravated from embryonic day E10.5 to E11.5.

Table 4: Phenotypes of PgpDN/DN embryos.

Parameter	E10.5	E11.5
Growth retardation	19 of 24	21 of 26
Heart beat	11 of 24	6 of 19
Internal hemorrhage	0 of 10 normal-sized embryos	3 of 5 normal-sized embryos
	3 of 14 growth-retarded embryos	7 of 14 growth-retarded embryos

E, embryonic day. The numbers of embryos showing the respective phenotypes relative to the total number of scored *Pgp*$^{DN/DN}$ embryos are given. Embryo size (growth retardation) was assessed relative to *Pgp*$^{WT/WT}$ littermate embryos. Massively deteriorated embryos were not included in the analysis.

4.2.2 Deletion of PGP activity in endothelial and hematopoietic cells

To examine whether these bleedings were caused by a functional defect of the endothelium or caused by a defect of the hematopoietic system, a second mouse model was generated. Breeding *Pgp*$^{flx/flx}$ mice with the Tie2-Cre driver line lead to a PGP inactivation in endothelial cells and in cells of the hematopoietic system such as red blood cells or lymphocytes. In contrast to the embryonic lethality observed upon whole-body ablation of PGP activity, mice with a deficiency of PGP activity in endothelial and hematopoietic cells (*Pgp*$^{flx/flx}$*; Tie2-Cre*$^{+/-}$) were born at the expected Mendelian ratios. Furthermore, these mice showed no hemorrhages, and were comparable to wildtype mice in terms of viability, growth and fertility (Segerer, Hadamek et al.; unpublished).

This indicates that PGP activity in endothelial and hematopoietic cells including red blood cells is not indispensable for life (Somoza and Beutler, 1983).

4.2.3 Effects of whole-body PGP inactivation on the cardiovascular system

Midgestation lethality in the mouse embryo is frequently due to an inadequate establishment of the embryonic cardiovascular system or to defective embryonic-maternal connections (Conway et al., 2003). A linear heart tube is formed and begins to beat by early E8.0 and blood and vessel formation is concurrently initiated in the embryo proper and in the extraembryonic yolk sac. By E8.5, a capillary plexus is established in the yolk sac. These primitive vessels undergo remodeling between E8.5 and E9.5, and ultimately connect to the embryo, thus providing a circulatory loop between the yolk sac and the embryo proper.

However, analysis of vascularization of globally PGP-deficient embryos and their yolk sac showed no obvious differences compared to their wildtype counterparts. Histochemical inspection showed that PGP inactivation resulted in a reduction of the embryonic blood vessel density in the placental labyrinth. Furthermore, examination of chorioallantoic placenta formation showed that none of six analyzed *Pgp*$^{DN/DN}$ embryos had accomplished chorioallantoic fusion (attachment of the allantois to the chorion, followed by the folding of the chorion into villi, into which the vasculature of the allantois grows to elaborate the placental labyrinth) by E8.5 (Segerer, Hadamek et al.; unpublished).

The vascular cell adhesion molecule 1 and its binding partner integrin $\alpha4\beta1$ (expressed in the allantoic mesoderm or chorionic trophoblast, respectively) are known to be critical for chorioallantoic fusion (Rossant and Cross, 2001). However, it was demonstrated that allantoides of all genotypes adhered to and spread on immobilized $\alpha4\beta1$ *in vitro* suggesting that the delay in chorioallantoic fusion in homozygously PGP-inactivated embryos was not

caused by a defect in integrin-mediated cell adhesion, but rather was a result of their general growth retardation (Segerer, Hadamek et al., unpublished).

Given the important role of protein tyrosine phosphorylation in vascular development and the previously observed involvement of PGP for EGF-induced signal transduction (Seifried et al., 2014), protein tyrosine phosphorylation levels in E10.5 *Pgp*$^{DN/DN}$ embryos compared to their wildtype counterparts were examined. Nevertheless, with the exception of a very faint band at ~150 kDa that appeared to be slightly increased in PGP-deficient embryos (see also ref. (Seifried et al., 2014)) there were no obvious alterations under these steady-state conditions (Segerer, Hadamek et al., unpublished).

Analysis of *Pgp*$^{DN/DN}$ embryo phenotypes as well as experiments to investigate potential effects of whole-body PGP inactivation on the cardiovascular systems were performed by Kerstin Hadamek.

Taken together, these data and the fact that Tie2-Cre-driven PGP inactivation did not result in embryonic lethality, argue that embryonic lethality upon whole-body PGP inactivation is not caused by a defect of the cardiovascular system. Additionally, it was demonstrated that loss of PGP phosphatase activity led to a growth defect with developmental delay after E8.5, resulting in a gradually deterioration and death of Pgp$^{DN/DN}$ embryos between E9.5 and E11.5 in utero.

4.2.4 Loss of PGP activity causes an oxygen-dependent proliferation defect

As described in **1.4.1**, it was shown that PGP is a phosphoglycolate phosphatase *in vitro*. Thus, the question arose if loss of phosphoglycolate phosphatase activity of PGP caused embryonic lethality.

To investigate the potential function of PGP as a PG phosphatase *in vivo*, the mechanisms leading to growth arrest in PGP-inactivated embryos had to be clarified in more detail. In the time between embryonic day E8.5 and E12.5, the growth of murine embryos is nearly exponential (Burns and Hassan, 2001) and embryo size increases such that systemic oxygen and nutrient supply by the mother become essential for the embryo. The supply of oxygen is ensured by the elaboration of the embryonic cardiovascular system and nutrient supply by placenta formation. At the same time, midgestational embryos transition from an environment that is physiologically low in oxygen (<2% O_2) to conditions that approach normoxia once maternal/fetal gaseous exchange has been established (Dunwoodie, 2009).

The potential impact of oxygen on PGP-dependent cell proliferation was investigated first. Here mouse embryonic fibroblasts (MEFs) generated from E8.5 embryos were analyzed. At

embryonic day E8.5 somite pair numbers (**Table 3**), as well embryo size were comparable in $Pgp^{WT/WT}$, $Pgp^{WT/DN}$ and $Pgp^{DN/DN}$ embryos (**Figure 40**).

However, whereas MEFs could easily be generated and cultivated from $Pgp^{WT/WT}$ and heterozygote $Pgp^{WT/DN}$ embryos at E8.5, MEFs derived from E8.5 $Pgp^{DN/DN}$ embryos did not grow under these standard culture conditions and died shortly after embryo dissociation and plating. In contrast, undissociated E8.5 embryo explants of all genotypes could be kept in culture for up to seven days and cellular outgrowths were observed in all explants. Although fewer cells grew out from $Pgp^{DN/DN}$ embryos, the explants did not die. Embryonic heart beats started within hours and were observed over the entire time period in explants of all genotypes. However, upon dissociation of the embryo explants and the reseeding of single cells, the percentage of proliferating $Pgp^{DN/DN}$ cells was again markedly reduced compared to $Pgp^{WT/WT}$ and $Pgp^{WT/DN}$ cells. $Pgp^{DN/DN}$ cells could not be cultured for longer than 72 hours after dissociation of the explants because they immediately stop growing and died. These observations suggested that hypoxic conditions –which are likely present in the interior of embryo explants – may sustain the viability and proliferation of PGP-deficient cells. To test this hypothesis a cell proliferation assay under normoxic (~20% O_2) and hypoxic (~1% O_2) conditions were performed. Indeed, when PGP-deficient MEFs were obtained by dissociation of embryo explants, their proliferation under normoxic conditions was clearly impaired compared to wildtype MEFs. Under hypoxic conditions however, the proliferation of PGP-inactivated MEFs was completely normalized (**Figure 41**).

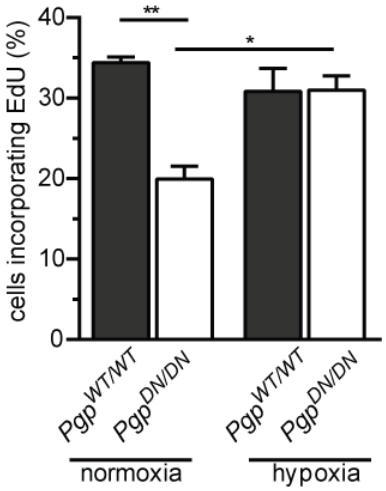

Figure 41: Cell proliferation assay of PGP-proficient or –deficient MEFs derived from embryo explant cultures under normoxia and hypoxia.
DNA synthesis was assessed based on the incorporation of the nucleotide analogue EdU. Nuclei were counterstained with DAPI, and the proportion of EdU-positive nuclei was quantified by fluorescence microscopy. Normoxic conditions were defined as ~20% O_2. For hypoxia, cells were kept at ~1% O_2 for 16 h. Shown are the mean values ± S.E.M. of n=3 independent experiments per condition and genotype. *, $p<0.05$; **, $p<0.01$.

These results clearly demonstrate that the oxygen tension present under *in vitro* normoxic conditions causes a cell-autonomous proliferation defect in PGP-inactivated cells.

The next step was to investigate the mechanistic link between exposure to normoxia and the block in proliferation observed in PGP-deficient cells or embryos.

The PGP substrate PG is produced during the repair of DNA strand breaks with 3'-PG termini that are generated after hydroxyl radical attack by oxidative stress before cleavage by phosphodiesterases (PDE) (Zhou et al., 2009, Zhou et al., 2005). DNA repair is crucial for the maintenance of genomic integrity during embryo growth and development. DNA repair genes capable of trimming 3'-PG ends are already expressed in E8.5 - E11.5 mouse embryos (Jaroudi and SenGupta, 2007). The time between embryonic day E8.5 - E11.5 is a developmental stage of nearly exponential DNA replication and cell proliferation (Burns and Hassan, 2001).

Thus, it was hypothesized that the DNA damage resulting from increasing exposure to oxygen during midgestation through systemic oxygen and nutrient supply by the mother may cause a PG-dependent inhibition of cell proliferation.

Little is known about the function of PG. As explained in more detail in **1.4.1.2**, it was demonstrated that PG is an inhibitor of enzymes involved in glucose homeostasis, such as triose phosphate isomerase (TPI), pyruvate kinase (Dougherty and Cleland, 1985) and phosphoenolpyruvate carboxykinase (Stiffin et al., 2008). Our focus was on TPI because it is an important metabolic regulator in cells.

Midgestational mouse embryos rely on both proliferative glycolytic and energy-producing oxidative metabolism (Johnson et al., 2003). TPI deficiency in humans results in a rare disease involving haemolytic anaemia (Stincone et al., 2014).

Thus, TPI activity in red blood cells isolated from $Pgp^{flx/flx}$ and $Pgp^{flx/flx}$; $Tie2\text{-}Cre^{+/-}$ mice was analyzed. **Figure 42** shows that the absence of PGP hydrolyzing activity and the potential, subsequent accumulation of phosphoglycolate in red blood cells isolated from $Pgp^{flx/flx}$; $Tie2\text{-}Cre^{+/-}$ mice indeed reduced TPI activity by ~25% compared to erythrocyte lysates obtained from $Pgp^{flx/flx}$ mice. In lysates of E8.5 $Pgp^{DN/DN}$ embryos, TPI activity was inhibited by ~34% compared to $Pgp^{WT/WT}$ embryos as well.

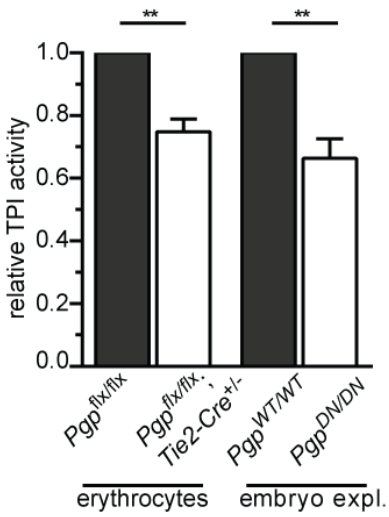

Figure 42: TPI activity assay of erythrocytes isolated from *Pgp*$^{flx/flx}$ and *Pgp*$^{flx/flx}$; *Tie2-Cre*$^{+/-}$ mice and in E8.5 embryo explant cultures.
Results are from three independent erythrocyte isolations from three individual mice or from three embryo explants per genotype and condition; Shown are the mean values ± S.E.M. of n=3 independent experiments per condition and genotype. **, $p<0.01$.

An attenuation, but not a complete PG-mediated inhibition of TPI activity is consistent with the fact that PG is a reversibly binding transition state analog of TPI substrates (Schnackerz and Gracy, 1991).

4.2.5 Loss of PGP activity leads to a metabolic shift towards increased lipogenesis

TPI constitutes a major branch point between carbohydrate and lipid metabolism (see **1.4.1.3**). In cells, TPI catalyzes the isomerization of dihydroxyacetone phosphate (DHAP) and glyceraldehyde 3'-phosphate (GADP), which are produced during glycolysis from glucose-derived fructose 1,6-bisphosphate. While DHAP exhibits a higher chemical stability, and consequently its formation is thermodynamically strongly favored over GADP production, only GADP can be utilized for the subsequent steps of glycolysis. TPI isomerizes DHAP to GADP to ensure the process of glycolysis. Because of that, the inhibition of TPI activity by phosphoglycolate even increases the thermodynamically favored formation of DHAP (Ralser et al., 2007).

Glycerol 3-phosphate dehydrogenase catalyzes the reduction of DHAP to glycerol 3-phosphate that provides the carbohydrate backbone that activated fatty acids are esterified with to build triglycerides (TGs) during lipogenesis.

Figure 43 shows that glycerol 3-phosphate (G3P) levels were elevated in E8.5 $Pgp^{DN/DN}$ embryos compared to $Pgp^{WT/WT}$ embryos. This is consistent with the hypothesis that by inhibition of TPI activity more DHAP is generated which can be converted to G3P.

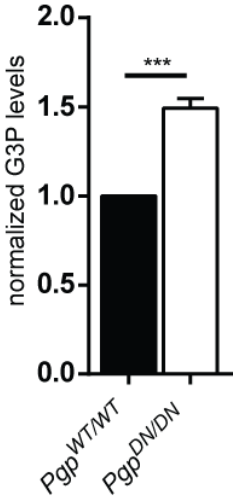

Figure 43: Determination of G3P levels of E8.5 embryo explant cultures by performing G3P colorimetric assays.
Results are from three pooled embryo lysates (consisting of 3-5 embryos) per genotype; Shown are the mean values ± S.E.M. of n=3 independent experiments per condition and genotype. ***, $p<0.001$.

To study the potential effects of PGP-inactivation on lipid metabolism, the lipid composition of E8.5 $Pgp^{WT/WT}$ and $Pgp^{DN/DN}$ embryo extracts was explored in lipidomic analyses using high resolution liquid chromatography/mass spectrometry together with Matthias Zundler.

Base peak ion chromatograms were analyzed first (**Figure 44A**). Whereas only few compounds were down-regulated, several compounds were up-regulated in $Pgp^{DN/DN}$ embryos (**Figure 44B**). Manual inspection of the two statistically most relevant down- and up-regulated PGP lipid markers showed only a slight decrease (7 and 9%) of the down-regulated markers in $Pgp^{DN/DN}$ embryos. In contrast, the peak areas of the two up-regulated compounds were 3-4 times higher in PGP mutant compared to wildtype embryos.

By comparing accurate masses of the molecular ions with the Metabolite and Tandem MS Database Metlin, the two up-regulated PGP lipid markers were identified as diglyceride (DG) species (DG-16:0-18:0 and DG-18:0-18:0).

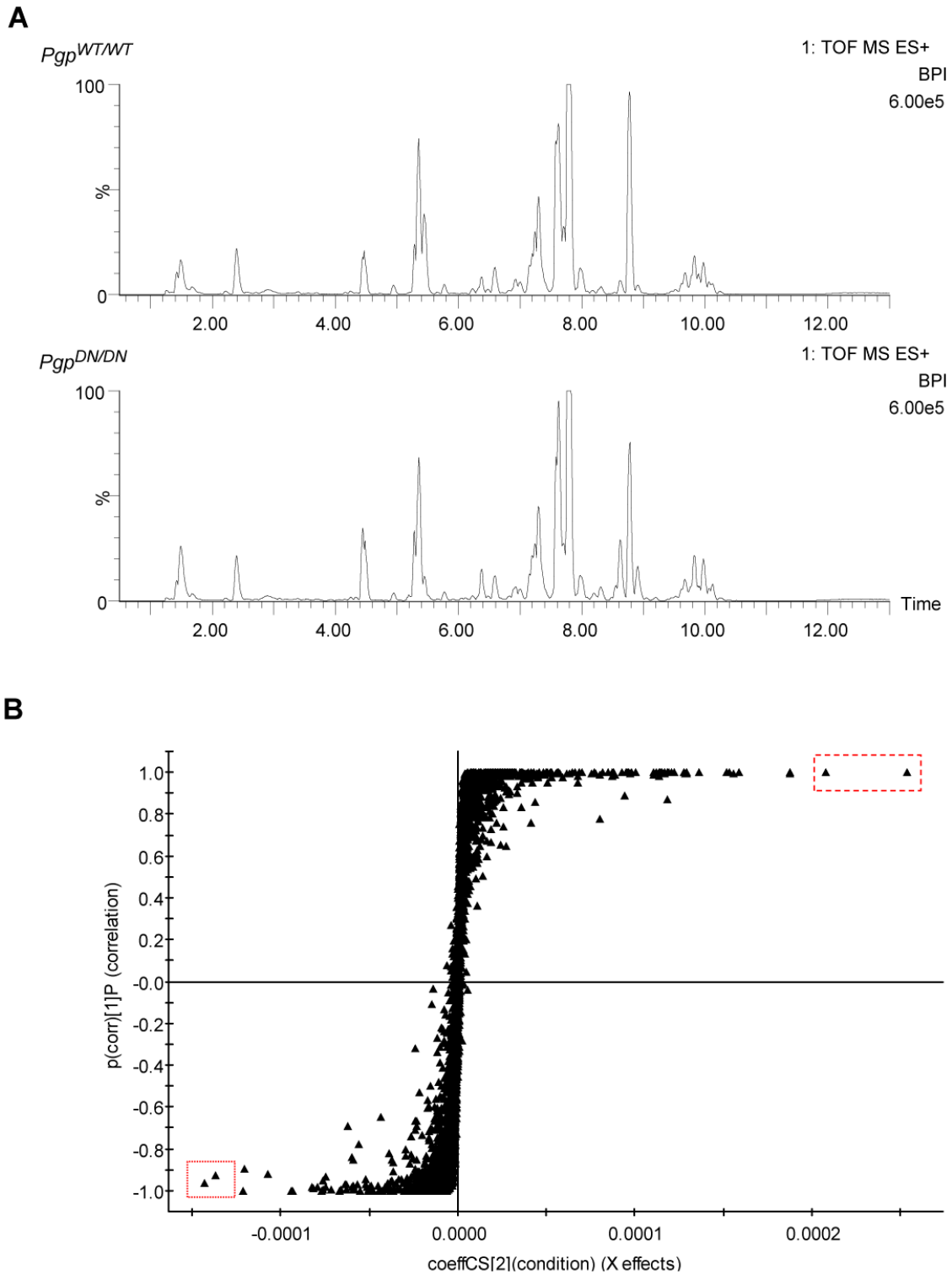

Figure 44: Glycerolipid profiling of E8.5 embryos by LC/MS.
A: Base peak ion chromatogram of total lipid extracts of pooled $Pgp^{WT/WT}$ (top) and $Pgp^{DN/DN}$ (bottom) embryos.
B: Identification of differentiating lipid compounds. After data preprocessing, 494 of the 3780 aligned compounds were significantly different in total lipid extracts of $Pgp^{WT/WT}$ and $Pgp^{DN/DN}$ embryos ($p \leq 0.02$, fold change ≥ 3). Orthogonal partial least square discriminant analysis (OPLS-DA) of all aligned compounds was performed to filter out statistically relevant lipid compounds that discriminate between $Pgp^{WT/WT}$ and $Pgp^{DN/DN}$ embryos. Lipid features that were significantly down- or up-regulated in the mutant embryos are marked with a dotted or dashed line box, respectively. By comparing accurate masses of the molecular ions with the Metabolite and Tandem MS Database Metlin, the two up-regulated PGP lipid markers were identified as diglyceride (DG) species (DG-16:0-18:0 and DG-18:0-18:0). The experiments were performed in collaboration with Dr. A. Fekete and Prof. Dr. M. J. Müller (Julius von Sachs Institute/Pharmaceutical Biology, University of Würzburg).

In an independent experiment using optimized ionization of DGs, glycerolipids in total lipid extracts of pooled E8.5 $Pgp^{WT/WT}$ and $Pgp^{DN/DN}$ embryos were profiled by Matthias Zundler using an in-house developed profiling software RLA-Tool (developed by Agnes Fekete and Prof. Dr. Martin J. Müller). **Figures 45B** show that retention time-aligned molecule ion and fragment ion spectra led to the identification of 14 DG-species. Consistent with the first experiment, an increase of total DGs in $Pgp^{DN/DN}$ embryos, with elevated levels of almost all profiled DGs was detected. Highly unsaturated DG species (DG-36:5, DG-36:6) were only found in $Pgp^{DN/DN}$ embryos (**Figure 45A**). Total DG content and the content of the identified DG species was normalized to the total endogenous phosphatidylcholine (PC) content determined by LC-MS, which was not affected by PGP activity.

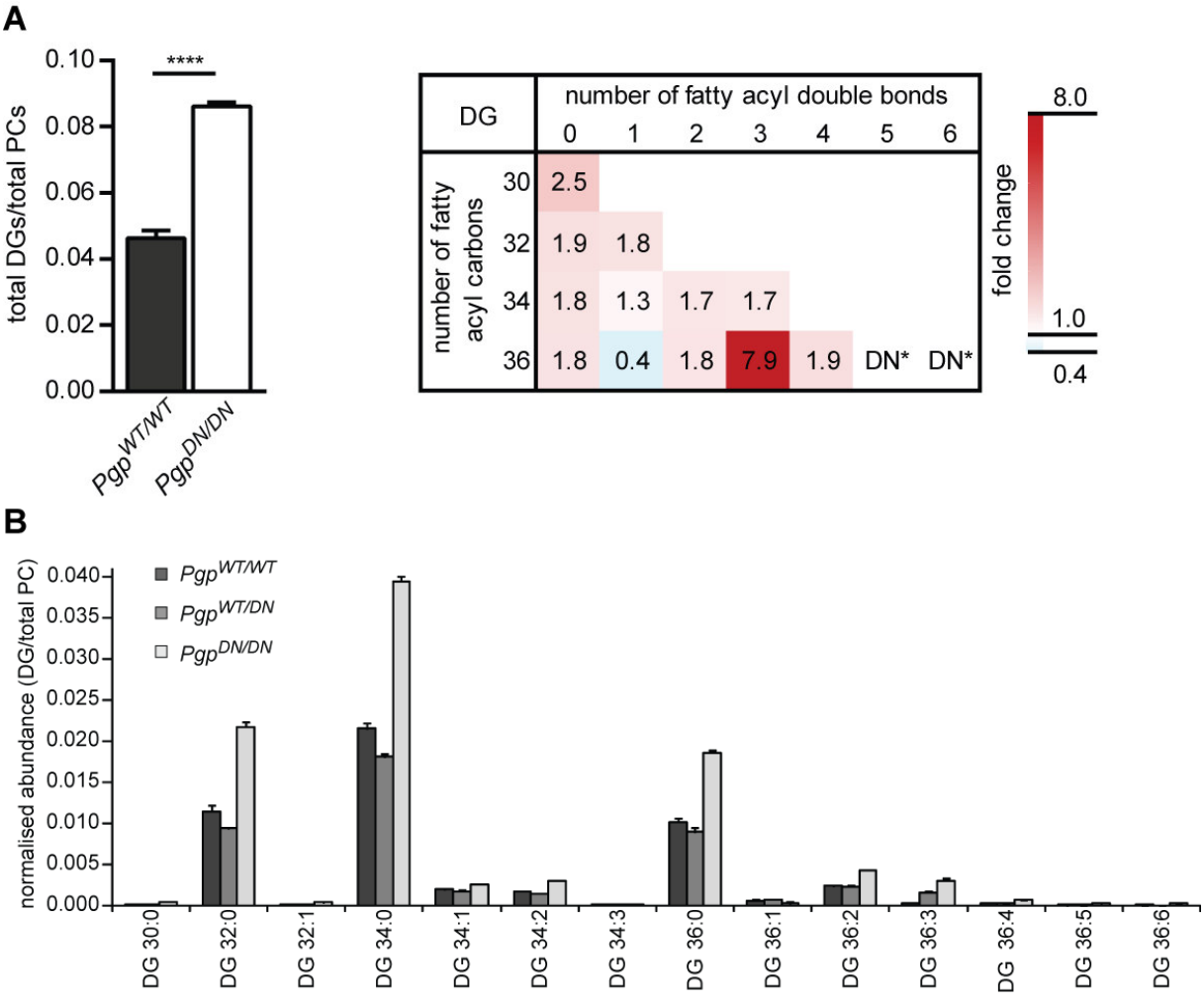

Figure 45: Mass spectrometry-based diglyceride profiling in total lipid extracts of pooled E8.5 embryos.
A: The total DG content was normalized to the total endogenous phosphatidylcholine (PC) content determined by LC-MS, which was not affected by PGP activity. The fold-change of individual DG species in $Pgp^{DN/DN}$ compared to $Pgp^{WT/WT}$ embryos was plotted according to the number of double bonds (columns) and carbons (rows) of the fatty acids esterified to glycerol. *, $p<0.05$; **, $p<0.01$; ****, $p<0.0001$.
B: Determination of endogenous DG species levels in E8.5 $Pgp^{WT/WT}$ (black columns), $Pgp^{WT/DN}$ (gray columns) or $Pgp^{DN/DN}$ embryos (light gray columns).

Furthermore, retention time-aligned molecule ion and fragment ion spectra led to the identification of 47 TG-species (**Figure 46A**).

The total TG content was also elevated in *Pgp*$^{DN/DN}$ embryos, and TG accumulation was more predominant for the unsaturated species, independent of the carbon number of the acyl chains (**Figure 46B**). Total TG content and the content of the single TG species were normalized to the total endogenous phosphatidylcholine (PC) content.

Unfortunately, monoacylglycerols (MGs) could not be reliably identified. Thus, it was not possible to distinguish whether increase in DG is caused by elevated lipogenesis (MG→DG) or by elevated lipolysis (TG→DG).

Taken together, these data argue that attenuated TPI activity caused by the inhibition by phosphoglycolate observed in *Pgp*$^{DN/DN}$ embryos diminishes the isomerization of DHAP to GADP. This leads to a shift toward DHAP formation and by accumulation of DHAP-derived glycerol 3-phosphate, which is utilized for TG-synthesis to elevated lipogenesis.

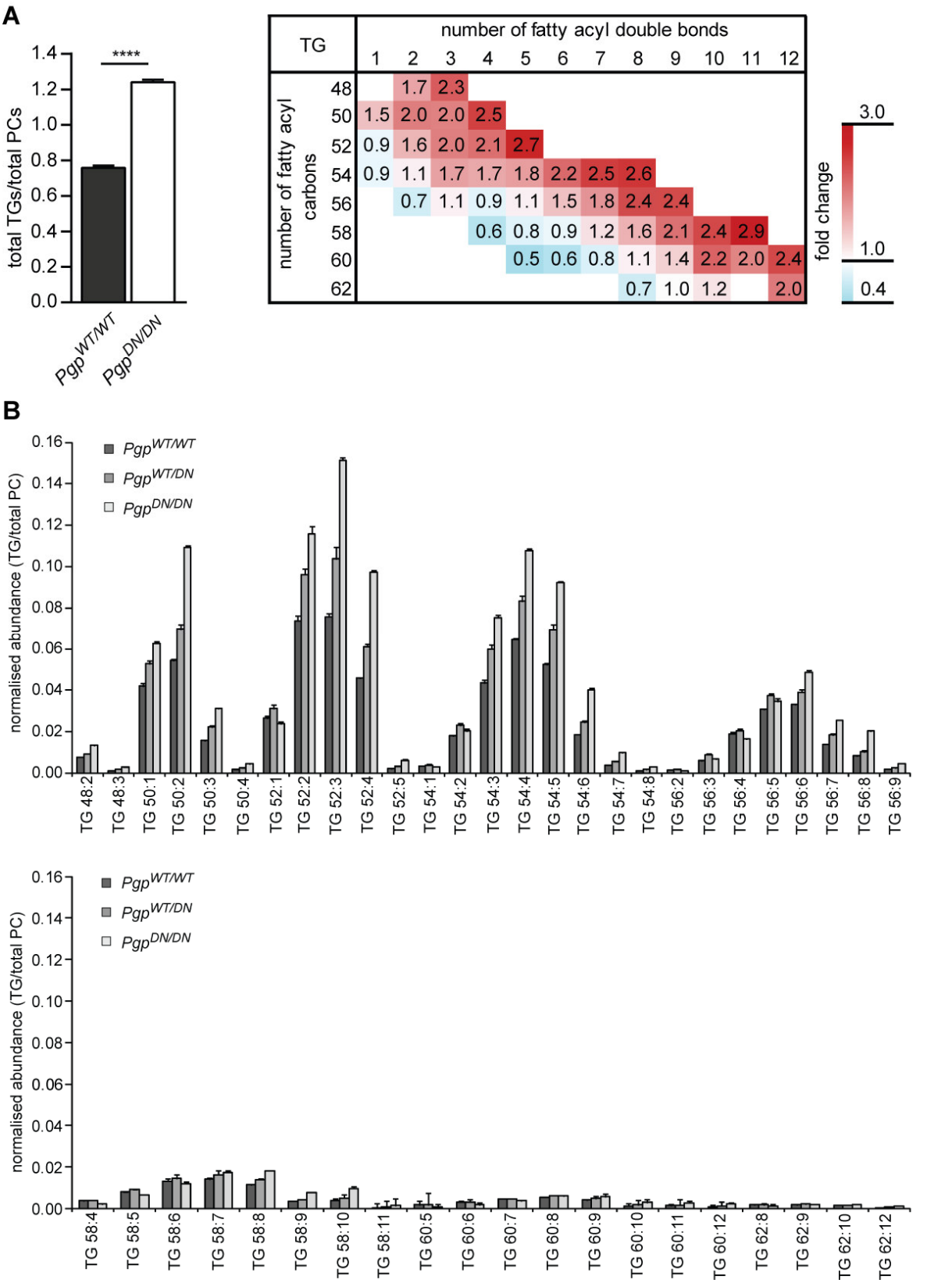

Figure 46: Mass spectrometry-based triglyceride profiling in total lipid extracts of pooled E8.5 embryos.
A: The total TG content was normalized to the total endogenous phosphatidylcholine (PC) content determined by LC-MS, which was not affected by PGP activity. The fold-change of individual TG species in *Pgp*$^{DN/DN}$ compared to *Pgp*$^{WT/WT}$ embryos was plotted according to the number of double bonds (columns) and carbons (rows) of the fatty acids esterified to glycerol. *, $p<0.05$; **, $p<0.01$; ****, $p<0.0001$.
B: Determination of endogenous TG levels in E8.5 *Pgp*$^{WT/WT}$ (black columns), *Pgp*$^{WT/DN}$ (gray columns) or *Pgp*$^{DN/DN}$ embryos (light gray columns).

4.2.6 PGP loss elevates energy-producing metabolism in an oxygen-dependent manner

Triglycerides function as a storage for fatty acids (FAs). FAs are an important source of energy by utilizing for ATP production. The process of TG breakdown starts with lipolysis, carried out by lipases and resulting in the occurrence of free FA, which are oxidized in the mitochondria (β-oxidation). Here, reduced nicotinamide adenine dinucleotide (NADH) and Flavin adenine dinucleotide $FADH_2$ are produced and utilized in the electron transport chain to produce ATP by oxidative phosphorylation (Berg JM, Tymoczko JL, Stryer L. Biochemistry. 5th edition; 2002).

Thus, it was investigated if PGP-deficiency-induced triglyceride elevation lead to changes of energy metabolism.

For this purpose, E8.5 embryos were analyzed. As an overall indicator of cellular energy status, total ATP content of E8.5 *Pgp*$^{DN/DN}$ and *Pgp*$^{WT/WT}$ embryos was initially measured using a luciferase-based ATP assay. Interestingly, ATP levels were markedly higher in PGP-inactivated embryos compared to wildtype embryos (**Figure 47**).

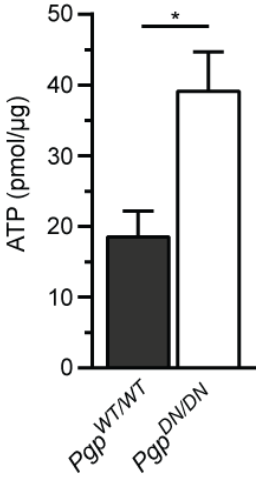

Figure 47: Determination of ATP levels.
Total ATP concentrations in PGP-proficient and PGP-deficient embryos. Shown are mean values ± S.E.M. of n=5 *Pgp*$^{WT/WT}$ and n=3 *Pgp*$^{DN/DN}$ embryos dissected at E8.5. *, $p<0.05$.

The effect of PGP inactivation on energy metabolism was investigated in more detail. Given the fact that it was not possible to keep *Pgp*$^{DN/DN}$ MEFs in culture under normoxic conditions (see **4.2.4**), the spermatogonial cell line GC1 as a model system was used to study PGP-dependent energy metabolism. In spermatogenesis, DNA repair proteins that trim 3'-PG ends and produce PG are thought to play an important role for chromatin dynamics (Jaroudi and SenGupta, 2007).

PGP is ubiquitously expressed but exhibits high expression levels in testis (Seifried et al., 2014). GC1 cells are derived from mouse testis and express high levels of PGP. Targeting of PGP by RNA interference using short hairpin RNA (shRNA) resulted in a reduction of PGP protein levels by ~80% (see **Figure 19**).

Similar to PGP-inactivated MEFs, PGP-depletion in GC1 cells decreased proliferation compared to control shRNA cells under normoxic conditions. Also in this case proliferation levels were normalized under hypoxic conditions (**Figure 48A** and **48B**).

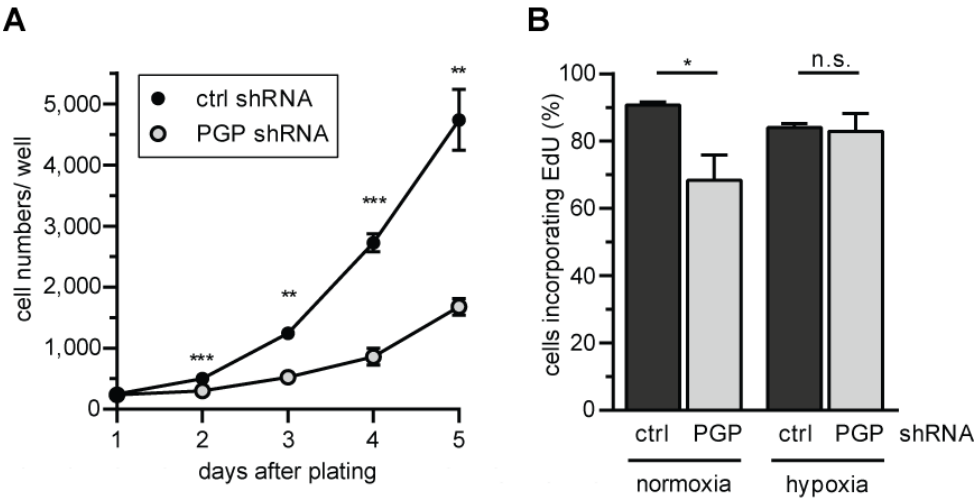

Figure 48: Cell proliferation of GC-1 cells.
A: Proliferation assay of GC1 cells stably expressing PGP-directed shRNA or control shRNA under normoxic (~20% O2) conditions. Cell proliferation was assessed by staining with H33342; the number of nuclei per well was quantified semi-automatically by fluorescence microscopy.
B: Effect of PGP depletion on the proliferation of GC1 cells cultured for 16 h under normoxic (~20% O_2) or hypoxic (~1% O_2) conditions. Cell proliferation was measured by EdU incorporation. Nuclei were counterstained with DAPI, and the proportion of EdU-positive nuclei was quantified by fluorescence microscopy. For (**A**) and (**B**), each data point represents mean values ± S.E.M. of n=3 independent experiments. *, $p<0.05$; **, $p<0.01$; ***, $p<0.001$.

Lipidomic analyses using high resolution liquid chromatography/mass spectrometry as described above were performed with GC1 cells as well.

The analysis of TG content revealed an increase in GC1 cells upon PGP downregulation. Especially longer chain and polyunsaturated TGs were significantly enriched (**Figure 49A)**. Seventy TG-species were identified (**Figure 49B**). Total TG content and the content of the identified TG species were normalized to the total endogenous phosphatidylcholine (PC) content, which was not affected on PGP expression.

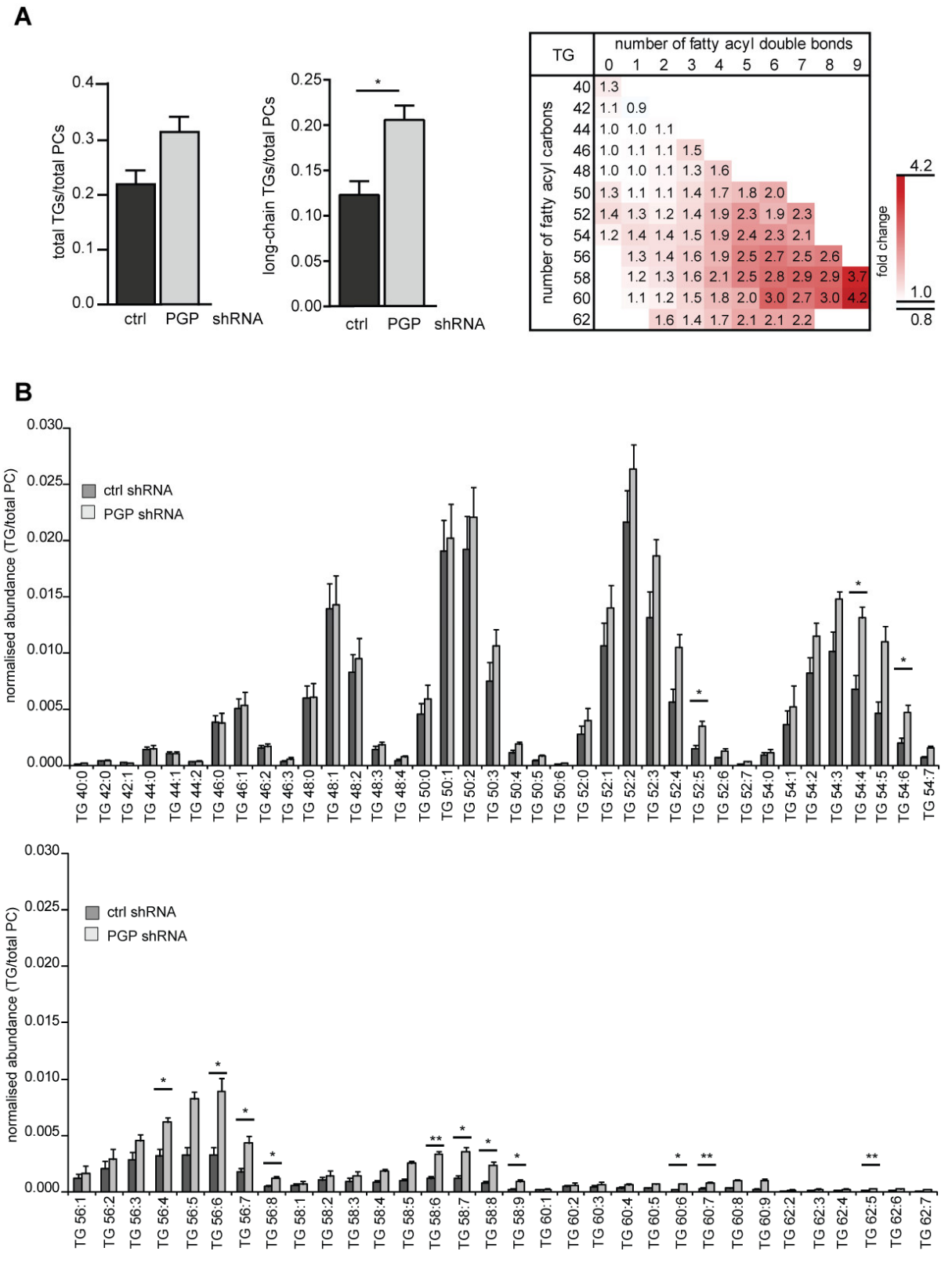

Figure 49: Mass spectrometry-based triglyceride (TG) profiling in total lipid extracts of control or PGP-depleted GC1 cells.

A: Total (left panel), or long-chain (middle panel) TG contents were compared after normalization to the total endogenous phosphatidylcholine (PC) contents. Right panel, fold-change of individual TG species in PGP-depleted compared to control shRNA cells.

B: Endogenous TG species levels in GC1 cells expressing control shRNA (black columns) or PGP shRNA (gray columns). Total TG content was normalised to the total phosphatidylcholine (PC) content determined by LC-MS. Results are mean values ± S.E.M. of *n*=3 experiments. *, $p<0.05$; **, $p<0.01$.

Thus, characteristics of genetically PGP-inactivated cells and embryos such as proliferation defect under normoxic conditions and the enrichment of triglycerides were recapitulated in PGP-depleted GC1 cells.

As a next step, total ATP content as an overall indicator of cellular energy status was determined in GC1 cells (**Figure 50**). Here, the luciferase-based ATP assay was used again. It was shown that cells in which PGP expression was suppressed by shRNA tended to have higher steady-state ATP levels compared to control shRNA cells under regular growth conditions, or when serum-starved cells were growing in the presence of glucose overnight. This difference was completely ablated by pre-incubation with atglistatin (Mayer et al., 2013), an inhibitor of the rate-limiting lipolytic enzyme adipose triglyceride lipase ATGL, suggesting a contribution of lipolysis-derived fatty acids to the elevated cellular ATP levels present in PGP-depleted cells.

To investigate the underlying mechanism further, palmitate was conjugated to BSA to make it bioavailable and used to study utilization of exogenous fatty acids. Serum-starved cells were incubated with palmitate in the presence or absence of glucose. In the presence of both palmitate and glucose, ATP levels in PGP-depleted cells were over 30% higher than in control shRNA cells. In comparison to serum-starved cells growing in the presence of glucose overnight, only ATP content of PGP shRNA expressing cells were slightly increased, suggesting that palmitate was utilized for fatty acid oxidation. However, serum-starved cells growing in the absence of glucose showed decreased ATP content to comparable levels in both cell types, suggesting that control shRNA and PGP shRNA cells differed in the utilization of glucose. This was consistent with the hypothesis that there is a shift towards energy-producing oxidative metabolism in cells lacking PGP activity.

The glucose- and palmitate-dependent overshoot of ATP levels in PGP-deficient cells was completely prevented by atglistatin-mediated inhibition of TG-breakdown. This was also the case by etomoxir-mediated inhibition of the carnitine palmitoyltransferase-1 (CPT-1) -dependent mitochondrial import of long-chain fatty acyl-CoA (Lopaschuk et al., 1988). These results strengthen the hypothesis that elevated ATP levels after loss of PGP activity were caused by increased lipolysis and fatty acid oxidation.

The impact of glucose supply was investigated in more detail. The glycolysis inhibitor 2-deoxy-D-glucose (2-DG, (Wick et al., 1955)), which competitively inhibit the isomerization of glucose 6-phosphate to fructose 6-phosphate, thereby blocking the supply of fructose 1,6-bisphosphate for GADP and DHAP generation was used. Treatment with 2-DG strongly reduced the cellular ATP content in both cell types, and abolished the ATP level elevation in PGP-deficient cells indicating again that the increased lipogenesis was dependent on the supply of DHAP which

functions as precursor of the glycerolipid backbone glycerol 3-phosphate. Thus, the downregulation of PGP in GC1 cells increased their ATP content in a glycolysis-, lipolysis-, and fatty acid oxidation-dependent manner.

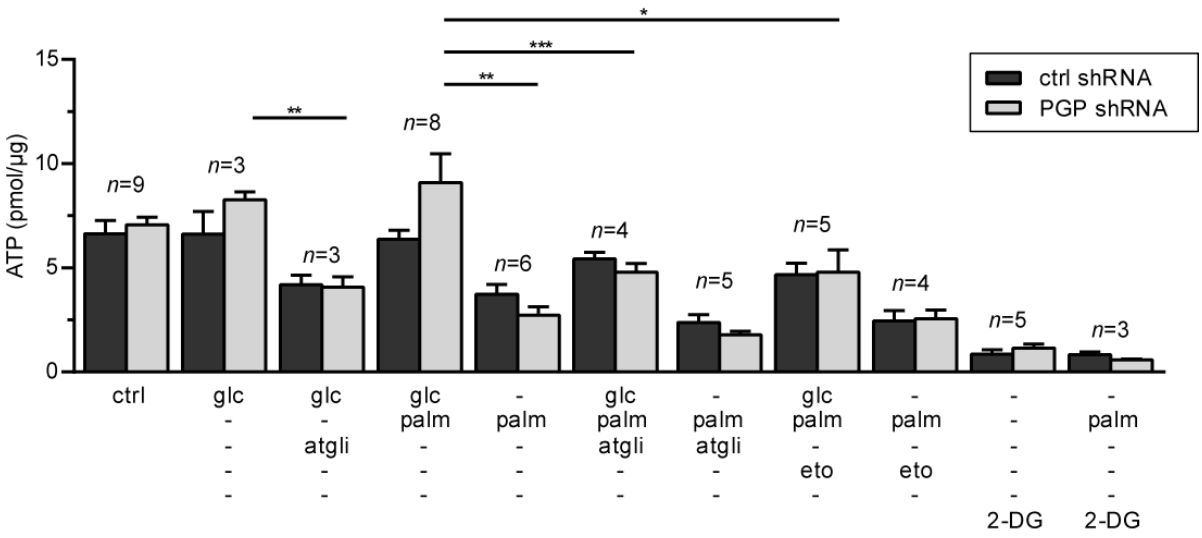

Figure 50: ATP determination of GC1 cells.
Control cells (ctrl) were grown in FCS- and glucose-containing medium. For all other conditions, cells were serum- and glucose starved, and either incubated with glucose (glc) or not ("–" in upper row) and/or with 2-deoxyglucose (2-DG), atglistatin (atgli), palmitate (palm), or etomoxir (eto). The number of n independent experiments performed for each condition is indicated above the bars. *, $p<0.05$; **, $p<0.01$, ***, $p<0.001$.

Because of these results, GC1 cells seemed to be an appropriate cell model to analyze the functions of PGP for energy metabolism further.

Oxygen consumption rates (OCR) were measured with an extracellular flux analyzer. **Figure 51A** shows that the basal and maximal mitochondrial respiration was elevated in PGP-deficient compared to control shRNA cells. Spare respiratory capacity and ATP production were increased as well in PGP-deficient cells whereas proton leak and mitochondrial coupling efficiency were not affected. Treatment of cells with the glycolysis inhibitor 2-deoxy-D-glucose (2-DG), the triglyceride lipase inhibitor atglistatin, or inhibition of mitochondrial fatty acid import and -oxidation with etomoxir before measuring oxygen consumption rates, abolished the elevated OCR of PGP-deficient GC1 cells and normalized ATP production.

Thus, increased energy production of PGP-deficient cells was a consequence of increased lipogenesis, lipolysis and fatty acid oxidation. Since 2-DG blocks the formation of fructose 1,6-bisphosphate-derived DHAP, these results strongly suggest that the increased lipogenesis was dependent on the supply of DHAP, and emphasize the key role of TPI as a branch point between glucose and lipid metabolism. The fact that the impact of inhibition with 2-DG on normalization of oxygen consumption rate was a bit lower than inhibition of lipolysis and fatty

acid oxidation suggests that the cells had still lipid storage available for mitochondrial respiration and ATP production.

Importantly, when PGP-depleted GC1 cells were cultured under hypoxic conditions (which increased the diminished proliferation of PGP-deficient cells, see **Figure 48A** and **48B**), OCR and ATP production in PGP-deficient or -proficient GC1 cells became indistinguishable (**Figure 51B**).

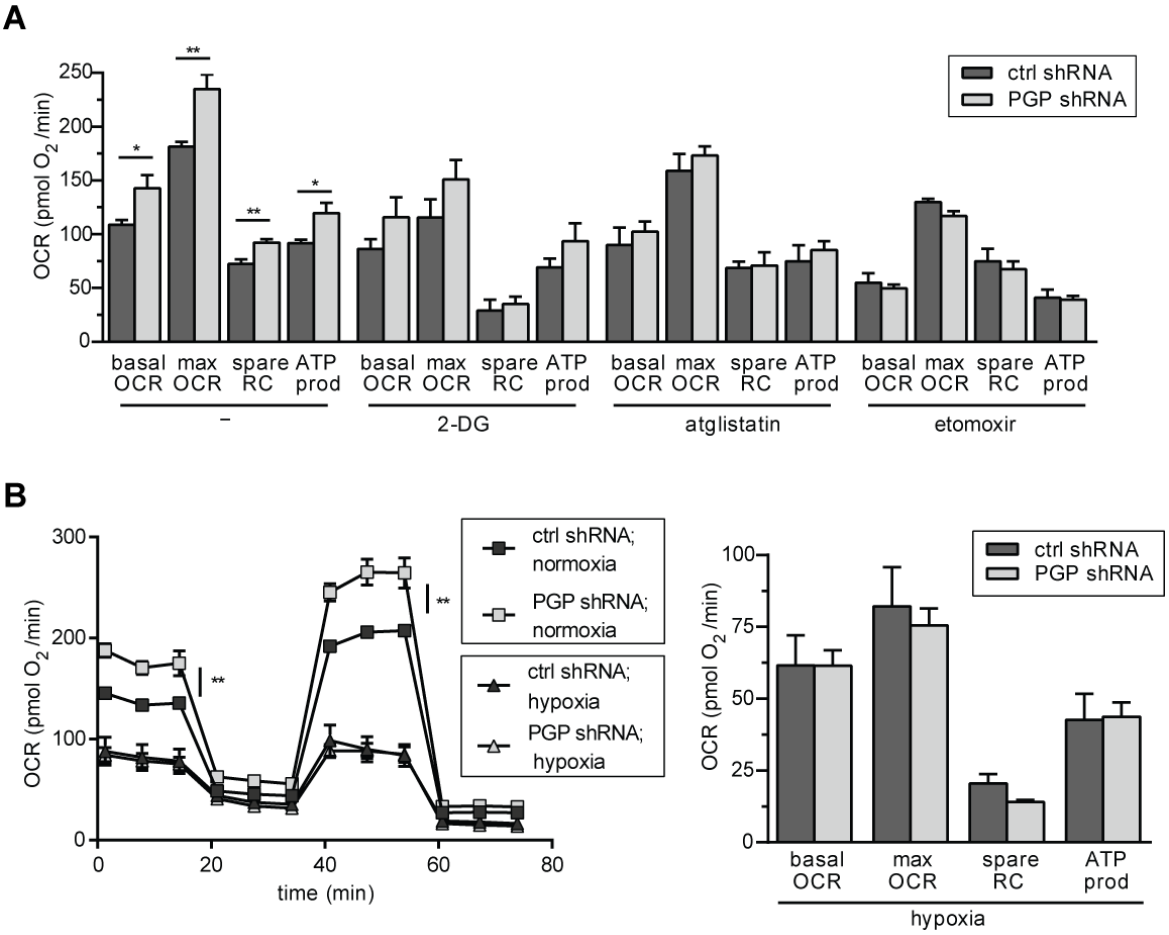

Figure 51: Analysis of cellular respiration.
A: Analysis of mitochondrial oxygen consumption rates (OCR) in PGP-depleted GC1 cells versus control shRNA cells cultured under normoxic (~20% O_2) conditions in the absence (n=6) or presence (n=3) of the indicated inhibitors. 2-DG, 2-deoxyglucose. Spare RC, spare respiratory capacity; ATP prod, ATP production. Mean values ± S.E.M. are given.
B: Mitochondrial OCR measurements in PGP-depleted GC1 cells and control shRNA cells cultured for 16 h under normoxic (~20% O_2) or hypoxic conditions (~3% O_2). Results are mean values ± S.E.M. of n=4 independent experiments. *, $p<0.05$; **, $p<0.01$.

These data demonstrate that the deficiency of PGP lead to elevated oxidative, energy-producing metabolism under normoxic conditions but not under hypoxic conditions.

5 Discussion

This thesis provides mechanistic insights into the role of the mammalian HAD-type phosphatase phosphoglycolate phosphatase PGP (also known as AUM) for receptor-induced cell spreading and cell migration. In addition, it describes for the first time a physiological function of PGP in cellular energy metabolism.

A model of the cell biological and physiological functions of PGP is displayed in **Figure 52**. The remaining open questions are indicated with a question mark and will be discussed in the following sections.

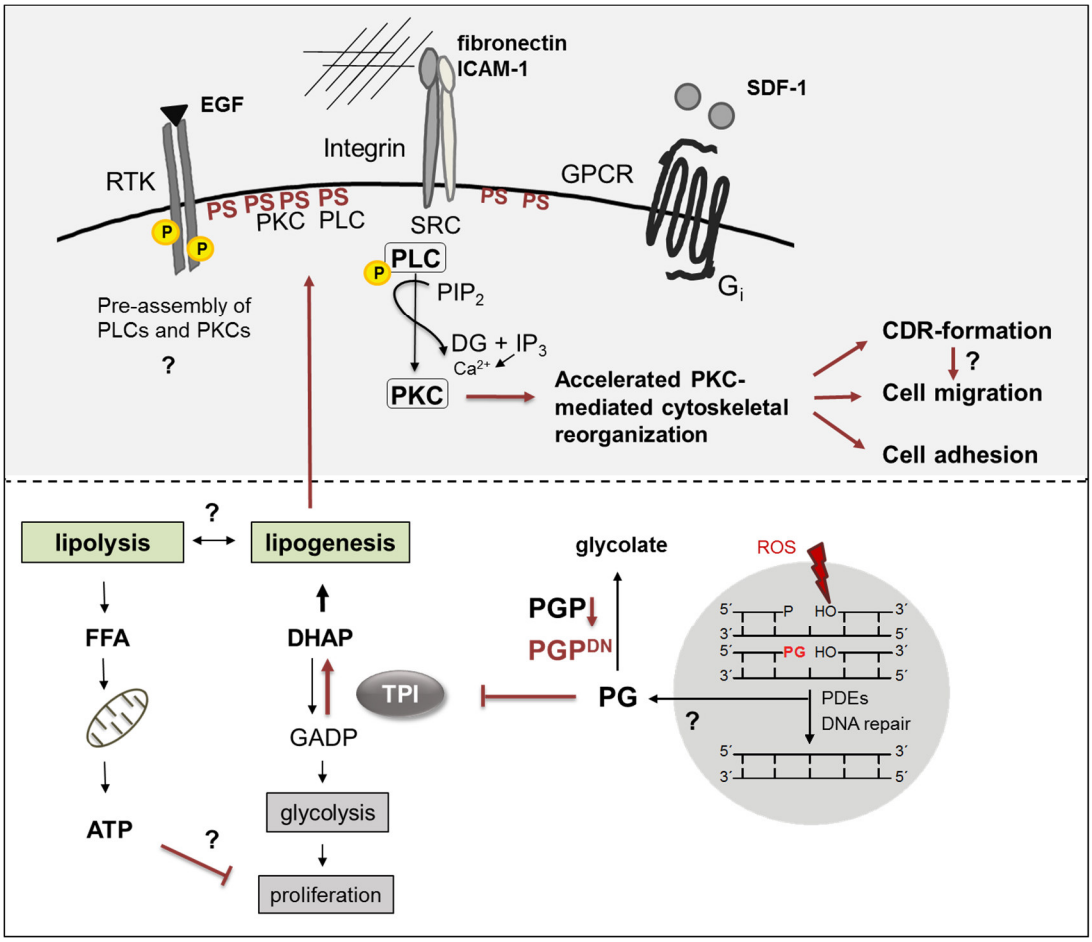

Figure 52: Model of a link between PGP-dependent bioenergetics and PGP functions for cell adhesion and migration.
As consequences of ROS-induced, oxidative DNA damage, 3'-PG termini are formed under homeostatic, normoxic conditions (bottom panel). Phosphodiesterases (PDEs) release PG, which is hydrolyzed by PGP in the cytosol. Genetic PGP inactivation by replacement of endogenous PGP with the catalytically inactive point mutant PGP^{D34N} (PGP^{DN}) prevents PG hydrolysis. PG attenuates TPI activity, causing a re-routing of the carbohydrate flux into triglyceride biosynthesis (lipogenesis), accompanied by an accumulation of the phospholipid phosphatidylserine (PS) in the plasma membrane of PGP-depleted GC1 cells. In GC1 cells and in PGP-inactivated mouse embryos, elevation of triglycerides is accompanied by increased triglyceride breakdown (lipolysis) and mitochondrial fatty acid oxidation. The resulting elevation of ATP levels, likely contributes to impaired cell proliferation.
Upper panel, elevated PS levels in the plasma membrane might lead to the pre-recruitment of signaling proteins such as PLCs and PKCs. In this way, RTK-, integrin- and GPCR-induced and PLC/PKC-mediated effects on the actin cytoskeleton are accelerated and enhanced.

5.1 Role of PGP for cell spreading and cell migration

Using the spermatogonial GC1 cell line, mouse lung endothelial cells and lymphocytes from *Pgp*$^{flx/flx}$ and *Pgp*$^{flx/flx}$; *Tie2-Cre*$^{+/-}$ mice, this study shows for the first time that PGP regulates cell spreading and cell migration downstream of fibronectin-binding integrins-, EGF receptors- and SDF1-induced GPCR signaling. PGP-inactivated cells were characterized by elevated CDR-formation and increased cell spreading and migration.

5.1.1 Does PGP primarily act as a PG phosphatase and/or as a tyrosine-directed phosphatase during cell spreading and migration?

Previous findings from our group suggested that PGP/AUM functions as a tyrosine-directed phosphatase *in vitro* and in cells, and as a regulator of RTK signaling. In a phospho-peptide screen with over 720 phosphorylated peptides, purified PGP exclusively dephosphorylated a small number of tyrosine-phosphorylated peptides and directly hydrolyzed tyrosine-phosphorylated proteins from HeLa cell extracts in a phosphatase overlay assay (Seifried et al., 2014). Furthermore, we demonstrated that PGP deficiency led to elevated tyrosine phosphorylation of some higher molecular weight proteins upon EGF stimulation (Seifried et al., 2014) and to elevated integrin-mediated cell adhesion (PhD thesis Ambrish Saxena).

In the beginning of this study, one emphasis was to find (a) potential tyrosine-phosphorylated substrate(s) of PGP, which might be involved in the regulation of integrin-mediated cell adhesion.

The integrin adhesome consists of a huge complex of tyrosine-phosphorylated proteins and many of these focal adhesion proteins are known to be tyrosine-phosphorylated after activation by cell adhesion to the ECM (Bass et al., 2008, Maher et al., 1985). Therefore, we postulated the existence of a tyrosine-phosphorylated protein substrate of PGP because it might explain the role of PGP for integrin-mediated cell adhesion, spreading and migration.

However, neither analysis of tyrosine phosphorylation levels of focal adhesion proteins in immunofluorescence experiments using TIRF microscopy, nor Western blot- or immunoprecipitation experiments showed changes in tyrosine phosphorylation of proteins involved in integrin signaling such as talin, paxillin or vinculin (data not shown).

We also observed PGP-dependent effects which occurred without integrin engagement. PGP-depleted cells migrated faster under basal conditions without fibronectin stimulation (see **Figure 27**), and PLCγ1 was also hyper-activated in cells seeded on poly-L-lysine and stimulated with EGF (see **Figure 31**), indicating that integrin engagement is not exclusively essential for PGP-dependent effects on cell migration and PLCγ1 activation. Another

possibility could be that PGP-depleted cells seeded on poly-L-lysine produce and secrete more fibronectin leading to integrin engagement and the observed cellular effects.

Cell adhesion, cell spreading and cell migration experiments were performed on the β1 integrin ligand fibronectin. There are at least two tyrosine phosphorylation sites located at the cytoplasmic domain of β1 integrin that modulate integrin function (Sakai et al., 1998). However, whether PGP affects integrin signaling directly at the level of the integrin receptor, has not yet been addressed.

Integrin-mediated effects were further augmented upon co-stimulation of GC1 cells with EGF. The activation of the EGF receptor is known to trigger a cascade of tyrosine phosphorylation events (Carpenter, 2000). Phosphorylation of tyrosine residues pY1045 (PhD thesis; Prashant Duraphe), pY1068 and pY1173 of the EGFR and phosphorylation on tyrosine residue 783 of PLCγ1 (this work, see **Figures 30** and **31**) were elevated in PGP-depleted cells.

PLCγ1 was extensively tested as a potential protein substrate of PGP. The results clearly demonstrate that PLCγ1 is not a direct PGP substrate. Thus, it appears more likely that the observed hyper-activation of PLCγ1 is a direct consequence of hyper-phosphorylation of the EGFR upon receptor activation. Especially, tyrosine residue pY1173 has been implicated in PLCγ1 binding and activation (Soler et al., 1994, Kim et al., 1991, Rotin et al., 1992).

In contrast to PLCγ1, it cannot currently be excluded that the EGFR itself might be a potential substrate of PGP. However, elevated lymphocyte migration in PGP-inactivated cells, which was observed independently of EGFR activation, and the observation that cell adhesion and migration on fibronectin were already elevated in PGP-depleted cells in the absence of EGF are arguments against this theory.

Several other proteins, which play roles in the crosstalk of RTK- and integrin signaling such as FAK, Src or p130cas (Moro et al., 2002) were also tested by Western blot analysis as potential PGP substrates, yet no changes in tyrosine phosphorylation levels were detected (data not shown).

Special attention was given to the analysis of Src as a potential PGP protein substrate. It was shown that PP2-mediated inhibition of Src family kinase (SFK) activity normalized PGP-dependent CDR formation and cell spreading upon integrin- and EGFR activation (see **Figures 25** and **32**). Furthermore, PP2 abolished PGP-dependent effects on lymphocyte migration upon GPCR- and integrin activation. In addition, hyper-phosphorylation of PLCγ1 was not detectable when SFK activity was inhibited.

However, phosphorylation levels at residues pY416 and pY527 of Src and other SFKs (that can also be detected because of cross-reactivity of the phospho-specific antibodies) were

unaltered in control shRNA and PGP shRNA expressing cells under basal conditions and also upon EGFR- and integrin activation, indicating that SFK activity itself was not changed in a PGP-dependent manner (see **Figures 31** and **32**).

It was reported that, SFK activity is essential for integrin-EGFR transactivation because Src mediates the integrin-EGFR macromolecular complex association (Moro et al., 2002).

Thus, it appears that although SFK activity is not directly altered by PGP, it is nevertheless required for integrin-, RTK- and GPCR cross-signaling to mediate PGP-dependent effects on CDR-formation, cell spreading and migration.

Therefore, the data obtained in this thesis do not support the hypothesis that PGP primarily acts as a tyrosine-directed protein phosphatase, but rather provide evidence that PGP regulates actin cytoskeleton reorganization, CDR formation, cell adhesion and migration by acting as a PG-directed phosphatase -as discussed in more detail in the following section.

Nevertheless, considering the large number of tyrosine-phosphorylated proteins involved in integrin-, RTK- and GPCR signaling (Case and Waterman, 2015, Zaidel-Bar and Geiger, 2010) and considering the fact that the closest PGP paralog chronophin dephosphorylates both the low molecular weight substrate pyridoxal 5'-phosphate and the protein substrates cofilin or the steroid receptor coactivator-3, the existence of PGP protein substrates cannot be excluded.

5.1.2 What is the link between upregulated PS levels and PGP-dependent effects on cell spreading and cell migration?

5.1.2.1 Functions of PS

In an untargeted lipidomic analysis of control shRNA and PGP shRNA expressing cells PS was found to be highly upregulated upon PGP depletion.

PS is a negative charged membrane-phospholipid which is actively held at the inner leaflets of the plasma membrane by the enzyme flippase (Segawa et al., 2014) and often associated with apoptosis (Marino and Kroemer, 2013a). During apoptosis, PS can flip to the extracellular leaflet, which acts as a signal for macrophages to engulf the cell (Fadok et al., 1998). This raises the question whether the accumulation of PS in PGP-depleted cells may indicate apoptosis.

In a TUNEL assay, which detects DNA fragmentation as a characteristic of apoptosis, it was shown that PGP-inactivated embryos do not display more apoptotic cells than wildtype embryos.

PGP-deficient GC1 cells and PGP-inactivated mouse embryonic fibroblasts (MEFs) isolated from E8.5 embryos proliferate less (see **Figures 41** and **48**). If these cells additionally undergo apoptosis at a higher rate was not tested yet. Therefore, it will be important to analyze the localization of PS in the plasma membrane. Accumulation of PS at the inner leaflets of the plasma membrane would substantiate our hypothesis that signal transduction is triggered by PS accumulation due to PGP loss, whereas PS accumulation in the extracellular leaflet of the plasma membrane would be a strong indicator of apoptosis. To analyze the subcellular localization of PS, FACS or immunostaining experiments of permeabilized versus non-permeabilized cells could be performed using a specific PS antibody (Mourdjeva et al., 2005) or Annexin V, which specifically binds to PS (Vermes et al., 1995).

PS is also implicated in signal transduction by recruitment and binding of signaling proteins such as vinculin, a protein of the adhesome (Case and Waterman, 2015). Importantly, PLCs and PKCs can bind to PS (Stace and Ktistakis, 2006, Kay and Grinstein, 2013), and PS is required for the activation of classical and atypical PKCs (Geraldes and King, 2010).

Potential mechanisms how elevated PS levels can lead to the observed PGP-dependent and PKC-mediated effects on cell adhesion, cell migration and CDR formation are discussed in the following section.

5.1.2.2 PS accumulation leads to catalyzed PKC-mediated signal transduction

It was demonstrated that PKC activity was upregulated in PGP-inactivated cells. This could be a result of a hyper-activation of PLCγ1 observed in cells lacking PGP. PLC activates PKCs by cleavage of the membrane phospholipid phosphatidylinositol 4,5-bisphosphat (PIP_2) to inositol 3- phosphate (IP_3) and diacylglyceride (DG). DG and Ca^{2+} released upon IP_3 receptor activation activate PKCs (Mochly-Rosen et al., 2012). However, it is also possible that classical and atypical PKCs are directly activated by PS at the plasma membrane independent of RTK-, integrin- or GPCR activation (**Figure 53(I)**).

Whereas, PS levels were found to be upregulated in unstimulated PGP-depleted cells, elevated PKC activity in PGP-inactivated lymphocytes was detected only after integrin- and GPCR activation. Thus, an activation of PKCs by PLC-mediated signaling upon receptor stimulation might be more likely than a direct activation by PS.

As mentioned above, PS is implicated in signal transduction by binding of signaling proteins. Thus, it is possible that upregulation of PS in the plasma membrane leads to a pre-recruitment of signaling proteins such as PLCs and PKCs (**Figure 53(II)**). After receptor activation, signal transduction might be triggered resulting in accelerated PKC-mediated cytoskeletal remodeling.

Upon loss of PGP activity, cell spreading and cell migration were elevated in a PKC-dependent manner, suggesting that actin reorganization proceeded faster. In addition, EGFR- as well as PLCγ1 hyper-activation resulting in PKC activation was detected already 3 minutes after EGF stimulation. Together with the described accelerated actin-breakdown after PKC activation in cells lacking PGP (see **Figure 34**), these data are consistent with the idea that a pre-assembly of signaling proteins leads to accelerated PKC-mediated actin reorganization.

To confirm this hypothesis in subsequent studies, it will be necessary to visualize a potential pre-recruitment of PKCs or PLCs to the plasma membrane. With fluorescently-tagged PKC or PLC constructs, subcellular localization in living cells could be investigated before and after receptor activation. By using activity sensors such as YFP-PH[PLCδ] (pleckstrin homology domain of human PLCδ1 fused to YFP), which specifically binds to PIP_2 in the plasma membrane, it may be possible to analyze subcellular localization as well as the activation of PLC (Sinnecker and Schaefer, 2004).

Another possibility of how PGP-dependent changes in PS levels may influence PGP-regulated cellular effects could be that PS accumulation in the plasma membrane leads to a receptor clustering of integrins and/or the EGFR (**Figure 53(III)**). As a consequence, transactivation of the receptors might be facilitated because of their close spatial proximity, or signal transduction might be accelerated as a result of assembly of signaling molecules involved in signal transduction of all these three receptors.

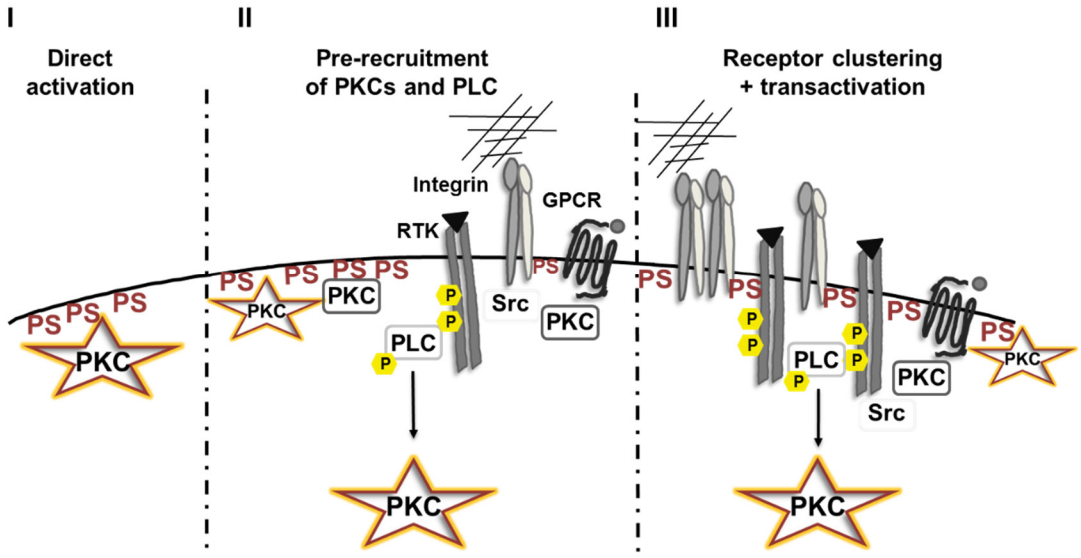

Figure 53: PKC activation mechanisms.
For details, see text above.

To test this hypothesis, a potential receptor clustering should be visualized by immunostaining of the receptors. By using antibodies that specifically detects active conformations of integrins

or by using phospho-specific antibodies against EGFR, it is additionally possible to make a statement about a potential transactivation of the receptors. The assumed pre-recruitment of signaling proteins may even increase the effect of receptor clustering.

One could also speculate if elevated PS levels lead to altered membrane fluidity. PS is a phospholipid with a negatively charged head group. Lipids in a cell membrane enriched with PS might be less densely packed and more motile because of the repulsion of the negatively charged head groups.

Alternatively, elevated PS levels may affect lipid raft composition and/or abundance. Lipid rafts are glycolipoprotein microdomains which are implicated in signal transduction by assembling signaling molecules and in receptor- and membrane protein trafficking (Pike, 2009). It was reported that PS levels are elevated 2-to 3-fold in lipid rafts compared with the plasma membrane (Pike et al., 2002).

To test if altered membrane composition influences membrane structure, transmission electron microscopy (TEM) and scanning electron microscopy (SEM) analyses of control shRNA and PGP shRNA expressing GC1 cells are currently ongoing.

5.1.3 Untargeted lipidomic analysis of GC-1 cells

In the untargeted lipidomic analysis of control shRNA and PGP shRNA expressing cells, 24 compounds were found to be highly upregulated in PGP-depleted cells in addition to triglycerides (see **Figure 36**). The four high abundance compounds were identified as PS species. However, there are still 20 low abundance compounds, which have not been identified yet.

During triglyceride biosynthesis also lipid signaling molecules and second messenger such as DG are generated (Spiegel et al., 1996). These compounds are usually not present in large quantities. Thus, it would be very important in order to better understand PGP-dependent signaling downstream of integrin-, EGFR and GPCR activation to identify the low abundance compounds as well.

Additionally, it is necessary to test if PS or other membrane lipids are upregulated in lymphocytes lacking PGP activity to strengthen the hypothesis that changes in plasma membrane composition causes PGP-dependent effects on cell migration.

To confirm that elevated PS levels in PGP-depleted cells leads to the observed effects on cell spreading and migration, it may be interesting to interfere in PS synthesis by modulating phosphatidylserine synthases with a shRNA approach or with a phosphatidylserine synthase

inhibitor such as inositol (Kelley et al., 1988). Intervention of PS synthesis should affect PGP-dependent cellular processes.

5.1.4 Inhibitor studies

To elucidate signaling pathways leading to elevated CDR formation and lymphocyte migration upon loss of PGP activity, key enzymes downstream of the integrins, EGFR and GPCRs were pharmacologically inhibited to show their involvement in PGP dependent cellular processes. It was demonstrated that PGP regulates CDR formation and directed lymphocyte migration in a PLC-, Src- and PKC-dependent manner (see **Figures 31, 32** and **33**). Although, structurally related negative controls of the employed inhibitors were used, off-target effects of the inhibitors cannot be excluded. Protein kinase inhibitors are not completely selective (Bain et al., 2007) and the phospholipase C inhibitor U73122 was shown to additionally possess activity against estrogen receptors (Cenni and Picard, 1999).

To further confirm the results achieved with the inhibitor studies, siRNA- or shRNA mediated downregulation of involved enzymes or the expression of catalytically inactive mutants can be performed.

5.1.5 Do elevated cellular ATP levels affect actin reorganization?

Another possibility could be that PGP inactivation elevates cell adhesion and cell migration through elevated ATP levels. It was demonstrated that downregulation of PGP in GC1 cells led to an increase of cellular ATP levels in a glycolysis-, lipolysis-, and fatty acid oxidation-dependent manner (see **Figure 50** and **51**).

In migrating cells, energy derived from ATP is utilized for cell movement. As explained in detail in **1.6**, during cell migration, actin filaments are reorganized in a highly dynamic manner. A process called treadmilling plays a critical role for actin remodeling at the leading edge of migrating cells (Pantaloni et al., 2001). Treadmilling describes the process of assembly of actin monomers at the plus end (barbed end) of actin filaments associated with the disassembly of actin at the minus end (pointed end) (Wegner, 1976) (**Figure 54**).

For polymerization of actin filaments ATP-bound actin (ATP-actin) is added at the barbed end. Profilin promotes the exchange of ADP-actin to ATP–actin under ATP hydrolysis. In addition, it binds to ATP-actin and directs it to the barbed end (Pring et al., 1992).

The extent of actin polymerization depends on the concentration of free ATP–actin. At high levels, the rate of actin assembly exceeds the rate of disassembly resulting in actin filament growth (Carlier et al., 2015).

Filament elongation towards plasma membrane leads to protrusions such as lamellipodia and is the driving force for cell motility. Hydrolysis of the bound ATP to ADP induces a conformational change of actin leading to weaker association with neighboring actin molecules and destabilization of the actin filaments. ADF/cofilin binding leads to the filament disassembly into shorter fragments and ADP-bound actin monomers (Carlier et al., 1997).

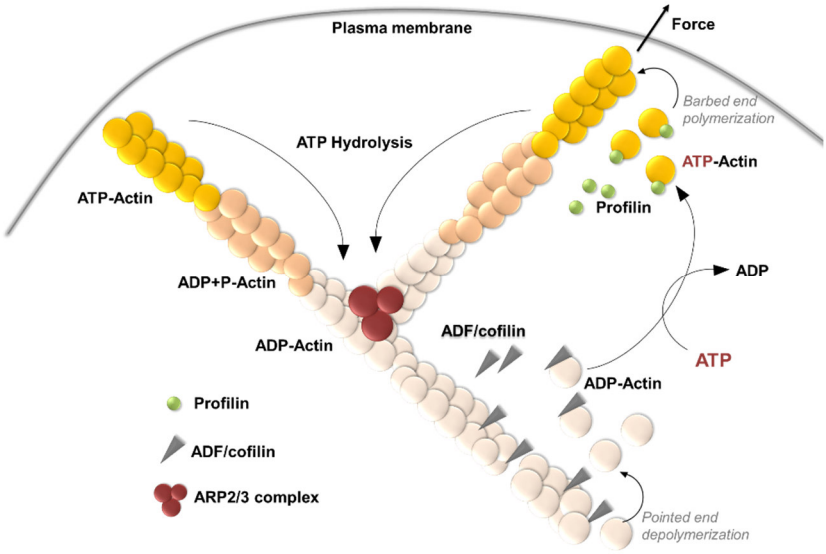

Figure 54: Treadmilling of actin filaments involved in the formation of plasma membrane protrusions and cell movement.
For details, see text above. The figure is adapted from (Carlier et al., 2015).

Thus, actin reorganization is an energy-dependent process. It was reported that chronophin, the closest relative of PGP, forms an ATP-sensing biosensor with the chaperone Hsp90 that regulates cofilin-dependent actin dynamics in an ATP-dependent manner (Huang et al., 2008). Cellular ATP depletion leads to a dissociation of the inhibitory chronophin/Hsp90 complex, and to elevated dephosphorylation and activation of cofilin by chronophin. Bamburg et al. could show that due to an inhibition of actin remodeling during anoxic stress in neurons, cellular ATP consumption is reduced by 50% (Bernstein and Bamburg, 2003). Thus, attenuation of actin turnover is a mechanism to save ATP under energy-deprived conditions. In addition, it was reported that cellular ATP depletion by treatment with the respiratory chain complex III inhibitor antimycin A leads to a decrease in ATP-actin monomers levels whereas ADP-actin levels stay unaltered. (Atkinson et al., 2004).

To the best of my knowledge, there are no reports connecting increased cellular ATP content to changes in actin-based processes such as cell adhesion and migration. It was demonstrated that elevated ATP levels in cells lacking PGP activity were caused by increased lipolysis and

fatty acid oxidation. To analyze if PGP-dependent cell migration is regulated by cellular ATP contents, control shRNA and PGP shRNA expressing cells could be treated with etomoxir, an inhibitor of the carnitine palmitoyltransferase-1 (CPT-1)-dependent mitochondrial import of long-chain fatty acyl-CoA or with atglistatin, an inhibitor of the rate-limiting lipolytic enzyme adipose triglyceride lipase ATGL to adjust lipolysis-induced changes in cellular ATP content, before analysis of cell migration.

5.1.6 CDR formation

PGP-depleted cells showed elevated formation of a ring-like membrane protrusion on the dorsal surface upon EGF stimulation. We identified this membrane structure as circular dorsal ruffle (CDR).

5.1.6.1 Signaling pathways involved in CDR formation

The signaling pathways leading to the formation of CDRs are currently poorly understood. Until now, about 20 proteins which localize to CDRs and are involved in their formation have been identified in the last few years (Hoon et al., 2012).

In this study, it was shown that PGP localizes to CDRs and decreases CDR formation. Next to the tumor suppressor p53, PGP is the only identified protein which negatively regulates CDR formation (Payne et al., 2014).

PGP-depleted cells showed significantly more CDRs. However, if this was due to altered signaling leading to the formation of CDRs is not fully answered yet.

It was shown that the EGFR was hyper-phosphorylated at auto-phosphorylation sites pY1173, pY1068 (this work) and pY1045 (PhD thesis Prashant Duraphe) upon EGF stimulation of PGP-depleted cells. In addition, PLCγ1 which is involved in PGP-dependent CDR formation was hyper-activated. Thus, CDR formation might be increased because EGFR signaling is elevated/hyper-activated upon loss of PGP activity.

PGP-depleted cells showed higher EGFR expression levels under basal conditions and thereby might be more responsive to EGF stimulation. Furthermore, the EGFR seemed to be degraded to a greater extent in control shRNA cells, upon EGF stimulation (see **Figure 30**). This suggests that the EGFR might exhibit prolonged signaling from the plasma membrane, which also might lead to elevated CDR formation in PGP shRNA expressing GC1 cells. Interestingly, a similar mechanism has been very recently proposed. It was reported that the tumor suppressor Merlin inhibits internalization and signaling of the EGFR by controlling tension at the actomyosin cytoskeleton (Chiasson-MacKenzie et al., 2015).

Another explanation for elevated CDR formation could be that PS accumulation, observed in PGP-depleted cells, alters plasma membrane composition and facilitates the formation of CDRs.

5.1.6.2 CDR functions

Until now the cellular functions of these transient, actin-rich membrane structures are not fully understood.

CDRs are often linked to receptor internalization. RTKs, in particular the EGF receptor, is known to be sequestered and internalized via CDRs (Orth et al., 2006). Upon internalization, RTKs can be either recycled or degraded (Sigismund et al., 2008).

As mentioned above, EGFR signaling is increased and prolonged (hyper-phosphorylation of the EGFR) in PGP-depleted cells. Elevated CDR formation and subsequent EGFR downregulation by degradation could be a negative feedback mechanism to limit EGFR signaling.

To analyze if EGFR is endocytosed via CDRs, internalization experiments were attempted in living cells by using labeled EGF. However, only a very low signal was detectable, indicating low expression levels of the EGFR, and receptor internalization was not observable in control shRNA or in PGP shRNA expressing cells.

Furthermore, Western blot analysis demonstrated that EGFR expression levels were higher in PGP-depleted cells upon EGF stimulation (see **Figure 30**), arguing against a potential degradation of the receptor due to elevated CDR formation.

Recently, a model was discussed that implicates CDR formation in integrin trafficking. It was demonstrated that αvβ3 integrins are internalized through macropinocytosis in CDRs on the dorsal cell surface upon PDGF stimulation (Gu et al., 2011). It is well established that integrin trafficking from the dorsal to the ventral surface leads to the creation of new adhesive sites to mediate cell spreading, adhesion or migration (Margadant et al., 2011). Integrins can be internalized by clathrin-dependent and caveolar endocytosis as well as via circular dorsal ruffles (Pellinen et al., 2008, Shi and Sottile, 2008, Gu et al., 2011).

Thus, the question arose if loss of PGP leads to increased cell spreading and cell migration because of elevated integrin internalization and/or trafficking via CDRs.

To answer this question, CDR formation was pharmacologically blocked by inhibition of signaling proteins, which are known to be essential for CDR formation (see **Figure 25**). The activity of the large GTPase dynamin was inhibited with dynasore, the activity of PI3K with wortmannin and Src family kinase (SFK) activities with PP2 before cell spreading assays were

performed. In every case, PGP-dependent cell spreading was normalized. These data led to the conclusion that PGP regulates cell spreading in a CDR-dependent manner and were consistent with our hypothesis that an increase in cell spreading of PGP-depleted cells is a consequence of increased integrin trafficking via CDRs.

It needs to be considered that inhibition of dynamin, PI3K and SFK not only dampens CDR formation, but also affects cell spreading *per se*. Especially Src is an important regulator of integrin-mediated cell adhesion (Cary et al., 2002). Furthermore, SFKs activate proteins involved in actin polymerization machinery such as WASP and WAVE (Takenawa and Suetsugu, 2007). PI3K, also identified as a regulator of integrin-mediated cell spreading (Zeller et al., 2010) activates the ARP2/3 complex via PAK1, a key molecule in the actin dynamics machinery (Yang et al., 2011, Vadlamudi et al., 2004). Dynamin regulates cell spreading either by promoting Rac trafficking (Schlunck et al., 2004) or by regulation of phospholipase D activity (Lee et al., 2015).

Thus, it will be difficult, if not to say impossible, to find a specific protein, which is only critical for CDR formation and which is not involved in signaling pathways leading to cell adhesion, cell migration and/or the reorganization of the actin cytoskeleton downstream of integrin- or RTK activation.

Furthermore, cell spreading was also elevated in PGP-inactivated mouse lung endothelial cells (isolated from *Pgp$^{flx/flx}$; Tie2-cre$^{+/-}$* mice) after co-stimulation with fibronectin and EGF. Though it was reported that endothelial cells display CDR formation upon vascular endothelial growth factor (VEGF) stimulation (Wu et al., 2003), stimulation with EGF, VEGF or PDGF did not induce CDR formation in wildtype or PGP-inactivated MLECs when plated on fibronectin.

These arguments are against the hypothesis that increased integrin trafficking via CDRs elevates cell spreading in PGP-depleted cells.

To analyze if PGP-dependent CDR formation affects integrin trafficking, internalization and recycling of integrins need to be investigated in living cells. In preliminary experiments which have already been performed, labeled fibronectin was used to visualize the receptors after ligand binding. However, no fibronectin internalization was observable upon EGF stimulation.

Taken together, it has so far not been possible to visualize integrin and RTK- trafficking. To strengthen the hypothesis that PGP-dependent effects on cell spreading and migration are a consequence of altered integrin trafficking, more experiments are required.

5.2 Physiological functions of PGP

To study the biological functions of PGP activity, E8.5 *Pgp*$^{WT/WT}$ and *Pgp*$^{DN/DN}$ embryos, MEFs generated from E8.5 embryos, red blood cells isolated from *Pgp*$^{flx/flx}$; *Tie2-Cre*$^{+/-}$ mice and GC1 cells were analyzed. It was shown that ablation of PGP activity causes (via inhibition of triose phosphate isomerase activity by PG) a switch from a predominantly glycolytic, proliferative, to an oxidative, energy-producing metabolism resulting in a block of cell proliferation. This metabolic shift is reversible upon oxygen deprivation and could explain why whole-body PGP inactivation results in growth arrest and the death of *Pgp*$^{DN/DN}$ embryos.

Because PG is likely derived from the repair of oxidative DNA damage (see **1.4.1.1**), PGP might play a role in the adaption of cellular bioenergetics and cell proliferation to the extent of DNA damage.

5.2.1 PGP inactivation leads to cell proliferation arrest

As a consequence of DNA damage, a well-known DNA damage response (DDR) mechanism is initiated to stop proliferation to ensure DNA repair or to trigger apoptosis, when the damage is not repairable (Jackson and Bartek, 2009). In eukaryotic cells, there are distinct control points, so-called cell cycle checkpoints, which ensure that cells pass accurate copies of their genomes on to the next generation. With the help of these checkpoints, the cell is able to detect damaged DNA and to coordinate cell-cycle progression with DNA repair. One prominent example of a DDR mechanism is the ATM (Ataxia telangiectasia mutated)/ATR (ATM- and RAD3-related) system. ATM and ATR are protein serine/threonine kinases and transduce signals after sensing DNA damage to effector proteins, which control cell cycle progression, such as p53 (Abraham, 2001).

In contrast to these well-studied cell cycle checkpoints, our potential DDR mechanism combines proliferation arrest and changes in metabolism. The PGP-dependent shift towards energy producing oxidative metabolism results in increased triglyceride formation and lipolysis-dependent ATP production.

It has been estimated that the repair of a single double-strand break (DSB) requires more than 10^4 ATP molecules (Hoeijmakers, 2009). Oxidative single-strand break (SSB) DNA repair also consumes ATP, and over-activity of the DNA repair enzyme poly(ADP-ribose) polymerase (PARP) can even deplete cellular ATP pools (Ha and Snyder, 1999) through inhibition of glycolysis (Andrabi et al., 2014).

Since ATP-consuming DNA repair processes are not expected to be altered by PGP-deficiency, the resulting ATP production in excess of demand likely contributes to the

proliferation arrest, for example by inhibition of rate limiting steps in glycolysis that are inhibited by a high ATP/AMP ratio (Locasale and Cantley, 2011). However, PGP-dependent mechanisms that inhibit cell proliferation warrant further investigation.

Previously, our group has shown that PGP dephosphorylates both ATP and ADP *in vitro* (Seifried et al., 2014). Given that intracellular ATP concentrations are generally in the range of 1-10 mM and about fivefold higher than the concentrations of ADP, the steady-state enzyme kinetics previously determined with purified PGP (ADP: K_m 0.4 mM, ATP: K_m 1.2 mM; (Seifried et al., 2014)) are consistent with an additional function of PGP as a cellular ATP/ADP phosphatase. It is possible that the rise in ATP levels upon PGP inactivation or depletion is a combined result of increased ATP production through fatty acid oxidation and decreased ATP hydrolysis.

To investigate the role of PGP as potential ATP/ADP phosphatase it may be informative to measure cellular ATP levels under hypoxic conditions. Elevated ATP levels in PGP-inactivated cells would indicate that missing ATP hydrolysis leads to ATP overshoot under hypoxia and that the cell proliferation defect of PGP-depleted/inactivated cells is not caused by an increase in cellular ATP levels.

5.2.2 Is PGP a PG phosphatase *in vitro* and *in vivo?*

The K_m of 0.3 mM PG (see **Figure 3**) that was determined for recombinant, murine PGP is similar to the value reported for the specific phosphoglycolate phosphatase GPH from *E. coli* (K_m 0.2 mM), which is involved in the hydrolysis of PG released by the activity of DNA repair enzymes (Teresa Pellicer et al., 2003).

Mass spectrometric quantification showed that 3'-PG termini constitute ~10% of all DNA sugar oxidation products produced by γ-irradiation or by treatment with the radiomimetic drug bleomycin (Chen et al., 2007); earlier studies estimated that ~25% of oxidative stress-induced (Bertoncini and Meneghini, 1995), or up to 50% of radiation-induced DNA strand breaks bear 3'-PG termini (Henner et al., 1983). Given the abundance of 3'-PG-containing lesions in DNA, the enzymatic properties of murine PGP appear to be well-adapted to a physiological function for PG dephosphorylation downstream of DNA repair but nevertheless further experiments are required.

Most important is to confirm the PGP hydrolyzing activity *in vivo.* For this purpose, it would be necessary to measure PG levels in cells, tissue and whole organs and to compare these levels in wildtype and PGP-inactivated cells/mice.

Established methods to determine PG levels include highly sensitive gas chromatography/mass spectrometry (Chen et al., 2007) and initial experiments to determine PG levels in blood samples from *Pgp*$^{flx/flx}$ and *Pgp*$^{flx/flx}$; *Tie2-Cre*$^{+/-}$ mice are currently ongoing.

5.2.3 Analysis of the link between DNA damage-derived PG and inhibition of TPI activity

To examine whether PG released after DNA damage is critical for TPI inhibition, enzymes involved in processing 3'-PG ends from DNA strand breaks such as tyrosyl-DNA phosphodiesterase (TDP1) (Chen et al., 2001) or AP endonuclease 1 (APE1) (Parsons et al., 2004) can be pharmacologically blocked (Al-Safi et al., 2012, Huang et al., 2011b). Treatment of PGP-inactivated cells with TDP1 and/or APE1 inhibitors should normalize TPI activity, demonstrating that PG derived from DNA damage causes TPI inhibition.

Another possibility could be to cultivate control and PGP-inactivated cells under hypoxia. Under hypoxic conditions, formation of 3'-PG DNA ends should be suppressed. A normalization of TPI activity of wildtype and PGP-inactivated cells would demonstrate that DNA damage and the resulting release of PG causes TPI inhibition upon PGP inactivation.

Additional cellular PG sources may also exist. Pyruvate kinase isolated from skeletal muscle has been reported to phosphorylate glycolate (Sasaki et al., 1987). However, the corresponding enzyme from red blood cells only exhibits low glycolate kinase activity, and a physiological relevance of pyruvate kinase for the maintenance of erythrocyte PG concentrations has been questioned.

5.2.4 Ablation of PGP activity only moderately inhibits TPI activity

As already mentioned in **1.4.1.2**, there are some reports identifying PG as an *in vitro* inhibitor of enzymes involved in glucose homeostasis. Because of its structural similarity to intermediates of glycolysis and the gluconeogenesis/glyceroneogenesis pathways, PG can inhibit triosephosphate isomerase (TPI) (Hartman et al., 1975), the phosphoenolpyruvate carboxykinase (PEPCK) (Stiffin et al., 2008), an enzyme critical for gluconeogenesis and glyceroneogenesis and pyruvate kinase (PK), another enzyme involved in glycolysis (Dougherty and Cleland, 1985).

PG inhibits purified TPI activity as a reversibly binding transition state analog of TPI substrates *in vitro* (Wolfenden, 1969). Consistent with this finding, TPI activity in PGP-deficient embryos and -cells was only moderately inhibited by ~34% (see **Figure 42**). A comparable reduction has been measured in a TPI-deficient yeast strain reconstituted with human TPI (Ralser et al., 2007). Using mass spectrometry, the authors of this study showed that an attenuation of TPI

activity by ~30% augmented intracellular DHAP and glucose 6-phosphate levels by ~25%, and doubled the concentration of the pentose phosphate pathway (PPP) intermediate 6-phosphogluconate. However, no marked changes of ribose 5-phosphate levels were detected under these conditions (Ralser et al., 2007). Thus, the attenuation of TPI activity observed in PGP-deficient embryos and cells is consistent with a TPI-dependent metabolic re-routing of carbohydrates into lipid biosynthesis and a concomitant increase in flux through the PPP (Stincone et al., 2014). The oxidative arm of the PPP supplies NADPH as an essential cofactor for antioxidant systems, allowing the cell to cope with an increased ROS load caused by elevated fatty acid oxidation. NADPH is also required for fatty acid biosynthesis, and the observed build-up of polyunsaturated fatty acids upon PGP loss may therefore be facilitated by PPP-mediated NADPH production.

So far, PG was only experimentally used as an *in vitro* inhibitor of PK, PEPCK and TPI. In this study, it was demonstrated that cellular PG levels were sufficient to attenuate TPI activity in PGP-inactivated cells. Whether the inhibition of PG hydrolysis upon loss of PGP activity affects the activities of the PG-dependent enzymes PK and PEPCK in cells and *in vivo,* has not yet been tested.

5.2.5 Glycolysis, gluconeogenesis and glyceroneogenesis as potential PG-regulated processes

PK catalyzes the phosphoryl-transfer from phosphoenolpyruvate (PEP) to ADP, which constitutes the final step of the glycolytic pathway leading to pyruvate production (Berg JM, Tymoczko JL, Stryer L. Biochemistry. 5th edition; 2002). Pyruvate is a key intermediate in several metabolic pathways including fatty acid synthesis.

PK and TPI inhibition might result in a complete block of glycolysis, and pyruvate as the final product of glycolysis cannot be used for ATP production in the tricarboxylic acid (TCA) cycle.

PEPCK catalyzes the conversion of oxaloacetate derived from pyruvate to phosphoenolpyruvate (PEP) which constitutes the rate-limiting step of gluconeogenesis (Berg JM, Tymoczko JL, Stryer L. Biochemistry. 5th edition; 2002). The following steps are almost the same as reversed glycolysis. Gluconeogenesis takes place mainly in the liver and to a small fraction in the kidney upon glucose deprivation. For gluconeogenesis non-carbohydrate substrates such as pyruvate derived for example from glucogenic amino acids, lactate or fatty acids are utilized for glucose biosynthesis to maintain blood glucose levels.

PEPCK is also a key enzyme in the metabolic pathway of glyceroneogenesis, which takes place upon glucose deficiency in the liver, but mainly in adipose tissue (Hanson and Reshef, 2003). Glyceroneogenesis is the branched arm of gluconeogenesis because the first steps

including the decarboxylation of oxaloacetate to PEP by PEPCK are the same as in gluconeogenesis. After DHAP production, glyceroneogenesis and gluconeogenesis diverge. DHAP is converted to G3P, which is usually derived from glucose under non-starvation conditions. G3P is esterified with activated fatty acids (FA-CoA) and provides the carbon backbone of triglycerides. Interestingly, about 30% of released fatty acids in adipose tissue and about 50% in non-adipose tissue are usually re-esterified during glyceroneogenesis (Reshef et al., 2003).

An overview over potential PG-regulated metabolic pathways is depicted in **Figure 55.**

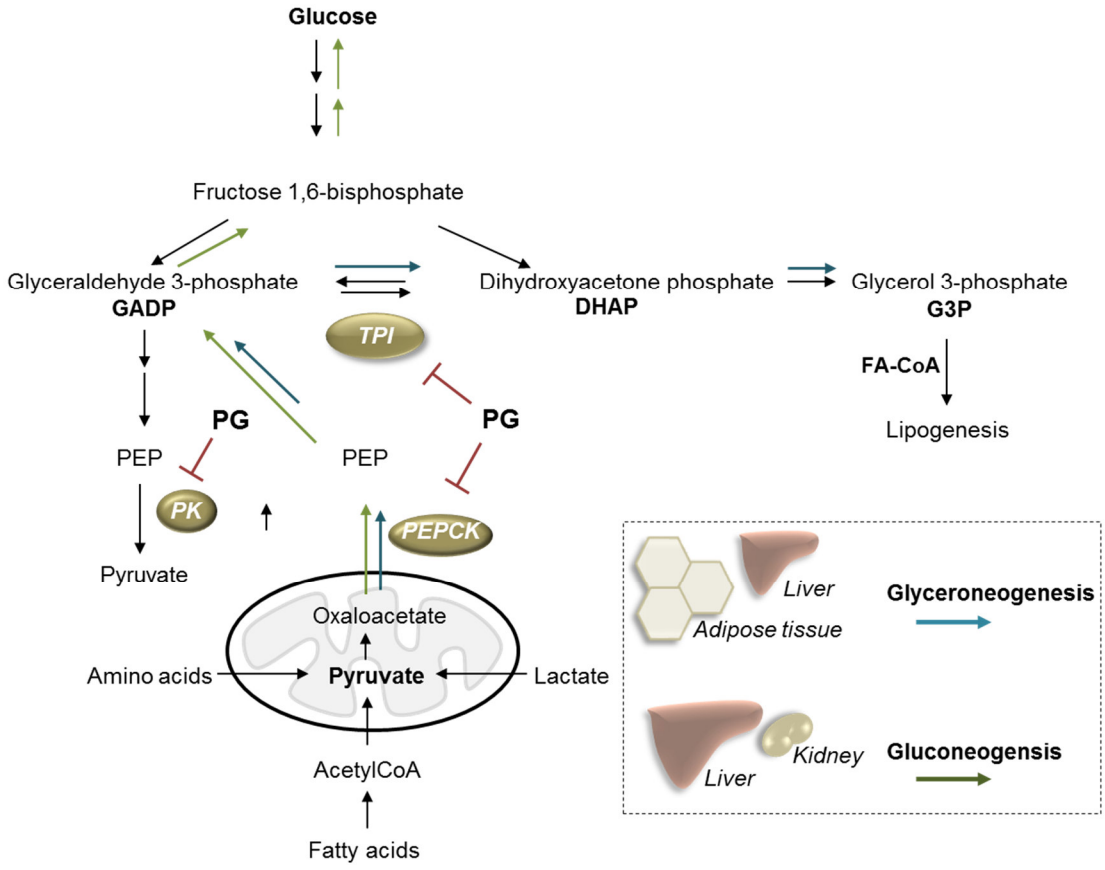

Figure 55: Glycolysis, gluconeogenesis and glyceroneogenesis as PG-regulated metabolic pathways. For details, see text above.

Human PEPCK can be found within the mitochondria and the cytosol. Very recently, it was reported that mitochondrial PEPCK enables tumor cells, which are growing under glucose deprivation, to use PEP supplied by glutamine to drive TCA cycle metabolism and for the production of glycolytic pathway intermediates required for cell proliferation (Vincent et al., 2015).

PG inhibits TPI and PK and thereby attenuates glycolytic cell proliferation. The inhibition of mitochondrial PEPCK by PG would even exclude the possibility for the cell to use glutamine for the synthesis of glycolytic pathway intermediates to ensure cell proliferation.

Taken together, our findings do not exclude the possibility that in addition to TPI, alterations in the activity of other PG-dependent enzymes contribute to the observed phenotype (Gruning et al., 2014, Gruning et al., 2011). The potential inhibition of PK- and PEPCK activity by PG reveals new roles for PGP as a kind of detoxification enzyme by dephosphorylating PG and thereby as an important regulator of carbohydrate and lipid metabolism.

5.2.6 TPI inhibition results in the accumulation of long-chain polyunsaturated fatty acids

The inhibition of TPI causes a block of glycolysis and increased lipogenesis. Interestingly, triglyceride (TG) species esterified with especially long-chain and polyunsaturated fatty acids accumulated after loss of PGP activity in cells and E8.5 embryos (see **Figures 46** and **49**).

The location of the double bonds within the unsaturated fatty acids can be critical for biological functions. Unfortunately, with our technical approach (see **3.2.7.2**) it was not possible to determine the exact positions of the double bonds within the fatty acids. There are already several well established methods to identify double bond positions in fatty acids using gas chromatography or high performance liquid chromatography (Mitchell et al., 2009)

Long-chain polyunsaturated fatty acids (PUFAs) are ligands of the peroxisome proliferator-activated receptors (PPARs) and have been implicated in the regulation of energy metabolism (Nakamura et al., 2014). In the last years, it became clear that PUFAs have some potential benefits. It was for example reported that the supply of ω-3 family of PUFAs reduces the risk of cardiovascular diseases (Thies et al., 2003, Hirafuji et al., 2003).

PUFAs also play a role in lipid rafts (Stillwell et al., 2005). The incorporation of PUFAs into membrane glycerolipids such as phosphatidylcholine, -ethanolamine and -serine affects formation, stability and fluidity of these membrane microdomains (Stillwell and Wassall, 2003). Phosphatidylserine levels were elevated in PGP shRNA expressing cells. Therefore, it would be interesting to determine whether the PS species in PGP-deficient cells contain PUFAs.

Furthermore, it was reported that the ω-3 family of PUFAs functions as antioxidants and decreases ROS production (Richard et al., 2008). In this context, consideration should be given to a potential role of PUFAs as antioxidants and as a protective mechanism in response to ROS production caused by elevated lipolysis.

Another interesting finding is that PUFAs can inhibit glycolysis by blocking the expression of glycolytic enzymes such as pyruvate kinase (Xu et al., 2006, Andrade-Vieira et al., 2013), and that they have also been reported to downregulate lipogenic enzymes such as fatty acid synthase (Dentin et al., 2005). This suggests that after lipolysis of TG species containing long-chain polyunsaturated fatty acids, the released PUFAs may on the one hand boost the metabolic shift towards lipogenesis by inhibiting the expression of glycolytic enzymes and on the other hand attenuate the increase of lipogenesis as a negative or protective feedback by inhibiting lipogenic enzymes.

5.2.7 PG inactivation leads to elevated lipogenesis and lipolysis

Triglyceride biosynthesis is an ATP-consuming process. However, ATP levels were increased in PGP-inactivated embryos and in cells (see **Figures 46** and **49**). By analyzing control shRNA and PGP shRNA expressing GC1 cells it was demonstrated that this overshoot of ATP was due to elevated lipolysis and fatty acid oxidation. In addition, measurements of oxygen consumption rates (OCR) showed that mitochondrial respiration and ATP production was elevated in a lipolysis and fatty acid oxidation dependent manner (see **Figure 51**). Thus, lipogenesis as well as lipolysis seem to be concomitantly elevated.

Therefore, the question arises, how these two functionally opposite processes that typically occur in a mutually exclusive manner can be concomitantly increased.

When nutrients are supplied, G3P derived from glucose is esterified either with exogenous fatty acids (FA) or with FA derived from *de novo* synthesis. Fatty acid biosynthesis starts by the generation of malonyl-CoA from acetyl-CoA catalyzed by the enzyme acetyl-CoA carboxylase (ACC) under ATP consumption (Currie et al., 2013). Acetyl-CoA is either derived from FA oxidation or from pyruvate in the mitochondria. It can be only provided for fatty acid synthesis under non-starving conditions when acetyl-CoA is not utilized for oxidation in the TCA cycle. After conversion to citrate via a tricarboxylate system, mitochondrial acetyl-CoA is transferred to the cytoplasm and is then utilized together with malonyl-CoA for fatty acid *de novo* synthesis. Lipogenesis takes place under ATP consumption in the cytosol of every cell but mainly in adipocytes (Ahmadian et al., 2007). Triglycerides are stored for future energy demand.

Under fasting conditions, when cellular ATP levels are low, lipolysis is induced. Lipolysis starts with the breakdown of triglycerides in the cytosol and the release of fatty acids (Zechner et al., 2012). The released fatty acids are activated by acyl-CoA synthase under ATP consumption. Activated fatty acids with a shorter chain can pass through the outer mitochondrial membrane, whereas longer chain fatty acids require a carnitine palmitoyltransferase 1 (CPT1) carrier to pass through the membrane (McGarry and Brown, 1997). Via a second carnitine-mediated

transfer, fatty acids reach the mitochondrial matrix and can be oxidized to acetyl-CoA (β-oxidation). Acetyl-CoA can enter the TCA cycle and generate NADH and $FADH_2$, which are utilized in the electron transport chain for ATP production by oxidative phosphorylation (OXPHOS) (Berg JM, Tymoczko JL, Stryer L. Biochemistry. 5th edition; 2002).

In order to react to energy requirements, the processes of lipolysis and lipogenesis are tightly regulated. One control point is the regulation of acetyl-CoA carboxylase (ACC) activity. In mammals, two isoforms have been identified. ACC1 is cytosolic and mainly expressed in liver and adipose tissue. ACC2 is located at the mitochondria associated with CPT1 (Brownsey et al., 1997).

The synthesis of malonyl-CoA from acetyl-CoA by ACC2 inhibits CPT1 (Rasmussen et al., 2002). Especially, longer chain fatty acids require CPT1 to enter the mitochondria for fatty acid oxidation. Hence, fatty acid oxidation is blocked while fatty acid synthesis takes place.

The activities of both isoforms are tightly regulated (Brownsey et al., 2006). Citrate, for example, activates ACC and longer chain fatty acids inhibit ACC activity. Hormone-mediated phosphorylation of ACC leads to changes of its activity. When cellular ATP levels are low, AMP-activated protein kinase (AMPK) can phosphorylate ACC and thereby inhibits its activity (Winder and Hardie, 1996). Glucagon release leads to PKA activation and ACC inhibition upon phosphorylation by PKA.

Figure 56 shows a simplified overview over the regulation of lipogenesis and lipolysis.

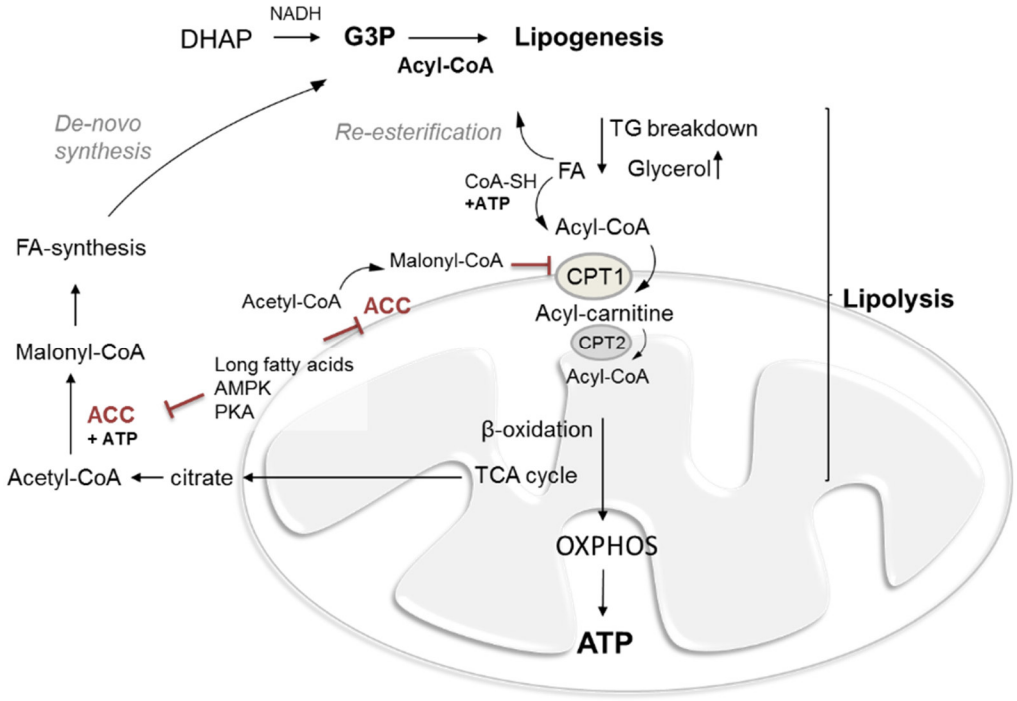

Figure 56: Regulation of lipogenesis and lipolysis.
For details, see text above.

So, how is it possible that PGP shRNA expressing GC1 cells show elevated lipogenesis and increased lipolysis-mediated mitochondrial respiration and ATP production?

Inhibition of TPI leads to a metabolic shift towards DHAP. In a reversible reaction, DHAP is reduced to G3P under NADH oxidation. It was reported that TPI deficiency results in DHAP accumulation. DHAP can be spontaneously degraded to cytotoxic methylglyoxal (Ahmed et al., 2003). To prevent this, G3P is utilized for TG synthesis to ensure that G3P is not converted back to DHAP by oxidation. Thus, *de novo* fatty acid synthesis might be activated and TGs are stored in lipid droplets.

Lipogenesis is an ATP-consuming process. However, glycolysis as an ATP-producing metabolic pathway might be completely blocked by PG-induced TPI and PK inhibition. Should this indeed be the case, PGP-depleted cells, will not be able to utilize glucose or glycolytic intermediates for their energetic or biosynthetic demands. Instead, they may have to use triglycerides, stored in lipid droplets for TCA cycle metabolism and OXPHOS to maintain energy homeostasis.

Breakdown of triglycerides leads to the release of fatty acids and glycerol. Since CPT1, which is necessary for mitochondrial transfer of long-chain fatty acids, might be blocked by malonyl-CoA upon *de novo* synthesis of fatty acids, only shorter chain fatty acids are oxidized and utilized for ATP production. Longer chain fatty acids, which are not able to enter the mitochondrial membrane, might be re-esterified for TG biosynthesis. This could be an explanation for the accumulation of especially long-chain triglyceride species upon PGP inactivation.

To answer the question how lipogenesis and lipolysis can take place at the same time, more experiments are required. For example, it has to be examined whether glycolysis is indeed blocked upon loss of PGP activity and if triglyceride levels are also elevated under oxygen deprivation conditions in PGP-deficient cells.

Taken together, this thesis characterizes the PG-directed phosphatase PGP as a metabolic phosphatase involved in the regulation of cell migration and cellular bioenergetics and suggests functional roles of PGP in glucose and lipid metabolism.

It will be of interest to study tissue-specific functions and regulation of PGP in the adult organism, which might provide new insights into important metabolic diseases, such as diabetes and adiposity (Zechner et al., 2012, Unger and Scherer, 2010).

6 Summary

Mammalian haloacid dehalogenase (HAD)-type phosphatases are a large and ubiquitous family of at least 40 human members. Many of them have important physiological functions, such as the regulation of intermediary metabolism and the modulation of enzyme activities, yet they are also linked to diseases such as cardiovascular or metabolic disorders and cancer. Still, most of the mammalian HAD phosphatases remain functionally uncharacterized.

This thesis reveals novel cell biological and physiological functions of the phosphoglycolate phosphatase PGP, also referred to as AUM. To this end, PGP was functionally characterized by performing analyses using purified recombinant proteins to investigate potential protein substrates of PGP, cell biological studies using the spermatogonial cell line GC1, primary mouse lung endothelial cells and lymphocytes, and a range of biochemical techniques to characterize *Pgp*-deficient mouse embryos.

To characterize the cell biological functions of PGP, its role downstream of RTK- and integrin signaling in the regulation of cell migration was investigated. It was shown that PGP inactivation elevates integrin- and RTK-induced circular dorsal ruffle (CDR) formation, cell spreading and cell migration. Furthermore, PGP was identified as a negative regulator of directed lymphocyte migration upon integrin- and GPCR activation.

The underlying mechanisms were analyzed further. It was demonstrated that PGP regulates CDR formation and cell migration in a PLC- and PKC-dependent manner, and that Src family kinase activities are required for the observed cellular effects. Upon integrin- and RTK activation, phosphorylation levels of tyrosine residues 1068 and 1173 of the EGF receptor were elevated and PLCγ1 was hyper-activated in PGP-deficient cells. Additionally, PGP-inactivated lymphocytes displayed elevated PKC activity, and PKC-mediated cytoskeletal remodeling was accelerated upon loss of PGP activity. Untargeted lipidomic analyses revealed that the membrane lipid phosphatidylserine (PS) was highly upregulated in PGP-depleted cells.

These data are consistent with the hypothesis that the accumulation of PS in the plasma membrane leads to a pre-assembly of signaling molecules such as PLCγ1 or PKCs that couple the activation of integrins, EGF receptors and GPCRs to accelerated cytoskeletal remodeling. Thus, this thesis shows that PGP can affect cell spreading and cell migration by acting as a PG-directed phosphatase.

To understand the physiological functions of PGP, conditionally PGP-inactivated mice were analyzed. Whole-body PGP inactivation led to an intrauterine growth defect with developmental delay after E8.5, resulting in a gradual deterioration and death of $Pgp^{DN/DN}$ embryos between E9.5 and E11.5. However, embryonic lethality upon whole-body PGP inactivation was not caused by a primary defect of the (cardio-) vascular system. Rather, PGP-

inactivated embryos died during the intrauterine transition from hypoxic to normoxic conditions. Therefore, the potential impact of oxygen on PGP-dependent cell proliferation was investigated. Analyses of mouse embryonic fibroblasts (MEFs) generated from E8.5 embryos and GC1 cells cultured under normoxic and hypoxic conditions revealed that normoxia (~20% O_2) causes a proliferation defect in PGP-inactivated cells, which can be rescued under hypoxic (~1% O_2) conditions. Mechanistically, it was found that the activity of triosephosphate isomerase (TPI), an enzyme previously described to be inhibited by phosphoglycolate (PG) *in vitro*, was attenuated in PGP-inactivated cells and embryos. TPI constitutes a critical branch point between carbohydrate- and lipid metabolism because it catalyzes the isomerization of the glycolytic intermediates dihydroxyacetone phosphate (DHAP, a precursor of the glycerol backbone required for triglyceride biosynthesis) and glyceraldehyde 3'-phosphate (GADP). Attenuation of TPI activity, likely explains the observed elevation of glycerol 3-phosphate levels and the increased TG biosynthesis (lipogenesis). Analyses of ATP levels and oxygen consumption rates (OCR) showed that mitochondrial respiration rates and ATP production were elevated in PGP-deficient cells in a lipolysis-dependent manner. However under hypoxic conditions (which corrected the impaired proliferation of PGP-inactivated cells), OCR and ATP production was indistinguishable between PGP-deficient and PGP-proficient cells. We therefore propose that the inhibition of TPI activity by PG accumulation due to loss of PGP activity shifts cellular bioenergetics from a pro-proliferative, glycolytic metabolism to a lipogenetic/lipolytic metabolism.

Taken together, PGP acts as a metabolic phosphatase involved in the regulation of cell migration, cell proliferation and cellular bioenergetics. This thesis constitutes the basis for further studies of the interfaces between these processes, and also suggests functions of PGP for glucose and lipid metabolism in the adult organism.

Zusammenfassung

Haloazid Dehalogenase (HAD)-Typ Phosphatasen in Säugetieren gehören zu einer großen ubiquitären Proteinfamilie, zu der auch mindestens 40 Phosphatasen, die im menschlichen Organismus vertreten sind, zählen. Eine Vielzahl dieser Phosphatasen hat wichtige physiologische Funktionen beispielsweise als regulatorische Enzyme im Metabolismus. Gleichzeitig werden sie in Verbindung mit Erkrankungen des kardiovaskulären Systems, Stoffwechselstörungen und Krebs gebracht. Dennoch sind die Funktionen vieler Mitglieder dieser Phosphatasen Familie bis heute weitestgehend unbekannt.

In der vorliegenden Arbeit wurden die zellbiologischen und physiologischen Funktionen der Phosphoglykolat-Phosphatase PGP, auch AUM genannt, charakterisiert. Zu diesem Zweck wurde mit gereinigtem Enzym nach potenziellen Protein-Substraten von PGP gesucht. Weiterhin wurden zellbiologische Studien mit der spermatogonialen GC1 Zelllinie sowie mit primären Endothelzellen und Lymphozyten durchgeführt. Mit biochemischen Methoden wurden zudem PGP-defiziente Mausembryonen charakterisiert.

Es wurde zunächst die Rolle von PGP für RTK- und integrin- induzierte Zellmigration untersucht. Dabei zeigte sich, dass PGP Inaktivierung die Zelladhäsion und Zellmigration steigerte. Gleichzeitig wurde eine vermehrte Bildung von RTK- und integrinvermittelten ringförmigen Plasmamembranausstülpungen, sogenannten Circular Dorsal Ruffles (CDR) auf der dorsalen Zelloberfläche beobachtet. PGP wurde zudem als negativer Regulator integrin- und GPCR-induzierter gerichteter Lymphozytenmigration identifiziert. Der zugrundeliegende molekulare Mechanismus wurde näher untersucht. Es konnte gezeigt werden, dass PGP die Bildung von CDRs und die gerichtetete Zellmigration in Abhängigkeit der Phospholipase C- (PLC-), Proteinkinase C- (PKC-) sowie Src Kinase-Aktivität steuert. Nach Integrin- und RTK-Aktivierung waren die Tyrosinreste 1068 und 1173 des EGF-Rezeptors in PGP-depletierten Zellen vermehrt phosphoryliert und PLCγ1 in diesen Zellen hyperaktiviert. Interessanterweise wurde zudem eine beschleunigte PKC-vermittelte Reorganisation des Zytoskeletts beobachtet. In stimulierten Lymphozyten führte PGP-Inaktivierung zu einer erhöhten PKC-Aktivität. Durch massenspektrometrische Analysen konnten erhöhte Spiegel des Membranlipids Phosphatidylserin (PS) in PGP-defizienten Zellen nachgewiesen werden. Diese Ergebnisse sind konsistent mit der Hypothese, dass die Anreicherung von PS in der Plasmamembran PGP-defizienter Zellen zu einer Vor-Rekrutierung von Signalproteinen führt, die die Aktivierung von Integrinen, EGF-Rezeptoren und GPCRs mit einer beschleunigten Zytoskelett-Reorganisation verbindet. Hierdurch konnte gezeigt werden, dass PGP durch die Dephosphorylierung von Phosphoglykolat die Zelladhäsion und Zellmigration reguliert.

Um die physiologischen Funktionen von PGP zu verstehen, wurden konditional PGP-inaktivierte Mäuse untersucht. Die Inaktivierung von PGP im gesamten Organismus führte zu einem Wachstumsdefekt ab Tag E8.5 und dem Tod der Embryonen im Uterus zwischen Tag E9.5 und E11.5. Die beobachtete embryonale Letalität war nicht durch einen Defekt des (kardio-)vaskulären Systems zu erklären.

PGP-inaktivierte Embryonen starben zu einem Zeitpunkt, an dem der intrauterine Übergang von einem hypoxischen zu einem normoxischen Millieu stattfindet. Der Einfluss von Sauerstoff wurde deshalb weiter untersucht. Zellwachstumsanalysen unter normoxischen und hypoxischen Bedingungen mit GC1 Zellen und embryonalen Maus-Fibroblasten, die aus E8.5 Embryonen gewonnen wurden zeigten, dass normoxische Bedingungen (~20% O_2) einen Wachstumsdefekt PGP-inaktivierter Zellen verursacht, wohingegen dies unter hypoxischen Bedingungen (~1% O_2) nicht der Fall war. Mechanistisch konnte gezeigt werden, dass die Aktivität der Triosephosphatisomerase (TPI), ein durch PG *in vitro* gehemmtes Enzym, in PGP inaktivierten Zellen und Embryonen vermindert war. TPI stellt einen entscheidenden Verzweigungspunkt des Glukose- und Lipidstoffwechsels dar. TPI katalysiert die Isomerisierung der aus der Glykolyse stammenden Intermediate Dihydroxyacetonphosphat (DHAP, eine Vorstufe des für die Triglycerid-Biosynthese benötigten Glycerol-Grundgerüsts) und Glyceraldehyd-3'-phosphat (GADP). Eine Verringerung der TPI-Aktivität in PGP-inaktivierten Zellen resultierte in erhöhten Glycerol-3-phosphat Spiegeln und einer gesteigerten Triglycerid-Biosynthese. Die Analyse des zellulären ATP Gehalts und des Sauerstoffverbrauchs bei der mitochondrialen Atmung zeigte, dass sowohl die ATP Produktion als auch die mitochondriale Atmung in Abhängigkeit der Lipolyse in PGP-defizienten Zellen erhöht waren. Unter hypoxischen Bedingungen, die zu einer Normalisierung der Zellproliferation führten, wiesen PGP-profiziente und -defiziente Zellen keinen Unterschied bezüglich ATP Produktion und mitochondrialer Atmung auf.

Wir vermuten deswegen, dass die Inhibierung der TPI-Aktivität durch PG-Anreicherung aufgrund ausbleibender Hydrolyse durch PGP zu einer Verschiebung des zellulären Energiehaushaltes von Seiten eines pro-proliferativ glykolytischen auf die Seite eines lipogenetisch/lipolytischen Metabolismus führt.

Zusammenfassend konnte gezeigt werden, dass PGP als eine metabolische Phosphatase Zellmigration, Zellproliferation wie auch den zellulären Energiehaushalt reguliert. Die vorliegende Arbeit stellt somit die Grundlage für weitere Untersuchungen an der Schnittschnelle dieser zellulären Prozesse dar und lässt auf eine wichtige Rolle von PGP im Glukose- und Lipidstoffwechsel im adulten Organismus schließen.

7 References

ABDELHAK, S., KALATZIS, V., HEILIG, R., COMPAIN, S., SAMSON, D., VINCENT, C., WEIL, D., CRUAUD, C., SAHLY, I., LEIBOVICI, M., BITNER-GLINDZICZ, M., FRANCIS, M., LACOMBE, D., VIGNERON, J., CHARACHON, R., BOVEN, K., BEDBEDER, P., VAN REGEMORTER, N., WEISSENBACH, J. & PETIT, C. 1997. A human homologue of the Drosophila eyes absent gene underlies branchio-oto-renal (BOR) syndrome and identifies a novel gene family. *Nat Genet,* 15**,** 157-64.

ABELLA, J. V., PARACHONIAK, C. A., SANGWAN, V. & PARK, M. 2010. Dorsal ruffle microdomains potentiate Met receptor tyrosine kinase signaling and down-regulation. *J Biol Chem,* 285**,** 24956-67.

ABERCROMBIE, M., HEAYSMAN, J. E. & PEGRUM, S. M. 1970. The locomotion of fibroblasts in culture. II. "RRuffling". *Exp Cell Res,* 60**,** 437-44.

ABERCROMBIE, M., HEAYSMAN, J. E. & PEGRUM, S. M. 1971. The locomotion of fibroblasts in culture. IV. Electron microscopy of the leading lamella. *Exp Cell Res,* 67**,** 359-67.

ABRAHAM, R. T. 2001. Cell cycle checkpoint signaling through the ATM and ATR kinases. *Genes & Development,* 15**,** 2177-2196.

AHMADIAN, M., DUNCAN, R. E., JAWORSKI, K., SARKADI-NAGY, E. & SUL, H. S. 2007. Triacylglycerol metabolism in adipose tissue. *Future Lipidol,* 2**,** 229-37.

AHMED, N., BATTAH, S., KARACHALIAS, N., BABAEI-JADIDI, R., HORANYI, M., BAROTI, K., HOLLAN, S. & THORNALLEY, P. J. 2003. Increased formation of methylglyoxal and protein glycation, oxidation and nitrosation in triosephosphate isomerase deficiency. *Biochim Biophys Acta,* 1639**,** 121-32.

AL-SAFI, R. I., ODDE, S., SHABAIK, Y. & NEAMATI, N. 2012. Small-molecule inhibitors of APE1 DNA repair function: an overview. *Curr Mol Pharmacol,* 5**,** 14-35.

ALBERTS B, JOHNSON A, LEWIS J, et al. Molecular Biology of the Cell. 4th edition; 2002

ALLEN, K. N. & DUNAWAY-MARIANO, D. 2009. Markers of fitness in a successful enzyme superfamily. *Curr Opin Struct Biol,* 19**,** 658-65.

ALONSO, A., SASIN, J., BOTTINI, N., FRIEDBERG, I., FRIEDBERG, I., OSTERMAN, A., GODZIK, A., HUNTER, T., DIXON, J. & MUSTELIN, T. 2004. Protein tyrosine phosphatases in the human genome. *Cell,* 117**,** 699-711.

ANDRABI, S. A., UMANAH, G. K., CHANG, C., STEVENS, D. A., KARUPPAGOUNDER, S. S., GAGNE, J. P., POIRIER, G. G., DAWSON, V. L. & DAWSON, T. M. 2014. Poly(ADP-ribose) polymerase-dependent energy depletion occurs through inhibition of glycolysis. *Proc Natl Acad Sci U S A,* 111**,** 10209-14.

ANDRADE-VIEIRA, R., HAN, J. H. & MARIGNANI, P. A. 2013. Omega-3 polyunsaturated fatty acid promotes the inhibition of glycolytic enzymes and mTOR signaling by regulating the tumor suppressor LKB1. *Cancer Biol Ther,* 14**,** 1050-8.

ANGERS-LOUSTAU, A., COTE, J. F., CHAREST, A., DOWBENKO, D., SPENCER, S., LASKY, L. A. & TREMBLAY, M. L. 1999. Protein tyrosine phosphatase-PEST regulates focal adhesion disassembly, migration, and cytokinesis in fibroblasts. *J Cell Biol,* 144**,** 1019-31.

ARAVIND, L. & KOONIN, E. V. 1998. The HD domain defines a new superfamily of metal-dependent phosphohydrolases. *Trends Biochem Sci,* 23**,** 469-72.

ARBER, S., BARBAYANNIS, F. A., HANSER, H., SCHNEIDER, C., STANYON, C. A., BERNARD, O. & CARONI, P. 1998. Regulation of actin dynamics through phosphorylation of cofilin by LIM-kinase. *Nature,* 393**,** 805-9.

ARCOLEO, J. P. & WEINSTEIN, I. B. 1985. Activation of protein kinase C by tumor promoting phorbol esters, teleocidin and aplysiatoxin in the absence of added calcium. *Carcinogenesis,* 6**,** 213-7.

ARNAOUT, M. A., GOODMAN, S. L. & XIONG, J. P. 2002. Coming to grips with integrin binding to ligands. *Curr Opin Cell Biol,* 14**,** 641-51.

ARTHUR, W. T. & BURRIDGE, K. 2001. RhoA inactivation by p190RhoGAP regulates cell spreading and migration by promoting membrane protrusion and polarity. *Mol Biol Cell,* 12**,** 2711-20.

ATKINSON, S. J., HOSFORD, M. A. & MOLITORIS, B. A. 2004. Mechanism of actin polymerization in cellular ATP depletion. *J Biol Chem,* 279**,** 5194-9.

AVRUCH, J., KHOKHLATCHEV, A., KYRIAKIS, J. M., LUO, Z., TZIVION, G., VAVVAS, D. & ZHANG, X. F. 2001. Ras activation of the Raf kinase: tyrosine kinase recruitment of the MAP kinase cascade. *Recent Prog Horm Res,* 56**,** 127-55.

AWAPARA, J., SANDMAN, R. P. & HANLY, C. 1962. Activation of DOPA decarboxylase by pyridoxal phosphate. *Arch Biochem Biophys,* 98**,** 520-5.

AZIMIFAR, S. B., BOTTCHER, R. T., ZANIVAN, S., GRASHOFF, C., KRUGER, M., LEGATE, K. R., MANN, M. & FASSLER, R. 2012. Induction of membrane circular dorsal ruffles requires co-signalling of integrin-ILK-complex and EGF receptor. *J Cell Sci,* 125**,** 435-48.

BADWEY, J. A. 1977. Phosphoglycolate phosphatase in human erythrocytes. *J Biol Chem,* 252**,** 2441-3.

BAIN, J., PLATER, L., ELLIOTT, M., SHPIRO, N., HASTIE, C. J., MCLAUCHLAN, H., KLEVERNIC, I., ARTHUR, J. S., ALESSI, D. R. & COHEN, P. 2007. The selectivity of protein kinase inhibitors: a further update. *Biochem J,* 408**,** 297-315.

BAMBURG, J. R. & BERNSTEIN, B. W. 2010. Roles of ADF/cofilin in actin polymerization and beyond. *F1000 Biol Rep,* 2.

BASS, M. D., MORGAN, M. R., ROACH, K. A., SETTLEMAN, J., GORYACHEV, A. B. & HUMPHRIES, M. J. 2008. p190RhoGAP is the convergence point of adhesion signals from alpha 5 beta 1 integrin and syndecan-4. *J Cell Biol,* 181**,** 1013-26.

BAUWE, H., HAGEMANN, M. & FERNIE, A. R. 2010. Photorespiration: players, partners and origin. *Trends Plant Sci,* 15**,** 330-6.

BAXTER, C. F. & ROBERTS, E. 1958. The gamma-aminobutyric acid-alpha-ketoglutaric acid transaminase of beef brain. *J Biol Chem,* 233**,** 1135-9.

BAZLEY, L. A. & GULLICK, W. J. 2005. The epidermal growth factor receptor family. *Endocr Relat Cancer,* 12 Suppl 1**,** S17-27.

BERG, JM, TYMOCZKO JL, STRYER L. Biochemistry. 5th edition; 2002

BERNSTEIN, B. W. & BAMBURG, J. R. 2003. Actin-ATP hydrolysis is a major energy drain for neurons. *J Neurosci,* 23**,** 1-6.

BERTONCINI, C. R. & MENEGHINI, R. 1995. DNA strand breaks produced by oxidative stress in mammalian cells exhibit 3'-phosphoglycolate termini. *Nucleic Acids Res,* 23**,** 2995-3002.

BETTATI, S., BENCI, S., CAMPANINI, B., RABONI, S., CHIRICO, G., BERETTA, S., SCHNACKERZ, K. D., HAZLETT, T. L., GRATTON, E. & MOZZARELLI, A. 2000. Role of pyridoxal 5'-phosphate in the structural stabilization of O-acetylserine sulfhydrylase. *J Biol Chem,* 275**,** 40244-51.

BISCARDI, J. S., ISHIZAWAR, R. C., SILVA, C. M. & PARSONS, S. J. 2000. Tyrosine kinase signalling in breast cancer: epidermal growth factor receptor and c-Src interactions in breast cancer. *Breast Cancer Res, 2***,** 203-10.

BISCARDI, J. S., MAA, M. C., TICE, D. A., COX, M. E., LEU, T. H. & PARSONS, S. J. 1999. c-Src-mediated phosphorylation of the epidermal growth factor receptor on Tyr845 and Tyr1101 is associated with modulation of receptor function. *J Biol Chem,* 274**,** 8335-43.

BLUME-JENSEN, P. & HUNTER, T. 2001. Oncogenic kinase signalling. *Nature,* 411**,** 355-65.

BRANDT, D., GIMONA, M., HILLMANN, M., HALLER, H. & MISCHAK, H. 2002. Protein kinase C induces actin reorganization via a Src- and Rho-dependent pathway. *J Biol Chem,* 277**,** 20903-10.

BREUNING, M. H., SNIJDEWINT, F. G., BRUNNER, H., VERWEST, A., IJDO, J. W., SARIS, J. J., DAUWERSE, J. G., BLONDEN, L., KEITH, T., CALLEN, D. F. & ET AL. 1990. Map of 16 polymorphic loci on the short arm of chromosome 16 close to the polycystic kidney disease gene (PKD1). *J Med Genet,* 27**,** 603-13.

BROWNSEY, R. W., BOONE, A. N., ELLIOTT, J. E., KULPA, J. E. & LEE, W. M. 2006. Regulation of acetyl-CoA carboxylase. *Biochem Soc Trans,* 34**,** 223-7.

BROWNSEY, R. W., ZHANDE, R. & BOONE, A. N. 1997. Isoforms of acetyl-CoA carboxylase: structures, regulatory properties and metabolic functions. *Biochem Soc Trans,* 25**,** 1232-8.

BRUNET, A., BONNI, A., ZIGMOND, M. J., LIN, M. Z., JUO, P., HU, L. S., ANDERSON, M. J., ARDEN, K. C., BLENIS, J. & GREENBERG, M. E. 1999. Akt Promotes Cell Survival by Phosphorylating and Inhibiting a Forkhead Transcription Factor. *Cell,* 96**,** 857-868.

BURDISSO, J. E., GONZALEZ, A. & ARREGUI, C. O. 2013. PTP1B promotes focal complex maturation, lamellar persistence and directional migration. *J Cell Sci,* 126**,** 1820-31.

BURNS, J. L. & HASSAN, A. B. 2001. Cell survival and proliferation are modified by insulin-like growth factor 2 between days 9 and 10 of mouse gestation. *Development,* 128**,** 3819-30.

BURROUGHS, A. M., ALLEN, K. N., DUNAWAY-MARIANO, D. & ARAVIND, L. 2006. Evolutionary genomics of the HAD superfamily: understanding the structural adaptations and catalytic diversity in a superfamily of phosphoesterases and allied enzymes. *J Mol Biol,* 361**,** 1003-34.

CAMPBELL, I. D. & HUMPHRIES, M. J. 2011. Integrin structure, activation, and interactions. *Cold Spring Harb Perspect Biol,* 3.

CARLIER, M. F., LAURENT, V., SANTOLINI, J., MELKI, R., DIDRY, D., XIA, G. X., HONG, Y., CHUA, N. H. & PANTALONI, D. 1997. Actin depolymerizing factor (ADF/cofilin) enhances the rate of filament turnover: implication in actin-based motility. *J Cell Biol,* 136**,** 1307-22.

CARLIER, M. F., PERNIER, J., MONTAVILLE, P., SHEKHAR, S. & KUHN, S. 2015. Control of polarized assembly of actin filaments in cell motility. *Cell Mol Life Sci,* 72**,** 3051-67.

CARPENTER, G. 2000. The EGF receptor: a nexus for trafficking and signaling. *BioEssays,* 22**,** 697-707.

CARY, L. A., KLINGHOFFER, R. A., SACHSENMAIER, C. & COOPER, J. A. 2002. Src Catalytic but Not Scaffolding Function Is Needed for Integrin-Regulated Tyrosine Phosphorylation, Cell Migration, and Cell Spreading. *Mol Cell Biol,* 22**,** 2427-40.

CASE, L. B. & WATERMAN, C. M. 2015. Integration of actin dynamics and cell adhesion by a three-dimensional, mechanosensitive molecular clutch. *Nat Cell Biol,* 17**,** 955-63.

CENNI, B. & PICARD, D. 1999. Two compounds commonly used for phospholipase C inhibition activate the nuclear estrogen receptors. *Biochem Biophys Res Commun,* 261**,** 340-4.

CHAN, G., NOGALSKI, M. T. & YUROCHKO, A. D. 2009. Activation of EGFR on monocytes is required for human cytomegalovirus entry and mediates cellular motility. *Proc Natl Acad Sci U S A,* 106**,** 22369-74.

CHEN, B., ZHOU, X., TAGHIZADEH, K., CHEN, J., STUBBE, J. & DEDON, P. C. 2007. GC/MS methods to quantify the 2-deoxypentos-4-ulose and 3'-phosphoglycolate pathways of 4' oxidation of 2-deoxyribose in DNA: application to DNA damage produced by gamma radiation and bleomycin. *Chem Res Toxicol,* 20**,** 1701-8.

CHEN, S., HOENE, M., LI, J., LI, Y., ZHAO, X., HARING, H. U., SCHLEICHER, E. D., WEIGERT, C., XU, G. & LEHMANN, R. 2013. Simultaneous extraction of metabolome and lipidome with methyl tert-butyl ether from a single small tissue sample for ultra-high performance liquid chromatography/mass spectrometry. *J Chromatogr A,* 1298**,** 9-16.

CHEN, S., INAMDAR, K. V., PFEIFFER, P., FELDMANN, E., HANNAH, M. F., YU, Y., LEE, J.-W., ZHOU, T., LEES-MILLER, S. P. & POVIRK, L. F. 2001. Accurate in Vitro End Joining of a DNA Double Strand Break with Partially Cohesive 3′-Overhangs and 3′-Phosphoglycolate Termini: EFFECT OF Ku ON REPAIR FIDELITY. *Journal of Biological Chemistry,* 276**,** 24323-24330.

CHHABRA, E. S. & HIGGS, H. N. 2007. The many faces of actin: matching assembly factors with cellular structures. *Nat Cell Biol,* 9**,** 1110-21.

CHIASSON-MACKENZIE, C., MORRIS, Z. S., BACA, Q., MORRIS, B., COKER, J. K., MIRCHEV, R., JENSEN, A. E., CAREY, T., STOTT, S. L., GOLAN, D. E. &

MCCLATCHEY, A. I. 2015. NF2/Merlin mediates contact-dependent inhibition of EGFR mobility and internalization via cortical actomyosin. *The Journal of Cell Biology,* 211**,** 391-405.

CHISHTI, A. H., KIM, A. C., MARFATIA, S. M., LUTCHMAN, M., HANSPAL, M., JINDAL, H., LIU, S. C., LOW, P. S., ROULEAU, G. A., MOHANDAS, N., CHASIS, J. A., CONBOY, J. G., GASCARD, P., TAKAKUWA, Y., HUANG, S. C., BENZ, E. J., JR., BRETSCHER, A., FEHON, R. G., GUSELLA, J. F., RAMESH, V., SOLOMON, F., MARCHESI, V. T., TSUKITA, S., TSUKITA, S., HOOVER, K. B. & ET AL. 1998. The FERM domain: a unique module involved in the linkage of cytoplasmic proteins to the membrane. *Trends Biochem Sci,* 23**,** 281-2.

CHO, J. H., KIM, H. O., KIM, K. S., YANG, D. H., SURH, C. D. & SPRENT, J. 2013. Unique features of naive CD8+ T cell activation by IL-2. *J Immunol,* 191**,** 5559-73.

CLARKE, J. C., HONEY, E. M., BEKKER, E., SNYMAN, L. C., RAYMOND, R. M., JR., LORD, C. & BROPHY, P. D. 2006. A novel nonsense mutation in the EYA1 gene associated with branchio-oto-renal/branchiootic syndrome in an Afrikaner kindred. *Clin Genet,* 70**,** 63-7.

COHEN, P. 2000. The regulation of protein function by multisite phosphorylation--a 25 year update. *Trends Biochem Sci,* 25**,** 596-601.

COHEN, P. 2001. The role of protein phosphorylation in human health and disease. The Sir Hans Krebs Medal Lecture. *Eur J Biochem,* 268**,** 5001-10.

COMBS, G. F. 2008. *The vitamins : fundamental aspects in nutrition and health,* Amsterdam ; Boston, Elsevier Academic Press.

COMMISSO, C., DAVIDSON, S. M., SOYDANER-AZELOGLU, R. G., PARKER, S. J., KAMPHORST, J. J., HACKETT, S., GRABOCKA, E., NOFAL, M., DREBIN, J. A., THOMPSON, C. B., RABINOWITZ, J. D., METALLO, C. M., VANDER HEIDEN, M. G. & BAR-SAGI, D. 2013. Macropinocytosis of protein is an amino acid supply route in Ras-transformed cells. *Nature,* 497**,** 633-7.

CONWAY, S. J., KRUZYNSKA-FREJTAG, A., KNEER, P. L., MACHNICKI, M. & KOUSHIK, S. V. 2003. What cardiovascular defect does my prenatal mouse mutant have, and why? *Genesis,* 35**,** 1-21.

CSAKI, L. S. & REUE, K. 2010. Lipins: multifunctional lipid metabolism proteins. *Annu Rev Nutr,* 30**,** 257-72.

CURRIE, E., SCHULZE, A., ZECHNER, R., WALTHER, TOBIAS C. & FARESE JR, ROBERT V. 2013. Cellular Fatty Acid Metabolism and Cancer. *Cell Metabolism,* 18**,** 153-161.

D'SOUZA, S. E., GINSBERG, M. H. & PLOW, E. F. 1991. Arginyl-glycyl-aspartic acid (RGD): a cell adhesion motif. *Trends in Biochemical Sciences,* 16**,** 246-250.

DAUM, G., KALMES, A., LEVKAU, B., WANG, Y., DAVIES, M. G. & CLOWES, A. W. 1998. Pervanadate inhibits mitogen-activated protein kinase kinase-1 in a p38MAPK-dependent manner. *FEBS Lett,* 427**,** 271-4.

DEJANA, E., TOURNIER-LASSERVE, E. & WEINSTEIN, B. M. 2009. The control of vascular integrity by endothelial cell junctions: molecular basis and pathological implications. *Dev Cell,* 16**,** 209-21.

DENTIN, R., BENHAMED, F., PEGORIER, J. P., FOUFELLE, F., VIOLLET, B., VAULONT, S., GIRARD, J. & POSTIC, C. 2005. Polyunsaturated fatty acids suppress glycolytic and lipogenic genes through the inhibition of ChREBP nuclear protein translocation. *J Clin Invest,* 115**,** 2843-54.

DHARMAWARDHANE, S., SCHURMANN, A., SELLS, M. A., CHERNOFF, J., SCHMID, S. L. & BOKOCH, G. M. 2000. Regulation of macropinocytosis by p21-activated kinase-1. *Mol Biol Cell,* 11**,** 3341-52.

DIAMOND, M. S., STAUNTON, D. E., MARLIN, S. D. & SPRINGER, T. A. 1991. Binding of the integrin Mac-1 (CD11b/CD18) to the third immunoglobulin-like domain of ICAM-1 (CD54) and its regulation by glycosylation. *Cell,* 65**,** 961-71.

DIMILLA, P., STONE, J., QUINN, J., ALBELDA, S. & LAUFFENBURGER, D. 1993. Maximal migration of human smooth muscle cells on fibronectin and type IV collagen occurs at an intermediate attachment strength. *The Journal of Cell Biology,* 122**,** 729-737.

DONKOR, J., SARIAHMETOGLU, M., DEWALD, J., BRINDLEY, D. N. & REUE, K. 2007. Three mammalian lipins act as phosphatidate phosphatases with distinct tissue expression patterns. *J Biol Chem,* 282**,** 3450-7.

DOS REMEDIOS, C. G., CHHABRA, D., KEKIC, M., DEDOVA, I. V., TSUBAKIHARA, M., BERRY, D. A. & NOSWORTHY, N. J. 2003. Actin Binding Proteins: Regulation of Cytoskeletal Microfilaments. *Physiological Reviews,* 83**,** 433-473.

DOUGHERTY, T. M. & CLELAND, W. W. 1985. pH studies on the chemical mechanism of rabbit muscle pyruvate kinase. 2. Physiological substrates and phosphoenol-alpha-ketobutyrate. *Biochemistry,* 24**,** 5875-80.

DOWNWARD, J., PARKER, P. & WATERFIELD, M. D. 1984. Autophosphorylation sites on the epidermal growth factor receptor. *Nature,* 311**,** 483-5.

DOWRICK, P., KENWORTHY, P., MCCANN, B. & WARN, R. 1993. Circular ruffle formation and closure lead to macropinocytosis in hepatocyte growth factor/scatter factor-treated cells. *Eur J Cell Biol,* 61**,** 44-53.

DUNN, K. W., KAMOCKA, M. M. & MCDONALD, J. H. 2011. A practical guide to evaluating colocalization in biological microscopy. *Am J Physiol Cell Physiol,* 300**,** C723-42.

DUNN, T. B. 1954. Normal and pathologic anatomy of the reticular tissue in laboratory mice, with a classification and discussion of neoplasms. *J Natl Cancer Inst,* 14**,** 1281-433.

DUNWOODIE, S. L. 2009. The role of hypoxia in development of the Mammalian embryo. *Dev Cell,* 17**,** 755-73.

DUONG-LY, K. C. & PETERSON, J. R. 2013. The human kinome and kinase inhibition. *Curr Protoc Pharmacol,* Chapter 2**,** Unit2.9.

DWYER, M. A., LOOGER, L. L. & HELLINGA, H. W. 2004. Computational design of a biologically active enzyme. *Science,* 304**,** 1967-71.

EVEN-FAITELSON, L. & RAVID, S. 2006. PAK1 and aPKCzeta regulate myosin II-B phosphorylation: a novel signaling pathway regulating filament assembly. *Mol Biol Cell,* 17**,** 2869-81.

EVENOU, J. P., WAGNER, J., ZENKE, G., BRINKMANN, V., WAGNER, K., KOVARIK, J., WELZENBACH, K. A., WEITZ-SCHMIDT, G., GUNTERMANN, C., TOWBIN, H., COTTENS, S., KAMINSKI, S., LETSCHKA, T., LUTZ-NICOLADONI, C., GRUBER, T., HERMANN-KLEITER, N., THUILLE, N. & BAIER, G. 2009. The potent protein kinase C-selective inhibitor AEB071 (sotrastaurin) represents a new class of immunosuppressive agents affecting early T-cell activation. *J Pharmacol Exp Ther,* 330**,** 792-801.

EWALD, H., MORS, O., FLINT, T., KOED, K., EIBERG, H. & KRUSE, T. A. 1995. A possible locus for manic depressive illness on chromosome 16p13. *Psychiatr Genet,* 5**,** 71-81.

FADOK, V. A., BRATTON, D. L., FRASCH, S. C., WARNER, M. L. & HENSON, P. M. 1998. The role of phosphatidylserine in recognition of apoptotic cells by phagocytes. *Cell Death Differ,* 5**,** 551-62.

FAGONE, P. & JACKOWSKI, S. 2009. Membrane phospholipid synthesis and endoplasmic reticulum function. *J Lipid Res,* 50**,** S311-6.

FLETCHER, D. A. & MULLINS, R. D. 2010. Cell mechanics and the cytoskeleton. *Nature,* 463**,** 485-492.

FONDA, M. L. 1992. Purification and characterization of vitamin B6-phosphate phosphatase from human erythrocytes. *J Biol Chem,* 267**,** 15978-83.

FUKATA, M., NAKAGAWA, M. & KAIBUCHI, K. 2003. Roles of Rho-family GTPases in cell polarisation and directional migration. *Curr Opin Cell Biol,* 15**,** 590-7.

GARTON, A. J., FLINT, A. J. & TONKS, N. K. 1996. Identification of p130(cas) as a substrate for the cytosolic protein tyrosine phosphatase PTP-PEST. *Mol Cell Biol,* 16**,** 6408-18.

GERALDES, P. & KING, G. L. 2010. Activation of protein kinase C isoforms and its impact on diabetic complications. *Circ Res,* 106**,** 1319-31.

GINSBERG, M. H., DU, X. & PLOW, E. F. 1992. Inside-out integrin signalling. *Current Opinion in Cell Biology,* 4**,** 766-771.

GIUBELLINO, A., BURKE, T. R., JR. & BOTTARO, D. P. 2008. Grb2 signaling in cell motility and cancer. *Expert Opin Ther Targets,* 12**,** 1021-33.

GOHLA, A., BIRKENFELD, J. & BOKOCH, G. M. 2005. Chronophin, a novel HAD-type serine protein phosphatase, regulates cofilin-dependent actin dynamics. *Nat Cell Biol,* 7**,** 21-9.

GRAVES, J. D. & KREBS, E. G. 1999. Protein phosphorylation and signal transduction. *Pharmacol Ther,* 82**,** 111-21.

GROVDAL, L. M., STANG, E., SORKIN, A. & MADSHUS, I. H. 2004. Direct interaction of Cbl with pTyr 1045 of the EGF receptor (EGFR) is required to sort the EGFR to lysosomes for degradation. *Exp Cell Res,* 300**,** 388-95.

GRUNING, N. M., DU, D., KELLER, M. A., LUISI, B. F. & RALSER, M. 2014. Inhibition of triosephosphate isomerase by phosphoenolpyruvate in the feedback-regulation of glycolysis. *Open Biol,* 4**,** 130232.

GRUNING, N. M., RINNERTHALER, M., BLUEMLEIN, K., MULLEDER, M., WAMELINK, M. M., LEHRACH, H., JAKOBS, C., BREITENBACH, M. & RALSER, M. 2011. Pyruvate kinase triggers a metabolic feedback loop that controls redox metabolism in respiring cells. *Cell Metab,* 14**,** 415-27.

GSCHWENDT, M., DIETERICH, S., RENNECKE, J., KITTSTEIN, W., MUELLER, H.-J. & JOHANNES, F.-J. 1996. Inhibition of protein kinase C μ by various inhibitors. Inhibition from protein kinase c isoenzymes. *FEBS Letters,* 392**,** 77-80.

GU, Z., NOSS, E. H., HSU, V. W. & BRENNER, M. B. 2011. Integrins traffic rapidly via circular dorsal ruffles and macropinocytosis during stimulated cell migration. *J Cell Biol,* 193**,** 61-70.

GUIDETTI, G. F., CANOBBIO, I. & TORTI, M. 2015. PI3K/Akt in platelet integrin signaling and implications in thrombosis. *Adv Biol Regul,* 59**,** 36-52.

GUILLOU, H., DEPRAZ-DEPLAND, A., PLANUS, E., VIANAY, B., CHAUSSY, J., GRICHINE, A., ALBIGES-RIZO, C. & BLOCK, M. R. 2008. Lamellipodia nucleation by filopodia depends on integrin occupancy and downstream Rac1 signaling. *Exp Cell Res,* 314**,** 478-88.

HA, H. C. & SNYDER, S. H. 1999. Poly(ADP-ribose) polymerase is a mediator of necrotic cell death by ATP depletion. *Proc Natl Acad Sci U S A,* 96**,** 13978-82.

HAENDELER, J., YIN, G., HOJO, Y., SAITO, Y., MELARAGNO, M., YAN, C., SHARMA, V. K., HELLER, M., AEBERSOLD, R. & BERK, B. C. 2003. GIT1 mediates Src-dependent activation of phospholipase Cgamma by angiotensin II and epidermal growth factor. *J Biol Chem,* 278**,** 49936-44.

HALPER, J. & KJAER, M. 2014. Basic components of connective tissues and extracellular matrix: elastin, fibrillin, fibulins, fibrinogen, fibronectin, laminin, tenascins and thrombospondins. *Adv Exp Med Biol,* 802**,** 31-47.

HANSON, R. W. & RESHEF, L. 2003. Glyceroneogenesis revisited. *Biochimie,* 85**,** 1199-205.

HARBURGER, D. S., BOUAOUINA, M. & CALDERWOOD, D. A. 2009. Kindlin-1 and -2 directly bind the C-terminal region of beta integrin cytoplasmic tails and exert integrin-specific activation effects. *J Biol Chem,* 284**,** 11485-97.

HARRINGTON, E. O., LOFFLER, J., NELSON, P. R., KENT, K. C., SIMONS, M. & WARE, J. A. 1997. Enhancement of migration by protein kinase Calpha and inhibition of proliferation and cell cycle progression by protein kinase Cdelta in capillary endothelial cells. *J Biol Chem,* 272**,** 7390-7.

HARTMAN, F. C., LAMURAGLIA, G. M., TOMOZAWA, Y. & WOLFENDEN, R. 1975. The influence of pH on the interaction of inhibitors with triosephosphate isomerase and determination of the pKa of the active-site carboxyl group. *Biochemistry,* 14**,** 5274-9.

HARTWIG, J. H., THELEN, M., ROSEN, A., JANMEY, P. A., NAIRN, A. C. & ADEREM, A. 1992. MARCKS is an actin filament crosslinking protein regulated by protein kinase C and calcium-calmodulin. *Nature,* 356**,** 618-22.

HENNER, W. D., RODRIGUEZ, L. O., HECHT, S. M. & HASELTINE, W. A. 1983. gamma Ray induced deoxyribonucleic acid strand breaks. 3' Glycolate termini. *J Biol Chem,* 258**,** 711-3.

HERBST, R. S. 2004. Review of epidermal growth factor receptor biology. *Int J Radiat Oncol Biol Phys,* 59**,** 21-6.

HIRAFUJI, M., MACHIDA, T., HAMAUE, N. & MINAMI, M. 2003. Cardiovascular protective effects of n-3 polyunsaturated fatty acids with special emphasis on docosahexaenoic acid. *J Pharmacol Sci,* 92**,** 308-16.

HOEIJMAKERS, J. H. 2009. DNA damage, aging, and cancer. *N Engl J Med,* 361**,** 1475-85.

HOON, J. L., WONG, W. K. & KOH, C. G. 2012. Functions and regulation of circular dorsal ruffles. *Mol Cell Biol,* 32**,** 4246-57.

HUANG, K. P. 1989. The mechanism of protein kinase C activation. *Trends Neurosci,* 12**,** 425-32.

HUANG, M., SATCHELL, L., DUHADAWAY, J. B., PRENDERGAST, G. C. & LAURY-KLEINTOP, L. D. 2011a. RhoB links PDGF signaling to cell migration by coordinating activation and localization of Cdc42 and Rac. *J Cell Biochem,* 112**,** 1572-84.

HUANG, S. N., POMMIER, Y. & MARCHAND, C. 2011b. Tyrosyl-DNA Phosphodiesterase 1 (Tdp1) inhibitors. *Expert Opin Ther Pat,* 21**,** 1285-92.

HUANG, T. Y., MINAMIDE, L. S., BAMBURG, J. R. & BOKOCH, G. M. 2008. Chronophin mediates an ATP-sensing mechanism for cofilin dephosphorylation and neuronal cofilin-actin rod formation. *Dev Cell,* 15**,** 691-703.

HUMMEL, J., SEGU, S., LI, Y., IRGANG, S., JUEPPNER, J. & GIAVALISCO, P. 2011. Ultra performance liquid chromatography and high resolution mass spectrometry for the analysis of plant lipids. *Front Plant Sci,* 2**,** 54.

HUNTER, T. 1995. Protein kinases and phosphatases: the yin and yang of protein phosphorylation and signaling. *Cell,* 80**,** 225-36.

HUTTENLOCHER, A. & HORWITZ, A. R. 2011. Integrins in cell migration. *Cold Spring Harb Perspect Biol,* 3**,** a005074.

HVAS, A. M., JUUL, S., BECH, P. & NEXO, E. 2004. Vitamin B6 level is associated with symptoms of depression. *Psychother Psychosom,* 73**,** 340-3.

HYNES, R. O. 1992. Integrins: versatility, modulation, and signaling in cell adhesion. *Cell,* 69**,** 11-25.

IWABU, A., SMITH, K., ALLEN, F. D., LAUFFENBURGER, D. A. & WELLS, A. 2004. Epidermal growth factor induces fibroblast contractility and motility via a protein kinase C delta-dependent pathway. *J Biol Chem,* 279**,** 14551-60.

IYAMA, T. & WILSON, D. M., 3RD 2013. DNA repair mechanisms in dividing and non-dividing cells. *DNA Repair (Amst),* 12**,** 620-36.

JACKSON, S. P. & BARTEK, J. 2009. The DNA-damage response in human biology and disease. *Nature,* 461**,** 1071-8.

JAROUDI, S. & SENGUPTA, S. 2007. DNA repair in mammalian embryos. *Mutat Res,* 635**,** 53-77.

JEMC, J. & REBAY, I. 2007. The eyes absent family of phosphotyrosine phosphatases: properties and roles in developmental regulation of transcription. *Annu Rev Biochem,* 76**,** 513-38.

JIMENEZ, C., PORTELA, R. A., MELLADO, M., RODRIGUEZ-FRADE, J. M., COLLARD, J., SERRANO, A., MARTINEZ, A. C., AVILA, J. & CARRERA, A. C. 2000. Role of the PI3K regulatory subunit in the control of actin organization and cell migration. *J Cell Biol,* 151**,** 249-62.

JOHNSON, M. T., MAHMOOD, S. & PATEL, M. S. 2003. Intermediary metabolism and energetics during murine early embryogenesis. *J Biol Chem,* 278**,** 31457-60.

JONES, N. P., PEAK, J., BRADER, S., ECCLES, S. A. & KATAN, M. 2005. PLCgamma1 is essential for early events in integrin signalling required for cell motility. *J Cell Sci,* 118**,** 2695-706.

KADAMUR, G. & ROSS, E. M. 2013. Mammalian phospholipase C. *Annu Rev Physiol,* 75**,** 127-54.

KANCHANAWONG, P., SHTENGEL, G., PASAPERA, A. M., RAMKO, E. B., DAVIDSON, M. W., HESS, H. F. & WATERMAN, C. M. 2010. Nanoscale architecture of integrin-based cell adhesions. *Nature,* 468**,** 580-4.

KAY, J. G. & GRINSTEIN, S. 2013. Phosphatidylserine-mediated cellular signaling. *Adv Exp Med Biol,* 991**,** 177-93.

KELLEY, M. J., BAILIS, A. M., HENRY, S. A. & CARMAN, G. M. 1988. Regulation of phospholipid biosynthesis in Saccharomyces cerevisiae by inositol. Inositol is an inhibitor of phosphatidylserine synthase activity. *J Biol Chem,* 263**,** 18078-85.

KESTLER, C., KNOBLOCH, G., TESSMER, I., JEANCLOS, E., SCHINDELIN, H. & GOHLA, A. 2014. Chronophin dimerization is required for proper positioning of its substrate specificity loop. *J Biol Chem,* 289**,** 3094-103.

KHOURY, G. A., BALIBAN, R. C. & FLOUDAS, C. A. 2011. Proteome-wide post-translational modification statistics: frequency analysis and curation of the swiss-prot database. *Sci Rep,* 1.

KIM, H. K., KIM, J. W., ZILBERSTEIN, A., MARGOLIS, B., KIM, J. G., SCHLESSINGER, J. & RHEE, S. G. 1991. PDGF stimulation of inositol phospholipid hydrolysis requires PLC-gamma 1 phosphorylation on tyrosine residues 783 and 1254. *Cell,* 65**,** 435-41.

KING, S. J., WORTH, D. C., SCALES, T. M. E., MONYPENNY, J., JONES, G. E. & PARSONS, M. 2011. β1 integrins regulate fibroblast chemotaxis through control of N-WASP stability. *The EMBO Journal,* 30**,** 1705-1718.

KIRKWOOD, J. S., MAIER, C. & STEVENS, J. F. 2013. Simultaneous, untargeted metabolic profiling of polar and non-polar metabolites by LC-Q-TOF mass spectrometry. *Curr Protoc Toxicol,* 0 4**,** Unit4.39.

KLEMKE, M., WESCHENFELDER, T., KONSTANDIN, M. H. & SAMSTAG, Y. 2007. High affinity interaction of integrin alpha4beta1 (VLA-4) and vascular cell adhesion molecule 1 (VCAM-1) enhances migration of human melanoma cells across activated endothelial cell layers. *J Cell Physiol,* 212**,** 368-74.

KNIGHT, J., HINSDALE, M. & HOLMES, R. 2012. Glycolate and 2-phosphoglycolate content of tissues measured by ion chromatography coupled to mass spectrometry. *Anal Biochem,* 421**,** 121-4.

KOLCH, W. & PITT, A. 2010. Functional proteomics to dissect tyrosine kinase signalling pathways in cancer. *Nat Rev Cancer,* 10**,** 618-629.

KRISHNAN, N., JEONG, D. G., JUNG, S. K., RYU, S. E., XIAO, A., ALLIS, C. D., KIM, S. J. & TONKS, N. K. 2009. Dephosphorylation of the C-terminal tyrosyl residue of the DNA damage-related histone H2A.X is mediated by the protein phosphatase eyes absent. *J Biol Chem,* 284**,** 16066-70.

KRUEGER, E. W., ORTH, J. D., CAO, H. & MCNIVEN, M. A. 2003. A dynamin-cortactin-Arp2/3 complex mediates actin reorganization in growth factor-stimulated cells. *Mol Biol Cell,* 14**,** 1085-96.

LAEMMLI, U. K. 1970. Cleavage of structural proteins during the assembly of the head of bacteriophage T4. *Nature,* 227**,** 680-5.

LAKSO, M., PICHEL, J. G., GORMAN, J. R., SAUER, B., OKAMOTO, Y., LEE, E., ALT, F. W. & WESTPHAL, H. 1996. Efficient in vivo manipulation of mouse genomic sequences at the zygote stage. *Proc Natl Acad Sci U S A,* 93**,** 5860-5.

LARSSON, C. 2006. Protein kinase C and the regulation of the actin cytoskeleton. *Cell Signal,* 18**,** 276-84.

LAUX, T., FUKAMI, K., THELEN, M., GOLUB, T., FREY, D. & CARONI, P. 2000. GAP43, MARCKS, and CAP23 modulate PI(4,5)P(2) at plasmalemmal rafts, and regulate cell cortex actin dynamics through a common mechanism. *J Cell Biol,* 149**,** 1455-72.

LAW, C. L., CHANDRAN, K. A., SIDORENKO, S. P. & CLARK, E. A. 1996. Phospholipase C-gamma1 interacts with conserved phosphotyrosyl residues in the linker region of Syk and is a substrate for Syk. *Mol Cell Biol,* 16**,** 1305-15.

LEE, C. S., KIM, J. M., GHIM, J., SUH, P. G. & RYU, S. H. 2015. GTP-dependent interaction between phospholipase D and dynamin modulates fibronectin-induced cell spreading. *Cell Signal,* 27**,** 2363-2370.

LEGATE, K. R., WICKSTROM, S. A. & FASSLER, R. 2009. Genetic and cell biological analysis of integrin outside-in signaling. *Genes Dev,* 23**,** 397-418.

LEGG, J. A., BOMPARD, G., DAWSON, J., MORRIS, H. L., ANDREW, N., COOPER, L., JOHNSTON, S. A., TRAMOUNTANIS, G. & MACHESKY, L. M. 2007. N-WASP involvement in dorsal ruffle formation in mouse embryonic fibroblasts. *Mol Biol Cell,* 18**,** 678-87.

LEVENTIS, P. A. & GRINSTEIN, S. 2010. The distribution and function of phosphatidylserine in cellular membranes. *Annu Rev Biophys,* 39**,** 407-27.

LI, C., LIANG, Y. Y., FENG, X. H., TSAI, S. Y., TSAI, M. J. & O'MALLEY, B. W. 2008. Essential phosphatases and a phospho-degron are critical for regulation of SRC-3/AIB1 coactivator function and turnover. *Mol Cell,* 31**,** 835-49.

LI, X., OGHI, K. A., ZHANG, J., KRONES, A., BUSH, K. T., GLASS, C. K., NIGAM, S. K., AGGARWAL, A. K., MAAS, R., ROSE, D. W. & ROSENFELD, M. G. 2003. Eya protein phosphatase activity regulates Six1-Dach-Eya transcriptional effects in mammalian organogenesis. *Nature,* 426**,** 247-54.

LIANG, F., LEE, S. Y., LIANG, J., LAWRENCE, D. S. & ZHANG, Z. Y. 2005. The role of protein-tyrosine phosphatase 1B in integrin signaling. *J Biol Chem,* 280**,** 24857-63.

LIBERTI, S., SACCO, F., CALDERONE, A., PERFETTO, L., IANNUCCELLI, M., PANNI, S., SANTONICO, E., PALMA, A., NARDOZZA, A. P., CASTAGNOLI, L. & CESARENI, G. 2013. HuPho: the human phosphatase portal. *Febs j,* 280**,** 379-87.

LIN, P. T., CHENG, C. H., LIAW, Y. P., LEE, B. J., LEE, T. W. & HUANG, Y. C. 2006. Low pyridoxal 5'-phosphate is associated with increased risk of coronary artery disease. *Nutrition,* 22**,** 1146-51.

LOCASALE, J. W. & CANTLEY, L. C. 2011. Metabolic flux and the regulation of mammalian cell growth. *Cell Metab,* 14**,** 443-51.

LOPASCHUK, G. D., WALL, S. R., OLLEY, P. M. & DAVIES, N. J. 1988. Etomoxir, a carnitine palmitoyltransferase I inhibitor, protects hearts from fatty acid-induced ischemic injury independent of changes in long chain acylcarnitine. *Circ Res,* 63**,** 1036-43.

LOWENSTEIN, E. J., DALY, R. J., BATZER, A. G., LI, W., MARGOLIS, B., LAMMERS, R., ULLRICH, A., SKOLNIK, E. Y., BAR-SAGI, D. & SCHLESSINGER, J. 1992. The SH2 and SH3 domain-containing protein GRB2 links receptor tyrosine kinases to ras signaling. *Cell,* 70**,** 431-442.

LU, Z., WANG, L., DUNAWAY-MARIANO, D. & ALLEN, K. N. 2009. Structure-function analysis of 2-keto-3-deoxy-D-glycero-D-galactonononate-9-phosphate phosphatase defines specificity elements in type C0 haloalkanoate dehalogenase family members. *J Biol Chem,* 284**,** 1224-33.

MAHER, P. A., PASQUALE, E. B., WANG, J. Y. & SINGER, S. J. 1985. Phosphotyrosine-containing proteins are concentrated in focal adhesions and intercellular junctions in normal cells. *Proc Natl Acad Sci U S A,* 82**,** 6576-80.

MARGADANT, C., MONSUUR, H. N., NORMAN, J. C. & SONNENBERG, A. 2011. Mechanisms of integrin activation and trafficking. *Curr Opin Cell Biol,* 23**,** 607-14.

MARINO, G. & KROEMER, G. 2013a. Mechanisms of apoptotic phosphatidylserine exposure. *Cell Res,* 23**,** 1247-1248.

MARINO, G. & KROEMER, G. 2013b. Mechanisms of apoptotic phosphatidylserine exposure. *Cell Res,* 23**,** 1247-8.

MAYER, N., SCHWEIGER, M., ROMAUCH, M., GRABNER, G. F., EICHMANN, T. O., FUCHS, E., IVKOVIC, J., HEIER, C., MRAK, I., LASS, A., HOFLER, G., FLEDELIUS, C., ZECHNER, R., ZIMMERMANN, R. & BREINBAUER, R. 2013. Development of small-molecule inhibitors targeting adipose triglyceride lipase. *Nat Chem Biol,* 9**,** 785-7.

MCGARRY, J. D. & BROWN, N. F. 1997. The Mitochondrial Carnitine Palmitoyltransferase System — From Concept to Molecular Analysis. *European Journal of Biochemistry,* 244**,** 1-14.

MELLSTRÖM, K., HELDIN, C.-H. & WESTERMARK, B. 1988. Induction of circular membrane ruffling on human fibroblasts by platelet-derived growth factor. *Experimental Cell Research,* 177**,** 347-359.

MELLSTROM, K., HELDIN, C. H. & WESTERMARK, B. 1988. Induction of circular membrane ruffling on human fibroblasts by platelet-derived growth factor. *Exp Cell Res,* 177**,** 347-59.

MILDVAN, A. S., XIA, Z., AZURMENDI, H. F., SARASWAT, V., LEGLER, P. M., MASSIAH, M. A., GABELLI, S. B., BIANCHET, M. A., KANG, L. W. & AMZEL, L. M. 2005. Structures and mechanisms of Nudix hydrolases. *Arch Biochem Biophys,* 433**,** 129-43.

MILLS, P. B., CAMUZEAUX, S. S., FOOTITT, E. J., MILLS, K. A., GISSEN, P., FISHER, L., DAS, K. B., VARADKAR, S. M., ZUBERI, S., MCWILLIAM, R., STODBERG, T., PLECKO, B., BAUMGARTNER, M. R., MAIER, O., CALVERT, S., RINEY, K., WOLF, N. I., LIVINGSTON, J. H., BALA, P., MOREL, C. F., FEILLET, F., RAIMONDI, F., DEL GIUDICE, E., CHONG, W. K., PITT, M. & CLAYTON, P. T. 2014. Epilepsy due to PNPO mutations: genotype, environment and treatment affect presentation and outcome. *Brain*.

MIRANTI, C. K., OHNO, S. & BRUGGE, J. S. 1999. Protein kinase C regulates integrin-induced activation of the extracellular regulated kinase pathway upstream of Shc. *J Biol Chem,* 274**,** 10571-81.

MITCHELL, T. W., PHAM, H., THOMAS, M. C. & BLANKSBY, S. J. 2009. Identification of double bond position in lipids: From GC to OzID. *Journal of Chromatography B,* 877**,** 2722-2735.

MITRA, S. K., HANSON, D. A. & SCHLAEPFER, D. D. 2005. Focal adhesion kinase: in command and control of cell motility. *Nat Rev Mol Cell Biol,* 6**,** 56-68.

MITRA, S. K. & SCHLAEPFER, D. D. 2006. Integrin-regulated FAK-Src signaling in normal and cancer cells. *Curr Opin Cell Biol,* 18**,** 516-23.

MOCHLY-ROSEN, D., DAS, K. & GRIMES, K. V. 2012. Protein kinase C, an elusive therapeutic target? *Nat Rev Drug Discov,* 11**,** 937-957.

MORO, L., DOLCE, L., CABODI, S., BERGATTO, E., BOERI ERBA, E., SMERIGLIO, M., TURCO, E., RETTA, S. F., GIUFFRIDA, M. G., VENTURINO, M., GODOVAC-ZIMMERMANN, J., CONTI, A., SCHAEFER, E., BEGUINOT, L., TACCHETTI, C., GAGGINI, P., SILENGO, L., TARONE, G. & DEFILIPPI, P. 2002. Integrin-induced epidermal growth factor (EGF) receptor activation requires c-Src and p130Cas and leads to phosphorylation of specific EGF receptor tyrosines. *J Biol Chem,* 277**,** 9405-14.

MOSER, M., LEGATE, K. R., ZENT, R. & FASSLER, R. 2009. The tail of integrins, talin, and kindlins. *Science,* 324**,** 895-9.

MOSER, M., NIESWANDT, B., USSAR, S., POZGAJOVA, M. & FASSLER, R. 2008. Kindlin-3 is essential for integrin activation and platelet aggregation. *Nat Med,* 14**,** 325-30.

MOURDJEVA, M., KYURKCHIEV, D., MANDINOVA, A., ALTANKOVA, I., KEHAYOV, I. & KYURKCHIEV, S. 2005. Dynamics of membrane translocation of phosphatidylserine during apoptosis detected by a monoclonal antibody. *Apoptosis,* 10**,** 209-17.

NAKAMURA, M. T., YUDELL, B. E. & LOOR, J. J. 2014. Regulation of energy metabolism by long-chain fatty acids. *Prog Lipid Res,* 53**,** 124-44.

NEWMAN, R. H., HU, J., RHO, H. S., XIE, Z., WOODARD, C., NEISWINGER, J., COOPER, C., SHIRLEY, M., CLARK, H. M., HU, S., HWANG, W., JEONG, J. S., WU, G., LIN, J., GAO, X., NI, Q., GOEL, R., XIA, S., JI, H., DALBY, K. N., BIRNBAUM, M. J., COLE, P. A., KNAPP, S., RYAZANOV, A. G., ZACK, D. J., BLACKSHAW, S., PAWSON, T., GINGRAS, A. C., DESIDERIO, S., PANDEY, A., TURK, B. E., ZHANG, J., ZHU, H. & QIAN, J. 2013. Construction of human activity-based phosphorylation networks. *Mol Syst Biol,* 9**,** 655.

NISHIZUKA, Y. 1995. Protein kinase C and lipid signaling for sustained cellular responses. *Faseb j,* 9**,** 484-96.

OLSEN, J. V., BLAGOEV, B., GNAD, F., MACEK, B., KUMAR, C., MORTENSEN, P. & MANN, M. 2006. Global, in vivo, and site-specific phosphorylation dynamics in signaling networks. *Cell,* 127**,** 635-48.

ORTH, J. D., KRUEGER, E. W., WELLER, S. G. & MCNIVEN, M. A. 2006. A novel endocytic mechanism of epidermal growth factor receptor sequestration and internalization. *Cancer Res,* 66**,** 3603-10.

ORTH, J. D. & MCNIVEN, M. A. 2006. Get off my back! Rapid receptor internalization through circular dorsal ruffles. *Cancer Res,* 66**,** 11094-6.

PALLEN, C. J. 2003. Protein tyrosine phosphatase alpha (PTPalpha): a Src family kinase activator and mediator of multiple biological effects. *Curr Top Med Chem,* 3**,** 821-35.
PANDEY, R. N., RANI, R., YEO, E. J., SPENCER, M., HU, S., LANG, R. A. & HEGDE, R. S. 2010. The Eyes Absent phosphatase-transactivator proteins promote proliferation, transformation, migration, and invasion of tumor cells. *Oncogene,* 29**,** 3715-22.
PANDYA, C., DUNAWAY-MARIANO, D., XIA, Y. & ALLEN, K. N. 2014. Structure-guided approach for detecting large domain inserts in protein sequences as illustrated using the haloacid dehalogenase superfamily. *Proteins*.
PANTALONI, D., LE CLAINCHE, C. & CARLIER, M. F. 2001. Mechanism of actin-based motility. *Science,* 292**,** 1502-6.
PARSONS, J. L., DIANOVA, I. I. & DIANOV, G. L. 2004. APE1 is the major 3′-phosphoglycolate activity in human cell extracts. *Nucleic Acids Research,* 32**,** 3531-3536.
PARSONS, S. J. & PARSONS, J. T. 2004. Src family kinases, key regulators of signal transduction. *Oncogene,* 23**,** 7906-9.
PAYNE, L. J., EVES, R. L., JIA, L. & MAK, A. S. 2014. p53 Down regulates PDGF-induced formation of circular dorsal ruffles in rat aortic smooth muscle cells. *PLoS One,* 9**,** e108257.
PELLICENA, P. & MILLER, W. T. 2001. Processive phosphorylation of p130Cas by Src depends on SH3-polyproline interactions. *J Biol Chem,* 276**,** 28190-6.
PELLINEN, T., TUOMI, S., ARJONEN, A., WOLF, M., EDGREN, H., MEYER, H., GROSSE, R., KITZING, T., RANTALA, J. K., KALLIONIEMI, O., FASSLER, R., KALLIO, M. & IVASKA, J. 2008. Integrin trafficking regulated by Rab21 is necessary for cytokinesis. *Dev Cell,* 15**,** 371-85.
PHILLIPS-MASON, P. J., KAUR, H., BURDEN-GULLEY, S. M., CRAIG, S. E. & BRADY-KALNAY, S. M. 2011. Identification of phospholipase C gamma1 as a protein tyrosine phosphatase mu substrate that regulates cell migration. *J Cell Biochem,* 112**,** 39-48.
PICCOLO, E., INNOMINATO, P. F., MARIGGIO, M. A., MAFFUCCI, T., IACOBELLI, S. & FALASCA, M. 2002. The mechanism involved in the regulation of phospholipase Cgamma1 activity in cell migration. *Oncogene,* 21**,** 6520-9.
PIKE, L. J. 2009. The challenge of lipid rafts. *J Lipid Res,* 50**,** S323-8.
PIKE, L. J., HAN, X., CHUNG, K. N. & GROSS, R. W. 2002. Lipid rafts are enriched in arachidonic acid and plasmenylethanolamine and their composition is independent of caveolin-1 expression: a quantitative electrospray ionization/mass spectrometric analysis. *Biochemistry,* 41**,** 2075-88.
PILS, B. & SCHULTZ, J. 2004. Evolution of the multifunctional protein tyrosine phosphatase family. *Mol Biol Evol,* 21**,** 625-31.
PLOW, E. F., HAAS, T. A., ZHANG, L., LOFTUS, J. & SMITH, J. W. 2000. Ligand binding to integrins. *J Biol Chem,* 275**,** 21785-8.
POLLARD, T. D., BLANCHOIN, L. & MULLINS, R. D. 2000. Molecular mechanisms controlling actin filament dynamics in nonmuscle cells. *Annu Rev Biophys Biomol Struct,* 29**,** 545-76.
PONTI, A., MACHACEK, M., GUPTON, S. L., WATERMAN-STORER, C. M. & DANUSER, G. 2004. Two distinct actin networks drive the protrusion of migrating cells. *Science,* 305**,** 1782-6.
PRING, M., WEBER, A. & BUBB, M. R. 1992. Profilin-actin complexes directly elongate actin filaments at the barbed end. *Biochemistry,* 31**,** 1827-36.
RABONI, S., PIOSELLI, B., BETTATI, S. & MOZZARELLI, A. 2003. The molecular pathway for the allosteric regulation of tryptophan synthase. *Biochim Biophys Acta,* 1647**,** 157-60.
RALSER, M., WAMELINK, M. M., KOWALD, A., GERISCH, B., HEEREN, G., STRUYS, E. A., KLIPP, E., JAKOBS, C., BREITENBACH, M., LEHRACH, H. & KROBITSCH, S. 2007. Dynamic rerouting of the carbohydrate flux is key to counteracting oxidative stress. *J Biol,* 6**,** 10.

RASMUSSEN, B. B., HOLMBACK, U. C., VOLPI, E., MORIO-LIONDORE, B., PADDON-JONES, D. & WOLFE, R. R. 2002. Malonyl coenzyme A and the regulation of functional carnitine palmitoyltransferase-1 activity and fat oxidation in human skeletal muscle. *J Clin Invest,* 110**,** 1687-93.

RAYAPUREDDI, J. P., KATTAMURI, C., STEINMETZ, B. D., FRANKFORT, B. J., OSTRIN, E. J., MARDON, G. & HEGDE, R. S. 2003. Eyes absent represents a class of protein tyrosine phosphatases. *Nature,* 426**,** 295-8.

REBAY, I., SILVER, S. J. & TOOTLE, T. L. 2005. New vision from Eyes absent: transcription factors as enzymes. *Trends Genet,* 21**,** 163-71.

REICHENBERGER, K. J., COLETTA, R. D., SCHULTE, A. P., VARELLA-GARCIA, M. & FORD, H. L. 2005. Gene amplification is a mechanism of Six1 overexpression in breast cancer. *Cancer Res,* 65**,** 2668-75.

REN, L., CHEN, X., LUECHAPANICHKUL, R., SELNER, N. G., MEYER, T. M., WAVREILLE, A. S., CHAN, R., IORIO, C., ZHOU, X., NEEL, B. G. & PEI, D. 2011. Substrate specificity of protein tyrosine phosphatases 1B, RPTPalpha, SHP-1, and SHP-2. *Biochemistry,* 50**,** 2339-56.

RESHEF, L., OLSWANG, Y., CASSUTO, H., BLUM, B., CRONIGER, C. M., KALHAN, S. C., TILGHMAN, S. M. & HANSON, R. W. 2003. Glyceroneogenesis and the Triglyceride/Fatty Acid Cycle. *Journal of Biological Chemistry,* 278**,** 30413-30416.

REUE, K. 2009. The lipin family: mutations and metabolism. *Curr Opin Lipidol,* 20**,** 165-70.

RICHARD, D., KEFI, K., BARBE, U., BAUSERO, P. & VISIOLI, F. 2008. Polyunsaturated fatty acids as antioxidants. *Pharmacol Res,* 57**,** 451-5.

RIVERA, G. M., ANTOKU, S., GELKOP, S., SHIN, N. Y., HANKS, S. K., PAWSON, T. & MAYER, B. J. 2006. Requirement of Nck adaptors for actin dynamics and cell migration stimulated by platelet-derived growth factor B. *Proceedings of the National Academy of Sciences,* 103**,** 9536-9541.

RODRIGUES, G. A., FALASCA, M., ZHANG, Z., ONG, S. H. & SCHLESSINGER, J. 2000. A novel positive feedback loop mediated by the docking protein Gab1 and phosphatidylinositol 3-kinase in epidermal growth factor receptor signaling. *Mol Cell Biol,* 20**,** 1448-59.

ROSE, Z. B. 1981. Phosphoglycolate phosphatase from human red blood cells. *Arch Biochem Biophys,* 208**,** 602-9.

ROSKOSKI, R., JR. 2005. Src kinase regulation by phosphorylation and dephosphorylation. *Biochem Biophys Res Commun,* 331**,** 1-14.

ROSSANT, J. & CROSS, J. C. 2001. Placental development: lessons from mouse mutants. *Nat Rev Genet,* 2**,** 538-48.

ROTIN, D., MARGOLIS, B., MOHAMMADI, M., DALY, R. J., DAUM, G., LI, N., FISCHER, E. H., BURGESS, W. H., ULLRICH, A. & SCHLESSINGER, J. 1992. SH2 domains prevent tyrosine dephosphorylation of the EGF receptor: identification of Tyr992 as the high-affinity binding site for SH2 domains of phospholipase C gamma. *Embo j,* 11**,** 559-67.

SAKAI, T., ZHANG, Q., FASSLER, R. & MOSHER, D. F. 1998. Modulation of beta1A integrin functions by tyrosine residues in the beta1 cytoplasmic domain. *J Cell Biol,* 141**,** 527-38.

SASAKI, H., FUJII, S., YOSHIZAKI, Y., NAKASHIMA, K. & KANEKO, T. 1987. Phosphoglycolate synthesis by human erythrocyte pyruvate kinase. *Acta Haematol,* 77**,** 83-6.

SCHIEBEL, J., KAPILASHRAMI, K., FEKETE, A., BOMMINENI, G. R., SCHAEFER, C. M., MUELLER, M. J., TONGE, P. J. & KISKER, C. 2013. Structural basis for the recognition of mycolic acid precursors by KasA, a condensing enzyme and drug target from Mycobacterium tuberculosis. *J Biol Chem,* 288**,** 34190-204.

SCHIRCH, V. & SZEBENYI, D. M. 2005. Serine hydroxymethyltransferase revisited. *Curr Opin Chem Biol,* 9**,** 482-7.

SCHLUNCK, G., DAMKE, H., KIOSSES, W. B., RUSK, N., SYMONS, M. H., WATERMAN-STORER, C. M., SCHMID, S. L. & SCHWARTZ, M. A. 2004. Modulation of Rac localization and function by dynamin. *Mol Biol Cell,* 15**,** 256-67.

SCHNACKERZ, K. D. & GRACY, R. W. 1991. Probing the catalytic sites of triosephosphate isomerase by 31P-NMR with reversibly and irreversibly binding substrate analogues. *Eur J Biochem,* 199**,** 231-8.

SEGAWA, K., KURATA, S., YANAGIHASHI, Y., BRUMMELKAMP, T. R., MATSUDA, F. & NAGATA, S. 2014. Caspase-mediated cleavage of phospholipid flippase for apoptotic phosphatidylserine exposure. *Science,* 344**,** 1164-8.

SEIFRIED, A., KNOBLOCH, G., DURAPHE, P. S., SEGERER, G., MANHARD, J., SCHINDELIN, H., SCHULTZ, J. & GOHLA, A. 2014. Evolutionary and structural analyses of mammalian haloacid dehalogenase-type phosphatases AUM and chronophin provide insight into the basis of their different substrate specificities. *J Biol Chem,* 289**,** 3416-31.

SEIFRIED, A., SCHULTZ, J. & GOHLA, A. 2013. Human HAD phosphatases: structure, mechanism, and roles in health and disease. *Febs j,* 280**,** 549-71.

SHI, F. & SOTTILE, J. 2008. Caveolin-1-dependent beta1 integrin endocytosis is a critical regulator of fibronectin turnover. *J Cell Sci,* 121**,** 2360-71.

SHI, Y. 2009. Serine/threonine phosphatases: mechanism through structure. *Cell,* 139**,** 468-84.

SCHULZE M., FEDORCHENKO O., ZINK TG., KNOBBE-THOMSON CB., KRAUS S., SCHWINN S., BEILHACK A., REIFENBERGER G., MONORANU CM., SIREN AL., JEANCLOS E.& GOHLA A. 2015. Chronophin is a glial tumour modifier involved in the regulation of glioblastoma growth and invasiveness. *Oncogen, accepted*

SIEG, D. J., HAUCK, C. R. & SCHLAEPFER, D. D. 1999. Required role of focal adhesion kinase (FAK) for integrin-stimulated cell migration. *J Cell Sci,* 112 (Pt 16)**,** 2677-91.

SIGAL, Y. J., MCDERMOTT, M. I. & MORRIS, A. J. 2005. Integral membrane lipid phosphatases/phosphotransferases: common structure and diverse functions. *Biochem J,* 387**,** 281-93.

SIGISMUND, S., ARGENZIO, E., TOSONI, D., CAVALLARO, E., POLO, S. & DI FIORE, P. P. 2008. Clathrin-mediated internalization is essential for sustained EGFR signaling but dispensable for degradation. *Dev Cell,* 15**,** 209-19.

SINNECKER, D. & SCHAEFER, M. 2004. Real-time analysis of phospholipase C activity during different patterns of receptor-induced Ca2+ responses in HEK293 cells. *Cell Calcium,* 35**,** 29-38.

SOLER, C., BEGUINOT, L. & CARPENTER, G. 1994. Individual epidermal growth factor receptor autophosphorylation sites do not stringently define association motifs for several SH2-containing proteins. *J Biol Chem,* 269**,** 12320-4.

SOMOZA, R. & BEUTLER, E. 1983. Phosphoglycolate phosphatase and 2,3-diphosphoglycerate in red cells of normal and anemic subjects. *Blood,* 62**,** 750-3.

SPIEGEL, S., FOSTER, D. & KOLESNICK, R. 1996. Signal transduction through lipid second messengers. *Curr Opin Cell Biol,* 8**,** 159-67.

STACE, C. L. & KTISTAKIS, N. T. 2006. Phosphatidic acid- and phosphatidylserine-binding proteins. *Biochim Biophys Acta,* 1761**,** 913-26.

STIFFIN, R. M., SULLIVAN, S. M., CARLSON, G. M. & HOLYOAK, T. 2008. Differential inhibition of cytosolic PEPCK by substrate analogues. Kinetic and structural characterization of inhibitor recognition. *Biochemistry,* 47**,** 2099-109.

STILLWELL, W., SHAIKH, S. R., ZEROUGA, M., SIDDIQUI, R. & WASSALL, S. R. 2005. Docosahexaenoic acid affects cell signaling by altering lipid rafts. *Reprod Nutr Dev,* 45**,** 559-79.

STILLWELL, W. & WASSALL, S. R. 2003. Docosahexaenoic acid: membrane properties of a unique fatty acid. *Chem Phys Lipids,* 126**,** 1-27.

STINCONE, A., PRIGIONE, A., CRAMER, T., WAMELINK, M. M., CAMPBELL, K., CHEUNG, E., OLIN-SANDOVAL, V., GRUNING, N., KRUGER, A., TAUQEER ALAM, M., KELLER, M. A., BREITENBACH, M., BRINDLE, K. M., RABINOWITZ, J. D. & RALSER, M. 2014. The return of metabolism: biochemistry and physiology of the pentose phosphate pathway. *Biol Rev Camb Philos Soc*.

SUETSUGU, S., YAMAZAKI, D., KURISU, S. & TAKENAWA, T. 2003. Differential roles of WAVE1 and WAVE2 in dorsal and peripheral ruffle formation for fibroblast cell migration. *Dev Cell,* 5**,** 595-609.

SVITKINA, T. M. & BORISY, G. G. 1999. Arp2/3 complex and actin depolymerizing factor/cofilin in dendritic organization and treadmilling of actin filament array in lamellipodia. *J Cell Biol,* 145**,** 1009-26.

SVITKINA, T. M., BULANOVA, E. A., CHAGA, O. Y., VIGNJEVIC, D. M., KOJIMA, S., VASILIEV, J. M. & BORISY, G. G. 2003. Mechanism of filopodia initiation by reorganization of a dendritic network. *J Cell Biol,* 160**,** 409-21.

TADOKORO, S., SHATTIL, S. J., ETO, K., TAI, V., LIDDINGTON, R. C., DE PEREDA, J. M., GINSBERG, M. H. & CALDERWOOD, D. A. 2003a. Talin binding to integrin beta tails: a final common step in integrin activation. *Science,* 302**,** 103-6.

TADOKORO, S., SHATTIL, S. J., ETO, K., TAI, V., LIDDINGTON, R. C., DE PEREDA, J. M., GINSBERG, M. H. & CALDERWOOD, D. A. 2003b. Talin Binding to Integrin ß Tails: A Final Common Step in Integrin Activation. *Science,* 302**,** 103-106.

TAKENAWA, T. & SUETSUGU, S. 2007. The WASP-WAVE protein network: connecting the membrane to the cytoskeleton. *Nat Rev Mol Cell Biol,* 8**,** 37-48.

TAMURA, M. & IWAMOTO, Y. 1989. The effect of platelet-derived growth factor on phagocytosis of cultured human trabecular cells. *Exp Eye Res,* 48**,** 761-70.

TERESA PELLICER, M., FELISA NUNEZ, M., AGUILAR, J., BADIA, J. & BALDOMA, L. 2003. Role of 2-phosphoglycolate phosphatase of Escherichia coli in metabolism of the 2-phosphoglycolate formed in DNA repair. *J Bacteriol,* 185**,** 5815-21.

THIES, F., GARRY, J. M., YAQOOB, P., RERKASEM, K., WILLIAMS, J., SHEARMAN, C. P., GALLAGHER, P. J., CALDER, P. C. & GRIMBLE, R. F. 2003. Association of n-3 polyunsaturated fatty acids with stability of atherosclerotic plaques: a randomised controlled trial. *Lancet,* 361**,** 477-85.

TOOTLE, T. L., SILVER, S. J., DAVIES, E. L., NEWMAN, V., LATEK, R. R., MILLS, I. A., SELENGUT, J. D., PARLIKAR, B. E. & REBAY, I. 2003. The transcription factor Eyes absent is a protein tyrosine phosphatase. *Nature,* 426**,** 299-302.

TVOROGOV, D., WANG, X. J., ZENT, R. & CARPENTER, G. 2005. Integrin-dependent PLC-gamma1 phosphorylation mediates fibronectin-dependent adhesion. *J Cell Sci,* 118**,** 601-10.

UBERSAX, J. A. & FERRELL, J. E., JR. 2007. Mechanisms of specificity in protein phosphorylation. *Nat Rev Mol Cell Biol,* 8**,** 530-41.

UNGER, R. H. & SCHERER, P. E. 2010. Gluttony, sloth and the metabolic syndrome: a roadmap to lipotoxicity. *Trends Endocrinol Metab,* 21**,** 345-52.

VADLAMUDI, R. K., LI, F., BARNES, C. J., BAGHERI-YARMAND, R. & KUMAR, R. 2004. p41-Arc subunit of human Arp2/3 complex is a p21-activated kinase-1-interacting substrate. *EMBO Rep,* 5**,** 154-60.

VERMES, I., HAANEN, C., STEFFENS-NAKKEN, H. & REUTELINGSPERGER, C. 1995. A novel assay for apoptosis. Flow cytometric detection of phosphatidylserine expression on early apoptotic cells using fluorescein labelled Annexin V. *J Immunol Methods,* 184**,** 39-51.

VINCENT, E. E., SERGUSHICHEV, A., GRISS, T., GINGRAS, M. C., SAMBORSKA, B., NTIMBANE, T., COELHO, P. P., BLAGIH, J., RAISSI, T. C., CHOINIERE, L., BRIDON, G., LOGINICHEVA, E., FLYNN, B. R., THOMAS, E. C., TAVARE, J. M., AVIZONIS, D., PAUSE, A., ELDER, D. J., ARTYOMOV, M. N. & JONES, R. G. 2015. Mitochondrial Phosphoenolpyruvate Carboxykinase Regulates Metabolic Adaptation and Enables Glucose-Independent Tumor Growth. *Mol Cell,* 60**,** 195-207.

VIRSHUP, D. M. & SHENOLIKAR, S. 2009. From Promiscuity to Precision: Protein Phosphatases Get a Makeover. *Molecular Cell,* 33**,** 537-545.

VOLKOV, Y., LONG, A., MCGRATH, S., NI EIDHIN, D. & KELLEHER, D. 2001. Crucial importance of PKC-beta(I) in LFA-1-mediated locomotion of activated T cells. *Nat Immunol,* 2**,** 508-14.

WANG, Z. & MORAN, M. F. 1996. Requirement for the adapter protein GRB2 in EGF receptor endocytosis. *Science,* 272**,** 1935-9.

WEBB, D. J., DONAIS, K., WHITMORE, L. A., THOMAS, S. M., TURNER, C. E., PARSONS, J. T. & HORWITZ, A. F. 2004. FAK-Src signalling through paxillin, ERK and MLCK regulates adhesion disassembly. *Nat Cell Biol,* 6**,** 154-161.

WEBB, D. J., PARSONS, J. T. & HORWITZ, A. F. 2002. Adhesion assembly, disassembly and turnover in migrating cells -- over and over and over again. *Nat Cell Biol,* 4**,** E97-100.

WEGNER, A. 1976. Head to tail polymerization of actin. *J Mol Biol,* 108**,** 139-50.

WEHRLE-HALLER, B. & IMHOF, B. A. 2003. Actin, microtubules and focal adhesion dynamics during cell migration. *Int J Biochem Cell Biol,* 35**,** 39-50.

WEISS, A. & LITTMAN, D. R. 1994. Signal transduction by lymphocyte antigen receptors. *Cell,* 76**,** 263-74.

WELCH, H. C., COADWELL, W. J., STEPHENS, L. R. & HAWKINS, P. T. 2003. Phosphoinositide 3-kinase-dependent activation of Rac. *FEBS Lett,* 546**,** 93-7.

WESTHOFF, M. A., SERRELS, B., FINCHAM, V. J., FRAME, M. C. & CARRAGHER, N. O. 2004. SRC-mediated phosphorylation of focal adhesion kinase couples actin and adhesion dynamics to survival signaling. *Mol Cell Biol,* 2**4,** 8113-33.

WICK, A. N., DRURY, D. R. & MORITA, T. N. 1955. 2-Deoxyglucose; a metabolic block for glucose. *Proc Soc Exp Biol Med,* 89**,** 579-82.

WIERZBICKA-PATYNOWSKI, I. & SCHWARZBAUER, J. E. 2003. The ins and outs of fibronectin matrix assembly. *J Cell Sci,* 116**,** 3269-76.

WINDER, W. W. & HARDIE, D. G. 1996. Inactivation of acetyl-CoA carboxylase and activation of AMP-activated protein kinase in muscle during exercise. *American Journal of Physiology - Endocrinology and Metabolism,* 270**,** E299-E304.

WINOGRAD-KATZ, S. E., FASSLER, R., GEIGER, B. & LEGATE, K. R. 2014. The integrin adhesome: from genes and proteins to human disease. *Nat Rev Mol Cell Biol,* 15**,** 273-88.

WOLFENDEN, R. 1969. Transition State Analogues for Enzyme Catalysis. *Nature,* 223**,** 704-705.

WOODS, A. & COUCHMAN, J. R. 1992. Protein kinase C involvement in focal adhesion formation. *J Cell Sci,* 101 (Pt 2)**,** 277-90.

WOZNIAK, M. A., MODZELEWSKA, K., KWONG, L. & KEELY, P. J. 2004. Focal adhesion regulation of cell behavior. *Biochimica et Biophysica Acta (BBA) - Molecular Cell Research,* 1692**,** 103-119.

WU, R. F., GU, Y., XU, Y. C., NWARIAKU, F. E. & TERADA, L. S. 2003. Vascular endothelial growth factor causes translocation of p47phox to membrane ruffles through WAVE1. *J Biol Chem,* 278**,** 36830-40.

XIA, P., AIELLO, L. P., ISHII, H., JIANG, Z. Y., PARK, D. J., ROBINSON, G. S., TAKAGI, H., NEWSOME, W. P., JIROUSEK, M. R. & KING, G. L. 1996. Characterization of vascular endothelial growth factor's effect on the activation of protein kinase C, its isoforms, and endothelial cell growth. *J Clin Invest,* 98**,** 2018-26.

XIAO, H., EVES, R., YEH, C., KAN, W., XU, F., MAK, A. S. & LIU, M. 2009. Phorbol ester-induced podosomes in normal human bronchial epithelial cells. *Journal of Cellular Physiology,* 218**,** 366-375.

XING, B., WANG, L., GUO, D., HUANG, J., ESPENEL, C., KREITZER, G., ZHANG, J. J., GUO, L. & HUANG, X. Y. 2013. Atypical protein kinase Clambda is critical for growth factor receptor-induced dorsal ruffle turnover and cell migration. *J Biol Chem,* 288**,** 32827-36.

XU, J., CHRISTIAN, B. & JUMP, D. B. 2006. Regulation of rat hepatic L-pyruvate kinase promoter composition and activity by glucose, n-3 polyunsaturated fatty acids, and peroxisome proliferator-activated receptor-alpha agonist. *J Biol Chem,* 281**,** 18351-62.

YANG, L., WANG, L. & ZHENG, Y. 2006. Gene targeting of Cdc42 and Cdc42GAP affirms the critical involvement of Cdc42 in filopodia induction, directed migration, and proliferation in primary mouse embryonic fibroblasts. *Mol Biol Cell,* 17**,** 4675-85.

YANG, Y., DU, J., HU, Z., LIU, J., TIAN, Y., ZHU, Y., WANG, L. & GU, L. 2011. Activation of Rac1-PI3K/Akt is required for epidermal growth factor-induced PAK1 activation and cell migration in MDA-MB-231 breast cancer cells. *J Biomed Res,* 25**,** 237-45.

YE, F. & PETRICH, B. G. 2011. Kindlin: helper, co-activator, or booster of talin in integrin activation? *Curr Opin Hematol,* 18**,** 356-60.

ZAIDEL-BAR, R. 2009. Evolution of complexity in the integrin adhesome. *J Cell Biol,* 186**,** 317-21.

ZAIDEL-BAR, R. & GEIGER, B. 2010. The switchable integrin adhesome. *Journal of Cell Science,* 123**,** 1385-1388.

ZAISS, D. M., VAN LOOSDREGT, J., GORLANI, A., BEKKER, C. P., GRONE, A., SIBILIA, M., VAN BERGEN EN HENEGOUWEN, P. M., ROOVERS, R. C., COFFER, P. J. & SIJTS, A. J. 2013. Amphiregulin enhances regulatory T cell-suppressive function via the epidermal growth factor receptor. *Immunity,* 38**,** 275-84.

ZAPPASODI, R., DI NICOLA, M., CARLO-STELLA, C., MORTARINI, R., MOLLA, A., VEGETTI, C., ALBANI, S., ANICHINI, A. & GIANNI, A. M. 2008. The effect of artificial antigen-presenting cells with preclustered anti-CD28/-CD3/-LFA-1 monoclonal antibodies on the induction of ex vivo expansion of functional human antitumor T cells. *Haematologica,* 93**,** 1523-34.

ZECHER, R. & WOLF, H. U. 1980. Partial purification and characterization of human erythrocyte phosphoglycollate phosphatase. *Biochem J,* 191**,** 117-24.

ZECHNER, R., ZIMMERMANN, R., EICHMANN, T. O., KOHLWEIN, S. D., HAEMMERLE, G., LASS, A. & MADEO, F. 2012. FAT SIGNALS--lipases and lipolysis in lipid metabolism and signaling. *Cell Metab,* 15**,** 279-91.

ZEHARIA, A., SHAAG, A., HOUTKOOPER, R. H., HINDI, T., DE LONLAY, P., EREZ, G., HUBERT, L., SAADA, A., DE KEYZER, Y., ESHEL, G., VAZ, F. M., PINES, O. & ELPELEG, O. 2008. Mutations in LPIN1 cause recurrent acute myoglobinuria in childhood. *Am J Hum Genet,* 83**,** 489-94.

ZELLER, K. S., IDEVALL-HAGREN, O., STEFANSSON, A., VELLING, T., JACKSON, S. P., DOWNWARD, J., TENGHOLM, A. & JOHANSSON, S. 2010. PI3-kinase p110alpha mediates beta1 integrin-induced Akt activation and membrane protrusion during cell attachment and initial spreading. *Cell Signal,* 22**,** 1838-48.

ZHANG, L., YANG, N., HUANG, J., BUCKANOVICH, R. J., LIANG, S., BARCHETTI, A., VEZZANI, C., O'BRIEN-JENKINS, A., WANG, J., WARD, M. R., COURREGES, M. C., FRACCHIOLI, S., MEDINA, A., KATSAROS, D., WEBER, B. L. & COUKOS, G. 2005. Transcriptional coactivator Drosophila eyes absent homologue 2 is up-regulated in epithelial ovarian cancer and promotes tumor growth. *Cancer Res,* 65**,** 925-32.

ZHANG, X. H., MA, J., SMITH-WARNER, S. A., LEE, J. E. & GIOVANNUCCI, E. 2013. Vitamin B6 and colorectal cancer: current evidence and future directions. *World J Gastroenterol,* 19**,** 1005-10.

ZHOU, T., AKOPIANTS, K., MOHAPATRA, S., LIN, P. S., VALERIE, K., RAMSDEN, D. A., LEES-MILLER, S. P. & POVIRK, L. F. 2009. Tyrosyl-DNA phosphodiesterase and the repair of 3'-phosphoglycolate-terminated DNA double-strand breaks. *DNA Repair (Amst),* 8**,** 901-11.

ZHOU, T., LEE, J. W., TATAVARTHI, H., LUPSKI, J. R., VALERIE, K. & POVIRK, L. F. 2005. Deficiency in 3'-phosphoglycolate processing in human cells with a hereditary mutation in tyrosyl-DNA phosphodiesterase (TDP1). *Nucleic Acids Res,* 33**,** 289-97.

ZHU, J., LUO, B. H., XIAO, T., ZHANG, C., NISHIDA, N. & SPRINGER, T. A. 2008. Structure of a complete integrin ectodomain in a physiologic resting state and activation and deactivation by applied forces. *Mol Cell,* 32**,** 849-61.

8 Appendix

8.1 Curriculum vitae

8.2 Publication list and conference contributions

Research articles

Ivanovska J, Tregubova A, Mahadevan V, Chakilam S, Gandesiri M, Benderska N, Ettle B, Hartmann A, Söder S, Ziesché E, Fischer T, Lautscham L, Fabry B, **Segerer G**, Gohla A, Schneider-Stock R (2013) Identification of DAPK as a scaffold protein for the LIMK/cofilin complex in TNF-induced apoptosis.*Int J Biochem Cell Biol.*; 45(8):1720-9.

Seifried A, Knobloch G, Duraphe PS, **Segerer G**, Manhard J, Schindelin H, Schultz J, Gohla A (2014) Evolutionary and structural analyses of mammalian haloacid dehalogenase-type phosphatases AUM and chronophin provide insight into the basis of their different substrate specificities. *J Biol Chem.*; 289(6):3416-31

Segerer G[*], Hadamek K[*], Seifried A, Zundler M, Fekete A, Mueller MJ, Koentgen F, Gessler M, Jeanclos E, Gohla A (2015) Phosphoglycolate phosphatase links DNA damage to metabolism and proliferation. (submitted)

Segerer G, Saxena A, Radenz M, Zundler M, Fekete A, Mueller MJ, Jeanclos E, Gohla A (2015) The phosphoglycolate phosphatase (PGP) regulates cell migration by altering plasma membrane composition. (in preparation)

[*]equal contribution

Oral Presentations

Date	Organizer	Presentation Title
March 2011	Annual retreat of the Department of pharmacology	'The role of AUM for cell-matrix adhesion'
July 2012	Annual retreat of the Department of pharmacology	'Analysis of AUM-dependent signaling'
July 2013	Annual retreat of the Department of pharmacology	'The role of the novel tyrosine phosphatase AUM for cell adhesion and migration'
Oktober 2013	Annual retreat of the Rudolf-Virchow-Center	'Should I stay or should I go-it`s up to AUM'
Oktober 2013	SFB688 Symposium	'Role of AUM for lymphocyte migration'
July 2014	Annual retreat of the Department of pharmacology	'The HAD-type phosphatase AUM regulates cell spreading and migration'

Poster presentation

Date	Organizer	Presentation Title
September 2011	Annual retreat of the Rudolf-Virchow-Center	'Analysis of AUM-dependent signaling'
Oktober 2012	Annual retreat of the Rudolf-Virchow-Center	'Analysis of AUM-dependent signaling'
February 2013	Gordon Research conference	'The novel tyrosine phosphatase AUM regulates circular dorsal ruffle formation and cell adhesion'
July 2014	FASEB Science Research conference	'The HAD-type phosphatase AUM regulates cell spreading and cell migration"
June 2015	EMBO Research conference	'The role of HAD-type phosphatase AUM for cell migration'

8.3 Affidavit

I hereby declare that my thesis entitled

'Characterization of cell biological and physiological functions of the phosphoglycolate phosphatase AUM'

is the result of my own work. I did not receive any help or support from commercial consultants. All sources and / or materials applied are listed and specified in the thesis.

Furthermore, I confirm that this thesis has not yet been submitted as part of another examination process neither in identical nor similar form.

Eidesstattliche Erklärung

Hiermit erkläre ich an Eides statt, die Dissertation

„Charakterisierung zellbiologischer und physiologischer Funktionen der Phosphoglykolat-Phosphatase AUM"

eigenständig, d.h. insbesondere selbständig und ohne Hilfe eines kommerziellen Promotionsberaters, angefertigt und keine anderen als die von mir angegebenen Quellen und Hilfsmittel verwendet zu haben.

Ich erkläre außerdem, dass die Dissertation weder in gleicher noch in ähnlicher Form bereits in einem anderen Prüfungsverfahren vorgelegen hat.

Würzburg……

Date Signature

8.4 Acknowledgments

I would like to start giving my sincere thanks to my primary supervisor Prof. Dr. Antje Gohla for the opportunity to work on these interesting and challenging projects and for the continuous support during my PhD thesis.

Thanks also to my other supervisors Prof. Dr. Dr. Manfred Schartl and PD Dr. Heike Hermanns for the helpful discussions about theoretical and technical aspects and for the supervision of my projects.

Special thanks to Dr. Elisabeth Jeanclos for an excellent technical and emotional support during my thesis.

Big thanks to Kerstin Hadamek, who contributed a lot to the projects and to Angelika Keller for their technical support and the nice working atmosphere. I also would like to thank Dr. Annegrit Seifried, who helped me with the metabolic studies and Dr. Gunnar Knobloch. Thanks also to the former members of the Gohla group, Markus Schulze, Beate Vogt, Karina Lamprecht and Ambrish Saxena.

I am very grateful to Matthias Zundler und Dr. Agnes Fekete for the good collaboration with lipidomic studies.

I am thankful to all the colleagues of the department of pharmacology, especially Sandra, Evelyn, Annette, Angela and Isabella for the good time inside and outside of the lab.

Finally, I would like to thank my family and friends.

This work is dedicated to Simon - my best friend and the greatest support you could wish for.